The oceanic response to Greenland melting: the effect of increasing model resolution

Dissertation

zur Erlangung des Doktorgrades

an der Mathematisch-Naturwissenschaftlichen Fakultät

der Christian-Albrechts-Universität

zu Kiel

vorgelegt von

Erik Behrens

Kiel

2013

Referent:	Prof. Claus W. Böning
Korreferent:	Prof. Torsten Kanzow
Tag der mündlichen Prüfung:	29.11.2013
Zum Druck genehmigt:	10.12.2013

Der Dekan

Abstract

This study investigates the oceanic response to an enhanced melting of the Greenland Ice Sheet. A series of forced ocean simulations with different horizontal resolutions from 0.5° to 0.05° is used. The main focus is to investigate the oceanic behaviour to a freshwater input within models of different horizontal resolutions and differing in the representation of mesoscale processes. In particular, the role of the mesoscale eddies on the spreading of freshwater in the subpolar North Atlantic is assessed. Two melting scenarios are realised, a strong meltwater release of 0.1 Sv as diagnosed by model data of climate models under high CO_2 conditions, and a more realistic melting scenario, where the diagnosed melting trend of 0.53 mSv/a from 1990 - 2009 is used. The simulations are based on the NEMO ocean sea-ice model and cover resolutions from coarse 0.5° (ORCA05), to eddy-permitting 0.25° (ORCA025), and to eddy-resolving 0.05° (VIKING20). VIKING20 is a new model development, and is based on a local grid refinement approach to reach grid sizes of about 3 km around Greenland.

In the both melting scenarios, the coarse resolution models (ORCA05 and ORCA025) suggest a prominent spreading of the meltwater from the Labrador Sea across the North Atlantic into the Nordic Seas. This hinders the formation of dense water masses, leading to an ongoing reduction in the AMOC. Conversely, results from VIKING20 reveal that mesoscale processes have a distinct potential to counteract the effect of the additional meltwater from Greenland. In comparison to coarser configurations, VIKING20 exhibits an equatorward export of meltwater from the Labrador Sea within the Deep Western Boundary Current and the potential to store meltwater in the northern Gulf Stream recirculation gyre. This results in less meltwater reaching the convection region of the Nordic Seas, and consequently in the realistic melting scenario no response in the AMOC is seen over three decades. The flow path of the North Atlantic Current, in particular the representation of the North-West Corner, is found to be a key factor determining the spread of freshwater in the North Atlantic. The presence of the North-West Corner, realistically reproduced in VIKING20, inhibits an enhanced eastward spreading of meltwater anomalies across the North Atlantic, preventing a pronounced freshwater leakage from the Subpolar Gyre into the Subtropical Gyre via the east Atlantic. This freshwater leakage is enhanced in both coarse configurations, especially in the strong melting case. In this artificial melting scenario the freshwater forcing predominates, such that the equatorward export along the North American coast and the presence of the North-West Corner are of minor importance in determining the oceanic response to meltwater spreading. Whereas in this case all configurations behave similarly and show a decline of the AMOC of about -40 % to -60 % after four decades, the AMOC reacts much less to the realistic melting scenario. These results emphases the need in climate projections to strive for both, realistic Greenland melting rates and represent mesoscale processes properly.

Zusammenfassung

In dieser Studie wurden die ozeanischen Auswirkungen auf ein verstärktes Abschmelzen des Grönländischen Eisschildes untersucht. Eine Serie von angetriebenen Ozeanmodellen mit unterschiedlicher horizontaler Auflösung von 0.5° bis 0.05° wurde hierfür benutzt. Der Hauptfokus der Untersuchung liegt auf den ozeanischen Auswirkungen auf den Schmelzwassereintrag und deren Auflösungsabhängigkeit. Im Besonderen ist die Rolle von mesoskaligen Wirbeln auf die Schmelzwasserausbreitung im Nordatlantik untersucht wurden. Zwei unterschiedliche Abschmelzszenarien wurden durchgeführt: ein Szenario mit starkem Schmelzwassereintrag von 0.1 Sv, wie er unter sehr hohen CO_2 Konzentrationen eintreten könnte und ein Szenario in dem der diagnostizierte Trend von 0.53 mSv/Jahr (1990-2009) verwendet wurde. Die Simulationen basieren auf dem NEMO Ozean-Seeeis-Modell und nutzen Auflösungen von groben 0.5° (ORCA05), wirbelerhaltenden 0.25° (ORCA025) und wirbelauflösenden 0.05° (VIKING20). Die VIKING20 Konfiguration ist eine Neuentwicklung und basiert auf einen lokalen Gitterverfeinerungsansatz, der es erlaubt Gitterweiten von ungefähr 3 km um Grönland zu erreichen.

In beiden Abschmelzszenarien zeigen die groben Modelle (ORCA05 und ORCA025) eine starke Schmelzwasserausbreitung von der Labrador See über den Nordatlantik in das Europäische Nordmeer. Dies beeinträchtigt die Bildung von dichten Wassermassen in dieser Region und führt zu einer fortschreitenden Abnahme der “AMOC”. Ergebnisse von VIKING20 zeigen im Gegensatz dazu ein deutliches Gegenwirkungspotential der mesoskaligen Wirbelprozesse auf das zusätzliche Schmelzwasser. Im Vergleich zu den gröberen Konfigurationen zeigt VIKING20 ein verstärken Export des Schmelzwasser von der Labrador See, teilweise mit dem tiefen westlichen Randstromes, nach Süden und die Fähigkeit das zusätzliche Schmelzwasser in der nördlichen Golfstromrezirkulation zu speichern. Dies führt dazu, dass weniger Schmelzwasser das Europäische Nordmeer erreicht und damit keine Reaktion der “AMOC” im realistischen Abschmelzszenario über drei Dekaden hervorgerufen wird. Es wurde herausgefunden, dass der Pfad des Nordatlantischen Stromes, ins besonderen die Repräsentation der “North-West Corner”, entscheidend für die Schmelzwasserausbreitung im Nordatlantik ist. Das Vorhandensein der “North-West Corner”, welches in VIKING20 der Fall ist, hemmt einen verstärkten Schmelzwasserexport, ausgehend vom Subpolaren Wirbel über den Ostatlantik in den Subtropischen Wirbel. In den beiden grob aufgelösten Konfigurationen und einem starken Abschmelzen von Grönland, ist dieser Exportpfad besonders deutlich. In diesem idealisierten Abschmelzszenario dominiert der Schmelzwassereintrag die ozeanische Reaktion und der nach Süden gerichtete Export von Schmelzwasser entlang der Amerikanischen Küste und das Vorhandensein der “North-West Corner” sind von geringerer Bedeutung. Dies resultiert in einer ähnlichen Abnahme der “AMOC” von -40 % bis -60 % über vier Dekaden, ungeachtet der Modellkonfiguration. In dem realistischen Abschmelzszenario fällt diese Reduktion der “AMOC” deutlich geringer aus. Die Ergebnisse bekräftigen die Notwendigkeit in zukünftigen Klimaprojektionen sowohl realistische Abschmelzraten also auch mesoskalige Prozesse zu berücksichtigen.

Contents

1. Introduction

Observations showed an enhanced melting of the Greenland Ice Sheet (GrIS) over the recent years (Rignot et al. (2010, 2011); Bamber et al. (2012)). The oceanic response to that additional meltwater is investigated in this study, using a set of numerical simulations. A conceptual consequence of the meltwater is a freshening of the subpolar North Atlantic and an accompanied reduction of the dense water mass formation, which could induce a decline of the Atlantic Meridional Overturning Circulation (AMOC). A weakening or shut down of the AMOC would have substantial climatic and environmental implications. Furthermore the melting from Greenland contributes to the global sea level rise, with consequences for all coastal areas (Cronin (2012); Church and White (2006)).

Over the past decades several surface freshening events in the subpolar North Atlantic, unrelated to a melting of Greenland, have been observed (Belkin (2004)). These Great Salinity Anomalies (GSA, Dickson et al. (1988)) were mainly triggered by enlarged freshwater transports from the Arctic Ocean through the Fram Strait or by local events in the Labrador Sea and Baffin Bay (Belkin (2004), Haak (2003)). During those events sea surface salinities (SSS) dropped up to -0.15 psu and propagated within the Subpolar Gyre (SPG) (Houghton and Visbeck (2002); Belkin (2004)). In some idealised simulations it was found that these anomalies have a disruptive effect on the deep water formation and overturning (Häkkinen (1999)). However, other studies found only a small impact on the AMOC of single GSA events (Haak (2003)) if that freshwater is distributed within the SPG. However, further studies prognosed that a freshwater anomaly of ~ 9000 km^3 within in the upper 1000 m of the Nordic Seas would alter the Denmark Strait Overflow significantly; two such events could trigger a shut down (Curry and Mauritzen (2005)). These results illustrate the importance of the amount and location of the freshwater for the oceanic response.

The total ice volume of Greenland ($\sim 2.93 \times 10^6$ km^3, Bamber et al. (2001)) and thus the available amount of meltwater (freshwater) is several times larger than those from GSAs (~ 9.000 km^3, Curry and Mauritzen (2005)). That is the reason, why strong attention has been paid on a melting of the GrIS and the linked freshwater spreading in the North Atlantic. Several modelling studies suggest a collapse of the meridional overturning if the freshwater forcing exceeds a certain thresholds (e.g. Rahmstorf (1996); Gregory et al. (2003, 2005)). A tipping point for that collapse is supposed to be around ~ 0.1 Sv (Rahmstorf (1996); Hofmann and Rahmstorf (2009); Gregory et al. (2003)).

The observed ice mass loss from Greenland in 2010 was around 300 Gt with an acceleration of about 20 Gt/year^2 (Rignot et al. (2011)). If that trend continues, the according meltwater fluxes from Greenland could reach 0.067 Sv (Swingedouw et al. (2012)) at the end of this century. Ice-sheet models forced with conditions from coupled climate models with high CO_2 concentrations, suggest a more drastic melting of the GrIS (Ridley et al. (2005)). The additional meltwater could cause a global sea level rise of about 7 m over 1000 years (Ridley et al. (2005)). That rise is equivalent to a freshwater flux in the order of 0.1 Sv over that time (Jungclaus et al. (2006a)). Even though paleo studies showed that a partial melting of the GrIS occurred in the past (Meese et al. (1997)), Greenland was not completely ice free for at least 11 million years. The oldest ice found there has an age of around 110000 years

(Neem community Members (2013)). A very recent study diagnosed an increasing runoff trend of 0.53 mSv/a for GrIS with large spatial variations (Bamber et al. (2012)) over the last decades. If remaining constant, that trend would lead to an additional meltwater flux from Greenland of about ~ 0.053 Sv at the end of the century. The flux is approximately half the required amount estimated for a shut-down of the Atlantic deep convection (Rahmstorf (1996)).

In the past decade, several ocean modelling studies have been conducted to investigate the impacts of a melting of the GrIS (e.g. Gerdes et al. (2006); Hu et al. (2009); Stammer (2008); Stouffer et al. (2006); Wang et al. (2012)). These studies have been often referred to as freshwater hosing simulations and have been used to investigate paleo and future melting events (e.g. Carlson et al. (2008)). In those simulations, freshwater is artificially added to the system and changes have been compared to a control simulation. Many of these studies used meltwater rates from Greenland of 0.1 Sv, to simulate melting conditions as they could occur in the near future, if global warming proceeds. Details of the meltwater release differed strongly between these studies. Some studies applied the freshwater flux constant in time over a large region 50°N-70°N (Stouffer et al. (2006)), while others dropped the freshwater along the entire coast of Greenland equally (Swingedouw et al. (2012); Weijer et al. (2012)) or spatially varying (Gerdes et al. (2006); Marsh et al. (2010); Stammer (2008)). It seems obvious that the release location is an important factor for the oceanic response: e.g. the freshwater forcing over the convection region led to a faster decline of the dense water mass formation compared to a release along the coast (Weijer et al. (2012)). More refined melting scenarios have been conducted by Hu et al. (2009), with simulations where the runoff increases over time, or in scenarios with increased runoff only during summer months, taking a seasonal cycle into account (Wang et al. (2012)). The results of these studies showed that temporal evolution of the meltwater forcing seem to be of minor importance for the oceanic response compared to amount of meltwater released. However, none of these studies took realistic, observed melting trend into account, but mostly assumed idealized scenarios with higher melting rates. That fact raises the question, how large is the range of the oceanic response between realistic and idealised melting conditions?

Most of these studies, except Weijer et al. (2012) use coarse models, with grid sizes several times larger than the baroclinic Rossby radius of deformation and thus not resolving small scale mesoscale processes, which are known to play a crucial role in the ocean (Chelton (2013); Lévy et al. (2010)). Many coarse models often suffer from large model biases, like shortcomings in the flow path of the North Atlantic Current (NAC), which cause a cold and fresh bias near Newfoundland (Eden et al. (2004)). None of these previous model studies resolved the West Greenland Current (WGC) eddies, which have been found to play an important role for the cross shelf transport of freshwater and for the deep water formation process in the interior Labrador Sea (Brandt et al. (2004); Gelderloos et al. (2011); Chanut et al. (2008)). The results of Weijer et al. (2012) showed a large impact of the horizontal resolution on the freshwater spreading in the North Atlantic and a more gradual decline of the mixed layer in a strong-eddying configuration, but used again freshwater fluxes of 0.1 Sv. An still open question is, how would an eddy resolving model react under a realistic melting scenario?

Irrespective of resolution, some studies use forced ocean-only simulations (Weijer et al. (2012); Wang et al. (2012); Gerdes et al. (2006)), while other studies are based on coupled ocean-atmosphere models (Stouffer et al. (2006)) including atmospheric feedbacks. In forced ocean simulations a negative atmospheric feedback is inhibited, which is stabilising the AMOC against perturbations (Griffies et al. (2009)). The results of Gerdes et al. (2006) showed that an active atmosphere is crucial for the long-term (beyond several decades) melting response. Contrary to this study, in a model-model intercomparison of Swingedouw et al. (2012) (a summary of this related study is found in section 4.2) no significantly different response between coupled and uncoupled models was found over a 40 year time span. That contradiction is possibly linked to details and differences in the freshwater forcing in both studies. However, it is clear that on longer time scales, beyond several decades, an active atmosphere is dominating the melting response. This fact raises the need for coupled simulations for long-term projections of the melting response.

Forced ocean simulations suffer from a further restriction, which is related to the missing of an active atmosphere (a summary of a related study is presented in section 4.1). To prevent long-term trends in water mass properties and in a subsequently drifting AMOC, which are related to uncertainties in the freshwater forcing and model biases, a relaxation of the modeled sea surface salinity (SSS) to a reference SSS is applied. That relaxation, often referred to as SSS restoring, counteracts salinity anomalies, which are induced especially in GrIS melting scenarios. However, studies of Wang et al. (2012); Marsh et al. (2010); Lorbacher et al. (2012); Gerdes et al. (2006) which applied a SSS relaxation, do not show a clear impact of this relaxation on the meltwater response in comparison to other studies. The missing of atmospheric feedbacks and the SSS relaxation is putting caveats against forced simulations. On the other hand, only forced simulations presently allow, with an acceptable amount of computing time, to resolve mesoscale processes in the ocean explicitly, a factor that seems to be relevant at least for the short term response (a few decades).

Irrespective of coupled or uncoupled models, the previous studies suggest that the amount of meltwater and its regional distribution are the main factors influencing the short-term oceanic response. In all simulations with a meltwater flux of about 0.1 Sv a decline of the AMOC is present. This decline depends on the initial AMOC state. Absolute AMOC reductions of about -3 Sv (Wang et al. (2012)), and -1 to -9 Sv (Stouffer et al. (2006)), and -2 to -5 Sv (Gerdes et al. (2006)), and -5 to -12 Sv (Weijer et al. (2012)), and -1 to -4 Sv (Swingedouw et al. (2012)) are found over the first 3 decades, while the mean AMOC transport varies between 10 Sv (Wang et al. (2012)) and 24 Sv (Weijer et al. (2012)). Relative to the initial AMOC state, all simulations show a broadly similar decline of -30 % to -50 % over that period.

Despite these previous studies, the relevance of small scale eddies and mesoscale processes on the melting response is still unclear. Furthermore, most studies assumed rather strong melting conditions, while the real observed trend has not been taken into account so far. That raises the following questions. How important is a gradual increase of meltwater fluxes for the oceanic response, in contrast

to a step function increase? How large is the difference in the oceanic response between realistic and idealised melting conditions? Most coarse resolution models suffer from large model biases (e.g. cold bias). Do these model biases influence the oceanic reaction? How would a highly realistic ocean simulation react to the observed melting trend?

A main goal of this study is to provide a systematic investigation of the oceanic response to an enhanced melting of the GrIS. The study covers the local reactions around Greenland, consequences for the deep water formation, and implications for the meridional transports. A special focus is set on the freshwater distribution in the North Atlantic and the importance of mesoscale processes affecting the spreading of freshwater anomalies. The investigation tries to assess the oceanic response with fairly realistic oceanic conditions, building on observed meltwater trends, in comparison to the previously used idealised scenario of a constant 0.1 Sv-melting rate. This comparison allows to quantify the uncertainties of the oceanic response for the near future.

In this study a suite of ocean only simulations with increasing horizontal resolution is used. The resolution varies between 0.5° (ORCA05), and 0.25° (ORCA025) and 0.05° (VIKING20). In the high resolution configuration (VIKING20) most of the mesoscale processes in the North Atlantic are resolved explicitly. The atmospheric forcing fields of CORE2 (Large and Yeager (2009)) have been applied to perform a six decade long reference hindcast simulation. In two different GrIS scenarios the oceanic response in comparison to the reference simulation has been analysed. The first melting scenario assumes meltwater fluxes of 0.1 Sv from Greenland and allows a comparison to previous studies. The second melting scenario takes the observed melting trend of 0.53 mSv/a (Bamber et al. (2012)) into account. In both melting scenarios a passive tracer was released according to the additional meltwater from Greenland to track its spreading.

The thesis is structured as follows. Chapter 2 introduces the numerical model and describes the different configurations. Furthermore, the performed simulations are characterised. The chapter also contains the methods, presented in this study. Chapter 3 provides a model assessment. The focus in this chapter is put on the gain of realism by increasing the horizontal resolution in comparison to observations. Chapter 4 summarises findings of related publications, which dealt with the impact of SSS restoring on the long-term AMOC evolution* (section 4.1) and the importance of atmospheric feedbacks in GrIS melting simulation** (section 4.2). Chapter 5 presents the oceanic response to a melting of Greenland under idealised and realistic melting conditions and shows the importance of mesoscale processes for the response. The last chapter 6 provides a summary and conclusion. The Appendix provides supporting material with respect to the sensitivity of the long-term AMOC tendency for the melting response.

* Behrens, E., Biastoch, A., & Böning, C. W. (2013). Spurious AMOC trends in global ocean sea-ice models related to subarctic freshwater forcing. Ocean Modelling, 69(39-49). doi:10.1016 / j.ocemod.2013.05.004

** Swingedouw, D., Rodehacke, C. B., Behrens, E., Menary, M., Olsen, S. M., Gao, Y., Mikolajewicz, U., Mignot, J., Biastoch, A. (2012). Decadal fingerprints of freshwater discharge around Greenland in a multi-model ensemble. Climate Dynamics, 41(3-4), 695–720. doi:10.1007/s00382-012-1479-9

2. Numerical model configurations, simulations and diagnostic methods

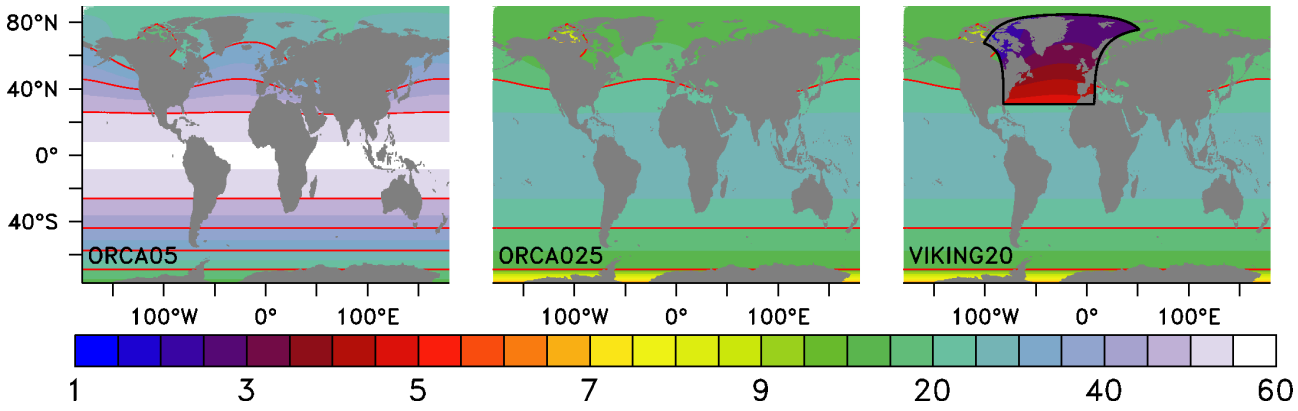

Figure 1.: Horizontal grid sizes for each individual model configuration in km. VIKING20 share the same global domain as ORCA025, but uses finer grid size for the North Atlantic (Nest) to resolve mesoscale processes in this region explicitly. The boundaries of the high resolution domain are indicated by the black frame. Each 10 km interval is contoured in red. Please note the none uniform scale, to highlight the fine mesh in VIKING20 in the subpolar North Atlantic.

2.1. Numerical model configurations

All model configurations build on the European ocean model system NEMO (Nucleus for European Modelling of the Ocean), developed in France (Madec (2008)). It is based on the hydrostatic primitive equations, and uses the Boussinesq approximation, and is discretised on an Arakawa C-grid (Arakawa and Lamb (1977)). Additional improvements of the model code and input data are accomplished through the DRAKKAR framework (DRAKKAR Group (2007)). This study uses three global configurations which differ in their horizontal resolution and thus in the representation of the mesoscale variability. All configurations have a global domain and do not suffer from boundary condition issues. The three utilised resolutions are a coarse (0.5°, ORCA05), medium (eddy permitting 0.25°, ORCA025) and high (eddy resolving 0.05°, VIKING20) resolution configuration. The eddy resolving configuration uses a local grid refinement realised by a two-way "nesting approach" (AGRIF, Debreu et al. (2008)), where a 0.05°-grid for the North Atlantic between 32°N and 85°N is embedded in a global (ORCA025) domain. It should be highlighted that VIKING20 is a new developed configuration with distinct focus on the North Atlantic. A detailed description is provided in section 2.2. Both other configurations are well tested configurations and used in several scientific studies (Behrens et al. (2012, 2013); Griffies et al. (2009); Böning et al. (2006); Biastoch et al. (2008a)). For the horizontal discretization a tri-polar grid is used, with two north poles over Canada and Siberia to avoid singularities at the geographic North Pole. The resulting horizontal grid sizes for each individual configuration are shown in Figure 1.

The coarse resolution (ORCA05) involves grid sizes of $\sim$ 55 km at the equator decreasing to $\sim$ 30 km in the Labrador Sea. The respective grid sizes of the other configurations are $\sim$ 15 km (ORCA025) and $\sim$ 3 km (VIKING20) in this region. All configurations have 46 vertical z-levels, with a partial cells scheme (Barnier et al. (2006)) to improve the near bottom flows. The vertical layer thickness

starts from 6 m at the surface and increases with depth to max 250 m. The bathymetry is based in all simulations on ETOPO (http://www.earthmodels.org/data-and-tools/topography/etopo) and GEBCO (http://www.gebco.net/) products. The configurations also use a viscos-plastic ocean-sea ice model (LIM2, (Fichefet and Maqueda (1997)) to simulate the sea-ice conditions in the high latitudes. For the turbulent vertical mixing a 1.5 level turbulent kinetic energy (TKE) scheme is applied (Blanke and Delecluse (1993); Madec et al. (1998)). Vertical mixing in cases of hydrostatic instability is parameterised by an enhanced vertical diffusion for tracer and momentum. Furthermore a energy and enstrophy conserving advection scheme is used (EEN, based on Arakawa and Hsu (1990)). A bottom boundary layer (BBL) parameterisation is used in ORCA05 and VIKING20 accomplished by diffusion on tracers. No improvements have been recognised in ORCA025, when the BBL was used (pers. comm. Jean-Marc Molines). The lateral viscosity for momentum is discretised by a horizontal bi-Laplacian and diffusion by an iso-neutral Laplacian scheme (parameter are provided in table 1).

2.2. General simulation strategy and reference simulation (REF)

In the following the term control or reference simulation will be used synonymously. All simulations are started from rest with initial conditions derived from Levitus (1998). For the atmospheric conditions the interannually varying forcing set of CORE 2 is used (Large and Yeager (2009)), which allows to compare model results with oceanic observations over the past 6 decades. This data set is based on reanalysis products for atmospheric quantities, like radiation and precipitation. These various data products have been used as input data for a coupled model simulation to obtain a global coverage and reliable global budgets. The atmospheric-oceanic fluxes are derived from bulk formula, described in (Large and Yeager (2009)). The atmospheric conditions during 1978-2007 have been used to perform a spinup simulation, to reduce large trends in the subsequent reference (hindcast) simulation (1948-2007). The period from 1978-2007 was chosen after a series of test experiments for the spinup, because the model trend in key quantities was smallest compared to other forcing periods (e.g. 1958-2007). The spinup state (end 2007) was then used as initial condition for the reference simulation (1948-2007). A schematic of the simulation strategy is provided in Figure 2. The first 10 years of the following reference simulation are affected by adaptation processes due to inconsistent atmospheric conditions (jump from 2007 back to 1948 atmospheric conditions), for example differences in the NAO phase. It should be noted that there is so far no concept avoiding jumps in simulations which are longer than the available forcing period. The initial thickness of the sea-ice is set to 3 m (1 m for the southern hemisphere) at the beginning of the spin up, due to a lack of reliable data in regions of freezing conditions. However it turns out that the initial condition of the sea-ice is of minor importance for the large scale hydrographic conditions. Additional sensitivity simulations with a spun-up sea-ice state as initial condition, did not show significant changes in drift of key quantities compared to simulations, which were initialised with the crude proxy. Within the first years of the spin-up, the sea-ice distribution and thickness adapts to conditions close to observations. The coastal runoff is based on Dai and Trenberth (2002) with

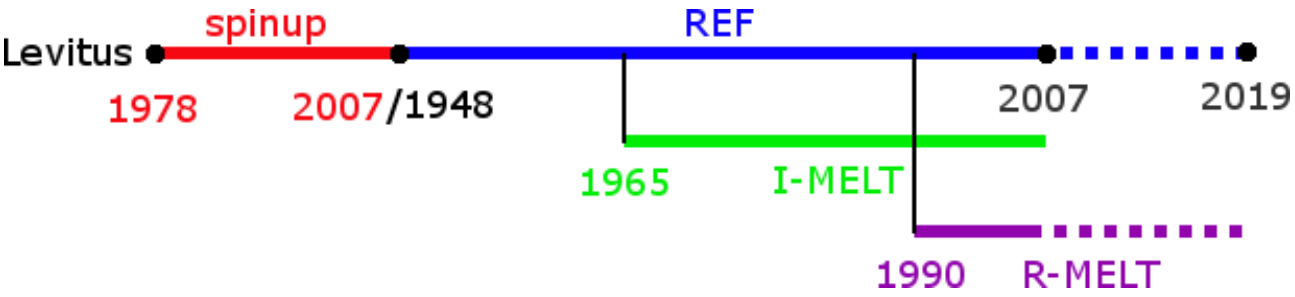

Figure 2.: Simulation strategy: The model simulation starts from rest with initial condition for temperature and salinity from Levitus (1998). The spinup simulation (red) uses the atmospheric forcing from 1978 to 2007. The reference simulation (REF, blue) is based on the spinup state and uses the atmospheric fields from1948 to 2007. Beyond 2007 a repetitive 2007 year forcing is used. The I-MELT simulation (green) is started in 1965 and is integrated until 2007. The R-MELT simulation (purple) is started in 1990 and is integrated until 2019.

some local modifications, which are described in Bourdallé Badie and Treguier (2006). The global applied runoff of approximately 1.2 Sv is in agreement with estimates derived from observations (Dai and Trenberth (2002)). The value of Arctic runoff adds up to 0.90 mSv, a bit lower than observations suggest. It should be also mentioned that the reference runoff value from Greenland (∼2 mSv) is very low compared to recent estimates (17 mSv - 22 mSv Greve (2000), Bamber et al. (2012)). An adaption to the observational estimate for future simulations is strongly recommended, although it may not affect the present melting simulations, since only anomalies to the reference simulations are investigated. However, such a modification would probably improve the positive salinity bias of all configurations in the Labrador Sea, where the models in the reference simulation tend to display a higher SSS than observations suggest. However, with respect to the coastal freshwater forcing large uncertainties are remaining, for example rates of terrestrial water storage (Pokhrel et al. (2012)). No geothermal heating is applied in any configuration.

A crucial point for the freshwater budget is the SSS-restoring required in ocean-only simulations to avoid long-term trends in water mass properties. Due to an inactive atmosphere a negative temperature feedback on the AMOC is missing (Griffies et al. (2009)). As a consequence the positive feedback by salinity is overemphasised and small variations in salinity and freshwater transport can introduce long-term drifts in water masses and the AMOC (Behrens et al. (2013)). To avoid such a drift a counteracting term is required, accomplished by a SSS restoring towards climatological values. The issue of SSS restoring was investigated intensively in a separate study (see Behrens et al. (2013), a summary is provided in section 4.1). All simulations use a “weak” salinity restoring with a piston velocity of 16.4 mm/d, which correspond to a 6 m surface layer and a restoring timescale of 1 year. The arbitrary restoring flux was further limited with a delta SSS criterion of 0.5 psu, suggested by the CORE protocol
(http://data1.gfdl.noaa.gov/~nnz/mom4/COREv2/doc/CORE_notes_15feb2012.pdf), to avoid dominating restoring fluxes. No restoring is applied in regions where sea-ice is present and in the vicinity of rivers as well as in a swath around Greenland (Figure 3).

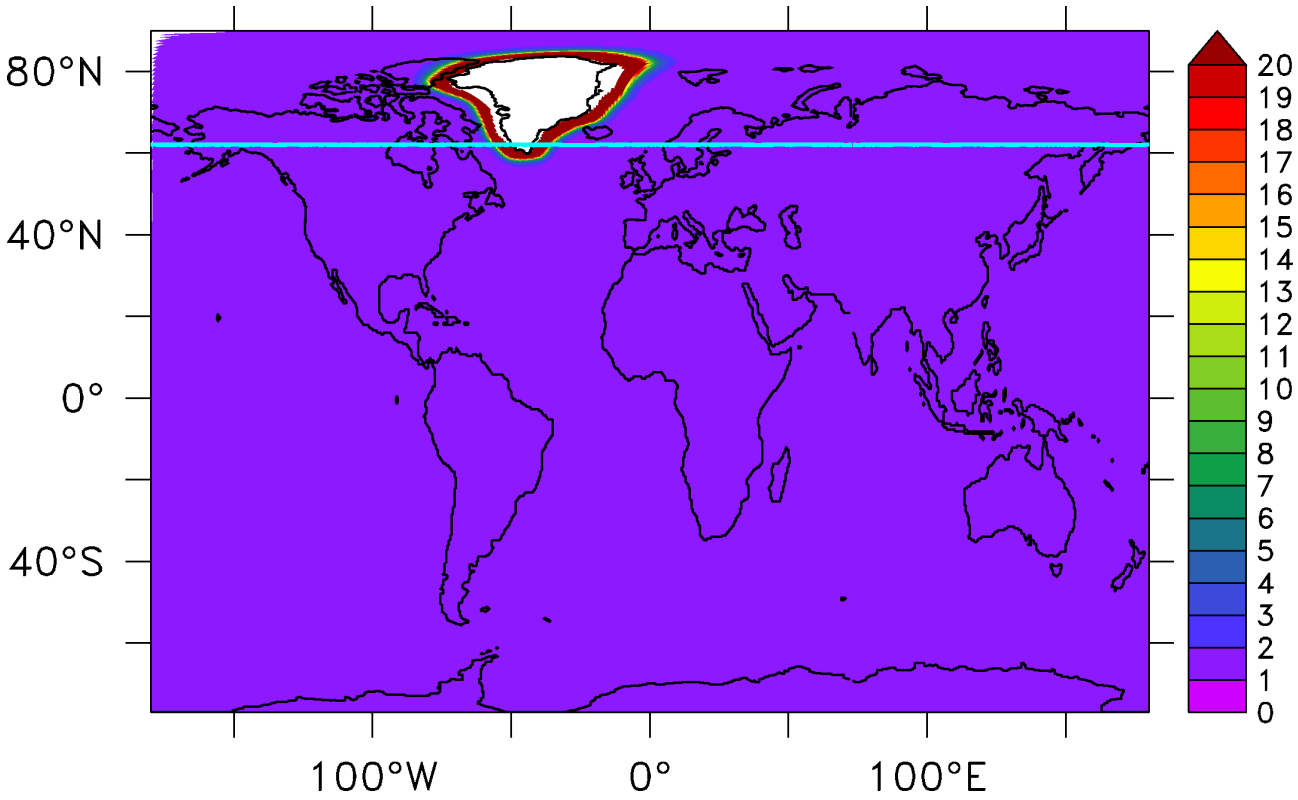

Figure 3.: The SSS restoring timescale in years used for the simulations is illustrated by the shading. The global default value is 1 year. No or weaker SSS restoring (according larger restoring timescales) is applied around the Greenland coast. Please note, an additional restoring flux limitation is used to limit the arbitrary restoring fluxes to maximal values of about ∼10% of the precipitation fluxes. North of the cyan line (62°N) the polar precipitation is reduced by 10% (14 mSv).

The spatial varying restoring field is used to avoid an immediate freshwater outtake by the SSS restoring in the Greenland melting simulations. Due to the additional freshwater and related SSS changes in such simulations, large counteracting restoring fluxes could inhibit the additional freshwater effect. In all simulations the original precipitation north of 62°N is reduced by 10 % (14 mSv, cyan line in Figure 3) to obtain reference simulations with little remaining drift in the water masses. The combination of the revised SSS restoring and rain reduction leads to simulations with fairly realistic values in AMOC and more important only little long-term drift. (Additional sensitivity simulations showed on the other hand that the long term AMOC trend, which is affected by the subarctic precipitation is of minor importance for the general GrIS melting response in idealised melting simulations; see Appendix)

The VIKING20-configuration: A new development

VIKING20 refers to the combined configuration, of a global ORCA025 configuration as base model and a local grid refinement embedded in the North Atlantic (between 32°N and 82°N, area is indicated in Figure 1). This configuration is a new development for dedicated studies of scientific questions regarding the North Atlantic circulation. A particular effort was made to implement the grid refinement also for the ice-model, which was not supported by NEMO/AGRIF before. The local grid refinement is accomplished by an AGRIF –zoom (Debreu et al. (2008)) with a horizontal resolution of 1/20°. The according refinement factor from the coarser model ORCA025 (1/4°) to the nested region is 5. This represents the maximum possible factor of refinement while avoiding problems at the interfaces between the nest and the base model. (pers. comm. Rachid Benshila). A resolution of 1/20° is used to obtain grid sizes smaller than the first baroclinic Rossby radius over the area of interest. That allows to resolve mesoscale eddies explicitly. For future configurations using higher resolutions ($< 1/20°$) the base model must have a higher resolution or an additional nest in the already nested domain has to been embedded. In the present case both "models" are actively linked with each other and exchange information during the run time (providing and sending of information partly over the entire nested domain or at the boundaries). This technique (two way nesting) allows to investigate the effect of increasing resolution in a certain region, but also the remote effect outside of the nested region like done in previous studies (e.g. Biastoch et al. (2008b)). The sea-ice model is very problematic in the nested region. Within the AGRIF zoom grid sizes of only a few kilometers are reached which mark the lowest threshold for the used sea-ice model (pers. comm. Gurvan Madec). At this grid size some of the underlying physical assumptions, like the un-elasticity of the sea ice become questionable. The impact of the rheology of sea-ice and ice-classes gain in importance for the results (Vancoppenolle et al. (2008)). For further model parameters details please see Table 1.

To initialise VIKING20 (1948) the conditions of the spin up simulation of ORCA025 (1978-2007) at the end of 2007 have been used. All reference simulations cover therefore at least the available forcing period of the interannual varying forcing fields from 1948-2007 (CORE2, Large and Yeager (2009)). The retrieved control simulation over the past 60 years is used for model validation with observations,

	ORCA05	ORCA025	VIKING20 (base-model/nest)
model time step	36 min	24 min	20 min / 4 min
horizontal diffusivity for momentum (bi-laplacian) in m^4/s^2	$1.2 \cdot 10^{12}$	$1.5 \cdot 10^{11}$	$1.5 \cdot 10^{11}/1 \cdot 10^{10}$
iso-neutral diffusivity for tracer (laplacian) in m^2/s	500	300	300/100

Table 1.: The most important model parameters, which vary between the model configurations.

which in general shows a good agreement to observed variability of key quantities (see chapter 3). The coarser configurations show some shortcomings to observation (e.g. position of the NAC), while VIKING20 matches key measures of the North Atlantic. In the following the two cases of melting scenarios (idealised I-MELT, realistic R-MELT) will be described in detail. Irrespective of the melting scenario all hosing simulations use the same model setup as the control simulation, the only difference is an increased runoff from Greenland, simulating an enhanced melting of the GrIS.

2.2.1. Idealised freshwater perturbation (I-MELT scenario)

The first melting scenario follows previous studies with a classical estimate for an increased coastal runoff from Greenland of 0.1 Sv (Gerdes et al. (2006); Wang et al. (2012); Stouffer et al. (2006); Swingedouw et al. (2012)). This value is based on ice-sheet simulation forced with model data from climate projection under large greenhouse gas emission, which produced a sea level rise of 7 m over the next 1000 years (Jungclaus et al. (2006a)). This sea level rise correspond to a mean meltwater flux in the order of 0.1 Sv. Large uncertainties about the real rates to be expected over the next century are still remaining (Swingedouw et al. (2012)). Therefore many studies used this idealised value to try to investigate the general oceanic response (Stouffer et al. (2006), Weijer et al. (2012)). It is also assumed that this runoff value could be a tipping point for the AMOC, from an "on" to an "off" mode (Hofmann and Rahmstorf (2009), Latif et al. (2000), Dijkstra (2007)). However there are large variations how this flux is applied among previous modelling studies. Some studies applied it over a relatively large region (Stouffer et al. (2006)), others only along the coast of Greenland (e.g. Swingedouw et al. (2012)). In the present case the additional freshwater flux (0.1 Sv) is applied constantly over time and equally distributed around the coast of Greenland (Figure 4) as done in Swingedouw et al. (2012). The hosing simulation is branched off from an oceanic state at the 31 December 1964 from the reference run. It therefore lasts 43 years, coinciding with the end of the available atmospheric reanalysis products of CORE 2 (2007). The seasonal amplitude of the modified Greenland runoff is unchanged. No smoothed transition from the reference runoff ($\sim$ 2 mSv) is applied. It should be mentioned that this scenario was the basis of the EU-THOR project (WP2). This scenario can be understood as an idealised case to simulate an extreme melting of Greenland which could lead to a shut down of the AMOC (Latif et al. (2000)). Figure 4 shows the spatial distribution of the coastal runoff (annual mean in m/a) for the reference case ("REF") and the idealised case ("I-MELT"). In the reference runoff there are

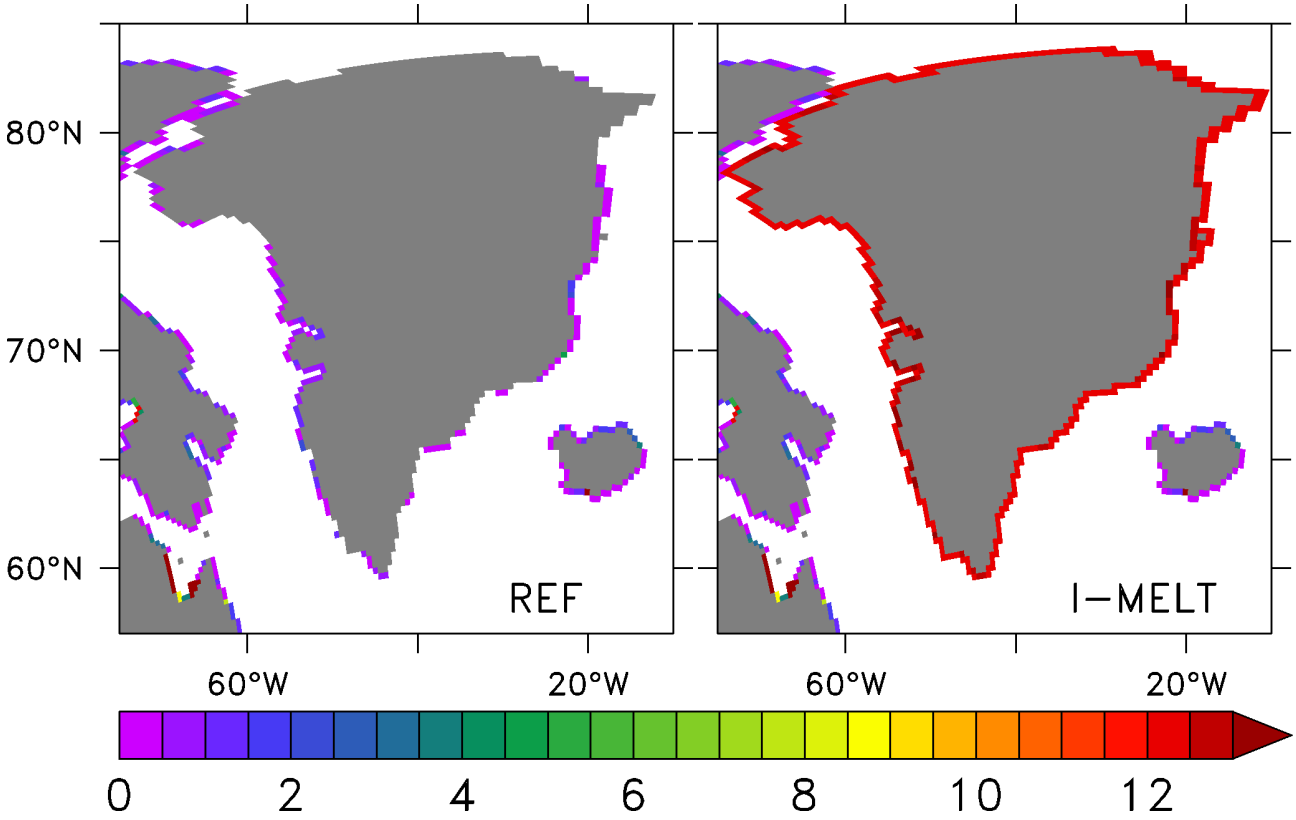

Figure 4.: Annual mean coastal runoff in m/a for the reference simulation (left panel) and the idealised runoff scenario I-MELT (right panel). Please note the different scales to Figure 5. The coastal runoff in the I-MELT scenario is increased by 0.1 Sv, and equally distributed around the coast of Greenland. The runoff is illustrated on the ORCA05 grid.

certain regions of the Greenland coast where no or very low coastal runoff is present. In the idealised scenario an anomaly of 0.1 Sv equally distributed along the entire Greenland coast is superimposed to the normal runoff.

2.2.2. Realistic freshwater perturbation (R-MELT scenario)

The second Greenland melting scenario adopts a more realistic, gradual increase in the runoff, where the estimated melting trend during 1990-2009 (0.53 mSv/a, Bamber et al. (2012)) was used to modify the reference coastal runoff from Greenland. This runoff estimate is based on regional mass balance model simulations for Greenland, forced with atmospheric conditions from ERA-40 and ERA-Interim for the period from 1958-2009. The runoff pattern from Greenland shows in this simulation large spatial variations in the runoff trend. The largest increasing trend of the runoff was found in the region of the Irminger basin, while certain regions displayed a negative trend. These individual trends where used to modify the reference runoff accordingly. The seasonal cycle is unchanged, therefore coastal runoff is also present during winter months, which could be improved in the future. The strong spatial variation can be seen in Figure 5. The melting simulations were started from an oceanic state of the reference simulation at the end of 1989 and was forced until 2007 with the available reanalysis products of CORE2. Beyond that period, the forcing of the year 2007 was repeated to prolong the simulation to the end of 2019. This approach has strong caveats and does not take real future atmospheric conditions into account. On the other hand since only anomalies from reference state are quantified, the prolongation seems to be a reasonable approach. More problematic could be the missing of any interannual variability beyond 2007, which would increase the noise level compared to the melting signal.

2.2.3. Run-off evolution in I-MELT and R-MELT

Figure 6a, illustrates the temporal evolution of the coastal integrated runoff from Greenland. As described above the mean reference runoff has a value of ∼2 mSv, and in the I-MELT scenario 0.1 Sv are constantly added. The R-MELT scenario starts at the reference value but describes a linear increase with a linear annual increase of 0.53 mSv. It would take therefore around 183 years to the reach the idealised runoff value (0.1 Sv). The amplitude of the seasonal cycle is un-changed between the different simulations. It should be remembered that the I-MELT simulation lasts 43 years while the R-MELT simulation only 30 years, therefore the amount of additional freshwater differs strongly between both simulations. The 43 year long simulation uses the entire available hindcast forcing period. For the 30 year simulation (R-MELT) the unknown real future evolution of atmospheric conditions and Greenland runoff are the limiting factors, making a prolongation beyond 2019 questionable. Figure 6b, shows how long it would take for the Greenland ice to melt completely. Estimates suggest a total volume of the Greenland ice-sheet of about 2.93×10^6 km^3 (green dashed line, Bamber et al. (2001)).

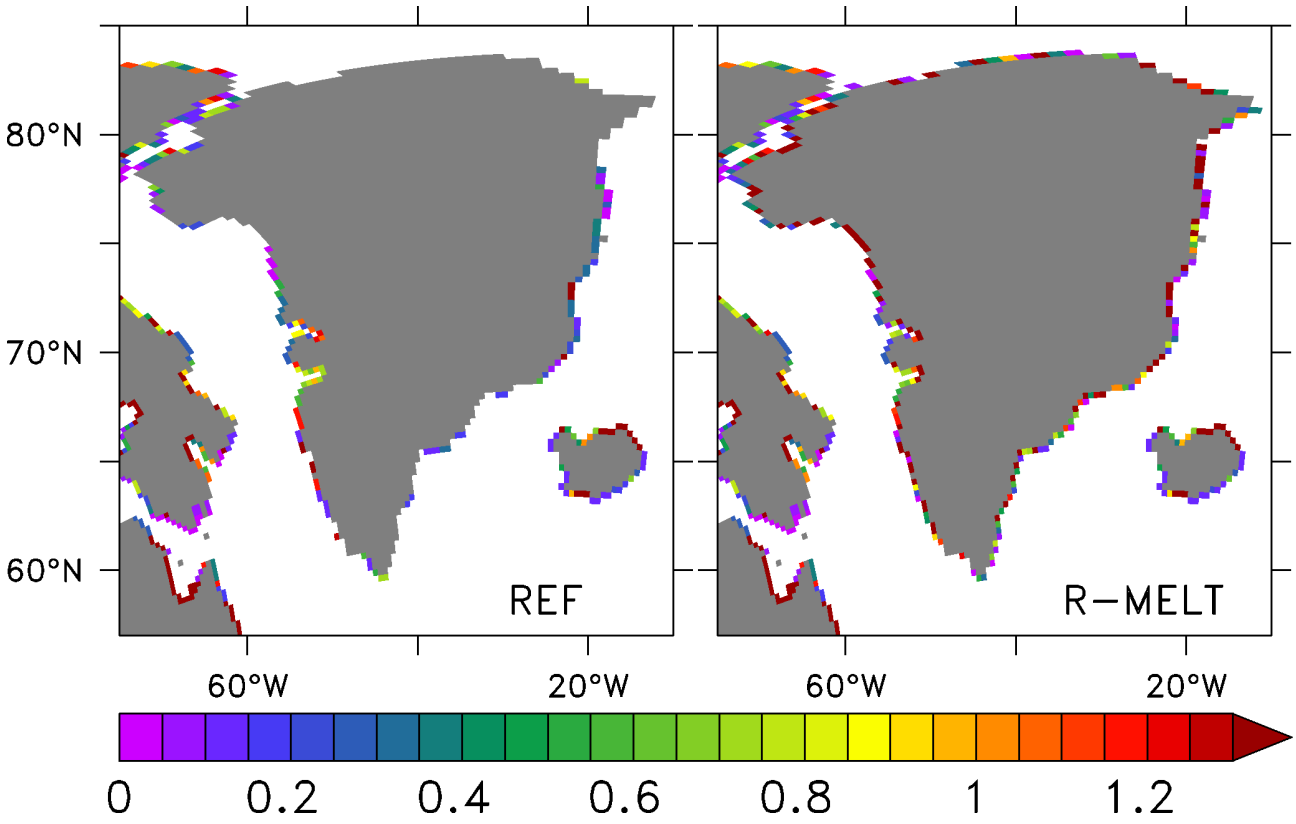

Figure 5.: Annual mean coastal runoff for the reference simulation (left panel) in m/a and for the R-MELT scenario (right panel) in 2019, where the runoff shows a linear trend of 0.53 mSv/a. Studies suggest a large increase of the coastal runoff to the Irminger Sea (Bamber et al. (2012)). Please not the different scales to Figure 4. The runoff is illustrated on the ORCA05 grid.

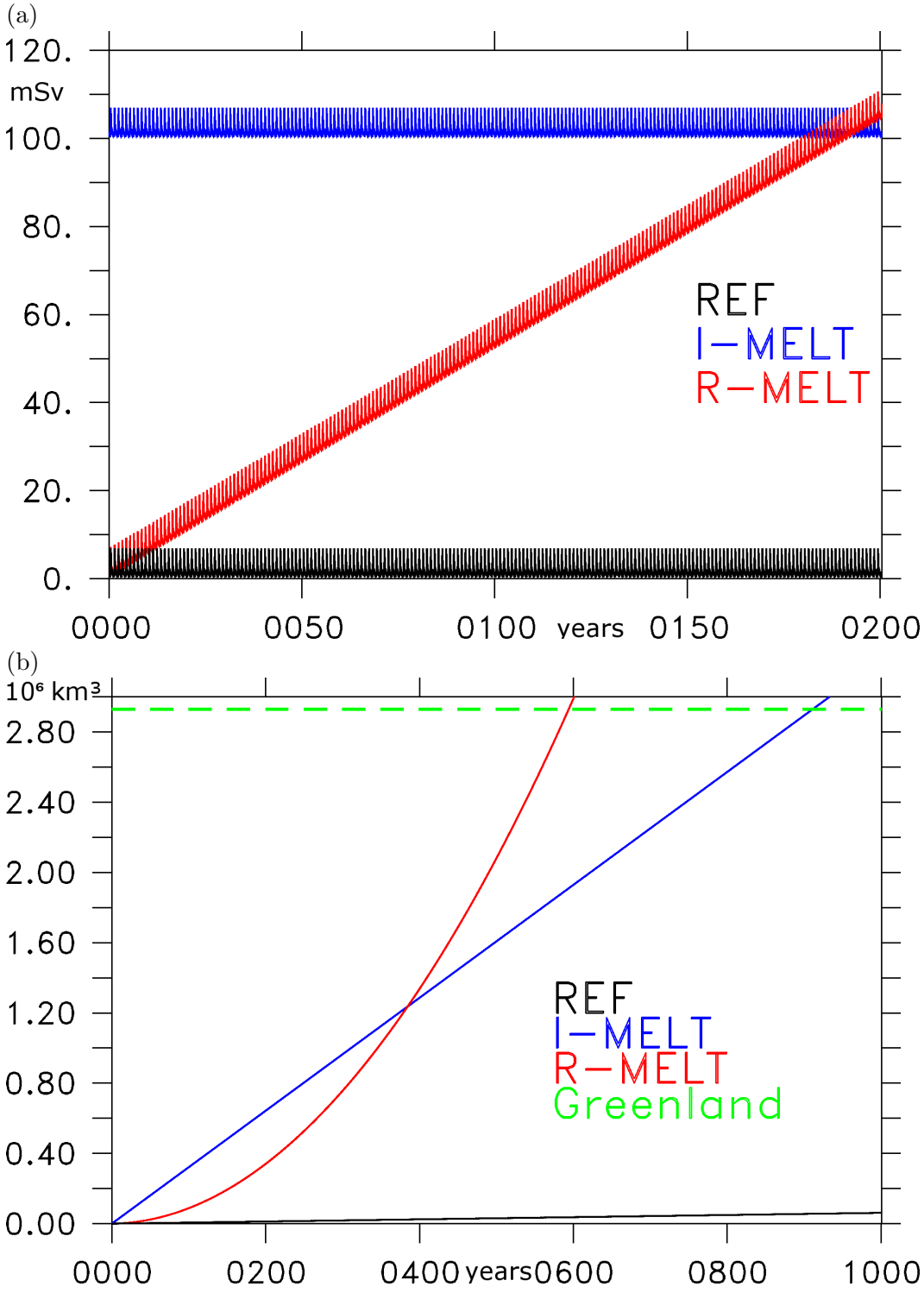

Figure 6.: Illustration of the different melting scenarios by depicting the (hypothetical) long-term evolution of the coastal runoff in (volume flux in mSv) over the first 200 years in (a) and (b) the total released freshwater volume (10^6km³) for the first 1000 years. The I-MELT scenario exhibits a constant additional release of 0.1 Sv (invariant in time) superimposed to the reference runoff with a seasonal variations. The R-MELT scenario describes a linear increase by 0.53 mSv/a of the reference runoff. The released volume of freshwater differs substantially between the I-MELT and R-MELT simulations for the first centuries. The total volume of the Greenland ice-sheet (2.93×10^6 km³) is indicated by the green dashed line. It would last approximately $\sim$ 580 years in the realistic and $\sim$ 880 years in the idealised melting scenario to melt the volume of Greenland completely. The actual amount of the reference runoff is nearly negligible compared to the volume of the GrIS.

In the R-MELT scenario it would take approximately around 580 years to melt the entire ice sheet approx. 300 years less than in the idealised case. However it is unlikely that Greenland ice will melt completely, as suggested by actual studies (Neem community Members (2013)).

2.2.4. Set of model experiments

Table 2 provides an overview about the main simulations (bold). For each configuration a reference simulation (REF) and two Greenland melting simulations have been conducted. The melting simulations differ in the applied melting scenario. The idealised GrIS melting scenario (I-MELT) with enhanced runoff from Greenland by 0.1 Sv branches off in 1965 from the reference simulation and lasts for 43 year. The second GrIS melting scenario takes a realistic melting (R-MELT) trend from Greenland into account. The runoff from Greenland increases each year by 0.53 mSv, starting in 1990 and follows results by Bamber et al. (2012). This simulation covers the period from 1990-2019. Due to the lack of atmospheric forcing beyond 2007, the atmospheric conditions of 2007 are repetitively applied to prolong the melting simulation to 2019 as well as the reference simulation. The additional sensitivity experiments performed in ORCA05 are used to investigate the sensitivity of the remaining sea surface salinity restoring. In REF NO 05 and the according hosing simulation I-MELT NO 05 no restoring of the SSS towards climatology is applied. In further sensitivity simulations the restoring fluxes from the reference simulation (REF 05) have been diagnosed and been applied to produce a second reference simulation without additional SSS restoring (REF-MIXED-05). This approach is referred to as mixed boundary conditions. The according melting simulation I-MELT MIXED 05 uses the same restoring fluxes as REF MIXED 05 and no further SSS-restoring. (see also Figure 2).

2.3. Diagnostic methods

The following section provides an account of the main diagnostics used assessing the model behaviour in the reference simulations and melting scenarios.

2.3.1. Tracking the meltwater: passive tracer versus salinity anomalies

An important concept in this study to track the meltwater from Greenland is accomplished by the release of a passive tracer according to the additional meltwater rates from Greenland. The amount of tracer being released each timestep at the Greenland coast is analogous to the coastal freshwater flux from Greenland. The spreading of this tracer is governed only by physical processes of advection and diffusion like the bulk of the meltwater from Greenland. Air-sea fluxes of tracer are prevented, which is not the case for the meltwater. The passive tracer allows tracking the meltwater directly without secondary effects (due to changes in the circulation). In this study most tracer concentrations

	configuration	period	SSS restoring	runoff
REF NO 05	ORCA05	1948-2007	0	
I-MELT NO 05	ORCA05	1965-2007	0	0.1 Sv
REF MIXED 05	ORCA05	1948-2007	MBC (0)	
I-MELT MIXED 05	ORCA05	1965-2007	MBC (0)	0.1 Sv
REF 05	ORCA05	1948-2007/2019	Weak+FL	
I-MELT 05	ORCA05	1965-2007	Weak+FL	0.1 Sv
R-MELT 05	ORCA05	1990-2019	Weak+FL	0.53 mSv/a
REF 025	ORCA025	1948-2007/2019	Weak+FL	
I-MELT 025	ORCA025	1965-2007	Weak+FL	0.1 Sv
R-MELT 025	ORCA025	1990-2019	Weak+FL	0.53 mSv/a
REF 005	VIKING20	1948-2007/2019	Weak+FL	
I-MELT 005	VIKING20	1965-2007	Weak+FL	0.1 Sv
R-MELT 005	VIKING20	1990-2019	Weak+FL	0.53 mSv/a

Table 2.: The table presents the most important simulations. The major simulations are highlighted in bold. The SSS restoring is kept unchanged in these main simulations. The applied SSS restoring is weak (piston velocity 16.4 mm/day) with an additional restoring flux limitation (referred to as "Weak-FL"). Deviations from the reference Greenland runoff are indicated in the last column, 0.1 Sv constant for the I-MELT scenario and a linear increasing runoff rate by 0.53 mSv/a in the R-MELT scenario. Additional sensitivity simulations in ORCA05 use no SSS restoring or mixed boundary conditions (MBC) to assess the sensitivity of the melting response to the restoring setting.

are diagnosed at the surface or as vertical integral, which proved to be the best means for illustration of the horizontal spreading. As an example, Figure 7 shows the surface tracer concentration (m^3/m^3) in VIKING20 after 1 year in the I-MELT scenario. Large amounts of meltwater are found within the Greenland boundary currents, penetrating into the Labrador Sea and in the Labrador Current. The corresponding SSS-anomaly between the hosing and reference simulation exhibits a meltwater related freshening in the boundary current of Greenland. This diagnostic shows positive and negative anomalies over the entire regions superimposed on the underlying melting signal, which are related to stochastic eddy activity or by melting related circulation changes. The passive tracers allows to distinguish between those direct and indirect meltwater effects.

2.3.2. Sections and regions to assess the oceanic response

A summary view of these sections and averaging regions used for assessing regional model behaviors are marked in Figure 8.

The hydrographic section AR7W

This hydrographic section is the most important transect in the Labrador Sea (see Figure 17 and 8), frequently repeated by various nations (USA, Canada, Germany). This section cuts directly through the entire Labrador Sea and is typically maintained in spring or early summer to investigate the

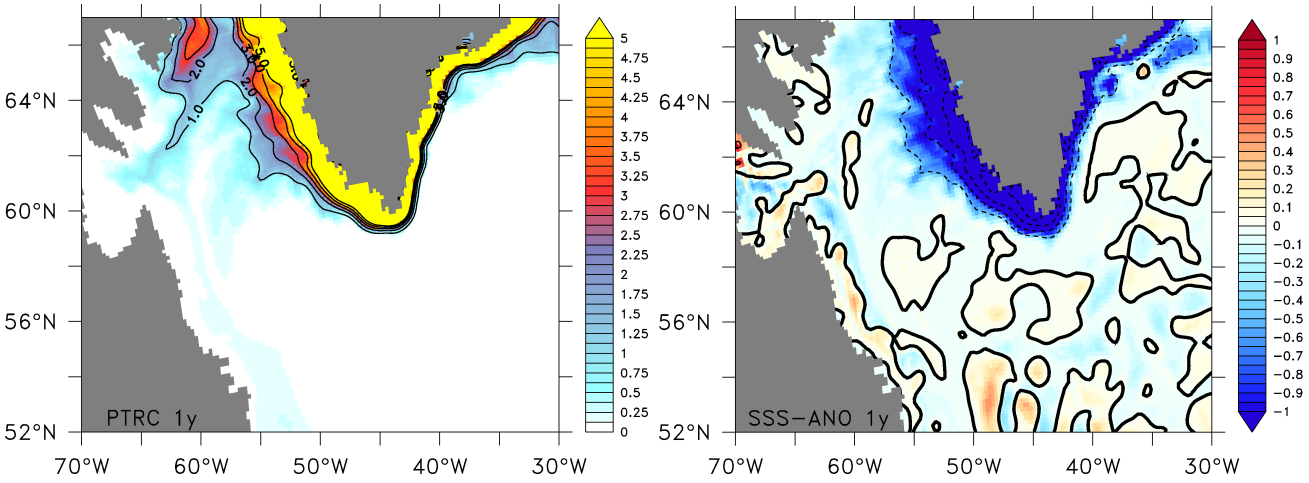

Figure 7.: Surface tracer concentration after 1 year in the I-MELT scenario in VIKING20 (10^{-2} m³/m³, left panel) and the corresponding SSS-anomaly (MELT minus REF) in psu at the same time (right panel). Each 1 $\times$ 10^{-2} m³/m³ interval is contour in the left panel and each 0.5 psu interval in the right panel.

winterly deep convection during the preceding winter months. A strong focus is set on the boundary currents on the Labrador and Greenland coast also covered by this section. For further details see section 3.4

The Central Labrador Sea

One focus of this thesis is to investigate the freshwater related effect on the deep water formation, which takes place in the central Labrador Sea. An area-mean over the central Labrador Sea is taken to diagnose changes there (red box marked with CL in Figure 8). Over this area temperature, salinity, Sea Surface Height (SSH) and the passive tracer are horizontally averaged at each depth level to gain a robust quantity to identify changes. (freshwater related results are presented in section 5.2.1). At this point it should be mentioned that the mean value of the barotropic sreamfunction over that box is taken as diagnostic for the SPG-strength, following the diagnostic present in Böning et al. (2006).

Heat and freshwater content in the subpolar North Atlantic (Boyer et al. 2007):

The region enclosed in the magenta line (50°N to Fram Strait in Figure 8, Baffin Bay and Baltic Sea excluded) is used for calculating heat and freshwater content changes in comparison to observed changes. These results can be compared with observations provided by Boyer et al. (2007) for the period from 1995-2006. The observations take only water depths between 0 - 2000 m into account. The according depth range is chosen for the model calculation (see subsection 2.3.5 and 2.3.4) as well. The measurements cover the period between 1955 and 2006, and show an anti-correlation between heat content and freshwater content over that region (Figure 9). That indicates strong advective processes/pulses from the south carrying salt and heat (negative freshwater) from the Subtropical

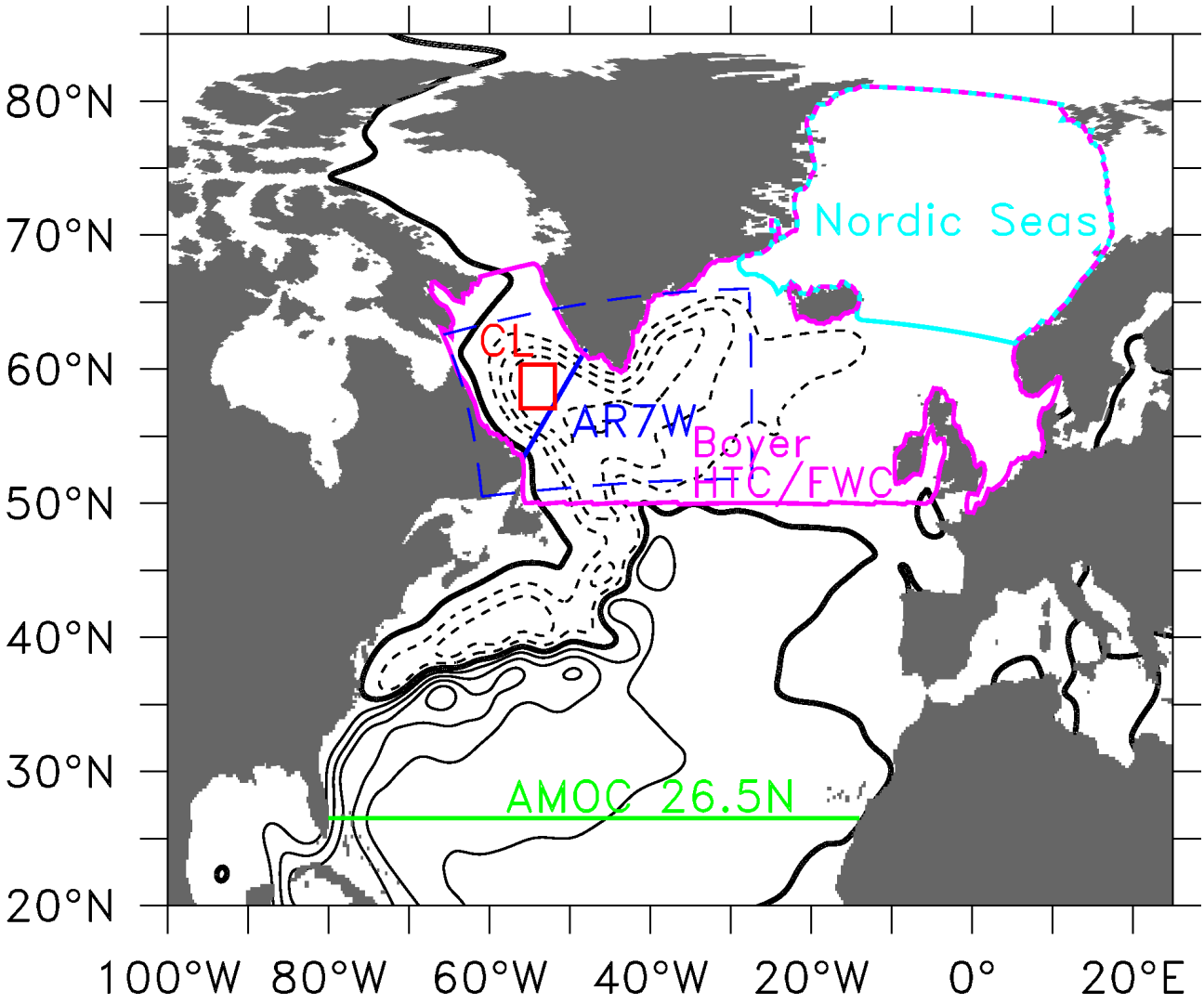

Figure 8.: Illustration of used sections and regions, which are utilised in this thesis. The black contour line indicates the mean barotropic streamfunction over the last decade in VIKING20 (10 Sv contour interval) to illustrated the large scale circulation. The AMOC is evaluated at 26.5° (green line). The enclosed magenta area is used to compute heat and freshwater content anomalies according to Boyer et al. (2007). The light blue enclosed area is taken to calculate area-means for the Nordic Seas and in red box for the Labrador Sea (CL), accordingly. The dark blue line across the Labrador Sea indicates the location of the hydrographic section AR7W and the dashed blue box shows the area which is used to compute Labrador Sea Water production rates.

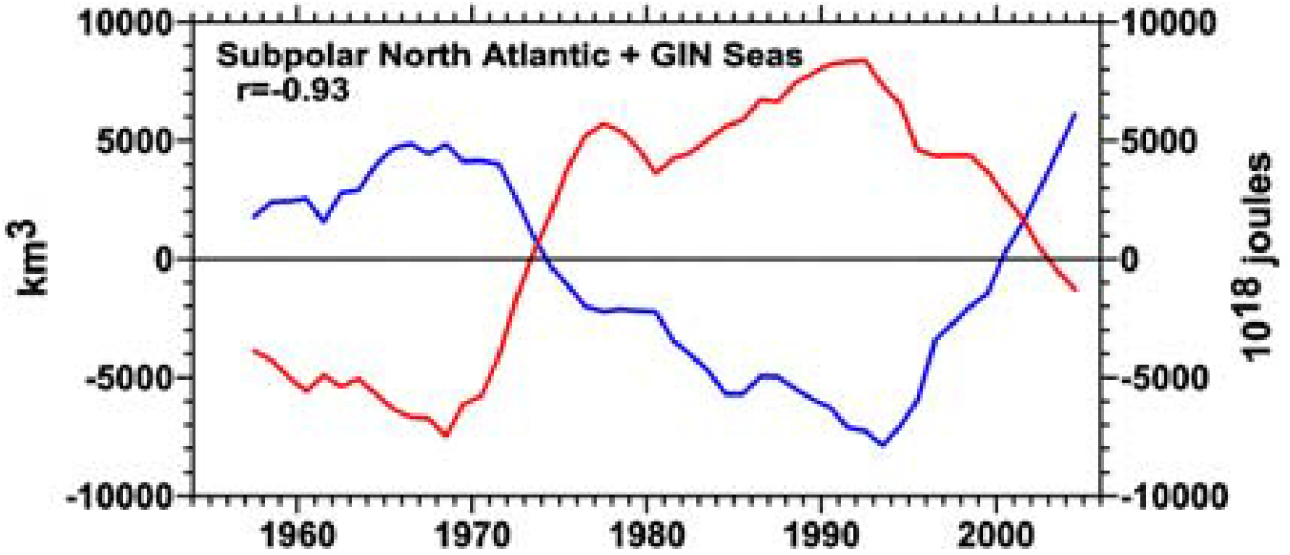

Figure 9.: Observed heat (red) and freshwater (blue) content anomaly over the subpolar North Atlantic for the upper 2000 m. Figure is adopted from Boyer et al. (2007). The region covers the North Atlantic (north of 50°N including the Nordic Seas). The Baffin Bay is excluded for this diagnostic. Figure 8 illustrates the region (magenta line).

Gyre (STG) via the Inter-Gyre-Gyre (connecting SPG and STG, Marshall et al. (2001)) to the SPG and leading to an increased heat content and a decreased freshwater content. All control simulations capture the observed variability, therefore anomalies of the melting simulations can be compared to the magnitude of natural variations. (For results please see section 5.3.3)

The Nordic Seas:

Despite the Labrador Sea, the Nordic Seas is a further a key region for the formation of dense water masses, more precisely the North Atlantic Deep Water (NADW). In the Nordic Seas the densest water masses in the subpolar North Atlantic are formed, with distinct water mass characteristics. These dense water masses exit the Nordic Seas via the Denmark Strait (sill depth ~620m), Island-Faroer and the Faroer-Shetland-Channel (1200m) southward and feed the lower limb of the AMOC. To investigate how this important region is affected by an enhanced Greenland melting and the implications for the formation process of dense water masses the area-mean over the cyan enclosed region is taken (Figure 8), similar to the central Labrador Sea diagnostic. The rather large area is chosen due to the fact that there are certain regions prone for deep water formation, differing between the model configurations.

AMOC 26.5°N:

A most important measurement with respect to the AMOC and benchmark for ocean models is given by the RAPID-MOCHA array at 26.5°N (Cunningham et al. (2010); Kanzow et al. (2010), see also Figure 11). The net transport timeseries across 26.5°N is available since March 2004 and

builds up to now a consistent measure for transport of volume and heat at that latitude. Since the meridional heat transport associated with the AMOC is a main contributor for the moderate climate of Northwestern Europe, large efforts have been undertaken to investigate changes of the AMOC and in the related meridional heat transport (Johns and Baringer (2011); Msadek et al. (2013)). Therefor these measurements are an important indicator for large scale changes with consequences for Europe. For the model validation as well as for investigating the melting related effect on the AMOC that latitude is chosen.

2.3.3. Assessing Labrador Sea Water production

One of the key effects of the additional meltwater input that needs to be assessed is the response of the convection. In the case of a melting of Greenland, the first response should be visible in the Labrador Sea, with implications on the formation of dense water masses. This dense water is referred to as Labrador Sea Water (LSW). Previous studies typically quantified the strength of convection, and indirectly, the LSW production by diagnosing the depth of the mixed layer depth (MLD) in the interior Labrador Sea during the winter season (e.g. Yashayaev and Loder (2009)). The MLD in this study is diagnosed from the ocean density σ_0. The MLD marks the depth where the density contrast to the surface exceeds 0.01 kg/m^3. A more rigorous estimate of the LSW production is provided by calculating the volume of homogenised water during winter conditions. In this case the MLD is horizontally integrated over the Labrador Sea and the annual maximum is diagnosed. In this study the calculation follows previous studies of Rhein et al. (2002) and Kieke et al. (2007). The volume of water where the convection reaches into a density range of 27.74 to 27.86 kg/m^3 is associated as LSW. The annual maximum divided by 1 year, provides the estimate for the annual LSW production.

2.3.4. Heat and freshwater content of the SPG

It is very useful to assess changes of temperature and salinity over a larger region as integral quantity. They allow a direct quantitative comparison with analysis of hydrographic observation (e.g. Boyer et al. (2007); Levitus (1998)). Thus, an assessment of the effects of the additional meltwater in relation to observed trends over the past decades can by made. Here we follow diagnostics of Boyer et al. (2007) for heat content and freshwater content changes in the subpolar North Atlantic. Freshwater content changes reflect the equivalent amount of freshwater which is required to obtain observed salinity changes. For this study a reference salinity of $S_{ref} = 34.8$ psu is assumed. The area for computing the heat and freshwater content reaches from 50°N up to the Fram Strait (Baffin Bay is excluded), but takes only the upper 2000 m into account, where ARGO data is available (consistent to Boyer et al. (2007)).

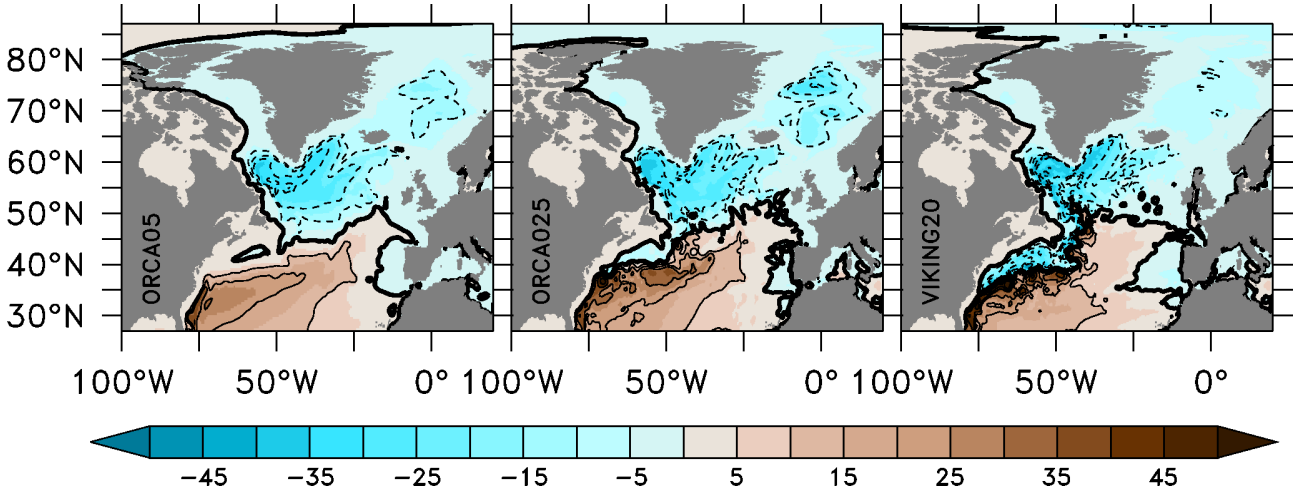

Figure 10.: Mean (1998-2007) barotropic streamfunction for ORCA05, ORCA025 and VIKING20 in Sv in the reference simulation. The contour lines illustrate a 10 Sv interval. Positive values indicate a anti-cyclonic and negative values a cyclonic circulation.

2.3.5. Volume transports of the large-scale circulation

In addition to the behaviour of individual currents systems, e.g. the boundary currents captured in the section 2.3.2, it is useful to assess the basin scale circulation. The two main features analysed here are the strength of the SPG and the AMOC.

For the SPG strength a useful diagnostic is the area-mean value of the barotropic streamfunction in the central Labrador Sea (Figure 8, red box marked with CL, Böning et al. (2006)). The area-mean provides a simple smoothing of the mesoscale noise, which is affecting, e.g. the streamfunction minimum. The value of the transport streamfunction in the Labrador Sea (see Figure 10), provides an indicator for the barotropic transport of the boundary currents, typically concentrated at the continental slopes.

These transports are hard to measure in the real ocean due to the rough geographical conditions. As found by Böning et al. (2006), changes in the SPG strength are tightly linked to changes in the SSH over that region (see also Figure 20 and 42) which allows for a continuous remote sensing by satellites.

A particular attention is paid on melting related changes in the AMOC, which would have important climatic consequences. Changes in the AMOC in response to changes in the deep water formation have been found meridionally coherent over the entire extent of the Atlantic Ocean (e.g. Behrens et al. (2013); Zhang (2010)). (see Figure 11a-b). A useful index that can be compared to observations is the change of the overturning transport at 26.5°N, where measurements in the RAPID program (Cunningham et al. (2010); Kanzow et al. (2010)) have provided a continuous record since March 2004.

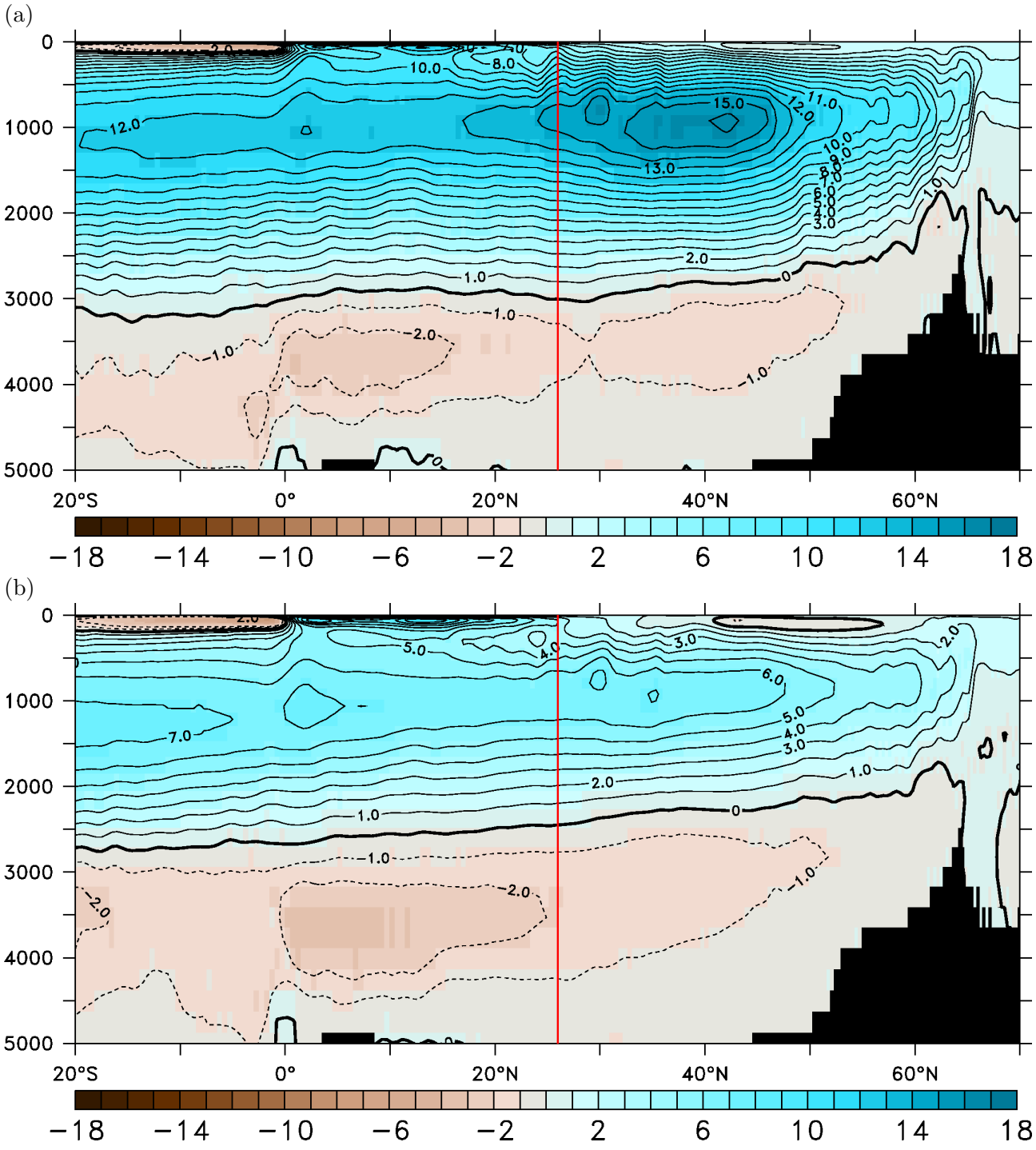

Figure 11.: Mean AMOC structure (1998-2007) from a ORCA05 simulation in Sv for a reference simulation in (a) and hosing simulation in (b). The latitude for diagnosing the AMOC (26.5°N) is highlighted by the red line. Each 1 Sv interval is contoured.

3. Model assessment

The representation of oceanic conditions varies significantly between the individual configurations. These differences reflect the increase in horizontal resolution from ORCA05, with grid sizes of about ∼30 km, to VIKING20, with only ∼3 km in the subpolar North Atlantic. Only the fine mesh of VIKING20 allows to explicitly resolve mesoscale features. Differences between the configurations are not only limited to the ocean surface, but occur also at depth. Of particular interest is the structure of the Deep Western Boundary Current (DWBC), a feature of significant importance for the AMOC. Previous ocean and climate have been characterized by deficits in the vertical structure of the DWBC due to issues in simulating the overflow process correctly.

3.1. Representation of the Denmark Strait Overflow Water (DSOW)

The DWBC is fed by dense water, which is formed in the Labrador and Nordic Seas. In the latter case the dense water has to pass through narrow passages from the Nordic Sea to the North Atlantic. An important passage is the Denmark Strait with sill depths of about 600 m. The dense water spills over the sill and descends along the Greenland coast (Girton and Sanford (2003)). This overflowing water is termed overflow, in this case, more precisely, Denmark Strait Overflow. Most coarse resolution models have shortcomings to resolve this process sufficiently. They normally tend to entrain too much surrounding water, which leads to an enhanced vertical mixing. The consequence of this is a lack of the densest observed water masses south of the ridges. This general problem of overflowing waters along topography is a principal shortcoming of z-level models. In these models large vertical steps between adjacent grid boxes can occur and these induce the large slopes. Improvements for these types of model were made by introducing the concept of partially vertical filled cells (partial steps, Barnier et al. (2006)) for a better representation of the bathymetry. In addition, further parameterisation have been developed to improve the overflows, e.g. streamtube (Danabasoglu et al. (2010)) or Lagrangian blobs (Bates et al. (2012)). Sigma-layer models are minor affect but show deficits in regions of weak vertical stratification, for example in the subtropics.

The large gradients between adjacent grid boxes in z-level models can be also reduced. An increase of the horizontal resolution results in a more realistic model bathymetry, with smaller steps and subsequently smaller gradients. The present set of configurations builds a perfect test case in this respect. The sill of Denmark Strait is the same in all different configurations. Figure 12 shows the mean current speed in the DSOW density range. Typically, water masses denser than 27.8 kg/m^3 are associated in the SPG with overflowing waters which are mainly fed by the DSOW (Jochumsen et al. (2012)). Since the maximum density (σ_0) in the Denmark Strait differs between the configurations, different iso-surface have been used to illustrate the overflowing water. The reason for the differences in density is related to downstream differences in the freshwater transport from the subpolar North Atlantic into the Nordic Sea, which is resolution dependent (Behrens et al. (2013)). First of all the lightest water in the Denmark Strait is found in ORCA025 (27.95 kg/m^3), which is connected to large scale overturning circulation strength (Behrens et al. (2013)). Observations suggest maximum values

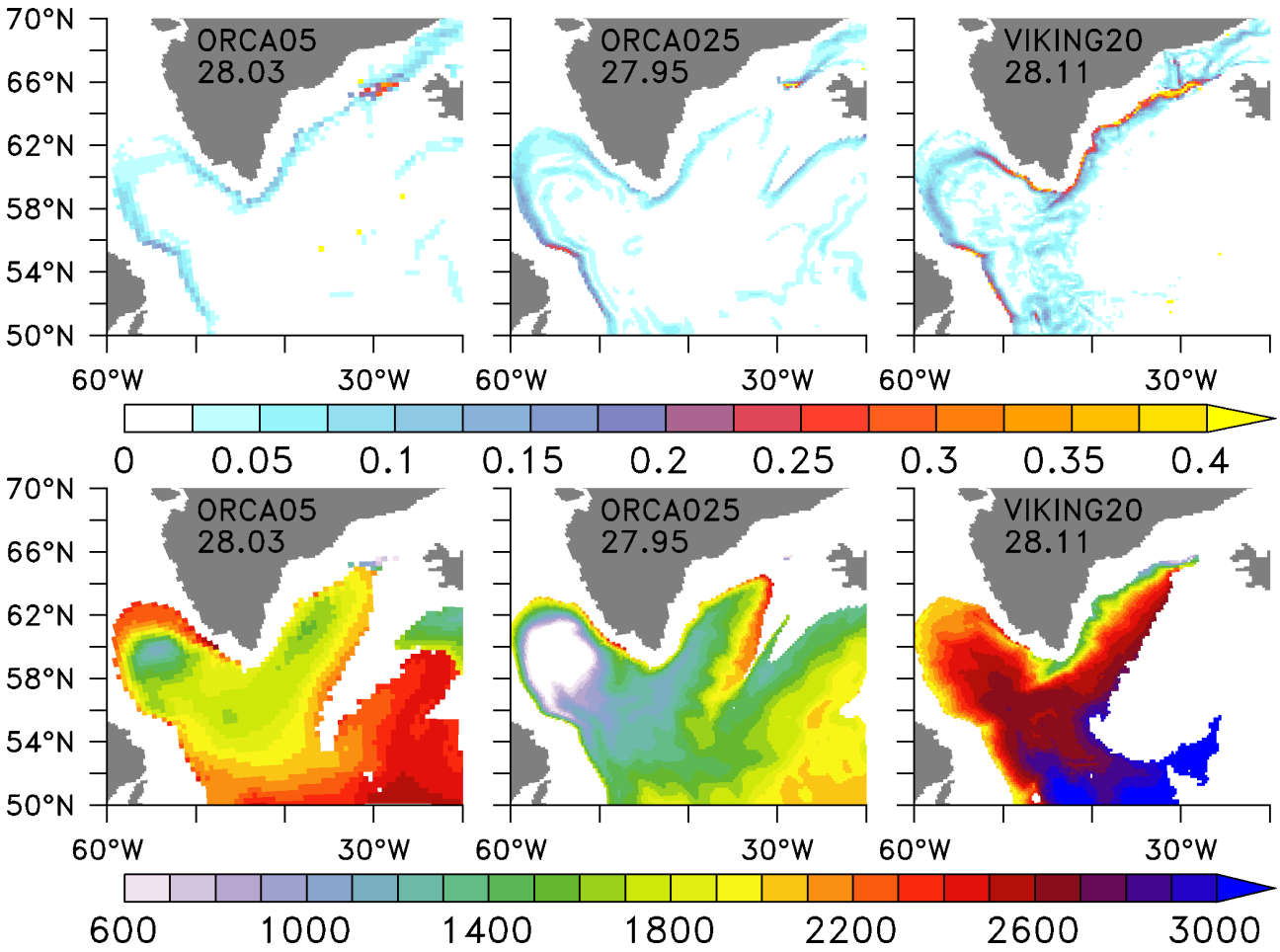

Figure 12.: Mean velocity (1998-2007) field (m/s) on σ_0 surface in the DSOW range, for each individual configurations in the reference simulation (upper panel). Depth (m) of corresponding iso-surface are shown in the lower panel. (Numbers indicate mean values of the densest waters in the Denmark Strait in kg/m^3 (σ_0). For ORCA05 and ORCA025 the iso-surface of 27.8 kg/m^3 and 27.9 kg/m^3 for VIKING20 was taken due to the different mean sigma values.)

of 28.1 kg/m^3 at the sill depth (Macrander et al. (2007); Jochumsen et al. (2012)). South of the sill a continuous flow is present in ORCA05 and VIKING20, flowing along Greenland southward. With increasing resolution current speeds increase and be close to the observed value at 53°N of about 0.3 m/s (Fischer et al. (2010)). It should be noted that below the chosen iso-surface of ORCA05 and ORCA025, no continuous boundary current is present due to model shortcomings (e.g. enhanced entrainment of surrounding water). In VIKING20 the strongest currents are found south of the sills, indicating a strong current of overflowing water. Downstream, the mean flow is also affected by strong cyclonic eddies (not shown), which is in agreement with recent observations (Brearley et al. (2012); Falina et al. (2012)). Along the entire flow path to the south the iso-surface descend, which is clearly seen in VIKING20 (lower panels). All configurations show depths of the iso-surface around 600 m at Denmark Strait. At the southern tip of Greenland the depth of the iso-surface exceeds 1400 m. Noticeable, is the lack of a continuous flow in ORCA025 south of the Denmark Strait, which indicates the shortcoming in the representation of the overflow. ORCA05 performs better than ORCA025 at that point. The reason is unclear, ORCA05 should show a large entrainment due to the additional eddy parameterisation. A remarkable feature is found in ORCA05 and ORCA025, which show a bulging of the iso-surface in the Labrador Sea. VIKING20 shows the opposite, which is in line with observations (Hall et al. (2013)). In the region of the Grand Banks, influences of the NAC are present, which are indicated by a depression of the isopycnal. Overall, VIKING20 exhibits a proper DSOW in the observed density range and shows the best agreement to the observed characteristics, like currents speeds and structure at key section in the subpolar North Atlantic. Both coarser configurations show distinct shortcomings compared to the observed characteristics and can not maintain a DSOW in the correct depths range.

3.2. The impact West Greenland Current eddies on the Labrador Sea convection

Deep water formation in the Labrador Sea

The Labrador Sea is known to be a crucial component of the subpolar North Atlantic and AMOC (Talley and McCartney (1982)). There are only a few locations where open ocean deep water formation occur. This formation process is strongly related to the NAO and governed by local surface heat fluxes (Hurrell et al. (2003)) . During positive NAO phases heat fluxes to the atmosphere are enhanced and cause higher dense water formation rates. Small mesoscale eddies play an important role for that formation process. The eddies are important for the freshwater transport from the WGC into the interior Labrador Sea (Lilly et al. (2003); Chanut et al. (2008)), as well as for the preconditioning and re-stratifying process of convection (Gelderloos et al. (2012)). They also affect the export of newly formed Labrador Sea Water (LSW) via exchanges with the DWBC (Brandt et al. (2007)). The representation of these processes is quite different between the used configurations (see section 3.6).

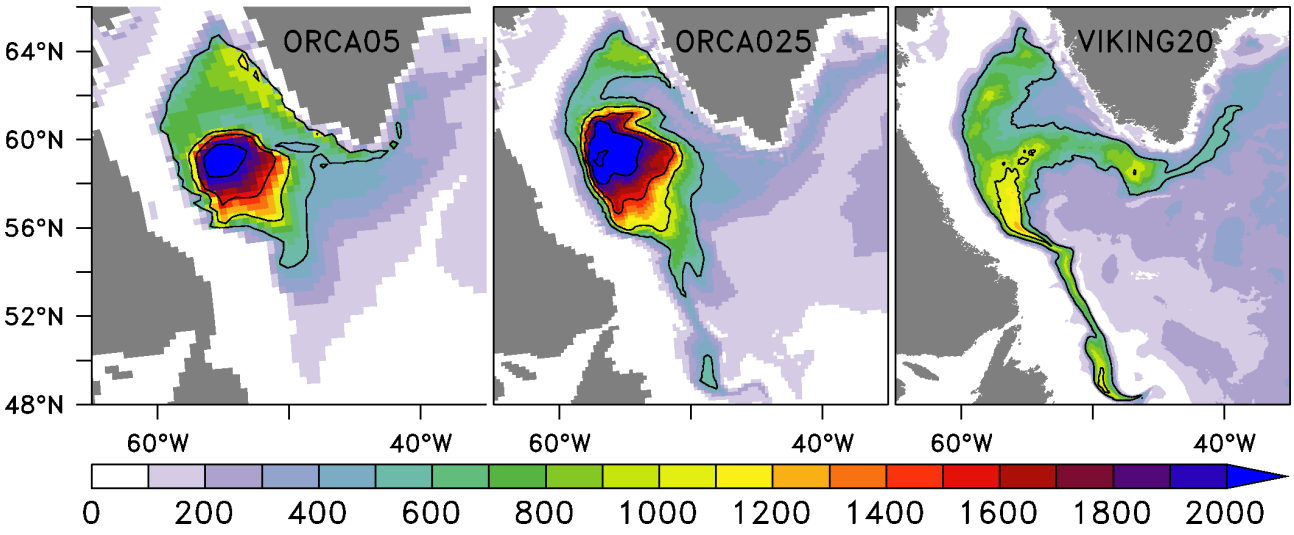

Figure 13.: Mean (1998-2007) March mixed layer (m) for the different configurations in the reference simulation. The contour interval is 500 m.

Only VIKING20 due to its the horizontal resolution and grid sizes of $\sim$ 3 km in this region has the ability to resolve these mesoscale processes explicitly. Both coarser configurations do not resolve this mesoscale processes sufficiently. As already described, ORCA05 uses an eddy parameterisation which is not the case for ORCA025. ORCA025 resolves some mesoscale processes at lower latitudes explicitly, which leads there to improvements compared to ORCA05. An additional eddy parameterisation in ORCA025 would counteract those achievements. An important class of mesoscale eddies in the Labrador Sea is the so-called WGC eddies (anti-cyclonic). They arr shed from the Cape Desolation into the interior Labrador Sea (Brandt et al. (2004); Eden and Böning (2002); Chanut et al. (2008)). The representation of these eddies is important for the shape for the convective region (a convection inhibiting effect) and depth of convection in the interior Labrador Sea as indicated in the following.

The mean March mixed layer depth in the Labrador Sea

The representation of the open ocean deep convection is an important, but difficult to reach, benchmark for ocean models, especially in coarse coupled models (Griffies et al. (2009); Swingedouw et al. (2012)). Figure 13 shows the March mixed layer depths (averaged 1998-2007) for all configurations. ORCA05 shows mixed layer depth in the observed maximum range of about 1700m during high positive NAO phases (Yashayaev and Loder (2009)), when the deep water formation is very intense. The convection pattern is very regular and centered in the interior Labrador Sea, which is in general agreement with the (sparse) observational evidence (Pickart et al. (2002)). In the medium resolution configuration (ORCA025) the depth of convection is too deep compared to observations and exceeds 2000 m. That fact is related to the missing effect of the WGC eddies (increasing the stratification), or their parameterisation. The very weak vertical stratification of the central Labrador Sea in both coarse configurations (see also Figure 18, especially in the deep ocean) points to additional deficits,

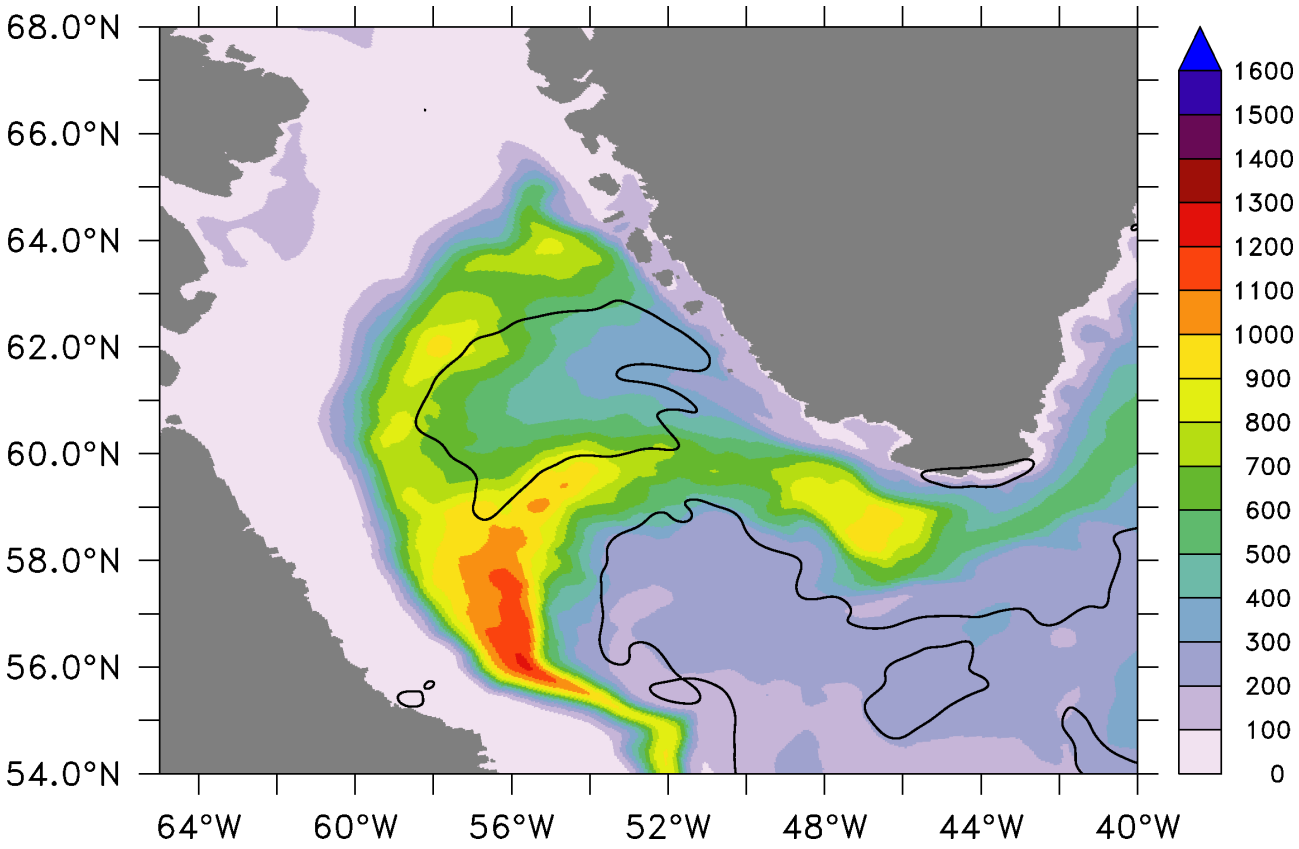

Figure 14.: The VIKING20 mean (1998-2007) March mixed layer depth in m and the 40 cm^2/s^2 mean EKE contour.

which are related to deficits in the DSOW (Figure 12). Thus, the overflowing water entrain too much surrounding waters and loses its unique water mass characteristics. The eddy resolving configuration (VIKING20) shows a more detailed pattern of convection than suggested by the other two configurations. The convection depth is reasonable, taking into account that convection does not reach depths of 1700 m each year in the real ocean during the period of 1998-2007 (Yashayaev (2007)). The shape of the convection in VIKING20 is strongly influenced by the presence of eddies and shows a large temporal variability (see Figure 14). This variability is not present in coarser configurations. Additional to the convection in the interior Labrador Sea,.a further convection region is seen at the southern tip of Greenland. The general convection pattern follows the described mid-depth recirculation pattern described by (Lavender et al. (2000)). These recirculation cells are characterised by low stratification, conducive for deep mixing. For the discussion of the GrIS melting response, it is necessary to take these differences in the convection in the Labrador Sea into account. It appears obvious that an important factor for the oceanic melting response is the general representation of convection and how much and how fast meltwater is carried from Greenland into this convective region.

The above mentioned relation between convection depth and presence of WGC eddies is illustrated in Figure 14 for VIKING20. A surface (3m) EKE contour line (40 cm^2/s^2) is superimposed on the mean (1998-2007) March mixed layer depth in VIKING20. The enclosed region in the interior Labrador Sea

matches with the area where lower mixed layer depth are present compared to the surrounding. That region is affected by anticyclonic WGC eddies, which increase the vertical stratification and inhibit winter convection. Influences of the NAC are present at the southern entrance of the Labrador Sea, mainly affected by anticyclonic eddies as well. In regions of low EKE the deepest mixed layer depths are found. That explains the two regions reaching from Greenland to Labrador which are characterised by a moderate convection activity. Both coarser configurations do not show any mesoscale activity in the Labrador Sea (not shown). Therefore a controlling factor for the convection is missing, which points again to the need to resolve eddies explicitly for a realistic reproduction of the deep convection pattern in the Labrador Sea.

3.3. The Deep Western Boundary Current at 53°N

Long-term continuous observations are sparse in the SPG due to the exceptional rough climatic conditions. The mooring array at 53°N, maintained by GEOMAR, constitutes for that reason a very valuable dataset of the strength of the boundary current in the SPG. The array is continuously occupied by moorings since 1997 and also part of annually repeated hydrographic sections (Fischer et al. (2010)). Unfortunately, the amount of moorings differ during the period, which makes a long-term transport calculation over the entire boundary current impossible. Based on all available data, an important insight in the boundary current structure and variability could be achieved (shown in Figure 15a). The observations show a strong barotropic southward flow at the continental slope. The strong Labrador current ($>$ 500m) is located at the shelf break and shows currents speed around 0.3 m/s to south. Below that current the flow speeds decrease slightly until the density range of DSOW water ($\sigma_0 > 27.88$ kg/m^3). At this depth a further strong southward core is present. Further offshore, hints of steady recirculations cells (Lavender-cells, Lavender et al. (2000)) are seen.

Most z-level models have difficulties to represent the overflow waters sufficiently, especially coarse models (see section 3.1). That fact causes strong biases in the current structure further downstream, and typically result in an absence of this deep DSOW core (not shown). VIKING20 behaves differently compared to most previous configurations (e.g. ORCA05 and ORCA025), and shows the best agreement to the observed current structure (Figure 15b). Both cores of high velocities are realistically captured, leading to fairly comparable transports over density classes across the section compared to observations (not shown). Both coarser configurations do not capture the deep intensification and therefore lack the comparison with observations (see also Figure 18d). Despite these shortcomings in the deep current structure of coarse models, all configurations capture the observed deep warming signal since the mid-1995 (Figure 16). Observations (colour) suggest a warming of about 0.5° K over the observed period. The coarse ORCA05 suggests the largest amplitude of decadal variability compared to the other configurations. Both higher resolution configurations seem to match the observational trend best. VIKING20 shows the smallest long-term trend overall, which seem to be related to lowest

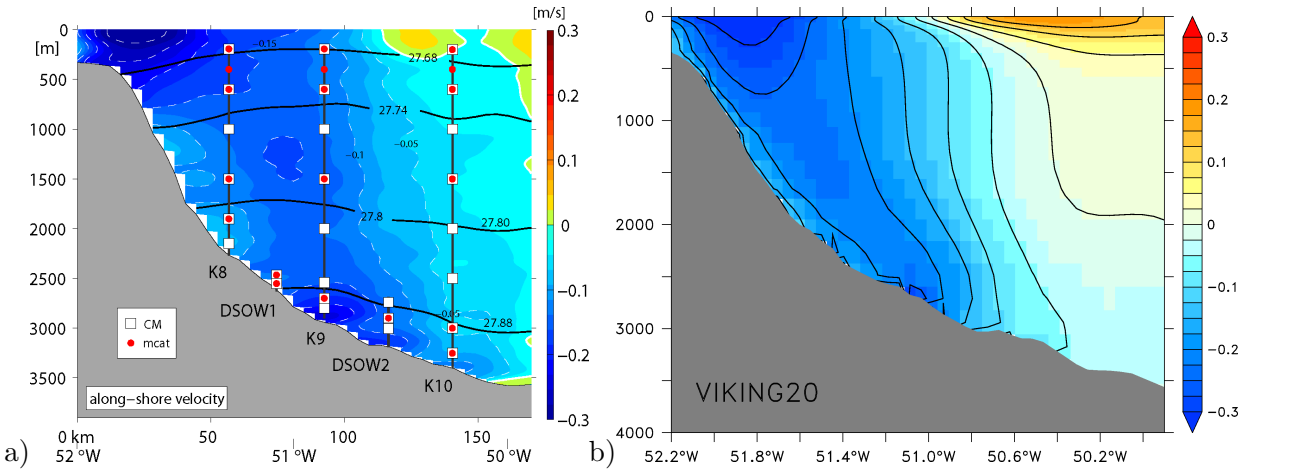

Figure 15.: Mean (1998-2007) cross-section velocity in m/s at 53°N, from (a) observation and (b) VIKING20. White contour lines in (a) and black in (b) indicate a 0.1 m/s interval. In (a) the positions of moorings are illustrated.

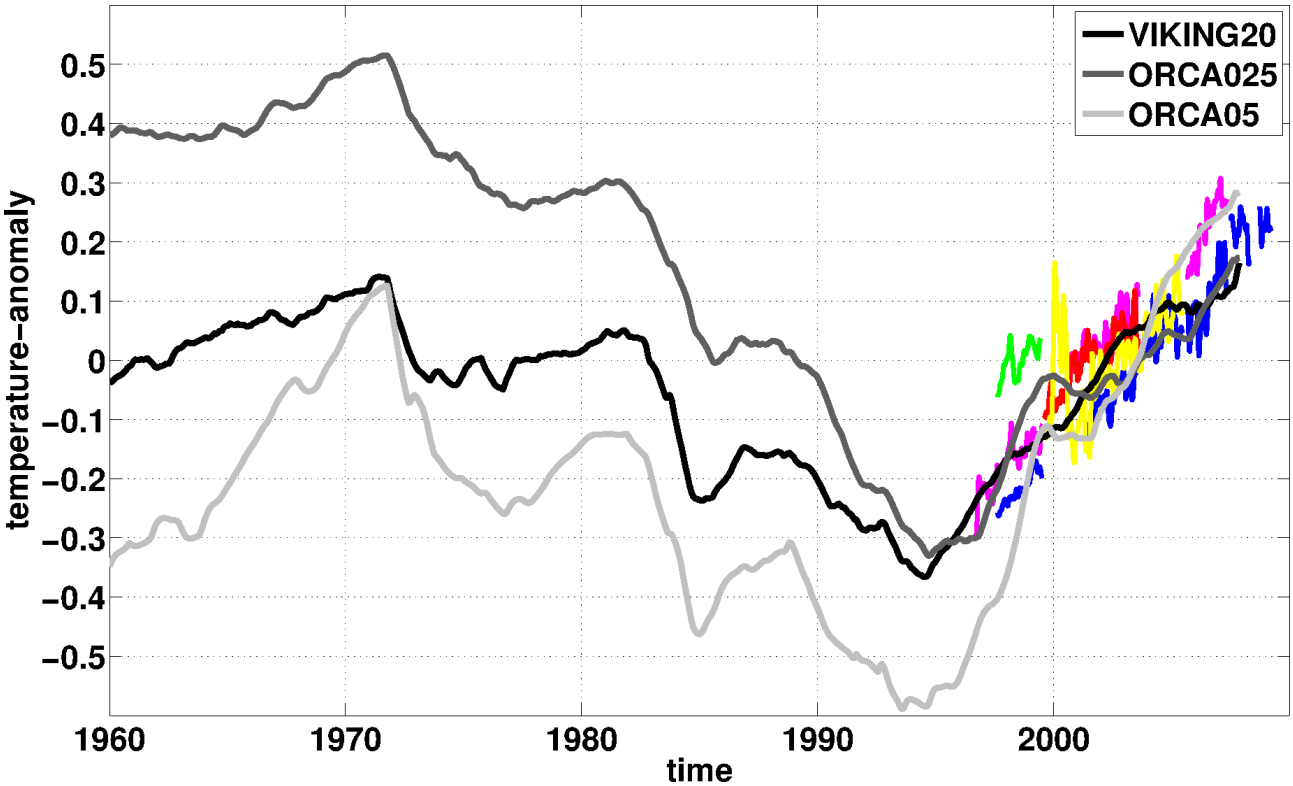

Figure 16.: The DWBC temperature anomaly (at 53°N) in °K at 1500 m for observation (colour) and model configuration. All temperature have been referenced to the mean from 1998 to 2007.

drift in the deep ocean compared to the other configurations. All simulations confirm that the observed warming is part of a decadal oscillation and still within the range of natural variability.

3.4. Mean hydrographic quantities along the AR7W section across the Labrador Sea

The hydrographic section (AR7W), shown in Figure 8, is occupied annually by various nations. This section provides a good view on the properties in the SPG and is used to investigate winterly deep mixing events. Beside changes in the interior, mostly related to convection, a strong focus is also set on the boundaries currents. The currents play an important role for the signal propagation within the SPG. The section off the Labrador coast is closely located to the 53°N mooring array, which is described above.

Observations along this section (Figure 17a) show a cap of freshwater (< 34.8 psu) at the ocean surface, at the coast reaching until the shelf break. The salinity increases with depth as well as in the deeper boundary current (Yashayaev (2007), Yashayaev and Loder (2009), Hall et al. (2013)) to around 34.9 psu. The DSOW layer is characterised by slightly lower salinities than the overlying waters. The fresh surface waters are thought to be fed by portions originating from Greenland meltwater and the Arctic Ocean (Belkin (2004)). The increased salinity in the Greenland boundary current at ∼500m depth is associated with the Irminger Current, transporting relatively warmer and saltier water from the NAC into the SPG. The deepest salinity maximum (2200 m - 3200 m) originates from North East Atlantic and enters the SPG through the Charlie-Gibs-Fracture-Zone (Yashayaev (2007)) and is referred to as NEADW (North East Atlantic Deep Water). This water mass is formed in the Nordic Sea with a large portion of direct Atlantic inflow water (high salinity) and returns through the Faroe Bank Channel into the subpolar North Atlantic (Hansen and Osterhus (2007)). The temperature distribution (Figure 17b) indicates these cold coastal boundary currents and a warm contribution of the Irminger Current. This water is characterised by temperature between 3.5°C and 5°C, which are located at both shelf breaks. The warm Irminger water is carried by the WGC-eddies into the interior and produces the far reaching warm signal, which originates from the Greenland coast. Temperatures below the Irminger water decrease to values around 1 °C at depth. In the interior Labrador Sea above 1600m a very well homogenised mass is present. This water is associated with ventilated water during winterly mixing events and forms the Labrador Sea Water. The density structure indicates a bowl shape structure below a sigma value of 27.77 kg/m^3 (σ_0). The elevated isopycnals on either side if the basin indicate strong cyclonic circulations.

All configurations (Figure 18a) show the fresh surface coastal currents (WGC and Labrador Current). ORCA05 does not well resolve the WGC, as indicated by highest salinity compared to the other two configurations. Along the Greenland shelf a salinity increase between 150-500 m is seen, associated with the Irminger Current. That increase is also present along the Canadian coast in ORCA05 and

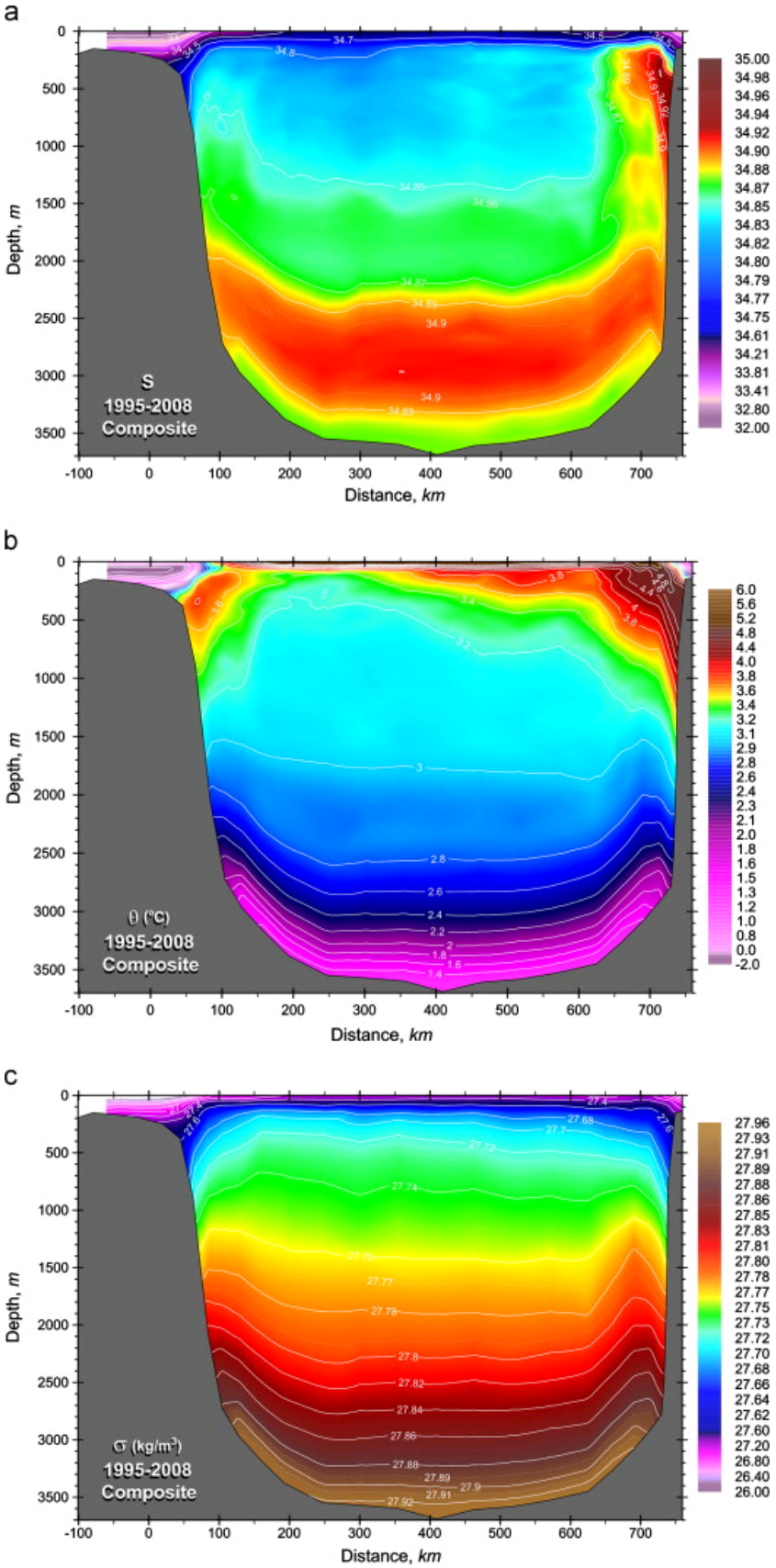

Figure 17.: Observed hydrographic properties along the AR7W section (1995-2008 composite), (a) salinity in psu, (b) temperature in ˚C and (c) density (σ_0) in kg/m^3, adopted from Hall et al. (2013)

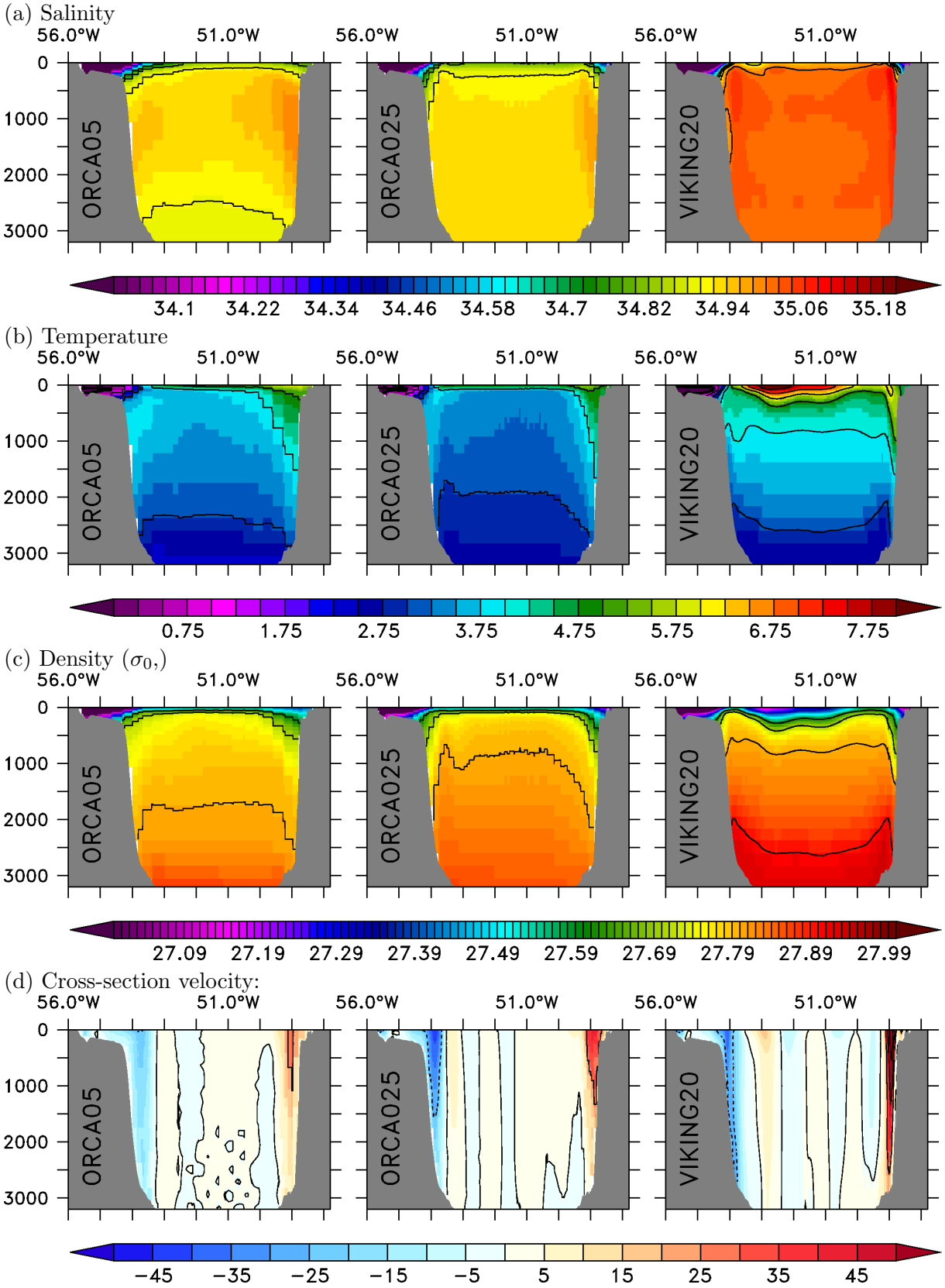

Figure 18.: Mean (1998-2007) hydrographic quantities along the AR7W section for the different configurations in the reference simulation: (a) salinity (psu), (b) temperature (°C), (c) Density (σ_0, kg/m^3) and (d) velocities (cm/s). Temperature contour lines mark each 1 °C interval, salinity contour lines mark salinities between 27.6 and 27.9 psu with a 0.1 contour interval, sigma contour lines mark values of 27 to 28 kg/m^3 with a 0.1 interval, velocity contour lines mark each 25 cm/s interval. Positive velocity values indicate a transport into the Labrador Sea.

VIKING20. In ORCA05 a local salinity minimum is visible at depths below 2000 m. That is in agreement with observations, suggesting lower salinities associated with the DSOW. VIKING20 shows some hints of NEADW by an increasing salinity at around 2500m. ORCA025 does not exhibit any vertical salinity structure in the interior. The general higher salinities in VIKING20 compared to the other two configurations are related to the improvements in the NAC and Irminger Current. The better representation of the NAC goes along with increased transports of saltier and warmer Irminger Water towards the SPG which is confirmed by observations (Yashayaev and Loder (2009)), while further increasing the positive salt bias in the Labrador Sea. However the deep salt maximum associated with NEADW (salinities ∼34.91) between 2500 m and 3000 m is underrepresented and points to shortcomings in the flow through Charlie-Gibs-Fracture-Zone associated with the Faroer Bank Channel outflow. A distinct salinity signal with NEADW would result in a better differentiation between NEADW and DSOW.

The temperature distribution (Figure 18b) along AR7W shows the coldest water on the west shelf (temperatures $< 1°C$). These cold waters represent the Labrador Current, carrying cold and fresh water to the south. In the central Labrador Sea the temperature decreases from top to bottom, which is in agreement with the summer biased observations. All simulations show the warm inflow of Irminger Water at the Greenland coast ($\sim$ 49°W) and the return flow along the Canadian shelf break. That is indicated by increased temperatures compared to the interior. The warmest water across the section is seen in VIKING20 in the central Labrador Sea. That surface intensified signal is missing in both coarser configurations. That warm surface signal can only be caused by direct contributions originating from the NAC via the North-West Corner (NW Corner). An associated signal with increased salinity is apparently missing. The contribution of water from the NW Corner is somehow questionable. There is no observational evidence confirming these results so far. However, RAFOS floats showed evidence of recirculations from the south Labrador Sea into the interior (Fischer and Schott (2002); Lavender et al. (2000)).

The temperature and salinity distribution is reflected in the density structure; its vertical structure is shown in the 3rd panel of Figure 18c. Contour lines show 27.6, 27.7, 27.8 and 27.9 kg/m^3 σ_0 levels. ORCA05 and ORCA025 show a similar distribution with a bulging of all isopycnals in the central Labrador Sea. VIKING20 on the other hand reveals a depression in the central Labrador Sea, which is in line with observations (Yashayaev and Loder (2009)). The largest densities are found at depths between 2500m and 3000m elevated at both coasts, indicating the Denmark Strait Overflow Water. That water mass is missing in both coarser configurations due to enlarged entrainment of surrounding water downstream of the Denmark Strait (see section 3.1 and Figure 15). It is also remarkable that the densest isopycnal in VIKING20 (27.9 kg/m^3) is not present in both coarser configurations.

The resulting cyclonic current structure is shown in Figure 18d. Prominent features are the inflow into the Labrador Sea (positive) at the Greenland coast and the outflow (negative) at the Canadian coast, exceeding 0.5 m/s in the higher resolution models. The flow shows a barotropic structure

(invariant with depth), while near the shelf edge baroclinic transports gain in importance. Close to the boundary currents, recirculation patterns are present indicating the proposed very stable Lavender cells (Lavender et al. (2000)). VIKING20 shows the best agreement to observations. This is also seen in the mooring array maintained by the GEOMAR at 53°N (see section 15). The observed transports in density classes are well captured by the modelled results in VIKING20, which is not the case for the other configurations.

3.5. The mean SSH pattern in the North Atlantic and the SSH-SPG index

The large scale horizontal flow field can be illustrated by using Sea Surface Height (SSH) from satellites (Landerer et al. (2007)). The SSH is, in this sense, a measure for the large scale horizontal pressure gradient, which is in geostrophic balance. Since 1992, global coverage by satellites available and gridded products are provided by AVISO (http://www.aviso.oceanobs.com). Figure 19 shows the mean SSH field for the observations and for the different configurations. The observations show two distinct gyres in the North Atlantic. The STG (anti-cyclonic) is indicated by positive values and the SPG (cyclonic) by negative values. The SPG is characterised by a depression of the SSH compared to the global average. The transition between both gyres in the north is accomplished by the NAC, transporting large amount of heat and salt to the north. The maximum of the SSH in observations is located close to Cape Hatteras; the place where the Gulf Stream detaches from the American coast. A minimum is located in the interior Labrador Sea and a further minimum in the northern Nordic Sea. Sea-ice cover and satellite tracks close to coastal regions are difficult and can cause large errors in observations. These products provide a valuable measure and benchmark for ocean models. All models show both gyres, while large difference in the transition zone are present. These differences are related to the flow path of the NAC. The path of the NAC differ largely between configurations. In both coarser configurations the path is too zonal across the North Atlantic. The consequences is a missing of the so-called NW Corner, east of Newfoundland, which leads to the a cold and fresh bias in this region (Weese and Bryan (2006)). VIKING20 shows the best agreement to the observed path compared to the other configurations. There are indications that the NW Corner is overestimated in VIKING20 compared to observations, which can be seen in a too further north extension into the Labrador Sea. It should be also noted that the satellite products are gridded on a coarse 1/3° x 1/3° grid which involves a potential smoothing effect.

Although the coarser configurations have problems in the path of the NAC, in other regions they produce reasonable results. An interesting application, is the SSH variability in the SPG. This diagnostic follows the study of , and links variations in the SSH with transport changes in the boundary currents, which reflects the SPG strength. (see Figure 42 for the link between SSH and SPG strength). This diagnostic elucidates the dynamic meaning of SSH changes. Figure 20 shows the model results and

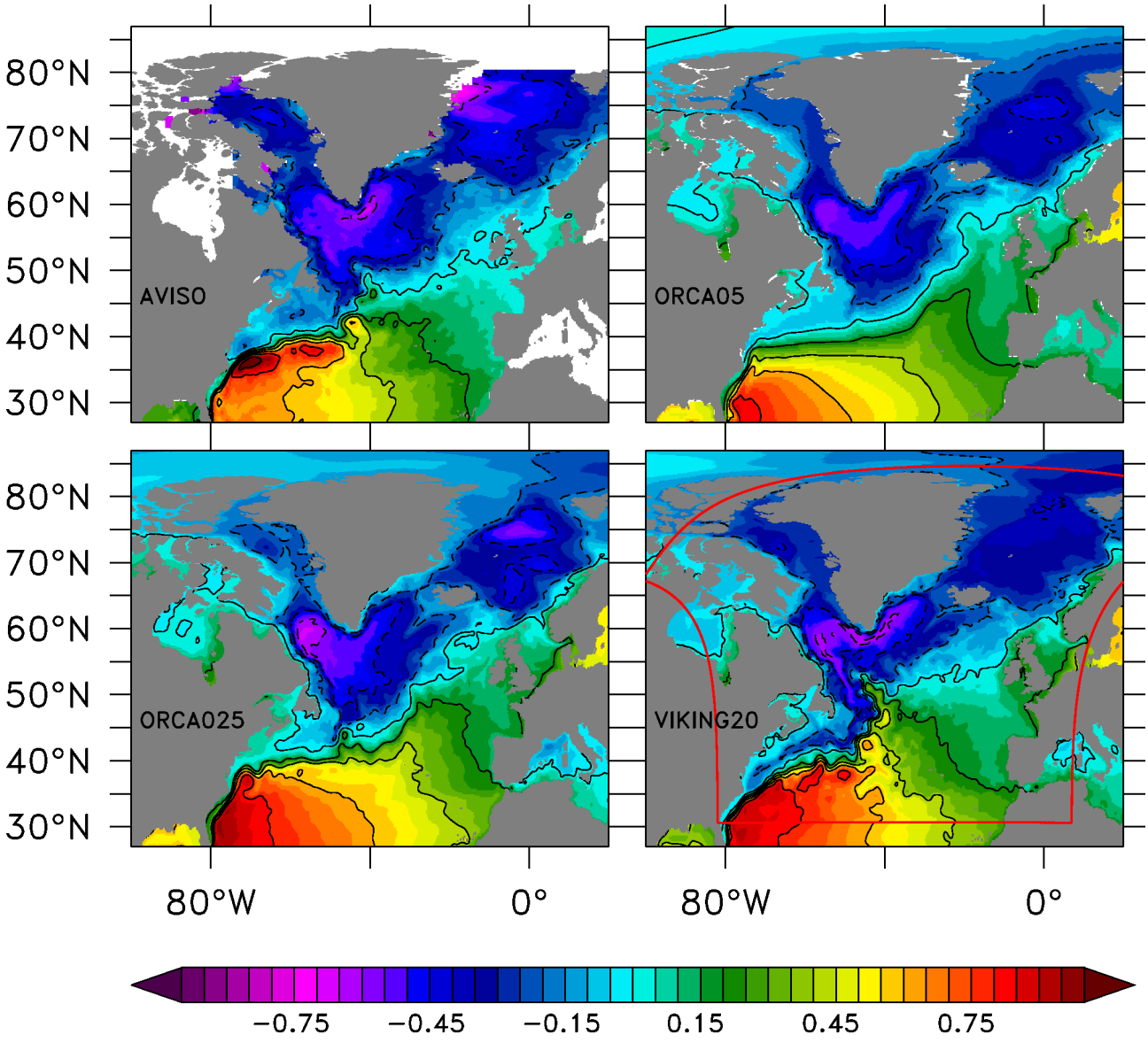

Figure 19.: Mean (1998-2007) SSH in m for observations (AVISO) and individual model configurations. Black contour lines indicate a 0.2 m interval. The area-mean of 0.56 m from the observation was taken as offset value for the model results. The red frame in VIKING20 indicate the region of the high resolution nest.

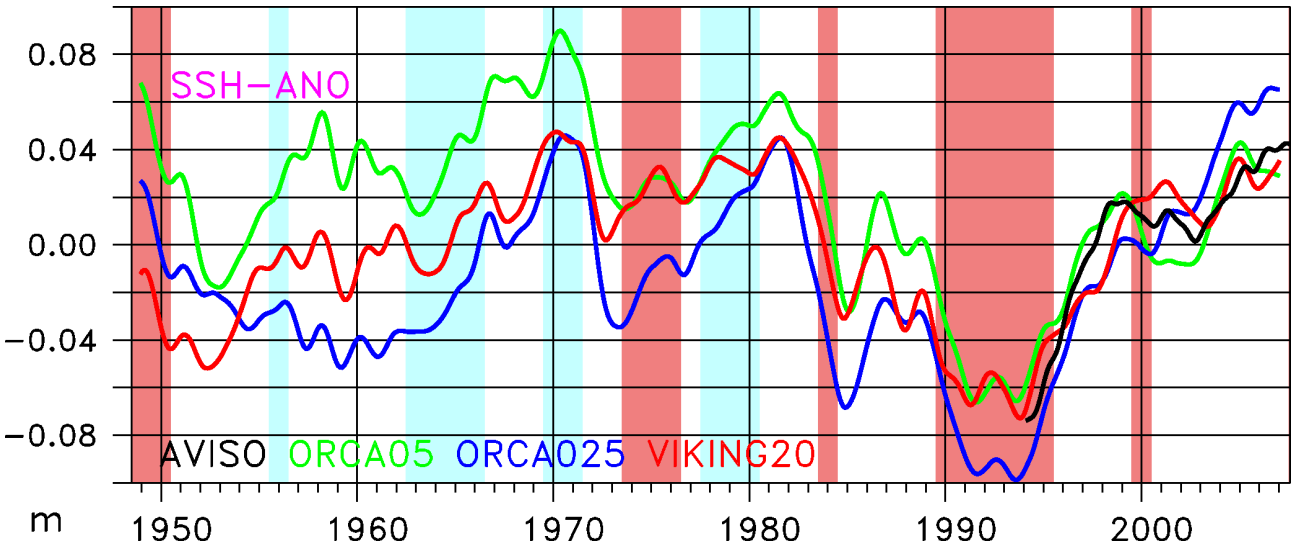

Figure 20.: SSH-anomaly in m over the central Labrador Sea (region marked with CL in Figure 8) for observations(black) and reference simulation of each model configurations, referenced to the individual mean from 1993-2007. The timeseries are interannual filtered. Red shading indicated positive NAO and blue negative NAO phases.

the timeseries from AVISO (black). Irrespectively of resolution, all models show the observed ssh rise since the early 1990. That SSH rise reflects a weakening of SPG-strength due to changes in the atmospheric conditions, which are indicated by the blue and red shading. The model results before the 1990 show a small spread between the configurations, while the variability is robust.

3.6. Representation of mesoscale eddies in the North Atlantic

Comparing the mesoscale variability between model and observations is achieved by diagnosing the SSH variance (figure 21) averaged over 1998-2007. SSH variance also allows comparisons of model results with satellite altimeter products provided by AVISO. The SSH variance distribution shows strong qualitative similarities to the eddy kinetic energy (EKE) for the near surface. Observations show large values along the flow path of the Gulf Stream, off Cape Hatteras, where the Gulf Stream separates from the American coast. After the detachment from the coast, the current begins to meander and form large rings with diameters up several hundred kilometer (Lee and Cornillon (1996)). Further offshore, the current separates into a southern branch heading toward the Azores Islands and a second branch following the topography towards Newfoundland. The north-west region of high values is referred to as the North-West Corner. Thereafter, the Gulf Stream crosses the subpolar North Atlantic eastward heading towards the Nordic Seas. In the Nordic Seas a hotspot of large SSH variance is seen in the observations, which is associated with Lofoten eddies being shed from the Norwegian coastal current (Rossby et al. (2009)).

A critical point with respect to the performed Greenland melting simulations is the region of the Labrador Sea. Observations suggest a tongue of large SSH variance originating from the west Green-

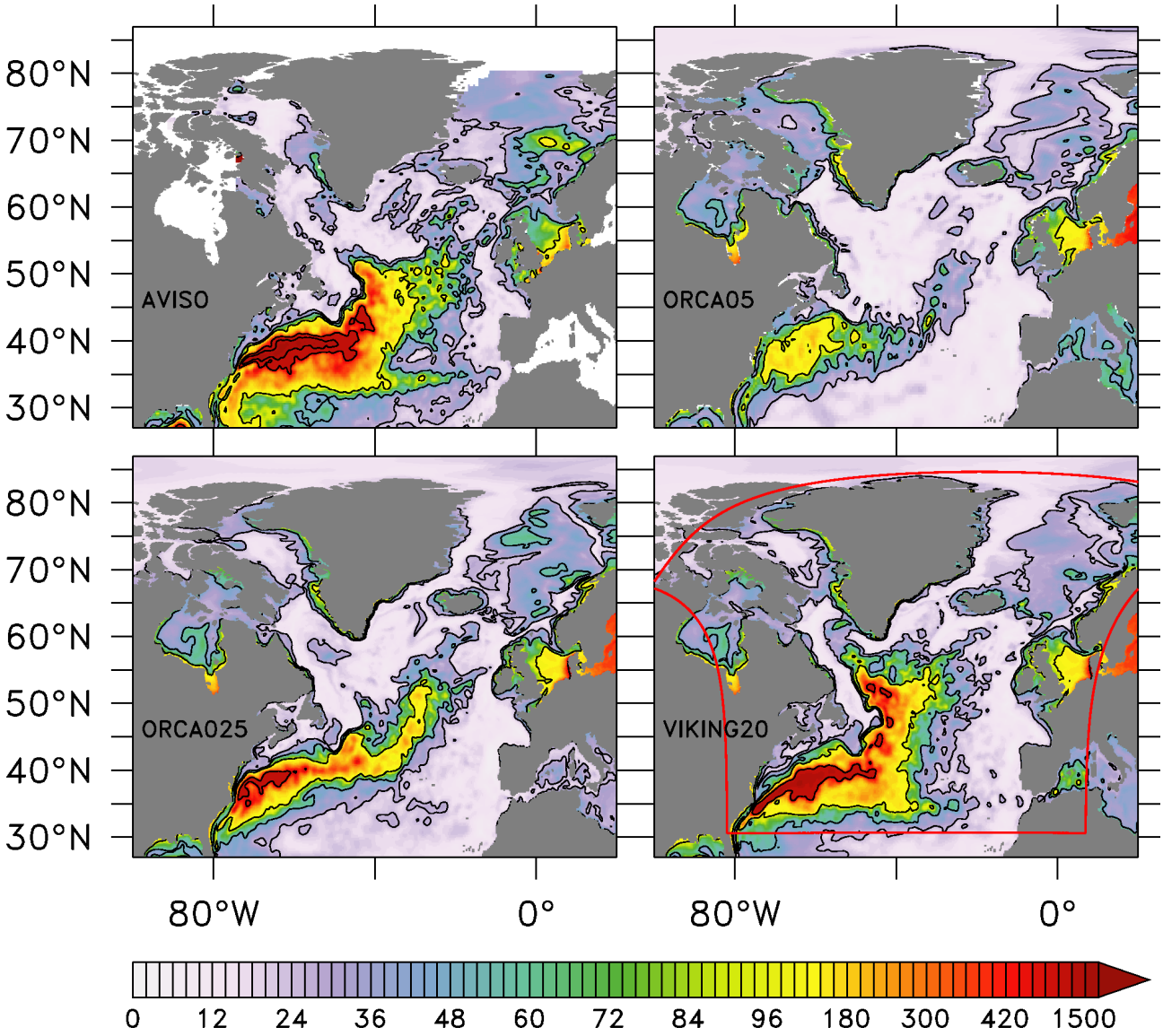

Figure 21.: Mean SSH variance (1998-2007) in cm^2 (contour lines indicate 25, 50,100 and 500 cm^2 levels) for the reference simulation of each model configuration in comparison to observations (AVISO). The SSH variance is used to illustrate the flow path of the NAC and its associated variability. ORCA05 and ORCA025 show distinct deficits in the NAC compared to the observations. The red box in the VIKING20 highlights the high resolution domain.

land coast into the Labrador Sea (Brandt et al. (2004)). The associated West Greenland Current Eddies (WGC eddies) are important for the cross-shelf transport of fresh coastal water into the interior Labrador Sea, and are being investigated intensively (Brandt et al. (2004); Gelderloos et al. (2011); Chanut et al. (2008)). Large values in the North Sea and Baltic are related to strong coastal wave processes. The model results of the coarser models show distinct deficit to that observed SSH variance pattern. An overall lag of variability is visible in ORCA05, with reduced levels in the Gulf Stream and subpolar North Atlantic region. It also exhibits the southward shift of the flow path of the NAC compared to observations. The Gulf Stream itself shows an overshooting at Cape Hatteras and after that, an overemphasised zonal branch clearly missing the NW Corner branch. Some improvements are seen by increasing the horizontal resolution from ORCA05 to ORCA025. The magnitude of variability in the Gulf Stream is better represented, while only little effect is seen on the general flow path. The NW Corner and the Azores branch are still missing. All these features are only visible in VIKING20, which shows the best agreement to the observations. Some deviations from observations are still seen in the path of Gulf Stream after the separation from the coast. That effect could be related to the southern boundary of the high resolution nest, which has an impact on the Gulf Stream and the representation of the Antilles Current. The connection of the WGC eddies to the NW Corner is questionable in VIKING20 and needs to be investigated further. The high variability of the Lofoten eddies is not well captured and possibly indicates a lack in the formation process of that kind of eddies. A too smoothed model bathymetry in the formation region can hinder the formation process.

4. Limitations of OGCMs with respect to Greenland melting simulations

In the following chapter, two important issues of OGCM´s, which limit the use of uncoupled models, will be discussed. The first point addresses the commonly used SSS-restoring in forced OGCM´s to reduce long-term drifts in water masses. This issue has been intensively investigated in Behrens et al. (2013) and the results are summarised in section 4.1. The second issue deals with the fact of a missing active atmosphere in OGCM´s. The surface ocean atmosphere heat fluxes take only a small portion of changes in ocean into account, but ignore all changes due to ocean-atmosphere feedbacks, which are important for the long-term oceanic response. An international model intercomparison that included results of the present experiments(Swingedouw et al. (2012)) found that this inactive atmosphere is of minor importance for the GrIS melting response over the first 4 decades. A summary of this study is provided in section 4.2, which also provides a comparison of GrIS melting results to previous studies.

4.1. SSS-restoring and its impact on the long-term AMOC behaviour

Forced ocean simulations over several decades typically suffer from drifting water masses (Behrens et al. (2013)) with implications on the large scale circulation. Model deficits and uncertainties in the applied atmospheric forcing fields, especially in the freshwater forcing, are a major contributing factor leading to an imbalance in the budget and inducing a drift. In addition, the lack of an active atmosphere exerting stabilizing feedbacks may increase the ongoing trend. Despite these general shortcomings, ocean-only simulations have been proved over the last decades to be an indispensable tool for the ocean research and suitable for specific research questions with focus of oceanic effects and involved mechanisms. Attempts of avoiding bulk formula (Paiva and Chassignet (2001)) for surface fluxes to reduce the model drift have not been successful either for heat fluxes (Barnier et al. (1995)) nor freshwater fluxes (Paiva and Chassignet (2001)). Their findings lead to the common practice of using bulk formula for heat and freshwater fluxes and a restoring of the modeled SSS towards observed climatology (e.g. Levitus (1998)). The SSS-restoring leads to an additional term in the net freshwater flux F_{net} in eq. 1.

$$F_{net} = F_{evap} - F_{precip} - F_{runoff} - F_{rest} \tag{1}$$

The induced freshwater restoring flux typically follows the formulation in eq.2, where the modelled SSS_{model} is relaxed to climatological values (Levitus (1998), SSS_{ref}).

$$F_{rest} = V_{piston} \frac{SSS_{model} - SSS_{ref}}{SSS_{model}} \tag{2}$$

The relaxation is applied each model time step with a coefficient for the restoring strength (often called piston velocity). The piston velocity (eq.3, V_{piston}) is defined in general as the first model layer thickness (H) divided by a restoring timescale (T_{rest}).

$$V_{piston} = \frac{H}{T_{rest}} \tag{3}$$

Thus, the longer this timescale the weaker is the restoring potential. The unavoidable SSS restoring is unfortunately a critical factor limiting the use of ocean-only simulations, especially in freshwater hosing experiments (for instance Greenland melting), where the effect of additional freshwater in the system is limited due to the counteracting restoring flux, acting against any salinity anomaly. Two approaches have been investigated to overcome the restoring issue: 1) limiting the restoring fluxes to a minimum with still realistic ocean states during the simulation period (very small remaining drift in water masses), or 2) by using mixed boundary condition. In the latter case the restoring fluxes have been diagnosed in a reference simulation with restoring and been applied in a second reference run with switched off SSS restoring instead. Both simulations should be identical. The first approach to limit the restoring fluxes to a minimum have been investigated successfully in detail in Behrens et al. (2013), leading in combination with small changes (within the range of uncertainty) in

the applied atmospheric precipitation, to a fairly realistic ocean state. Limited restoring fluxes mean that the restoring fluxes cannot exceed approximately 10% of the precipitation flux, which is a large improvement compared to previous simulations (e.g. in Griffies et al. (2009)). The resulting best guess setting of these sensitivity simulations (with little remaining drift) was then used to perform the Greenland melting simulations (for according results see chapter 5), which builds the main part of this thesis. The second approach with mixed boundary conditions was also conducted, but only in ORCA05 with idealised melting scenario and showed no obvious difference to the simulations with SSS restoring (see Appendix). The restoring work can be considered as preparatory work for the GrIS experiments. In the following section the main results of Behrens et al. (2013) will be summarised. More details are given in the according publication.

Starting point of this investigation

The applied SSS restoring setting varies largely between different ocean models and limit model intercomparisons Griffies et al. (2009). However, there is a recent tendency to decrease this unphysical factor which may indicate a positive development and improvements of ocean models as well as improvements in the applied atmospheric forcing products (Danabasoglu in prep.). In previous simulations salinity restoring was typical applied over the entire water column and in sea-ice covered regions (Griffies et al. (2009)). Due to the model and forcing improvements the restoring timescales of about 30 days for a 6 m surface layer in previous simulations has been increased during the recent years to values of about 180 days (Danabasoglu in prep., see also the CORE 2 protocol for the recommendations: http://data1.gfdl.noaa.gov/~nnz/mom4/COREv2/doc/CORE_notes_15feb2012.pdf) in comparison to Griffies et al. (2009)). Restoring settings with 30 days and applied over the water column build the starting point for the work here presented, where the sensitivity of the AMOC on the different restoring settings and modification in the polar precipitation was investigated.

4.1.1. Experimental setup

A series of ocean-only simulations coupled to a sea-ice model, in two different horizontal resolutions (0.5° - ORCA05; 0.25° - ORCA025), have been conducted to study the effect of the SSS restoring on the large scale overturning circulation. The restoring timescale varies between 30 and 365 days. In some simulations the restoring flux was further limited according to eq. 4, which follows recommendations of the CORE 2 protocol (http://data1.gfdl.noaa.gov/~nnz/mom4/COREv2/doc/CORE_notes_15feb2012.pdf).

$$0.5 \leq \| \, SSS_{model} - SSS_{ref} \, \| \tag{4}$$

The restoring is only applied in sea-ice free regions at the ocean surface (for a detailed list see table 3). Additional to changes in restoring timescale also reductions in the sub-polar precipitation, within the

experiments	configuration	piston velocity, Vpiston [mm/d] and (restoring timescale)	restoring flux limitation (eq. 4)	precipitation reduction
NO 05	ORCA05	0	no	0
WEAK 05	ORCA05	16.4 (365 days)	no	0
WEAK+FL 05	ORCA05	16.4 (365 days)	yes	0
RED+FL 7,5% 05	ORCA05	16.4 (365 days)	yes	-7,5%
RED+FL 10% 05	ORCA05	16.4 (365 days)	yes	-10%
STRONG 05	ORCA05	193.5 (30 days)	no	0
WEAK 025	ORCA025	16.4 (365 days)	no	0
WEAK+FL 025	ORCA025	16.4 (365 days)	yes	0
RED+FL 7,5% 025	ORCA025	16.4 (365 days)	yes	-7,5%
RED+FL 10% 025	ORCA025	16.4 (365 days)	yes	-10%

Table 3.: Table of performed experiments. The simulations differ mainly in the strength of the applied SSS restoring, the rain reduction north of 55°N and the horizontal resolution.The suffix NO, WEAK and STRONG indicated the the restoring, while RED indicated a reduction of the polar precipitation north of 50°N. All rain reduction simulation use the same restoring setting as WEAK+FL. FL refers to an additional restoring flux limitation to 0.5 psu between model SSS and climatology.

range of uncertainties, have been conducted (up to 30 mSv north of 55°N). The simulation period cover ∼80 years using the CORE2 interannual forcing (1948-2006, Large and Yeager (2009)) and have been initialised from rest with Levitus (1998) as initial ocean state. The first 20 years of the simulation (integrated with 1958-1977 atmospheric conditions) are in general associated with a model spinup phase, where the initial adaption of water masses and currents takes place. That adapted oceanic state was used in the following as initial state for the reference period (1958-2006). Using two model configurations with different horizontal resolution allows an estimate for the resolution dependence of the results. In total, 10 simulations have been performed (see table 3). The notation is the following:

Diagnostics

The presented diagnostics have a large scale quantifying character to ensure their meaningfulness and robustness. Small scale (also short term) effects are beyond the scope of this study (like effects close to interfaces, boundary currents, coast, ice edges). Most diagnostics shown are averages over the last decade of the reference simulation (1997-2006), when the differences between the simulations are largest.

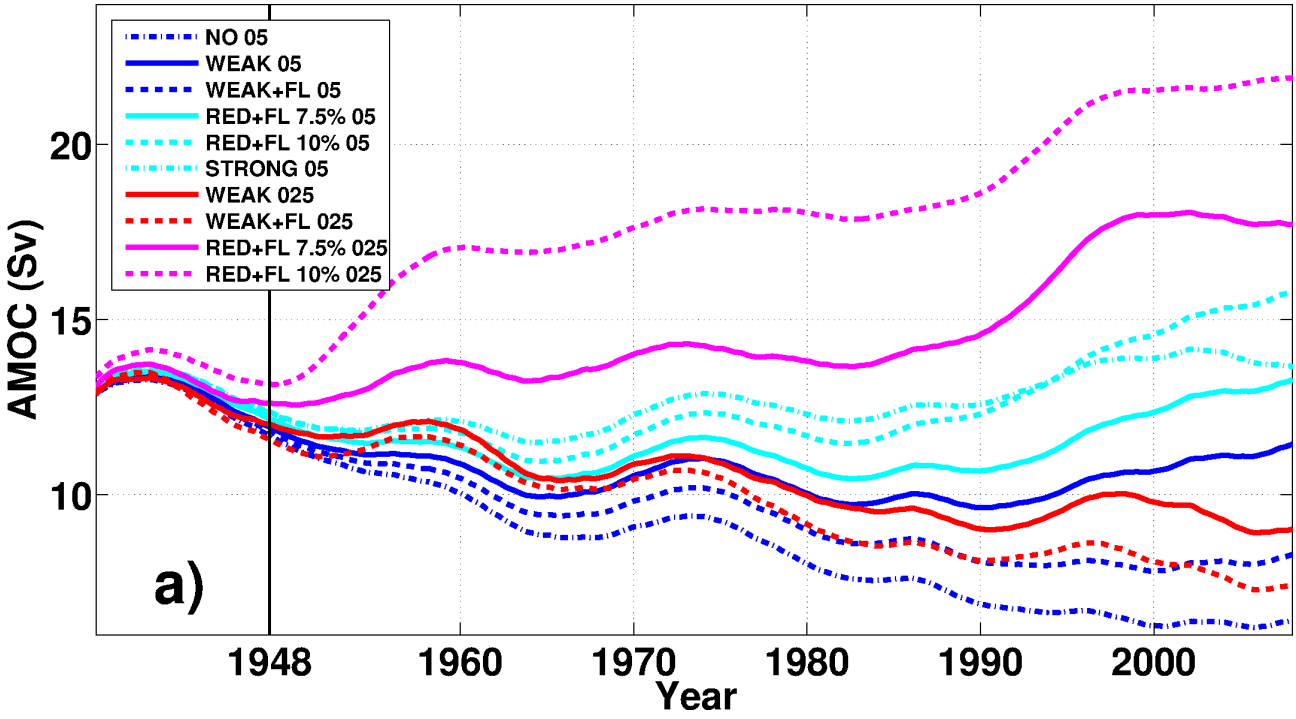

Figure 22.: AMOC (Sv) time series (36°N, a lowpath filter is applied (> 10 years)), in simulations differing in the freshwater forcing and resolution. The black line in 1948 indicates the end of the spinup period. Simulations with reduced polar precipitation show a positive impact on the AMOC. All simulation start from the same initial conditions (Levitus (1998)). For the spinup simulation the atmospheric conditions form 1958-1977 have been used. The Figure is adopted from Behrens et al. (2013).

4.1.2. The main findings about the impacts of the surface freshwater forcing on the large scale circulation in the North Atlantic

It is shown that the choice of the restoring timescale and changes in the subarctic precipitation have a substantial impact on the long-term AMOC (36°N) evolution (Figure 22), in line with findings of Griffies et al. (2009). On the other hand the interanual variability was quite robust among all simulations respectively the underlying long-term trend (not shown). This results highlight the importance of local, wind induced Ekman transport changes which affect the AMOC locally on interannual timescale, in line with results by Biastoch et al. (2008a). Irrespectively of the local wind fluctuations the long-term AMOC changes show a meridional coherent pattern. That points to large scale changes in the source water masses of the lower limb of the AMOC, originating from Nordic Seas, rather than to changes in the surface limb being more affected by local wind changes.

The simulation with no SSS restoring (NO 05) shows an ongoing decline over the entire forcing period with an AMOC value of around 8 Sv after 80 years (Figure 22). This result implies that the formation rate of dense water masses in the high latitudes is not maintained sufficiently and the present positive feedback (lower salt transports to the north and an ongoing freshening) leads to the ongoing decline. With applied "weak" restoring (WEAK 05) the decline decreases and turns in ∼1990 to an upward

trend with a mean 12 Sv at the end of the simulation. Observational estimates suggest mean values around ∼18.5 Sv (Cunningham et al. (2010)) at 26.5°N, while the maximum is supposed to be around 36°N. A further increase of the restoring strength to timescales of 30 days (STRONG 05) shifts the reversal point to earlier stages (1965) and produces a final value of 14 Sv. A limitation of the restoring fluxes (following eq. 4) increases the trend to lower AMOC values again (comparison between WEAK 05 and WEAK+FL 05). Keeping this setting and reducing the subarctic precipitation by 22 mSv and 30 mSv has on the other hand a remarkable positive effect on the AMOC. The freshwater flux north of 55°N varies between 280 mSv (NCEP) and 340 mSv (CORE 1) among different atmospheric reanalysis products and indicated that these modifications in the precipitation flux are within the range of uncertainties even with these reductions. The coastal runoff contributes approximately 100 mSv to these values (Trenberth (2010)). The reversal point in these simulations is similar to STRONG 05 but the final values are 14 Sv (RED05+FL 7,5%) and 16 Sv (RED025+FL 10%). Results with increased resolution of WEAK025 and WEAK025+FL show a similar behaviour to the 0.5° model results. On the other hand, changes in the subarctic precipitation have a larger impact on the AMOC and point to a higher sensitivity with respect to the freshwater forcing and overcoming the declining initial tendency. The values at the end of the simulation are 17 Sv (RED025+FL 7,5%) and 22 Sv (RED025+FL 10%). The higher sensitivity is related to improvements in the NAC current in terms of freshwater pathways and heat transport as well as improvements in the formation process of dense water masses in the Nordic and Labrador Sea, between ORCA05 and ORCA025.

The reasons for the strong sensitivity of the long-term AMOC evolution to the restoring setting and modifications in the subpolar precipitation will be discussed in the following. Changes in the restoring setting and precipitation have an effect on the fresh water flux budget at the ocean surface according to eq. 1. A typical net surface freshwater flux pattern derived from ORCA05 (STRONG 05) is shown in Figure 23a. Positive values (mm/d) indicate freshwater fluxes from the ocean towards the atmosphere. Expected positive fluxes occur in the subtropics and in the course of the NAC in the Newfoundland basin. Negative fluxes occur along the east coast of North America after the separation of the Gulf Stream from the coast (Cape Hatteras), in the Labrador Sea and partly in the Nordic Seas. The positive pattern in the subtropics is expected, due to northeasterly trades (warm and dry) increasing the evaporation and carrying the moisture towards the equator. The comparison between the net surface fluxes and the restoring fluxes (Figure 23b) shows some striking similarities in the flux pattern. In some regions the contribution of the restoring fluxes to the budget is substantial, like in the course of the NAC. Large negative restoring fluxes are found along the North American coast and around Greenland while a positive hotspot emerges in the Newfoundland basin. Some portion of this pattern is caused by deficits in the SSS reference (Levitus (1998)) which does not reflect sharp fresh coastal currents. For instance the East Greenland Current (EGC) is resolved reasonably by the models but not by the climatology which leads to an artificial salinification in that region, with implication for the Labrador Sea (Rattan et al. (2010)). As a consequence of the arbitrary positive restoring flux in the EGC in combination with a too low runoff from Greenland (see section 4.1.3, 2 mSv compared

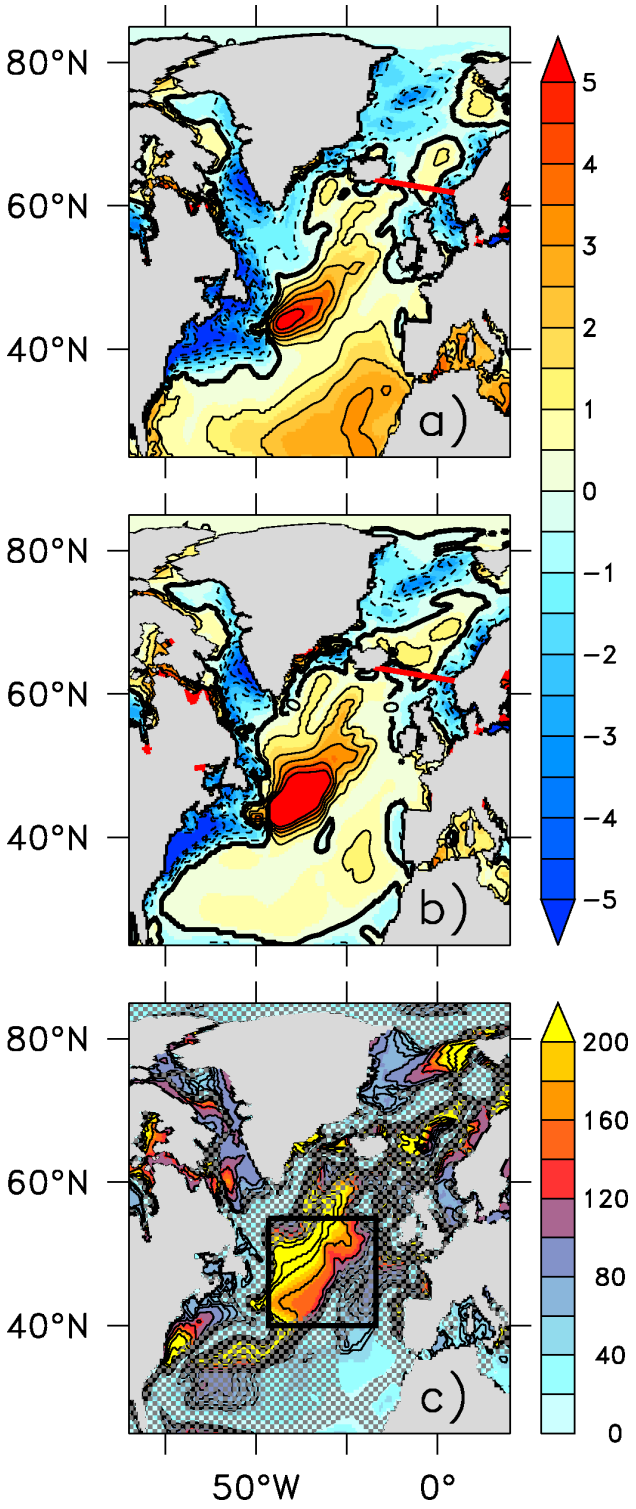

Figure 23.: a-c) Surface fluxes averaged over the last decade of STRONG 05; (a) Net freshwater flux (mm/d), (b) Restoring freshwater flux (mm/d); (c) Fraction between restoring flux and net freshwater flux in %. Areas where the restoring fluxes are smaller than 50% of the precipitation are shaded in (c). The red line in (a-b) indicates the section to compute freshwater transports into the Nordic Seas. The black box in (c) shows the region for evaluating the surface freshwater fluxes. In (a-b) each 1 mm/d interval is contoured and each 20% interval in (c). The Figure is adopted from Behrens et al. (2013).

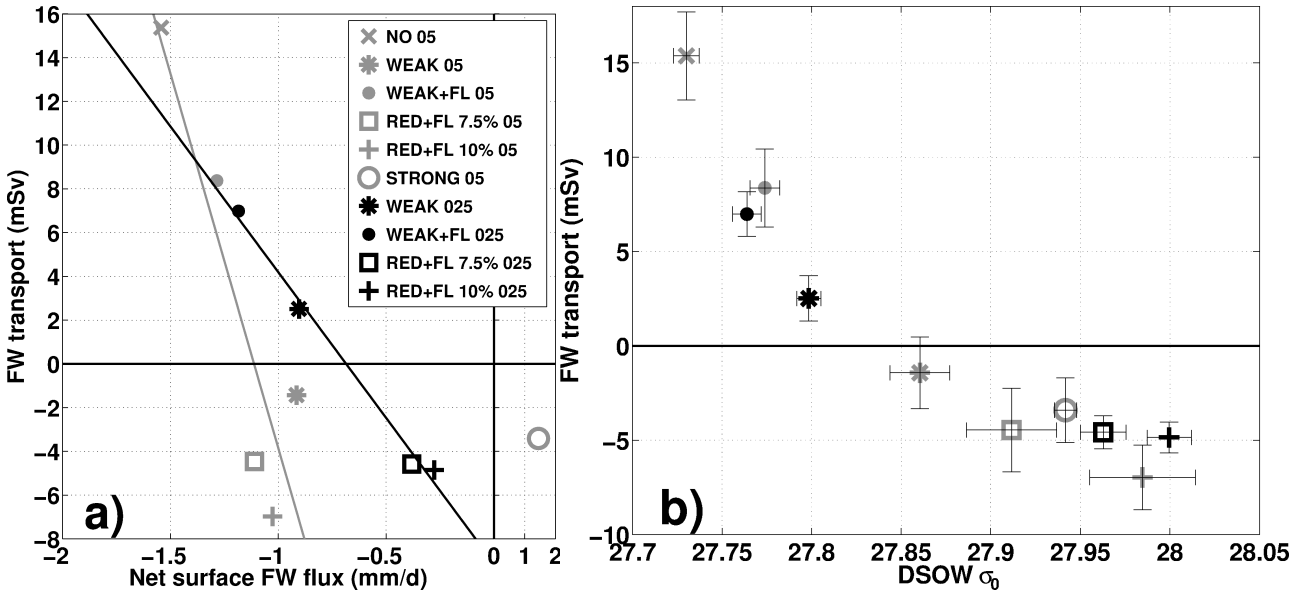

Figure 24.: (a) Relation between integrated surface freshwater flux between (50°W-20°W, 40°N-55°N, black box in Figure 23) and freshwater transports across Island and Norway (see Figure 23, red line) into Nordic Seas for each simulation averaged over the last decade (1997-2006), (b) Relation between mean (1997-2006) freshwater transport across Island and Norway and DSOW density for each simulation. Error bars indicate the interannual variability. The Figure is adopted from Behrens et al. (2013).

to expected 17-22 mSv, Bamber et al. (2012); Greve (2000)) the SSS is increased over the Labrador Sea and this is the reason for the negative restoring fluxes over that area. A further reason for the large restoring fluxes (e.g. along the NAC) is the discrepancy in the model representation of the ocean circulation. Deviations from the observed flowpath of the NAC in the model (i.e. overshooting Gulf Stream) cause negative restoring fluxes north of Cape Hatteras, indicating a too northern course of the Gulf Stream. This is a common known bias in coarse ocean models (Jungclaus et al. (2006b)). Further upstream, the flow path is too zonal across the subpolar North Atlantic with a not well represented NW Corner. This misrepresentation is indicated by the positive hotspot of the restoring fluxes suggesting too low salinity over this region in comparison to observations. To reduce this fresh model bias the restoring fluxes are largest in this area leading to an increase in the salinity locally. The restoring itself does not fix the model deficit but weakens its importance and consequences (see section 4.1.3). A measure for the significance of the restoring fluxes is shown by the fraction to the prescribed precipitation. In the regions earlier mentioned the restoring fluxes are the dominating and controlling factor for the surface net freshwater flux (same magnitude as the precipitation flux). In that context, the region in the Newfoundland basin is a key region for the long-term AMOC evolution as shown in Figure 23c .

It is obvious that the choice of restoring strength controls the net surface freshwater flux in this region, with implications for the northward freshwater transport into the Nordic Seas (Figure 24; section is marked in Figure 23a and b. Depending on the choice of the surface flux formulation the sign of

the northward freshwater transport turns from positive (no and weak+fl restoring) to negative in all other simulations. The freshwater transport and the involved positive feedback via AMOC and related meridional heat and freshwater anomalies are the crucial controlling factors for the source water masses of the dense overflows generated in the Nordic Seas, like indicated in Figure 24b. Less freshwater transport into the Nordic Seas goes along with increased density of the overflow, highlighting the importance of salinity. The temperature contribution is of minor importance in that respect. In experiments with strong restoring or precipitation modification over the subarctic region, densities in the range of observations are obtained (Jochumsen et al. (2012)). The repercussion of the density of DSOW feeding the lower limb of the AMOC have been already mentioned and described by Latif et al. (2006). The present results support their findings.

In summary, it is shown that the DSOW density is closely linked to the freshwater transport from the subpolar North Atlantic into the Nordic Seas which is strongly affected by the restoring over the Newfoundland Basin (model related bias) and thus controlled by the formulation of the restoring flux over that region or by changes in the applied precipitation north of 55°N.

4.1.3. Consequences for the surface freshwater forcing in Greenland melting simulations

The overall goal of this study was to find a model setup with SSS restoring reduced to a minimum and with acceptable small drift in the water masses to overcome the dominating role of the SSS restoring, which was present in previous model simulations. There is no concept so far which allows to switch off the SSS restoring completely without deteriorating model results by the model drift. Running coarse models in a quasi-equilibrium state (Danabasoglu et al. (1996)), over more than a few thousands of years might be an option, but not applicable for high resolution simulations requiring large amounts of computing time. That fact raises the need for model settings with little initial and long-term trend. It is found that accurate boundary conditions are essential for long-term behaviour of model results and small changes can have substantial implications for the long-term model drift. The precipitation in the high latitudes shows uncertainties around 10-15% between different atmospheric reanalysis products (not shown). Probably a similar value can be estimated for the coastal runoff in subarctic-arctic vicinity. For example estimates from Greenland under present conditions vary between ∼22 mSv (Bamber et al. (2012)) and ∼17 mSv (Greve (2000)). The study presented here showed that modifications within this range of uncertainties (Figure Fig. 24b) in the freshwater forcing can control the long-term (∼100 years) AMOC tendency while the interannual variability is unrelated to the long-term AMOC behaviour. The overall aim of future studies should be to decrease the SSS restoring effect as much as possible to values small compared to the applied precipitation fluxes. This reduction calls for further improvements in model physics and probably, a forcing methodology which, at least partially, accounts for the important atmospheric feedbacks in a physically more realistic manner than the bulk formulation and for precise forcing dataset.

Model	Institute	Type	Ocean resolution	Reference
HadCM3	Hadley Centre	AOGCM	1.25° , L20	Gordon et al. (2000)
IPSLCM5A	Institute Pierre Simon Laplace	AOGCM	2°, L31	Dufresne et al. (2013)
MPI-ESM	MPI	EBM	1.5°, L40	Jungclaus et al. (2013)
ORCA05	GEOMAR	OGCM	0.5°, L46	Behrens et al. (2013)
EC-Earth	DMI	AOGCM	1° , L42	Sterl et al. (2011)
BCM2	NERSC	AOGCM	2.8°, L35 isopycnal	Otterå et al. (2010)

Table 4.: Model overview and description. AOGCM reflects coupled ocean-atmosphere models, OGCM stands for a forced ocean-only model and EBM for Energy Balance Model. ORCA05 has the highest horizontal resolution in comparison to the other models.

4.2. The role of atmospheric feedbacks in GrIS melting scenarios

As a part of the EU-THOR project a large model intercomparison was initiated to assess the oceanic response to a melting of Greenland. In the according study of Swingedouw et al. (2012), 5 state-of-the-art coupled ocean-atmosphere models and one forced ocean model (see Table 4) were used to perform a 43 year long (1965-2007) idealised melting simulation (enhanced runoff from Greenland by 0.1 Sv, constant in time and equally distributed along the Greenland coast; the setting is identical to the I-MELT scenario described in section 2.2.1) and compared with results from an unperturbed control (reference) simulation. The horizontal resolution in the ocean varies from 2.8° (BCM2) to 0.5° (ORCA05) between the different models (for more details see Swingedouw et al. (2012)). The latter model (ORCA05) is considered as the connecting link between coarse coupled models on the one side and the high resolution ocean-only simulations as part of this thesis.

Common features between all models are found in the time evolution of the freshwater signal, here diagnosed in the SSS (Figure 25) averaged over the last 10 years (1996-2005). The negative salinity signal originates from the Greenland coast and spreads into the Baffin Bay, where the largest salinity signal over the entire water column can be found throughout the entire simulation period. Later, the anomaly penetrates into the Labrador Sea and follows the main circulation, partly into the Nordic Seas and partly in the SPG within the Canary Current. The latter-mentioned part (comma shape pattern) was found to provide an export pathway of freshwater anomaly to leave the subpolar North Atlantic with corresponding implications for the AMOC. Only BCM2 does not show the freshwater leakage to the STG. It seems clear that the comma shape signal is driven to certain amount by direct advection of meltwater into that area, and partly related to changes in the STG (contraction/expansion, passively forced). A differentiation between both contributions is only possible if a passive tracer is released to mark the meltwater from Greenland directly which is fortunately the case in the forced ocean-only simulation of ORCA05. A common positive SSS anomaly among all models is present in the Arctic Ocean and is considered to be related to the Atlantic inflow, which in contrast to the control simulation, has not interacted with surrounding surface water due to increased stratification in the melting simulations. The Atlantic inflowing water has been shielded from the surface by the meltwater

cap from Greenland which results in an outcropping in this region with distinct saltier characteristics. The magnitude of these anomalies differs between models but is a common feature. The explanation of the outcropping of Atlantic water in the Arctic Ocean is also aided by corresponding SST anomalies averaged over the last decade (Figure 26). Except for BCM2, all models show a warming signal in the Nordic and Barents Sea. A common cooling, similar in structure as the SSS anomaly (comma shape), is present in the Labrador Sea, south of the Greenland-Scotland ridges and along the south east edge of the STG.

Melting response: no significant effect of atmospheric feedbacks over first decades is found

The described surface anomaly patterns of SSS and SST with according relevance for the atmospheric condition seem very robust and are also present in other recent studies (Gerdes et al. (2006); Hu et al. (2009); Stouffer et al. (2006); Wang et al. (2012)) with slight variations in magnitude and location. The short-term melting response was investigated by Marsh et al. (2010), which is based on ORCA025 simulations with relative strong SSS-restoring. Based on the results of Swingedouw et al. (2012), no fundamental difference is seen in the anomaly pattern between AOGCM and OGCM over several decades, suggesting that atmospheric feedbacks are minor important for the first 4 decades at least. The study by Gerdes et al. (2006) proposed the opposite but used coarse (∼2°) OGCMs with a strong SSS-restoring with a timescale of 60 days for a 10 m surface layer (piston velocity of 166 mm/day). The forced model in Swingedouw et al. (2012) used a much weaker SSS-restoring (365 days for a 6 m surface layer (piston velocity of 16 mm/day) and a additional restoring flux limitation following eq. 4), which could be the reason for the different behaviour and conclusion. Anyway, these anomaly patterns of temperature and salinity go along with a reduction in the deep water formation rates feeding the lower limb of the overturning and lead to a reduction in the large scale AMOC here diagnosed at 26.5°N (Figure 27). The reduction accounts for 1 to 4 Sv (after 35 years) over the hosing period. It should be mentioned that mean AMOC values of ∼15 Sv of all models are around 3-4 Sv lower than observational estimates of 18.7 ± 2.1 (Cunningham et al. (2010)). With respect to the AMOC response two groups can be identified: a group with a larger AMOC response EC-EARTH, ORCA05 and BCM2 (3-4 Sv) and on the other side MPI-ESM, IPSL and HadCM3 (1-2 Sv) with a weaker response. When taking the initial AMOC state into account, then these results are in broad agreement to previous studies, showing a weakening of -30% to -50% in AMOC strength over a ∼ 30 year period (Wang et al. (2012); Stouffer et al. (2006); Gerdes et al. (2006); Weijer et al. (2012)) with a comparable meltwater flux. The AMOC response in general does not show any clear difference between coupled and uncoupled models and confirms the minor importance for atmospheric feedbacks on this timescales. Even forced simulations with strong SSS restoring of 30 days (Wang et al. (2012)) show a distinct declining AMOC response, which is not inhibited by the counteracting SSS restoring or missing of atmospheric feedbacks. These results confirm findings of Swingedouw et al. (2012), which

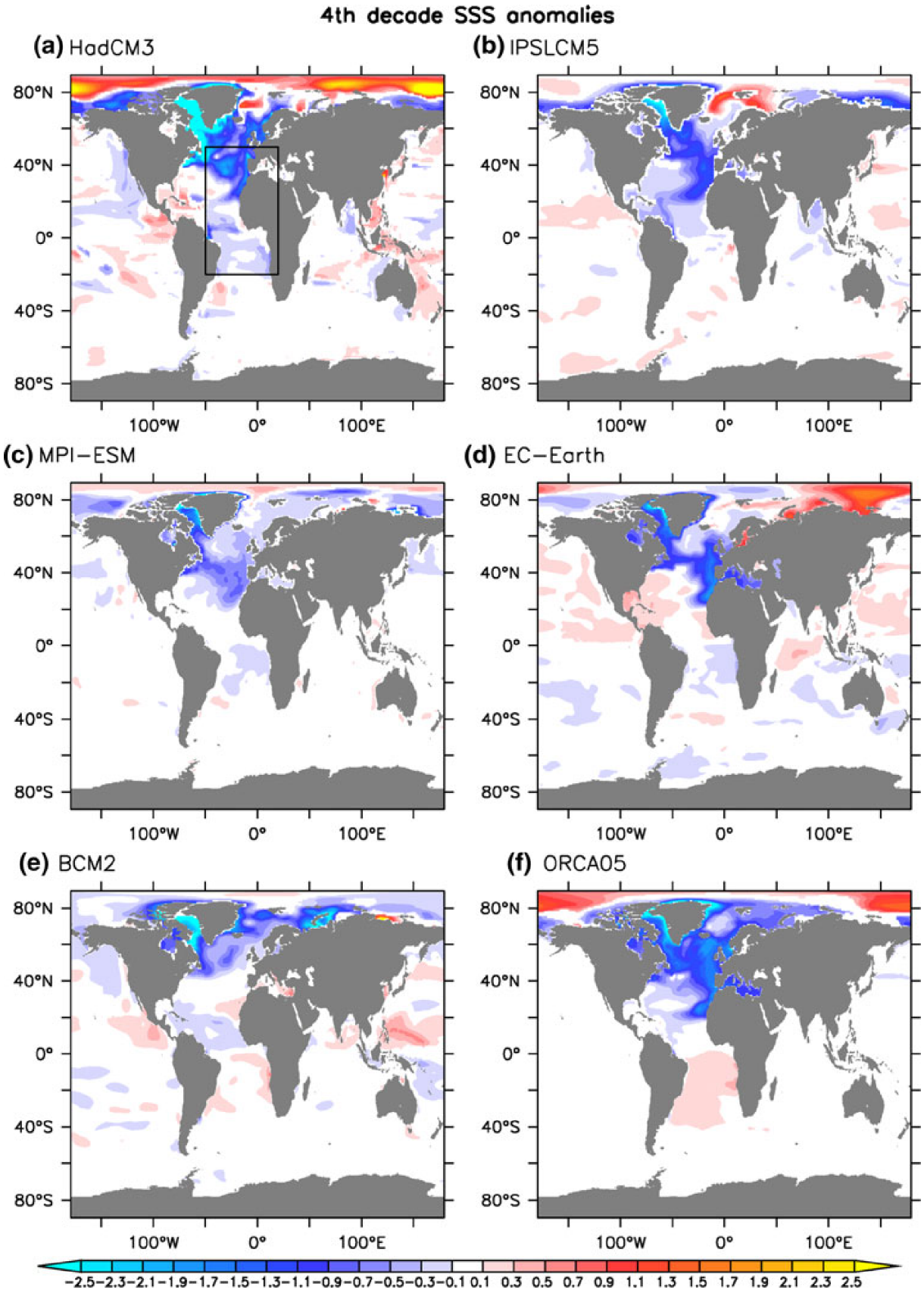

Figure 25.: SSS anomaly (psu) between hosing and control simulation over the 4th decade (1996-2005) for different models. Figure is adopted from Swingedouw et al. (2012).

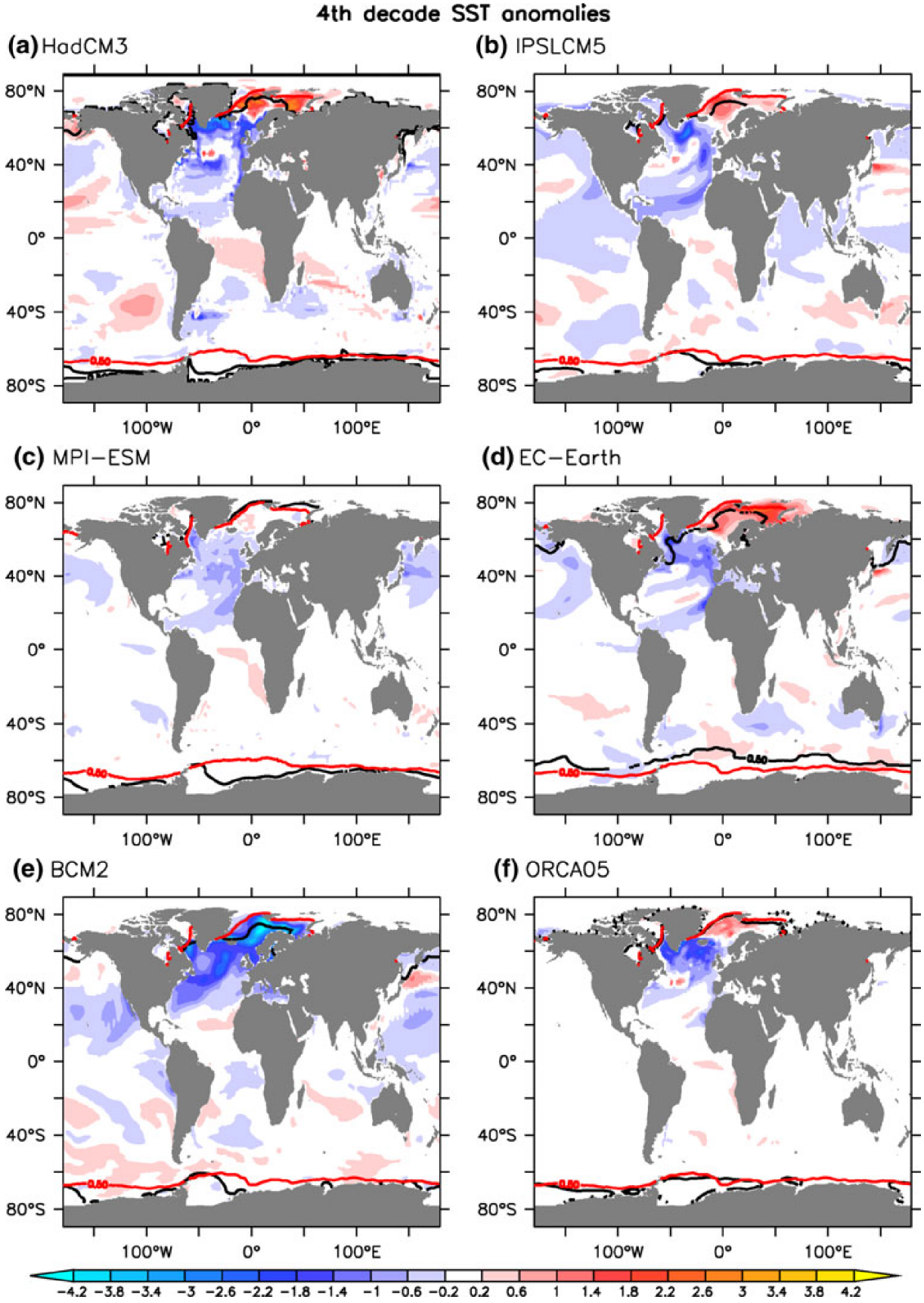

Figure 26.: SST anomaly (°K) between hosing and control simulation over the 4th decade (1996-2005) for different models. Figure is adopted from Swingedouw et al. (2012). The red contour line represent the observed sea-ice edge and in the black line illustrates the modelled sea-ice edge.

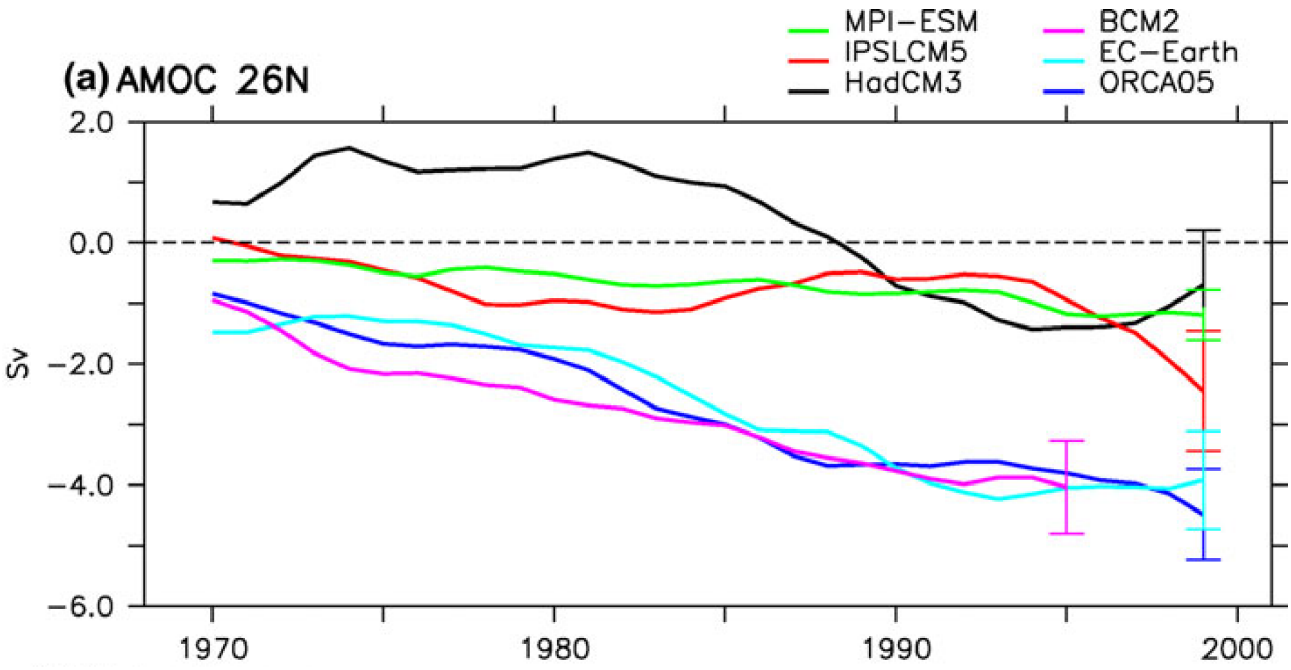

Figure 27.: Temporal evolution of AMOC anomalies between hosing and reference simulation at 26°N in Sv for the individual models. Figure is adopted from Swingedouw et al. (2012). The timeseries are based on annual means.

suggested a minor importance of atmospheric feedbacks for the melting response over the first few decades.

The dependence of the melting response on resolution

However the large spread in the AMOC response is considered to be related to general differences in the representation of the large scale Atlantic Ocean circulation where coarse models have their difficulties, e.g. cold bias of the NAC related to the southwards shift of the NAC path. From that idea rose that an increasing resolution, leading to improvements in the circulation, might have an impact on the melting response. Results from Weijer et al. (2012) showed that the response of the mixed layer is more gradual in a strong-eddying configuration, while the AMOC response in total (absolute change) is larger in the higher resolved case. Their results also suggest a faster signal propagation within the DWBC current in the strong-eddy simulation, if it is sufficiently resolved. However, a clear robust statement about the impact of increasing resolution is still missing. Results from Condron and Winsor (2011) in a simulation of the freshwater release from Lake Agassiz (5 Sv) in a coarse (2.6°) and a medium (1/6°) resolution suggest that the SSS anomalies in the coarse configuration propagate eastward over the subpolar North Atlantic and travel to the north and south (comma shape) along the European coast similar to Swingedouw et al. (2012). On the other hand, in the medium-resolution configuration, these SSS anomalies seem to travel more along the American coast and do not enter the Nordic Sea within the simulation period of 7 years. SSS anomalies are found after 7 years in a zonal

band around 20°N and 40°N over the Atlantic. Spence et al. (2008) investigated the same melting event with model resolutions ranging from coarse (1.8° × 3.6°) to higher (0.2° × 0.4°) resolutions and slight differences in the applied freshwater anomaly (1.75 Sv over 3 years). Only little effect of resolution effect on the AMOC response was found, but hints that, with higher resolution and improved deep water formation, the impact on the melting would be weaker.

Results from these studies indicated some effects of resolution but a clear picture is still absent and the need of a clear, precise examination of the resolution dependence and the impact on a melting of the GrIS is emphasised. The results of such a comparison are now presented in the following chapter, including a coarse model (ORCA05, some results are included in (Swingedouw et al. (2012)) with 0.5° horizontal resolution, a medium configuration (ORCA025) with 0.25° and an eddy resolving resolution (VIKING20) with 1/20° horizontal resolution. For a detailed model description see section 2.1 and 2.2. The oceanic response to two melting scenarios will be discussed, an idealised (0.1 Sv) and a more realistic (0.53 mSv/a increase following Bamber et al. (2012)) (see section 2.2.1 and 2.2.2 for information about details of the melting scenario). The results are presented starting from the source region around Greenland towards larger spacial and temporal scales. The focus is put on the resolution dependence and the effect of the different melting scenarios.

5. The oceanic response to a melting of the GrIS: the effect of model resolution

The following chapter constitutes the main part of this thesis, where a melting of the GrIS is simulated and the oceanic response to the additional freshwater is investigated. The focus is set on the resolution dependence and the effect of the mesoscale variability representation within three configurations. The horizontal resolutions of these configurations is 0.5°, 0.25° and 0.05°. These investigations with ocean-only simulations are complemented by a collaborative model - model intercomparison with coupled models to investigate the effect of an active atmospheric response which is limited in forced simulations. A summary of this model - model intercomparison (Swingedouw et al. (2012)) is presented in section 4.2 and mark the starting point of this study. Two different types of GrIS melting scenarios have been conducted. Additional to an idealised Greenland melting scenario (0.1 Sv, constant) which is used in the model - model intercomparison, a second more realistic melting scenario (0.53 mSv/year linear increase) was conducted. These both scenarios allow to assess the importance of the melting scenario to the oceanic response.

5.1. The local response around Greenland

In this section, the local and initial (short-term over the first 5 years) response to a GrIS melting with respect to resolution dependence and applied melting scenario will be discussed. For details of the experimental setup see chapter 2. It is clear that the initial response is first found along the Greenland coast, where the additional meltwater enters the ocean and acts on the actual ocean state. The boundary currents carry the corresponding anomalies of temperature and salinity towards Baffin Bay as well as into the Labrador Sea. Some portion of temperature and salinity anomalies are not directly related to the direct presence of meltwater but rather induced by circulation changes.

Response in the I-MELT scenario

Meltwater spreading (passive tracer)

The spreading of the additional meltwater from Greenland can be best traced using a passive tracer, released in combination with the additional runoff from Greenland to mark the additional meltwater directly (for more details see section 2.3.1). The sequence of this surface spreading over the first 5 years (initial period) is shown in Figure 28. Highest concentration (above 0.05 m^3/m^3) are found within the boundary current around Greenland after 1 year. The tracer is carried with the main circulation towards Baffin Bay, and is penetrating into the Canadian Archipelago towards the Arctic Ocean. A spreading from the boundary current of Greenland (WGC) into the Labrador Sea is a common feature among all configurations. The signal is most diffuse in the ORCA05 and more defined with higher resolution when small scale currents can be resolved explicitly.

After 2 years the meltwater from Baffin Bay enters the Labrador Sea and joins the meltwater emerging from the WGC, transporting the meltwater with the Labrador Current to the south along the shelf-break of Labrador. A quite interesting eastward spreading north of Iceland is present in all simulations, probably related to local wind events (also seen in the SSS anomalies) or by recirculations within EGC into the Nordic Seas. Recent studies (Våge et al. (2011)) showed that same portion of the DSOW is formed north of Iceland. That formation is very sensitive to freshwater and could lead to fast response in the DSOW with repercussions on the AMOC. The interior Labrador Sea, which is critical for the deep water formation (LSW), shows the highest tracer concentrations and homogenised coverage with meltwater (tracer) in the coarser resolution. In comparison to the other configurations, it seems that the tracer diffusivity is overestimated in ORCA05, partly related to the GM, eddy parameterisation. In the southern part of the Labrador Current some recirculations towards the interior of the Labrador Sea are visible (marked by red triangles in the middle panels). These recirculations carry some meltwater fraction back into the convective region. This feature seems consistent with the observed trajectories of floats released at 53°N done by Fischer and Schott (2002); Lavender et al. (2000) suggesting recirculation cells. These recirculations are unfortunately not seen in a more recent study

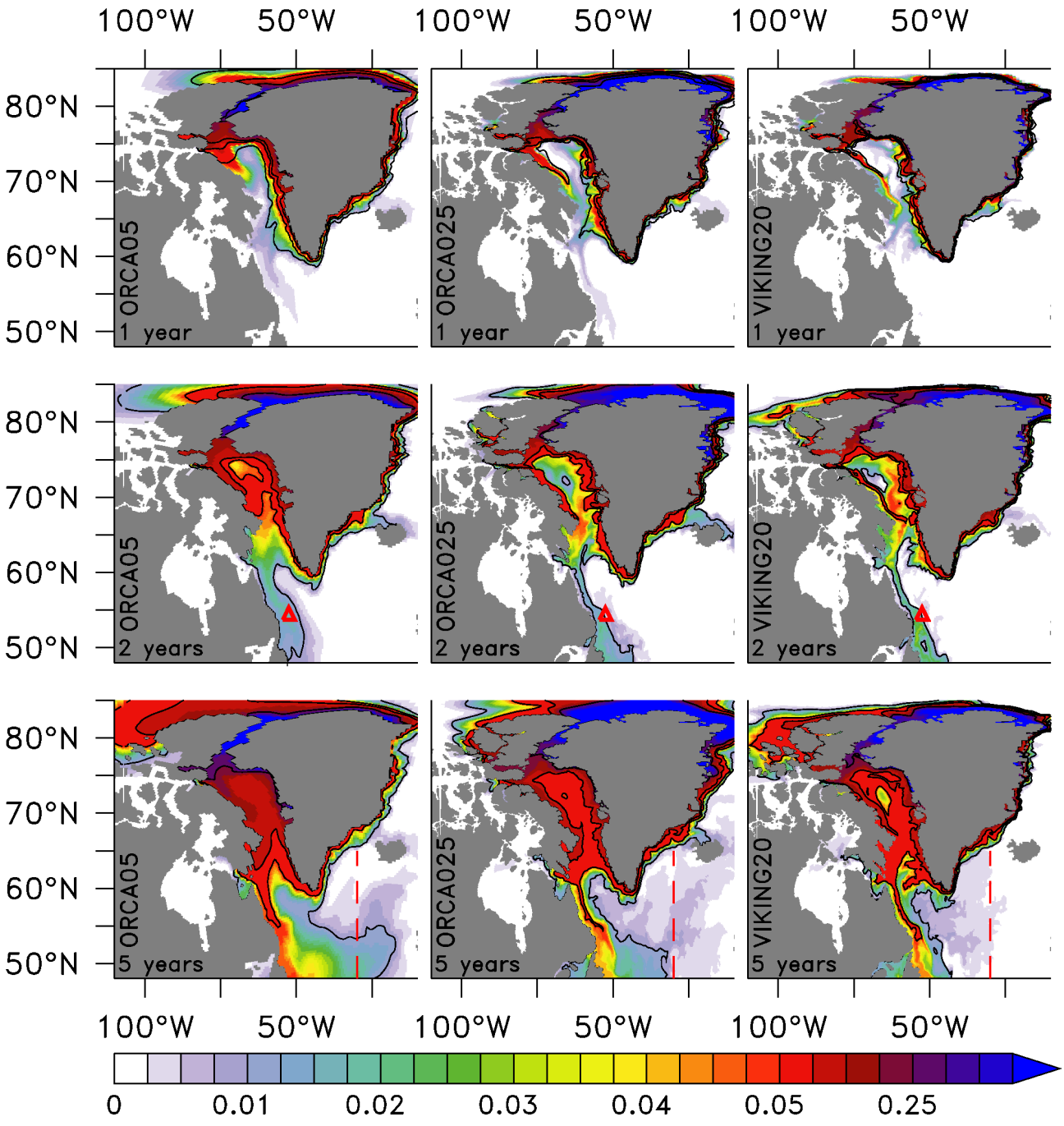

Figure 28.: Spreading of the additional meltwater: Surface passive tracer spreading in the different model configurations in (m^3/m^3) for the first 5 years of the hosing simulation (is based on monthly means). Contour lines represent concentrations of 0.01, 0.05, 0.1 and 0.25 m^3/m^3 to aid the visual inspection. The red triangle in the middle panels indicates the recirculation from the Labrador current towards the interior Labrador Sea, which could carry some portion of water from the NAC in cases of a well located NW Corner. The red dashed line is for visual guidance to gauge the eastward spreading of meltwater and related anomalies into the subpolar North Atlantic.

by Bower et al. (2013) about interior pathways. The high resolution configuration shows the most fine-structure elements there, pointing to small scale processes (mesoscale) controlling the cross-shelf transport in the "real ocean". It appears that not all passages through the Canadian Archipelago are well represented in the coarse ORCA05. The Jones Sound is a dead end in ORCA05 (no throughflow), while the other configurations maintain a northward throughflow of meltwater towards the Norwegian Bay and further north. This export pathway of meltwater is in contradiction with studies suggesting that all water in that spot originating from the Pacific Ocean (Jones (2003)) and not from Atlantic proper. Melting related circulation changes open this new export pathway which is not present in the unperturbed simulation.

After 5 years the tracer concentration in the interior Labrador Sea shows similar values 0.005-0.015 m^3/m^3 among all configurations, but with large contrast to the boundary current concentration, carrying the host of meltwater. It should be mentioned that the meltwater transport in the Labrador Sea is accomplished by the mean currents and an additional contribution in VIKING20 associated with WGC eddies, carrying meltwater from the fresh boundary current into the interior (red tongue, south of the mean flow pathway in the Labrador Sea). The WGC eddy contribution should be investigated more in details, but is beyond the scope of this work. Irrespectively of that, there are some indications that the eastward and northeastward penetration within ORCA05 and ORCA025 in the SPG (outside the Labrador Sea) is enhanced compared to results of VIKING20 (visualised by the red dashed line). The meltwater has already crossed the Reykjanes Ridge in both coarser configurations but not in VIKING20 where meltwater has partly entered the Irminger Sea. The spreading within the Arctic Ocean exposes further differences; the propagation of the meltwater in VIKING20 is more concentrated to the Greenland coast and to the Canadian Arctic Archipelago. ORCA025 shows, in comparison, a more northward spreading (towards the north pole) and ORCA05 a west and northward path.

SSS response

The corresponding SSS anomaly pattern (Figure 29) is strongly related to the presence of meltwater described above. An immediate freshening of the coastal waters of Greenland is present with values exceeding -1 psu after 1 year. After 2 years, the freshening signal from the Greenland coast arrives to the north of Iceland. This pattern was also seen in the tracer spreading, with possible consequences for the DSOW formation.

After 5 years the surface freshening is more broadly distributed. In ORCA05, a strong homogenous salinity anomaly ($<$ -1 psu) is present in Baffin Bay. Both higher resolved configurations exhibit a larger contrast between the boundary current and interior compared to ORCA05. The salinity anomaly in the interior Labrador Sea is similar for all configurations ($\sim$ -0.4 psu), while the eastward and north eastward penetration into the subpolar North Atlantic shows again the differences described earlier. In the coarse ORCA05 a "fresh finger" is propagating towards the Iceland-Scotland ridge and crosses the Mid Atlantic Ridge (visual aided by the red dashed line in Figure 29). This feature is

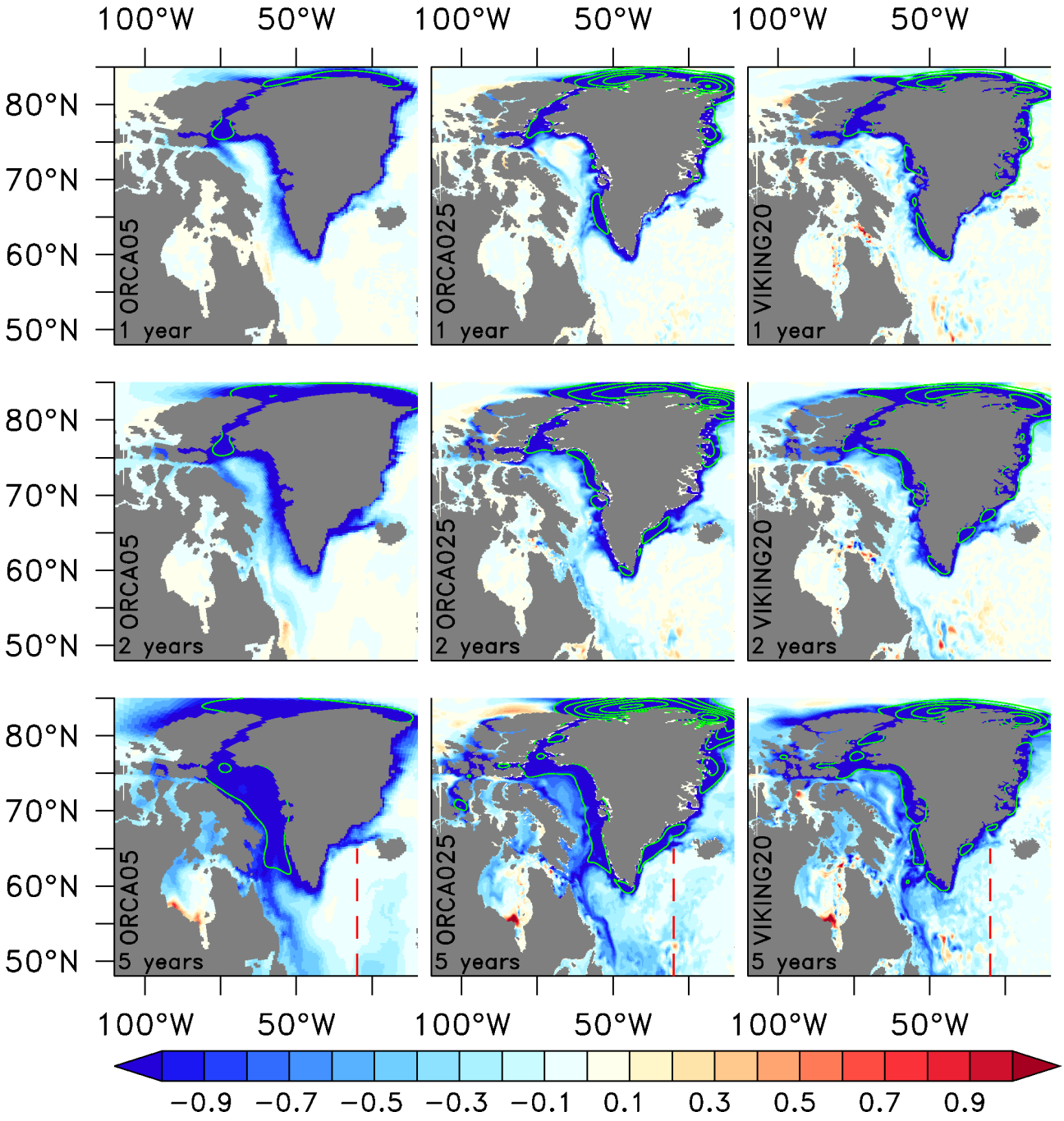

Figure 29.: Initial (short-term) SSS (psu) anomalies (are based on monthly means) for the different model configurations for the first 5 years of the hosing simulation. Green contour lines indicate anomaly intervals of 1 psu. The red dashed line is for visual guidance to gauge the eastward spreading of meltwater and related anomalies into the subpolar North Atlantic.

found further west in ORCA025 and which is not present in VIKING20 at all, where only a few signals are seen east of the Reykjanes Ridge. Obviously that spreading is strongly affected by eddies and the representation of the NW Corner, which differs quite substantially between the configurations. As shown earlier (section 3.6) VIKING20 fits best the observed characteristics of the flow path and variability of the NAC. There are only minor differences between the passive tracer distribution and the SSS-anomaly pattern during that period. That result confirms that most of the visible SSS anomalies are directly induced by the presence of meltwater and changes in the circulation, which induce salinity anomalies are of minor importance.

SST response

The SST anomaly pattern is more diverse than the SSS response (Figure 30), because meltwater affects salinity but not temperature directly. Temperature is more related to changes in the circulation, vertical stratification and surface heat fluxes. Changes in the SST due to heat fluxes are crucial for atmospheric conditions but are beyond the scope of this study. It should be noted that the coastal runoff has the same temperature as the SST of the grid box which it enters. In the real world this runoff would probably be colder than the surrounding ocean. This effect should be taken into account and analyzed in future studies.

After one year a cooling ($\sim$ -0.8 °K) of the EGC and WGC south of 65°N is a common feature for all configurations. This pattern is related to an increased stratification in the boundary current which leads to less deep mixing during winter. The resulting negative anomalies can exceed more than -1 °K. This pattern is robust among all configurations and is enhanced in the high resolution configuration which resolves the boundary currents more in detail. Positive anomalies are found at the northern coast of Greenland in all configurations. In VIKING20 anomalies exceeding $\pm$ 1 °K are present in the NAC and Irminger Sea which are related to the presence of local mesoscale eddies. A warming signal in the Labrador Current in ORCA05 is not supported in the other configurations. The cooling signal in the boundary current around Greenland becomes more pronounced and expands to the north of Iceland during the simulation.

After 5 years, a large cooling response is seen in VIKING20 over the entire Labrador Sea ($<$ -1 °K), compared to the other simulations. This cooling in VIKING20 seems to be related to larger amounts of warmer Irminger Sea water in the control simulation compared to the coarser configurations, which is not longer maintained in the hosing simulation. The flow of Irminger water differs greatly between the configurations, which is also related to the path of the NAC and the representation of the NW Corner. The positive anomaly north of Greenland is still present among all configurations, but does not develop further after 1 year.

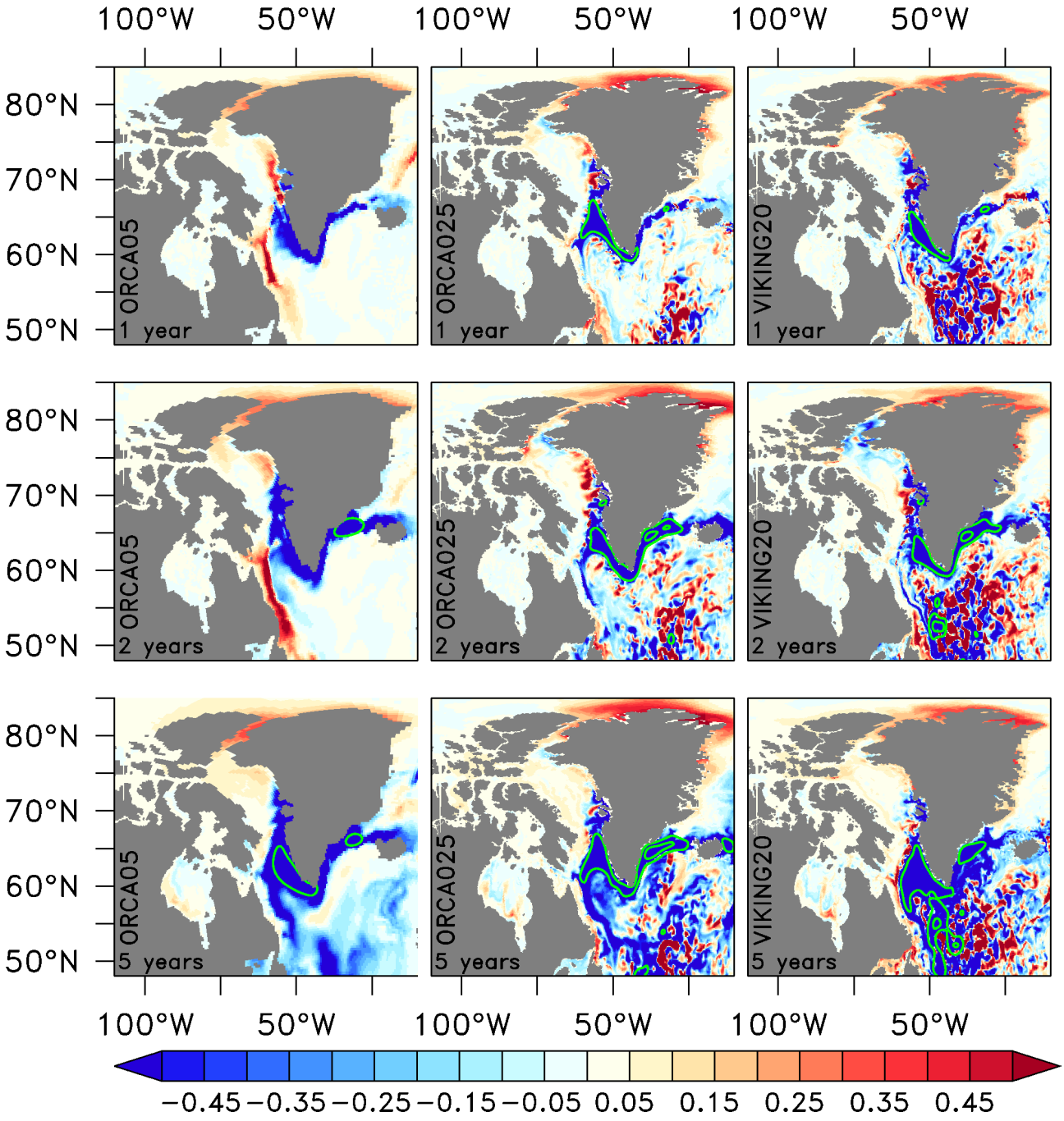

Figure 30.: Initial (short-term) SST (°K) anomalies (are based on monthly means) for the different configurations for the first 5 years of the hosing simulation. Green contour lines indicate anomaly intervals of 1 °K.

Sea ice response

The additional meltwater decreases the salinity and increases the freezing point of water, so for fixed temperatures freezing conditions are more likely. The separate effect of temperature (T) and salinity (S) changes are shown in Figures 29 and 30. In regions where fresh and cold anomalies occur simultaneously, there is an increase in ice fraction (e.g. in the EGC, Figure 31), except for the WGC which exhibits unchanged conditions. The largest positive signals are related to a southward shift of the ice edges in the Labrador Sea, Irminger Sea and parts of Baffin Bay (Figure 31, blue contour line). In the presence of sea-ice the surface heat fluxes between ocean and atmosphere are interrupted which prevents the ocean from a further cooling during the winter season. This interruption would results in a positive SST anomaly compared to ice-free case. The effect of this mechanism is not seen here. Relatively little change with respect to time and resolution is seen in the sea-ice response compared to the temperature and salinity responses.

Response in the R-MELT scenario

In the realistic melting scenario the amount of freshwater released after 5 years is substantially different compared to the idealised scenario. In the realistic scenario, only 236 km^3 of additional freshwater has entered the ocean after 5 years, while in the idealised scenario 15768 km^3 has been released during the same period. The total amount of freshwater in the R-MELT scenario is therefore only 1.5% of the amount of the idealised scenario. The relatively low amount of meltwater is not sufficient to produce significant anomalies compared to the natural seasonal, interannual and stochastical variability in the system over this time span. Therefore only the surface passive tracer distribution after 5 years is shown in Figure 32. The spreading of the meltwater in idealised and realistic scenarios are similar but the magnitude of the concentrations is lower in the latter case. High concentrations are found around the Greenland coast and the tracer is advected into Baffin Bay, resulting in high concentrations there. The tracer follows also the Labrador Current into the SPG. The spreading to the north of Iceland is also present and the eastward penetration into the subpolar North Atlantic is weakest in VIKING20 (across the red dashed line). Some differences with respect to the idealised scenario are seen in the spreading into the Arctic Ocean. The high concentrations north of Ellesmere Island and in the Canadian Arctic Archipelago in the idealised case are not visible in the realistic melting case, probably because of lower and non uniform release rates at the northern coast of Greenland. Despite that difference, the similarities dominate and lead to the conclusion that at least over this time span the spatially varying runoff from Greenland compared to the uniform release is of minor importance for the meltwater spreading. On the other hand, the amount of freshwater seems to be a relevant effect on ocean density and the resulting circulation changes.

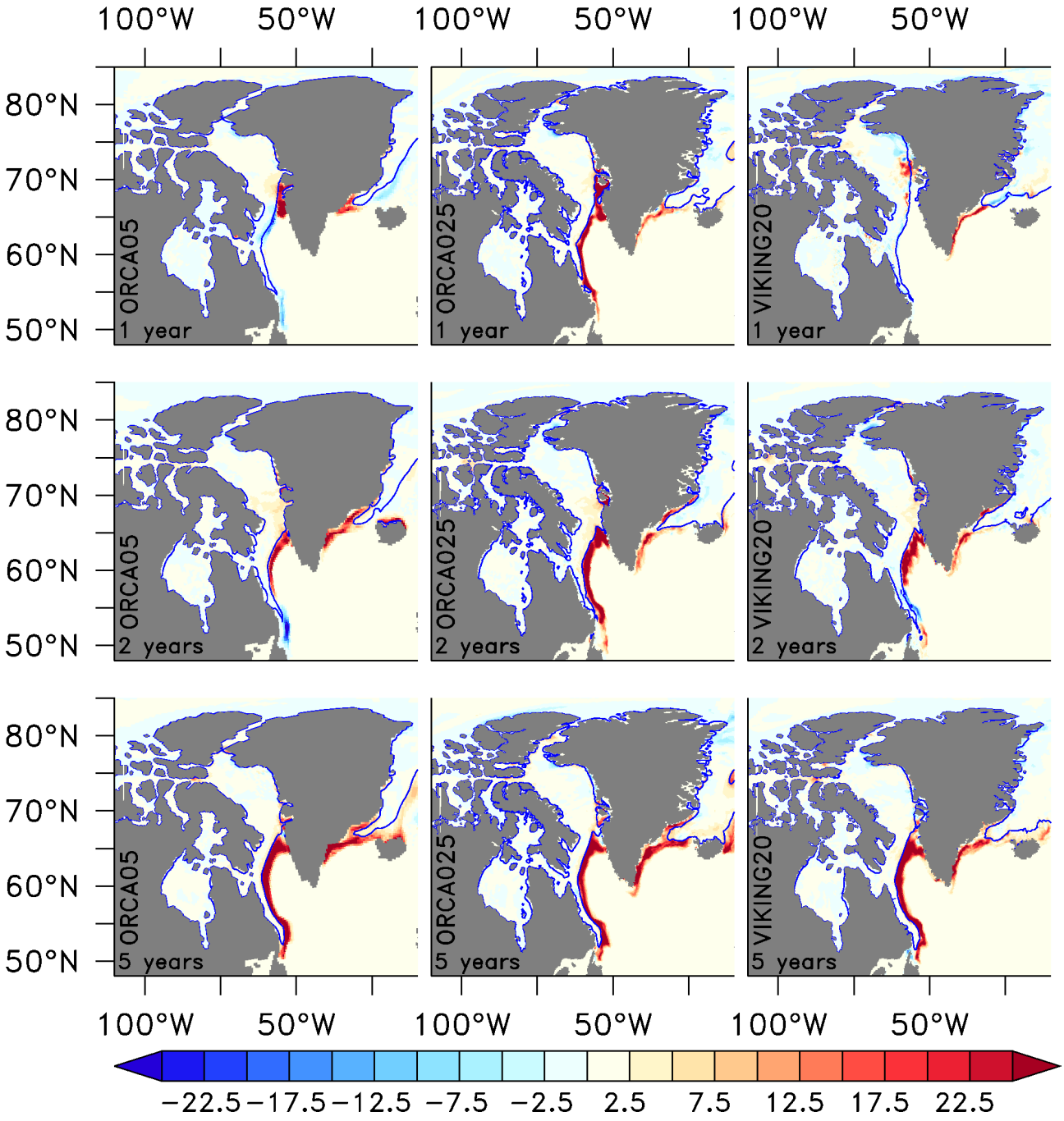

Figure 31.: Anomalies of the March sea-ice concentration for the different configuration (%) for the first 5 years of the hosing simulation. The blue contour line indicates the sea ice edge in the reference simulation during the same period (75% level).

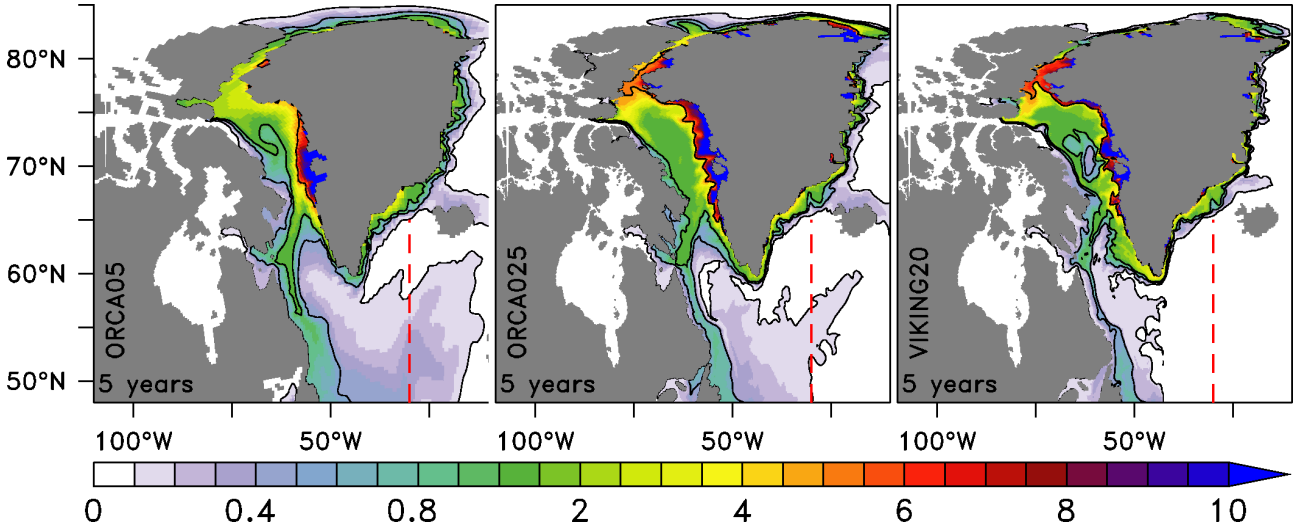

Figure 32.: Spreading of the additional meltwater: Surface initial tracer spreading in the different configurations (in 10^{-3} m^3/m^3) after 5 years of the hosing simulation (is based on monthly means). Contour lines represent concentrations of 0.1, 0.5, 1 and 5 $\times$ 10^{-3} m^3/m^3. The red dashed line is for visual guidance to gauge the eastward spreading of meltwater into the subpolar North Atlantic.

Summary of the short-term and local response

During the initial to short-term response over the first 5 years of melting, anomalies emerge from the release area along the Greenland coast, propagate with the main circulation into the Baffin Bay and the Labrador Sea and penetrate into the interior. For this period anomalies in the realistic melting scenario are small compared to natural variability. A surface freshening of the boundary currents of Greenland is present and anomalies exceeds in the I-MELT scenario -1 psu after 1 year. This freshening goes along with a surface cooling (lower than -1 °K) over the EGC and WGC south of 65°N and a surface warming ($\sim$ 0.2 °K) north of Greenland. The freshening and cooling cause an extension of the sea ice edges in the Labrador Sea and Irminger Sea. The eastward penetration into the subpolar North Atlantic is affected by the representation of the NW Corner and the actual stochastical state of the eddy field associated with the NAC. In both coarser configurations this eastward spreading over the subpolar North Atlantic is enhanced compared to VIKING20, which characterises the most prominent difference between the configurations. Despite that, differences in the spreading of the freshwater into the Labrador Sea are seen, with implications for the response to the deep convection. The coarse ORCA05 shows the largest and fastest freshwater spreading into the region. In ORCA025 the freshwater penetrates only from south accomplished by recirculations from the Labrador Current into the interior Labrador Sea. The WGC eddies in VIKING20 cause for an additional contribution from the north in comparison to ORCA025 during that time.

5.2. Response of the Labrador Sea

After investigating the short-term and initial implications, the effect on the long-term regional scale is explored. The focus is on the Labrador Sea, since the deep winter convection in that area is the trigger for further large scale changes, presented later. In the subsections 5.2.1 and 5.2.3 changes in the Labrador Sea will be discussed, and associated responses in dense water formation in section 5.2.2. Changes in the dense water formation rates have potential implications for the SPG circulation and for large scale anomalies (section 5.2.4). Specifically, changes in the SPG transport influence the northward transport of freshwater and heat into the Nordic Sea (Levermann and Born (2007)). That area is crucial for the formation of overflow water masses, that feed the lower limb of the AMOC. The evolution in the Nordic Seas is discussed in the next section (5.3), because of its importance on the large scale behaviour.

5.2.1. Spreading of freshwater anomalies

In the following the area-mean over the interior Labrador Sea (the area is marked with CL in Figure 8) is taken to show the time evolution of anomalies in response to a melting of the GrIS.

Response in the I-MELT scenario

The upper panels (a) of (Figure 33) show the temperature anomalies compared to the control simulation. Over the entire hosing period (43 years) a cooling of the near surface waters ($<$ 100 m) is present, exceeding values of about 1.5 °K. Below that layer a positive anomaly emerges due to the reduction in the replenishment of dense cool water masses by deep convection. The depth of convection is indicated by the black curve, representing the MLD in the control simulation and the red curves in the melting simulation (March values). The mixed layer depth in the control simulations shows the expected interannual variations with NAO related peaks in the early 1970s, 1980s and 1990s. During these periods pronounced deep water formation was observed (Yashayaev and Loder (2009)). The largest interannual amplitudes with respect to convection are seen in ORCA025. That is related to the described shortcoming in the overestimation of convection due to the missing of the eddy related effect (increasing the stratification, see section 3.2). Lowest interannual variations are found in VIKING20, pointing to a very variable pattern of convection, related to the stochastic eddy distribution. The same behaviour is also seen in the LSW production rates. However, peaks in the 1970s, 1980s and 1990 are visible, indicating phases of higher convection activity. The convection in the hosing simulation is shut down ($<$ 100 m) approximately after 5 years, while ORCA025 still show some shallower (800 m) convection events still in the mid 1970´s (see also LSW production diagnostic in section 2.3.3 and 5.2.2). At the end of the hosing simulation the positive temperature (mid depth) anomaly seems to switch to a negative sign related to a decrease in the meridional heat transport (see section 5.4.3).

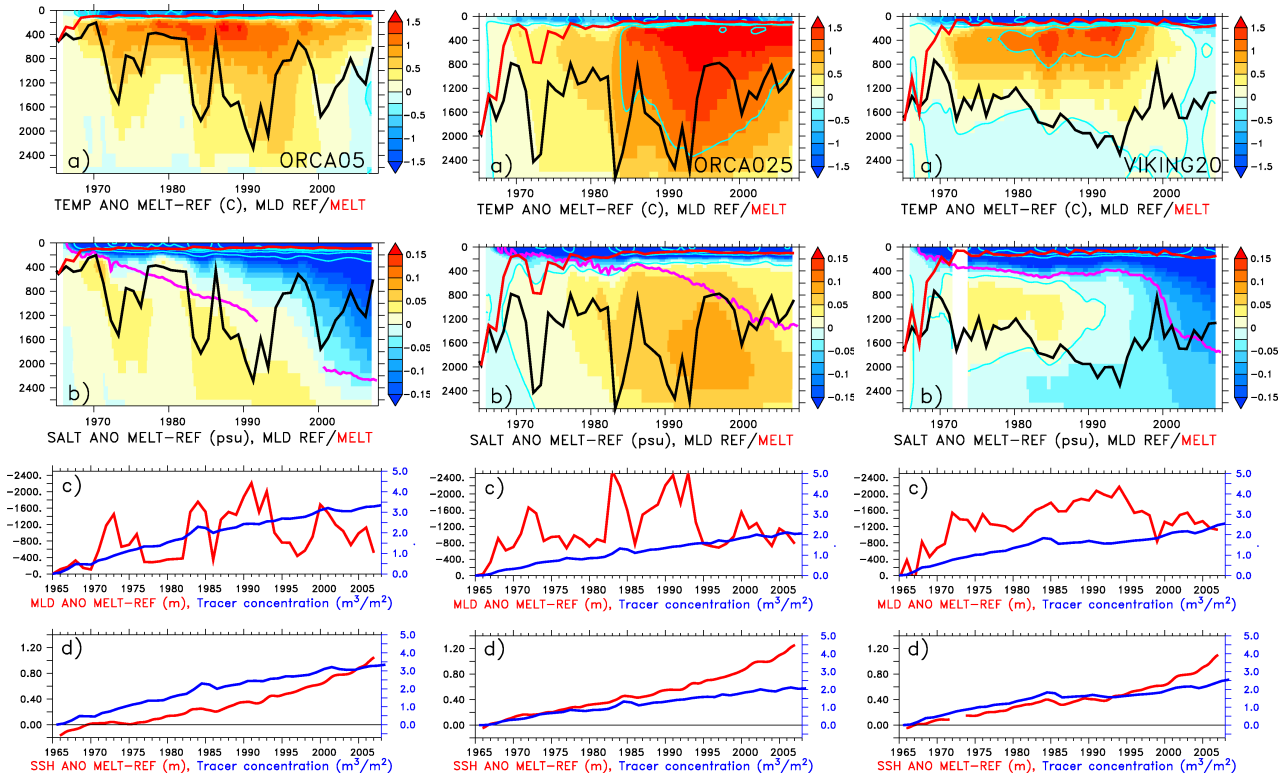

Figure 33.: Hydrographic anomalies between hosing (I-MELT) and reference (REF) simulation in the different model configurations: (a) temperature (in °K, light blue contour lines mark a 1°K interval), (b) Salinity (in psu, light blue contour lines mark a 0.5 psu interval), (c) March-MLD (m, in red) and vertical integrated passive tracer concentration (m^3/m^2, in blue) and (d) SSH (m, in red) and vertical integrated passive tracer concentration (m^3/m^2, blue). The thick lines in (a) and (b) indicate the March-MLD in the reference (black) and hosing (red) simulation. The magenta line in (b) mark the 0.0006 m^3/m^3 isosurface of the passive tracer. All anomalies are interannually filtered.

The salinity anomalies, (second panel, (b)) show a surface enhanced freshening slowly penetrating to depths of around 2000 m. An exception represents ORCA025 where the negative anomalies stays at the ocean surface over the entire hosing period. ORCA025 shows the largest positive anomaly below 400 m from 1975 onward instead. The slight positive anomaly is related to the reduced replenishment of LSW, also present in VIKING20, which does not last over the entire hosing period. The magenta line indicates the presence of meltwater from Greenland derived from the passive tracer concentration (contour line mark 0.0006 m^3/m^3). In ORCA05 and VIKING20 this line follows nicely the downward penetration of the negative salinity anomaly, which is not seen in ORCA025. It is noteworthy that the deep negative freshening signal in VIKING20 emerging after 1980 is not directly related to the presence of Greenland meltwater, implying that this anomaly is induced by circulation changes instead. Less fresher water is carried in this depth range into the Labrador Sea. The distinct reasons have to be investigated further, but might by related to enhanced meridional freshwater transport in VIKING20 (Figure 65) during that time.

The third panel row shows the linkage between the amount of meltwater (vertical integral, blue curve) and March MLD anomaly (red curve). The amount of meltwater (tracer) increases in all simulations, largest in ORCA05, weaker in VIKING20 and lowest in ORCA025 and reach values of 3.2 m^3/m^2, 2.5 m^3/m^2 and 2 m^3/m^2, respectively at the end of the hosing simulation. Taking VIKING20 as reference, leads to the conclusion that the coarse model (ORCA05) overestimates the transport of meltwater into the interior Labrador Sea and ORCA025 underestimates that transport, but overestimates the related MLD response.

Related to the changes in the LSW formation are changes in the strength of the SPG, reflected in the SSH in the central Labrador Sea. The SSH response is shown in the lower panel row ((d), red curve). A steady increase is common feature among all configurations. A SSH rise of about $\sim$ 1.0 m over the 43 year long hosing simulation is seen in the interior Labrador Sea in all configurations coincident with the increasing meltwater amount (blue curve), with a closest linkage in VIKING20. The discrepancies after 2000 are obviously caused by changes in the large scale circulation and not directly related to the amount of meltwater. The global SSH rise in a 0.1 Sv melting scenario is $\sim$ 8.8 mm/year (Wang et al. (2012)), accumulating to 37.8 cm over a 43 period. That estimate indicates that local changes in the interior Labrador Sea are approximately 3 times larger than the expected global mean rise, pointing to a strong regional varying pattern (see Figure 49), consistent with studies by (Landerer et al. (2007); Cronin (2012)). The observed SSH rise from 1961 to 2003 account for 1.8 mm/year (Pokhrel et al. (2012)), which reflects that the proposed raise is about 5 times larger than the observed trend; (since 1993 a trend of $\sim$ 3 mm/year is observed (IPCC 2013)). Despite the general similar response in all different configurations, differences are seen with respect to the timing, magnitude and depth penetration. Some differences are caused by the differences in the general convection pattern, but also by enhanced lateral mixing of freshwater from the boundary into the convective region in ORCA05 (see also Figure 28) compared to VIKING20.

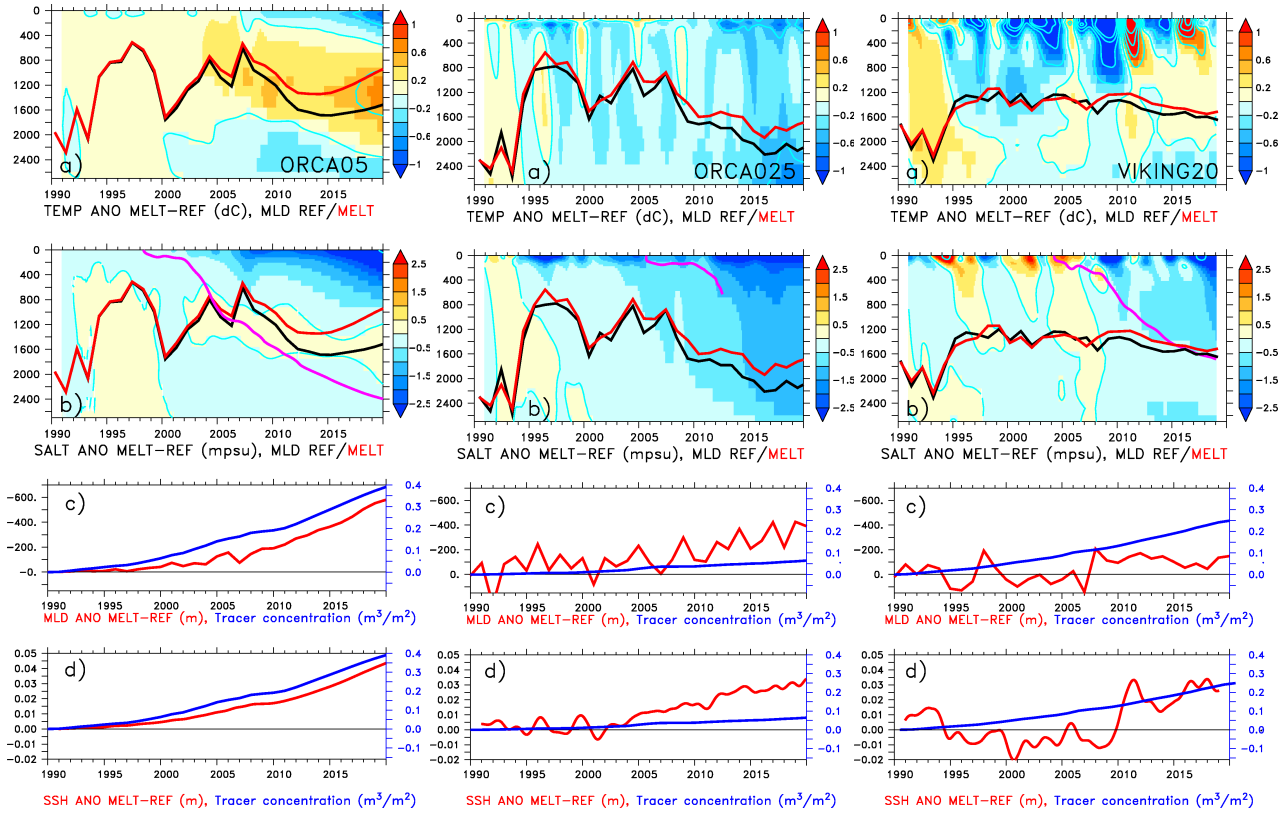

Figure 34.: Hydrographic anomalies between hosing (R-MELT) and reference (REF) simulation in the different model configurations: (a) temperature (in °dK, light blue contour lines mark a 0.5°dK interval), (b) salinity (in mpsu, light blue contour lines mark a 5 mpsu interval), (c) March-MLD (m, in red) and vertical integrated passive tracer concentration (m^3/m^2, in blue) and (d) SSH (m, in red) and vertical integrated passive tracer concentration (m^3/m^2, in blue). The thick lines in (a) and (b) indicate the March-MLD in the reference (black) and hosing (red) simulation. All anomalies are interannually filtered.

Response in the R-MELT scenario

With realistic runoff from Greenland the expected anomalies should be smaller (Figure 34), due to the much lower released amount of meltwater compared to the idealised melting scenario at similar stages. Interestingly, the temperature anomaly (upper panel, (a)) follows only in the coarse ORCA05 the behaviour of the idealised scenario. A cooling at the surface and a warming signal at depth (400 m - 2000 m) is observed. (Note that the results beyond 2007 use an artificial repeated atmospheric forcing with no further interannual variability; in principle it can be argued that the hosing induced tendency is persistent beyond 2007). It is also interesting that the above seen strong warming in ORCA025 is not observable in the realistic melting scenario. A general cooling tendency by $\sim$ -0.05 °K is present instead. The VIKING20 results show a strongly varying signal which is associated with the presence of individual eddies. A clear temperature signal is therefore not seen over the 30 year long simulation period. With respect to the March MLD response, the largest decline of the MLD by $\sim$ -500 m (REF MLD (black) and R-MELT (red)) occurs in ORCA05, while ORCA025 ($\sim$ -400 m) and VIKING20 ($\sim$ -100 m) show a much weaker response, respectively.

The salinity anomalies in (b) exhibit the already above described (surface intensified) freshening signal superimposed by mesoscale variability in VIKING20. The freshening exceeds -0.025 psu in the near surface layer around 2010. The deepest penetration of the freshening below 2000 m is visible in ORCA025, while ORCA05 and VIKING20 suggest anomalies to stay in the upper 1200 m, and further developing (intensifying) over the hosing period. The penetration of anomalies to depth below 2000 m in ORCA025 suggest a too deep convection during winter time, which is consistent with earlier results (section 3.2).

The above suggested close relation between the presence of meltwater (blue curve) and the reduction of convection (red curve) now only holds (third panel row, (c)) for ORCA05. With higher resolution this relation seems to fade or being more affected by the mesoscale variability, especially in VIKING20. ORCA05 shows the largest meltwater amount (0.4 m^3/m^2) and the largest MLD response. ORCA025 on the other hand shows the lowest meltwater amount (0.1 m^3/m^2) with a lower MLD response, while VIKING20 shows an intermediate amount (0.25 m^3/m^2) of meltwater but nearly no response in the depth of convection.

Concerning the evolution of the SSH anomaly (lower panel, (d), red curve), the results suggest a rise by 3-4 cm over the 30 year long simulation (global mean 2.75 cm), closely linked to the amount of meltwater in ORCA05. ORCA025 and VIKING20 suggest a relative large amplitude of natural variability in the SSH anomaly, largest in VIKING20, superimposed of a positive tendency. The decline between 1990 to 2010 in VIKING20 could be related to the NAO condition, which cause an increase of SPG circulation and an according decrease in SSH. Due to a larger decrease in the mixed layer depths at this stage in both coarser models, these atmospheric anomaly might be inhibited to speed up the SPG.

Summary

In the idealised scenario a cooling and freshening (larger than -1 °K and -1 psu) of the near surface layers and some warming of intermediate layers (normally ventilated) is seen in all configurations. The cooling and freshening signal in the idealised scenario seems to be present in the realistic scenario as well, but with a distinctly weaker magnitude and superimposed by natural (mesoscale) variability in the higher resolution configurations. The prominence of such stochastic variability makes it difficult to trace the melting related signals in those configurations under realistic meltwater forcing. The projected warming (of the ventilated layer) in the idealised simulations is not seen in the realistic scenarios. An exception represents the coarse ORCA05, due to a larger impact on the convection induced by larger cross-shelf transports of freshwater in the interior compared to the other configurations. In the idealised case after a few years ($\sim$ 5) the convection is shut down which is not seen under a realistic melting scenario. In these realistic simulations the largest reduction is present in ORCA05 ($\sim$ -500 m) and significantly reduced with increasing resolution. The SSH rise is projected to be between 1.2 m and 3-4 cm in the idealised and realistic scenario at the end of hosing simulation, respectively. That

rise is distinct larger than the global mean. In general, the impact of the melting scenario seems to be crucial for the response on the convection. A fast shutdown of convection within a few years only occurs in the idealised melting scenario but not under realistic meltwater forcing. In addition, in the 0.05°-case with resolved mesoscale eddies, nearly no change in the convection is encountered. That behaviour points to some compensating effects when eddies are explicitly resolved, i.e.changes in the path of the WGC eddies in idealised melting scenario.

5.2.2. Labrador Sea Water formation

In the following, a revised integral diagnostic for the convection strength in the Labrador Sea is used. This diagnostic is based on the production rates of dense water masses being formed during the winter time convection in the Labrador Sea. The diagnostic is similar to diagnostics presented by Kieke et al. (2007); Rhein et al. (2011, 2002). They calculated production rates from CFC concentrations in a certain density range. The water mass was then associated as LSW water (sigma interval 27.74 - 27.8). Details of the computation of LSW production rates are provided in section 2.3.3. Observations suggest rates between 8 and 11 Sv during NAO^+ years, while the production reduces to 2 Sv during "normal" atmospheric conditions (Rhein et al. (2002)). Figure 35 shows the estimated production rates for the individual configurations for the control simulations (black), I-MELT (blue) and R-MELT (red). ORCA025 and VIKING20 show production rates within the observed range, with some interannual variations. Some differences from observational estimates are expected due to differences in the computation of the LSW formations rates. ORCA05 overestimates the production of that water mass by a factor of two compared to observations and to the other configurations. There are also certain periods where no LSW production takes place (e.g. in 1970 in ORCA05). The other configurations always suggest a yearly LSW production rate by at least 2 Sv. Only ORCA05 shows a strong connection to the NAO phase, with distinct positive peaks during NAO^+ phases. Both higher resolution configurations show during theses phases also some slight increase, but especially in VIKING20 the interannual variability is dominated by other factors, probably by the amount of WGC eddies or due to the methodology. With respect to the larger convection pattern in ORCA025 (see section 3.2), it seems counter intuitive that ORCA025 produce less LSW than ORCA05. But the deep density structure in Labrador Sea was not taken into account in the previous "pure" March MLD diagnostic. The density structure of the Labrador Sea is shown in section 5.2.3 and reinforces the calculated LSW rates for ORCA05 and ORCA025.

The response in the I-MELT scenario (blue curves) leads to a fast shut down of LSW production in all configurations (within 5 years), slightly longer retained in ORCA025 (anomalies are shown in Figure 36). However, a northward shift of the WGC eddy pathway is observed in VIKING20 in the I-MELT scenario (not shown). This shift seems to be connected with the boundary current transport and formation processes of the WGC eddies near Cape Desolation. That shift produces a lower meltwater transport accomplished by WGC eddies into the central Labrador Sea, which counteracts

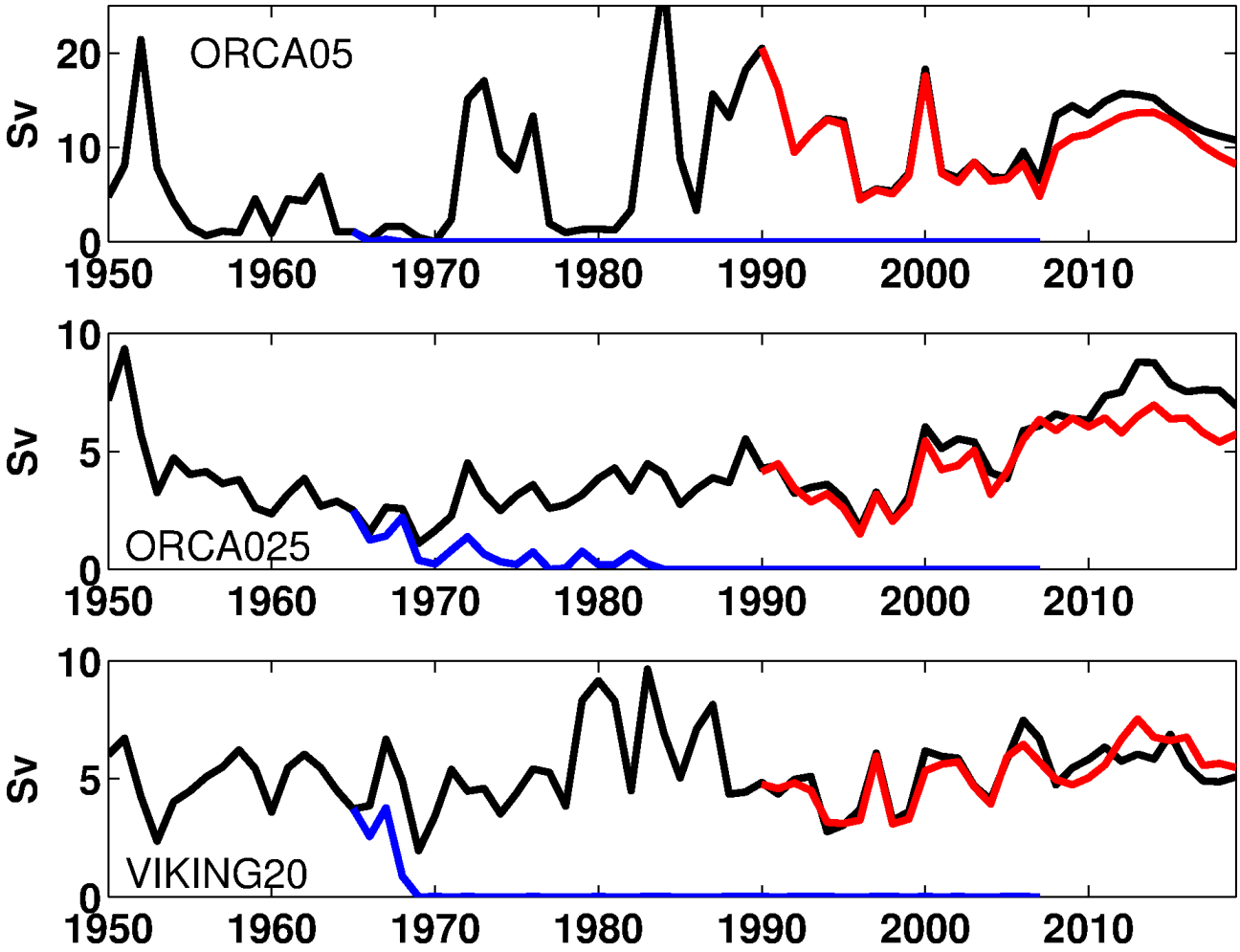

Figure 35.: Annual Labrador Sea Water production rates in the different model configurations in Sv. The reference simulation is illustrated in black, the I-MELT scenario in blue and the R-MELT scenario in red. For details of the computation see section 2.3.3.

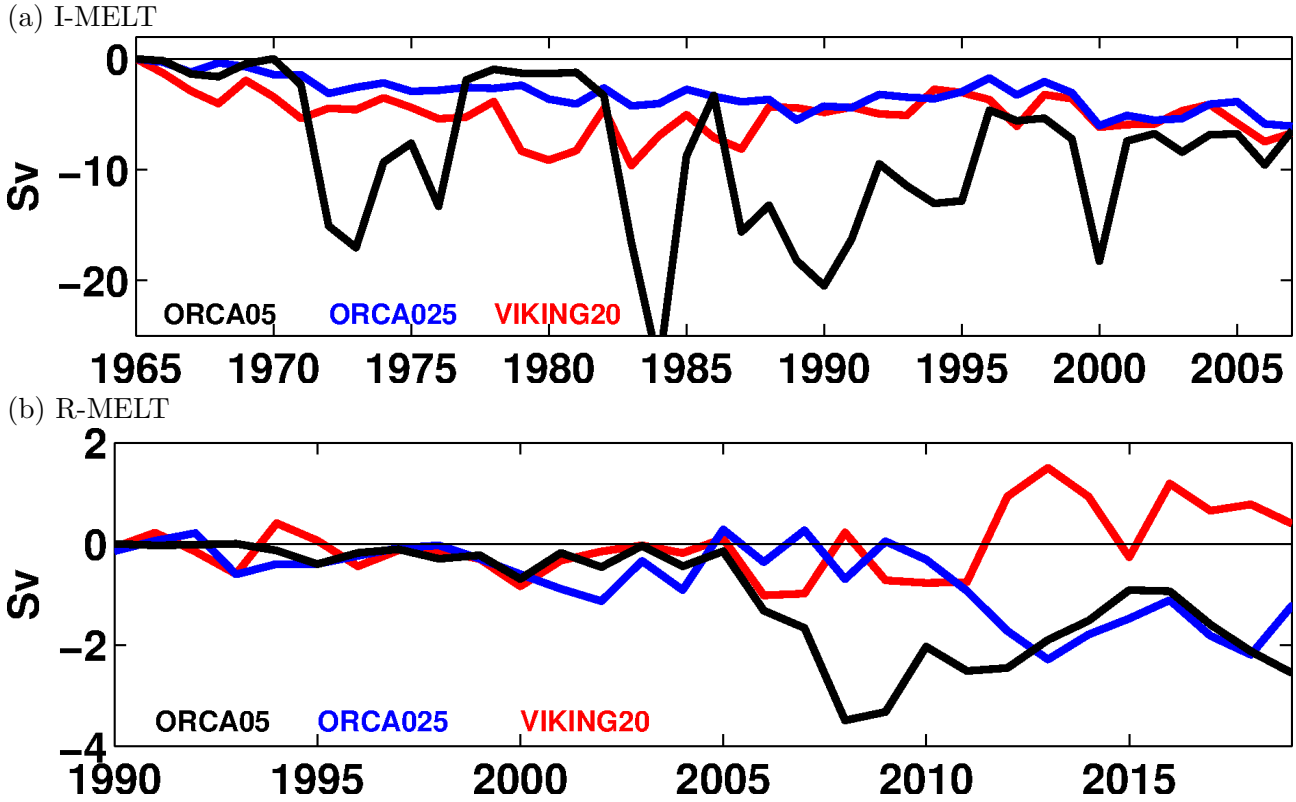

Figure 36.: Annual Labrador Sea Water production rate anomalies in Sv for the different model configurations for the I-MELT scenario in (a) and R-MELT scenario in (b).

the additional meltwater forcing. The northward pathway should support deep convection in the end. Nevertheless, that mechanism seems to be small compared to the amount of additional meltwater being released, and in consequence a similar response among all configurations is observed. In the realistic melting scenario production rates decrease by only $\sim$ -2 Sv in ORCA05 and ORCA025 after 30 years (Figure 36), while production rates slightly increase ($\sim$ 1 Sv) in VIKING20 above rates of the control simulation. That indicates again a possible counteracting mechanism related to the resolved mesoscale eddies in VIKING20 in comparison to ORCA025 and ORCA05. These results also confirm the findings derived from the area-mean diagnostic in the central Labrador Sea above (see Figures 33 and 34). An exception is VIKING20 in the R-MELT case. In that simulation VIKING20 shows a slight ($\sim$ 100 m) decrease in the convection depth at the end of the R-MELT simulation (MLD-diagnostic), while the LSW production rate suggests a little increase in the production of dense water masses with implications for the SPG strength.

5.2.3. Hydrographic changes across the Labrador Sea (AR7W section)

In this subsection the hydrographic properties along the hydrographic section AR7W will be discussed. This diagnostics is important to identify changes in the boundary current, which play a crucial role for the propagation and advection of anomalies in the interior Labrador Sea. (see also section 3.4 for

a comparison of mean hydrographic quantities along AR7W to observations)

Response in the I-MELT scenario

In the following the time evolution of anomalies in I-MELT scenario is investigated. Differences are based on monthly means at certain times after the hosing has started. The salinity anomalies (Figure 37) show the expected freshening in the surface layer originating from both boundary currents at the Canadian and Greenland coast. A pronounced freshening ($\sim$ -0.5 psu) is visible at the Greenland coast already within the first year. Negative anomalies above -0.3 psu cover the upper 100 m along the section after 5 years. In the VIKING20 configuration some freshening penetrates to depth (500 m) in the interior Labrador Sea. That behaviour is not present in the other configurations. This spreading is possibly induced by WGC eddies carrying a part of the meltwater from the WGC directly into the convective region (also confirmed by tracer analyses). The surface freshening continues over the entire hosing period and exceeds values of -1 psu. Unexpectedly, positive anomalies occur in ORCA025 after 20 years small in the depth range between 250 - 2500 m, which are not present in both other configurations. Meanwhile, VIKING20 exhibits a freshening in the DSOW range, which is clearly visible at the Greenland coast (freshening of about -0.15 psu).

The corresponding temperature anomalies are shown in the Figure 38. A cooling of ($\sim$ -0.5 °K) the WGC within the first year is a common feature among all configurations. The cooling progresses during time and spreads over the entire section in the upper 200 m, and reaches values up to $\sim$ -2 °K. This cooling is induced by a increased stratification due to the additional meltwater, which results in a decrease of the winterly convection, especially during winter seasons. As consequence of this decrease an opposing warming signal develops in the depth range of the previously ventilated water column. That signal is slowly enhancing and penetrating further to depth over time. The positive temperature anomaly exceeds 1.5 °K and is most striking in ORCA025, which is connected to the overestimation of the Labrador Sea convection in this configuration. It should be mentioned that this deep warming switches after 3-4 decades the signal, due to a reduction of the meridional heat transport (see 5.4.3) to the north induced by a overturning weakening.

The combined effect of temperature and salinity changes on density (σ_0) is displayed in Figure 39. The contour lines (iso-values 27.6, 27.7, 27.8 and 27.9 kg/m^3) indicate the mean state of the reference simulation at that time to guide the interpretation of the anomalies. Negative anomalies are developed within the first year in the coastal currents at the Labrador and Greenland coast. This negative anomaly progresses during time further into the interior Labrador Sea and to depth and counteracts the “normal” cross-section density gradient. As consequence the horizontal pressure gradient reduces over the Labrador Sea and induces a decrease of the SPG circulation over that period. (see section 5.2.4)

The according velocity changes are shown in Figure 40. The mean flow direction of the reference

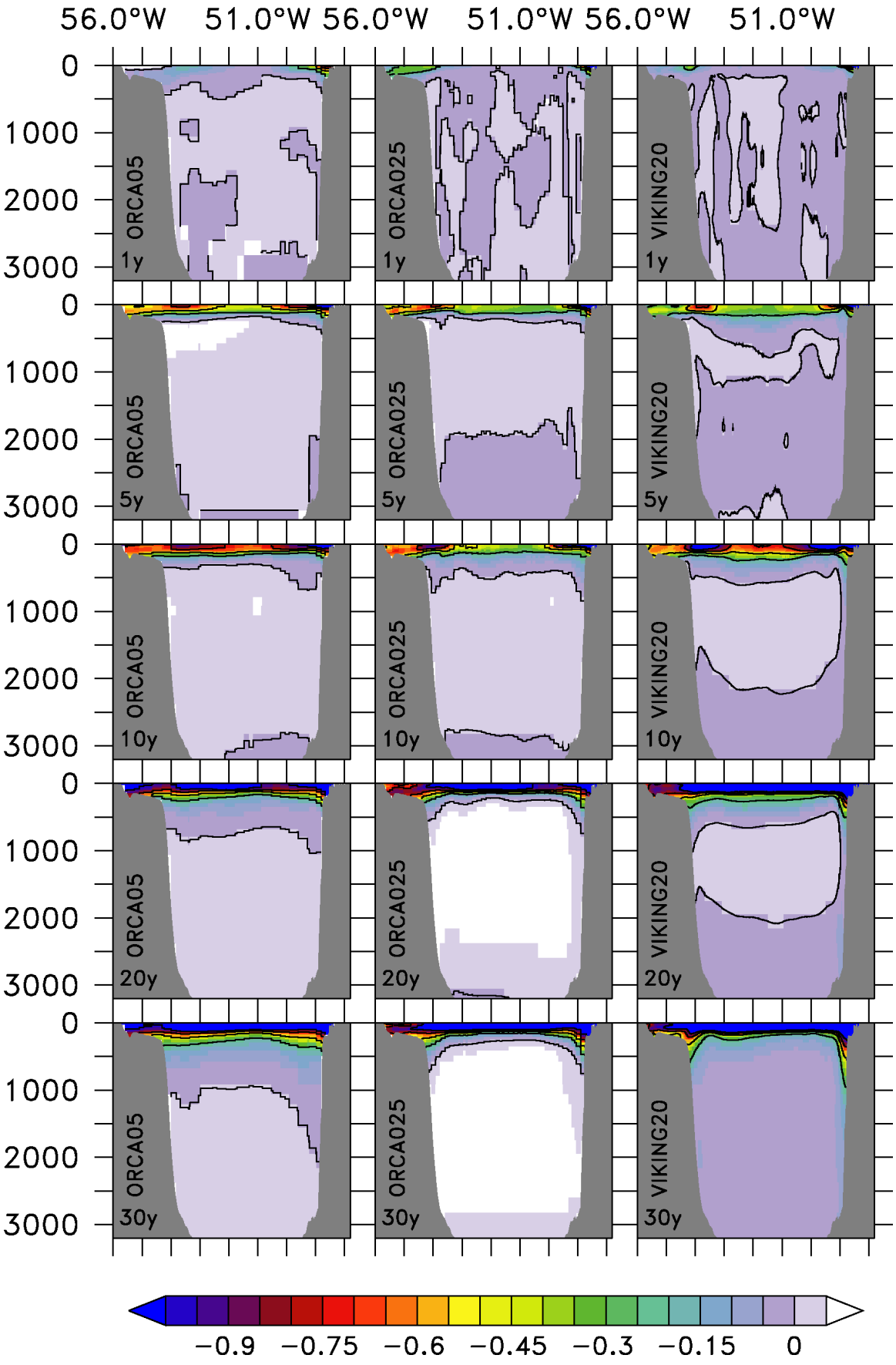

Figure 37.: Salinity anomalies (psu, are based on monthly means) between I-MELT and reference simulation along the AR7W section in the different model configurations for the first 30 years of the hosing simulation. Each 0.25 psu interval is contoured.

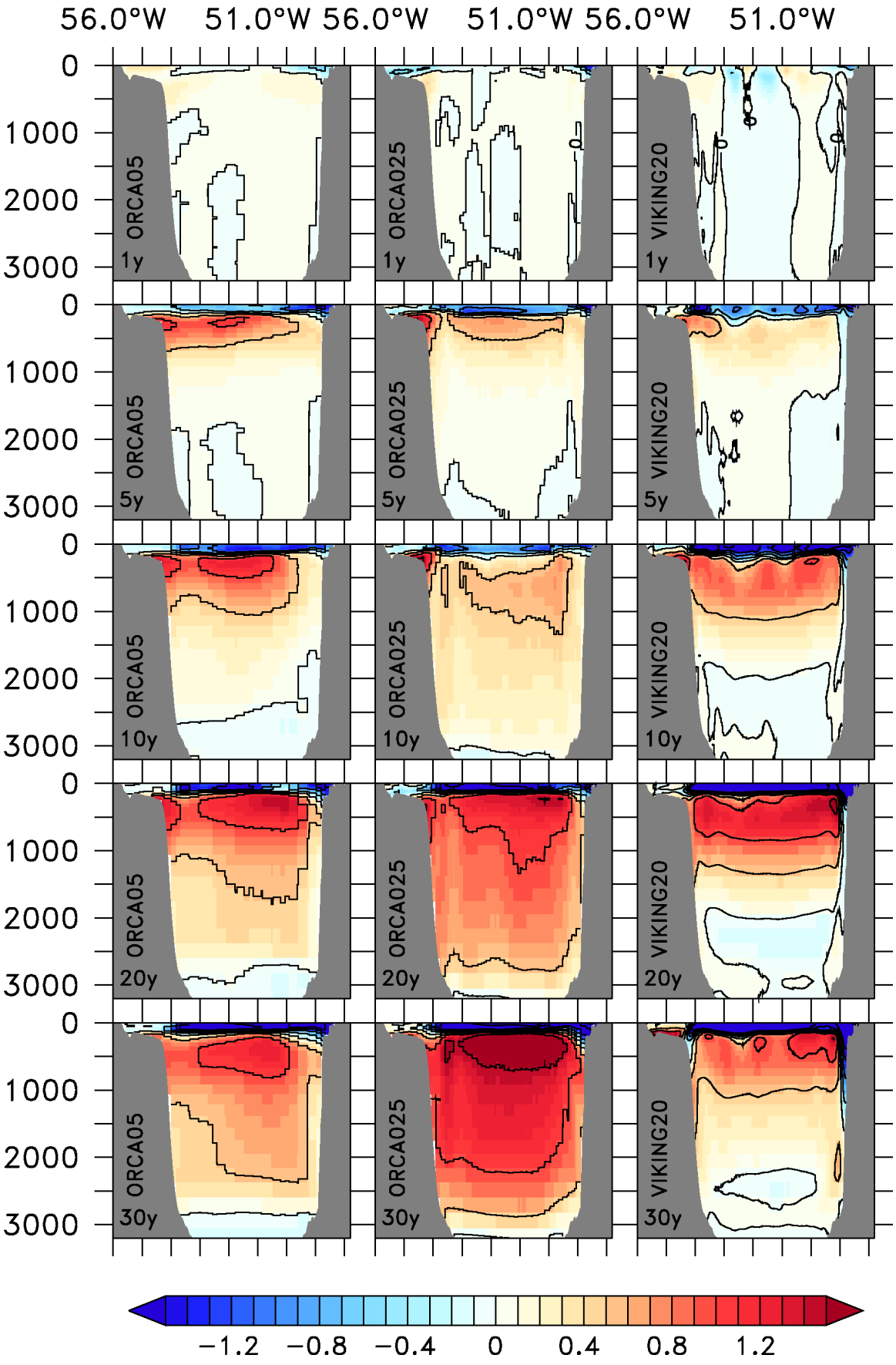

Figure 38.: Temperature anomalies (°K, are based on monthly means) between I-MELT and reference simulation along the AR7W section in the different model configurations for the first 30 years of the hosing simulation. Each 0.5 °K interval is contoured.

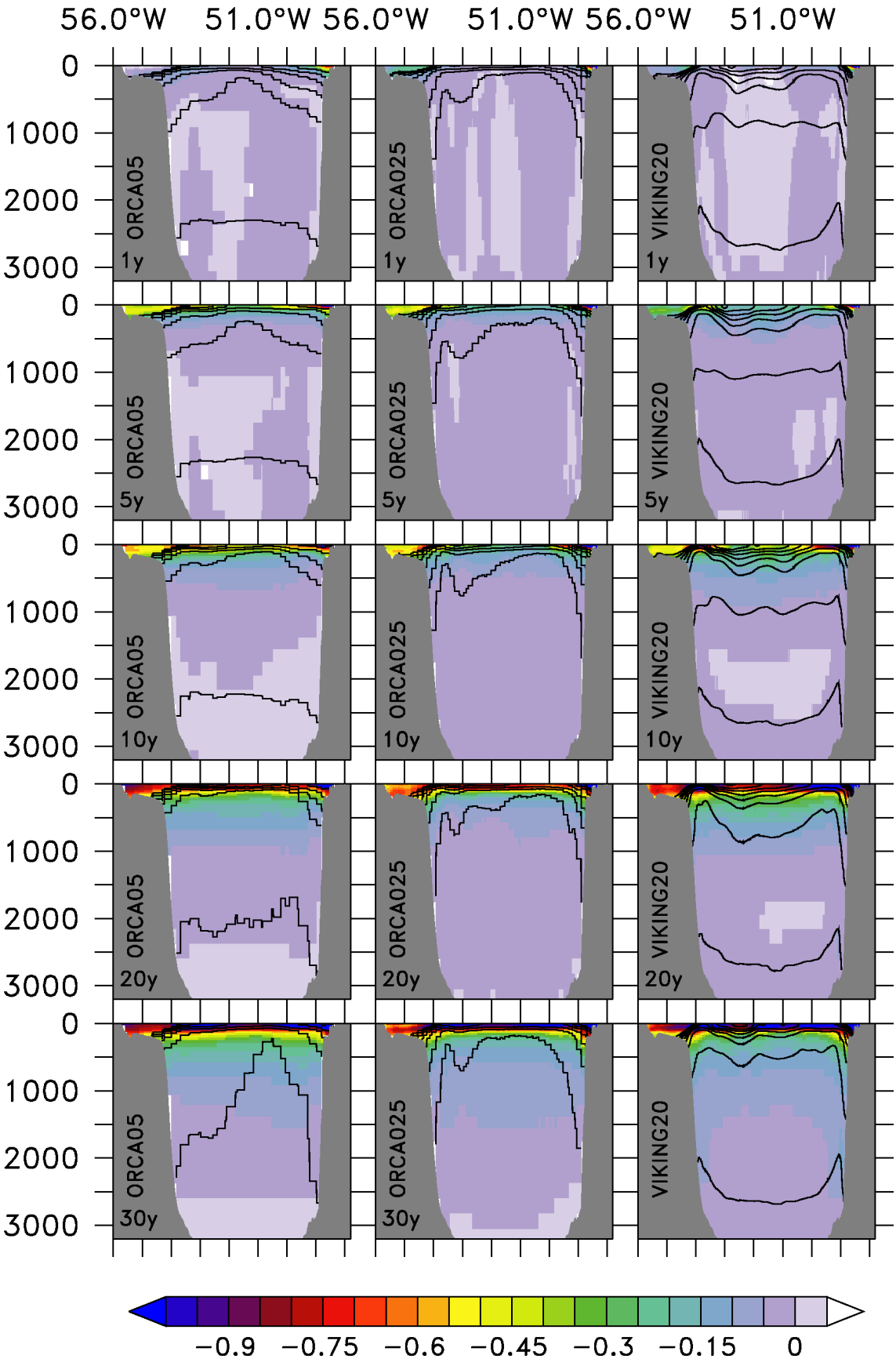

Figure 39.: Sigma density anomalies (σ_0,kg/m^3, are based on monthly means) between I-MELT and reference simulation along the AR7W section in the different model configurations for the first 30 years of the hosing simulation. The levels between 27.2 kg/m^3 and 28.2 kg/m^3 with a 0.1 kg/m^3 interval from the reference simulation are contoured.

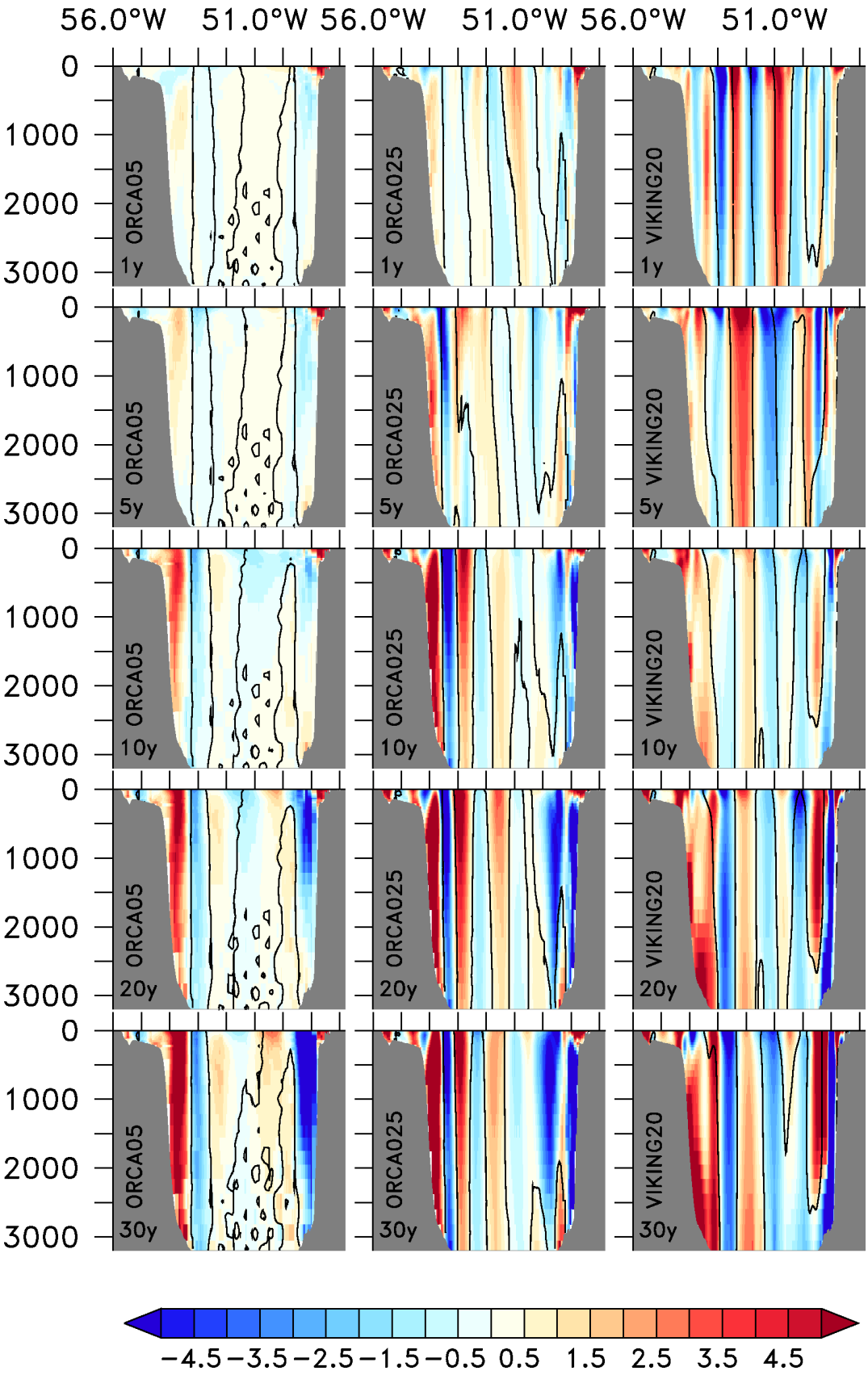

Figure 40.: Cross section velocity anomalies (cm/s) along the AR7W section in the different model configurations for the first 30 years of the hosing simulation, are based on yearly averages. The 0 level from the reference simulation are contoured to identify the direction and shifts of current bands. The large positive anomaly at 54°W after 10 years indicate a weakening of the current from the Labrador Sea to the subpolar North Atlantic. At the Greenland coast (49°W) a weakening is indicated by the negative anomaly at the continental slope.

simulation is again visualised by the contour line (0 contour) of the cross-section velocity during the individual periods. The corresponding anomalies are shown in colour. An immediately strengthening of the shelf currents at the Greenland coast (positive anomaly, upper 200 m) is present in all simulations east of 49°W. Further off shore, the current speeds into the Labrador Sea are decreased (negative anomalies) as suggested by the density changes after 3 decades. A related weakening at Labrador coast (positive anomaly) is also present and pointing to an overall weakening of the SPG circulation over the 3 decades. The largest changes at the Labrador coast occur in ORCA05 and ORCA025 in the upper 2500 m (weakening of currents speeds indicated by positive anomalies). However, VIKING20 indicates relative little changes in that depth range in comparison to both other configurations. VIKING20 reveals the largest changes in the overflow (DSOW) depth instead, which is present at depth below 2500 m and present at both coasts.

Response in R-MELT scenario after 30 years

In the following paragraph anomalies after 30 years in the R-MELT scenario (Figure 41) are presented, similar to the I-MELT scenario results above. First of all it seems clear, that the anomalies in the R-MELT scenario are much weaker compared to the I-MELT scenario, due to lower freshwater release in that scenario during that time. Many anomalies are small compared to the natural variability over the first decades (not shown). That is the reason why anomalies are only presented at the end of the hosing simulation (after 30 years) with adapted anomaly ranges. Negative salinity anomalies (Figure 41, first panel) are concentrated at the boundary currents (as in the I-MELT results) in the shelf regions with deviations of -0.1 psu from the references state. While in ORCA05, the negative anomaly covers nearly the entire surface of the Labrador Sea, the anomalies are much weaker in ORCA025 and hardly seen in VIKING20 at all. In this configuration a fresh anomaly occurs in a subsurface band between 500 m - 1500 m, while the surface layer shows a lower freshening compared to the subsurface interior central Labrador Sea. In comparison to the I-MELT scenario no positive anomaly is found in ORCA025, but some small positive anomalies are visible in ORCA05 at the Canadian coast in the depth range of 1000 m - 1500 m and penetrating into the central Labrador Sea.

The reason for that salinification in ORCA05 are yet unknown, but coincides with positive temperature anomalies and lower current speeds (Figure 41, 2nd panel) at this locations. These anomalies are probably induced by lower transports and indicating lower freshwater transport at that depth layer. At that point it is unclear if this is a robust and persisting pattern. The temperature anomaly pattern shows the earlier described (I-MELT) surface cooling in ORCA05 and ORCA025 with temperature changes around -0.1 °K. Due to the presence of eddies the anomaly pattern in VIKING20 is highly affected. However, the higher resolution configurations suggest a cooling near the coastal regions, i.e. in the shelf currents and the deep layers at the Greenland coast. The slight warming signal in the interior is induced again by a reduction in the winterly convection.

The combined effect of T and S changes on the density (σ_0) are presented in the 3rd panel (Figure 41).

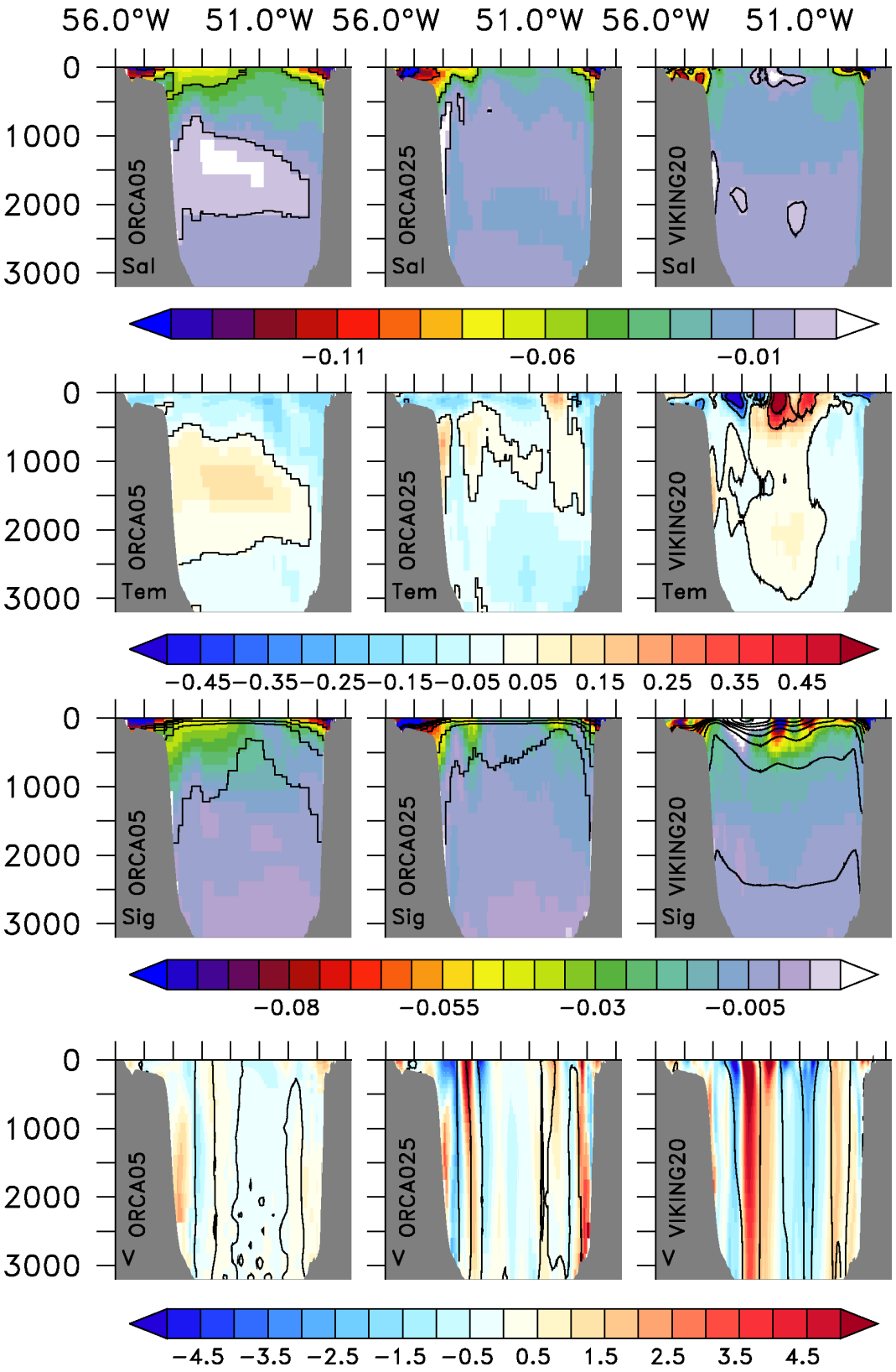

Figure 41.: Anomalies along the AR7W section for hydrographic quantities in the different configurations after 30 years in the R-MELT scenario. Upper panel shows salinity anomalies (psu), in the panel below temperature anomalies (°K) are illustrated. The panel beneath shows sigma anomalies (kg/m^3, σ_0) and cross section velocity anomalies (cm/s) in the bottom panel. Salinity contour lines mark each 0.05 psu interval and 0.25 °K for temperature. The sigma levels between 27.2 and 28.2 are marked with a 0.1 interval from the reference simulation and the 0 velocity contour of the reference simulation in the bottom panel.

Overall the earlier described response in the I-MELT scenario with negative anomalies at the surface is confirmed in the R-MELT results. The reduction is pronounced in the coastal shelf regions (exceeding -0.1 kg/m^3). Due to the spatial pattern of these negative anomalies the effect on the barotropic gyre transport is not straight forward as in the I-MELT simulations, which indicated a decrease. (Results from the barotropic streamfunction are provided in section 5.2.4)

However the anomalies of the current speeds suggest a strengthening of the currents at the shelf of Greenland (positive anomaly) and in the deep layers below $\sim$ 1500 m at least in ORCA025 and VIKING20 (contrary to I-MELT) results. ORCA025 exhibits a pronounced signal at the continental slope of Greenland (positive anomalies). An overall weakening instead is seen at both shelfbreaks between 500 m and 1500 m, which is robust among all configurations. At the Labrador coast a net strengthening effect is visible in ORCA025 and VIKING20, which is concentrated in the near surface and overflow layers. That strengthening is also visible at the Greenland coast (positive anomalies). ORCA05 confirms that increase but shows the smallest increase in comparison to the other configurations.

Summary of the melting response on hydrographic quantities along the AR7W section:

Irrespective of the configurations and melting scenario, all simulations showed surface intensified anomalies. These anomalies appear first in the source region at the Greenland coast and propagate within the boundary currents around the Labrador Sea. Therefore the largest signals are visible in boundary currents over the entire period. Due to lateral mixing processes anomalies reach the interior and affect the deep water formation, which results in subsequent anomalies. The largest lateral mixing exhibits ORCA05.

Inconsistencies between the melting scenarios are seen in the transports of boundary currents. The I-MELT results suggest a weakening signal of the entire boundary current system over the first 30 years. The R-MELT scenario exhibits a strengthening of the deep and surface currents instead after 30 years and a slight weakening at the intermediate depth levels (500 m - 2500 m). Later presented diagnostics link that response to differences in the atmospheric condition between I-MELT and R-MELT. (see section 5.2.4) The clear warming signal of the not longer ventilated deep water masses in the interior Labrador Sea in the I-MELT scenario is only partially visible in the R-MELT simulation. That difference is caused by a not complete shut down of the deep convection in the realistic melting case.

With respect to resolution, it seems obvious that ORCA05 shows an enhanced tendency for lateral mixing, which carries anomalies from the boundary currents into the interior Labrador Sea. However very robust signals are seen in the boundary current system among all configurations. The interior of the Labrador Sea seems more influenced by the presence of eddies, at least in VIKING20 in the R-MELT scenario.

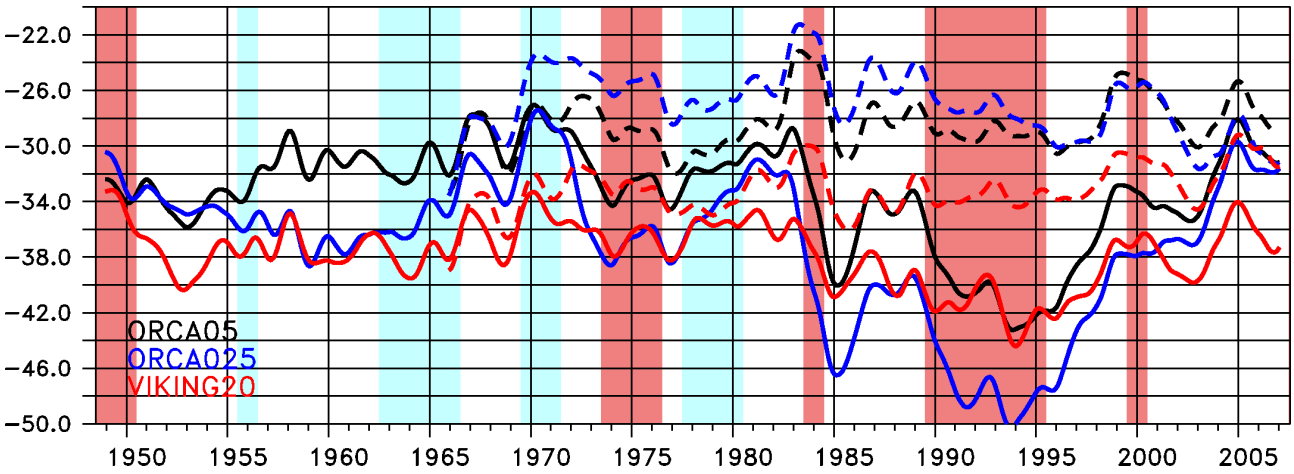

Figure 42.: Barotropic transport in the SPG: SPG strength for the reference (solid) and hosing (dashed, I-MELT) simulation in Sv in the different model configurations. Blue and red shading indicates NAO^- and NAO^+ phases, respectively. The timeseries are interannually filtered. Negative transport values indicate a cyclonic circulation.

5.2.4. Changes of the SPG transport

In the following section the volume transport changes within the SPG will be discussed. This diagnostic provides a quantified picture of the earlier shown anomalies in the boundary current along the AR7W section. The volume transport given by the barotropic streamfunction is closely linked to SSH changes in the central Labrador Sea (Böning et al. (2006)), further discussed in section 2.3.5.

Response in the I-MELT scenario

The negative values (in Figure 42) indicate a cyclonic gyre circulation for the reference simulations (solid lines). The reference simulations show large variability on interannual to decadal timescales. The interannual variability is linked to the NAO phase indicated by the red (NAO^+) and blue (NAO^-) shading. Previous studies (Hurrell et al. (2003)) showed that the persistence of a NAO phase plays a crucial role for the gyre transport due to involved feedbacks. Positive NAO phases (red shading) correlate with a strengthening (more negative) behaviour of the gyre transport and vice versa for NAO^- conditions. During positive NAO phases the westerly winds and heat loss over the interior Labrador Sea are enhanced during winter months (Hurrell et al. (2003)). These enhanced heat fluxes lead to pronounced winterly convection and increase the cross gyre density gradient and result in an increase in the gyre transport (Böning et al. (2006)). Increasing tendencies are seen in the mid 1970s, 1980s and early 1990s in agreement with Hurrell et al. (2003). These transport changes are concentrated in the boundary current (not shown). Irrespectively of the mean value of the reference simulations, all reference simulations show the same variability on interannual to decadal timescales with small differences on shorter timescale.

The hosing simulations (Figure42, dashed curves) do not suggest any long-term decline over the

entire hosing period (43 years), while a large weakening is seen during the 3rd decade (1985-1994), which is in agreement with previous shown diagnostics. Differences between reference and hosing simulation have vanished at the end of the hosing period. It should be noted that transports in certain density classes are considerably affected by a melting of GrIS, especially transports of dense water masses. However during the hosing simulation large hydrographic anomalies occur in comparison to the reference simulation. They are induced by the shut down of the winterly deep convection in the hosing simulations, which normally leads to an increase in the SPG strength, especially during NAO^+ phase. The consequence is that the SPG strength is to a certain extent decoupled from the local atmospheric forcing, which triggers most of the interannual-decadal variability in the reference simulation. The hosing simulations exhibit an interesting result in this context. It is known that the SPG is driven by buoyancy forcing and wind stress (Spall and Pickart (2001)). Since the atmospheric conditions, the wind stress forcing explicitly, are the same among all simulations a differentiation between wind and buoyancy driven induced variability of SPG is possible. Variability which is consistent between reference and hosing simulation can only be wind induced. For example the gyre intensification during and after the positive NAO phase in the mid 1980s is seen in all simulations. That result reflects that most of that variability is triggered mainly by windstress changes. That behaviour is in contrast to the early 1990s where a strengthening of the gyre is only seen in the reference simulation but not in the hosing simulations. These behaviour explains the suggested weakening over the first 3 decades, seen in the AR7W diagnostic. The strength of that response differs between the configurations. ORCA025 shows the largest weakening of the gyre by about 25 Sv (∼50%) during the mid 1990s. ORCA05 and VIKING20 suggest a weakening of about 15 Sv (∼35%) and 12 Sv (∼27%), respectively. From that it can be concluded that the eddy effect in the Labrador Sea has a damping effect for freshwater perturbations. These results are somehow in contrast to the LSW diagnostic, which suggested the largest decline in LSW production rates in ORCA05.

Response in the R-MELT scenario

As expected, the response in the R-MELT simulation is weaker and does not even show a clear qualitative tendency (Figure 43), like the overall slight weakening in the I-MELT cases. The anomalies are strongly affected by mesoscale processes, therefore large variations are seen in the anomalies of VIKING20 and ORCA025. In contrast, ORCA05 does not resolve such features and shows a weakening of about 0.5 Sv in 2020. The other two simulations show a strengthening tendency of the SPG by about -1 Sv in 2020. The reason for this discrepancy between ORCA05 and the other configurations should be related to the differences in the response at mixed layer depth. Apparently, ORCA05 shows the largest decline in the mixed layer depth (Figure 34) as well as the largest reduction in LSW production (Figure 36b) of all configurations.

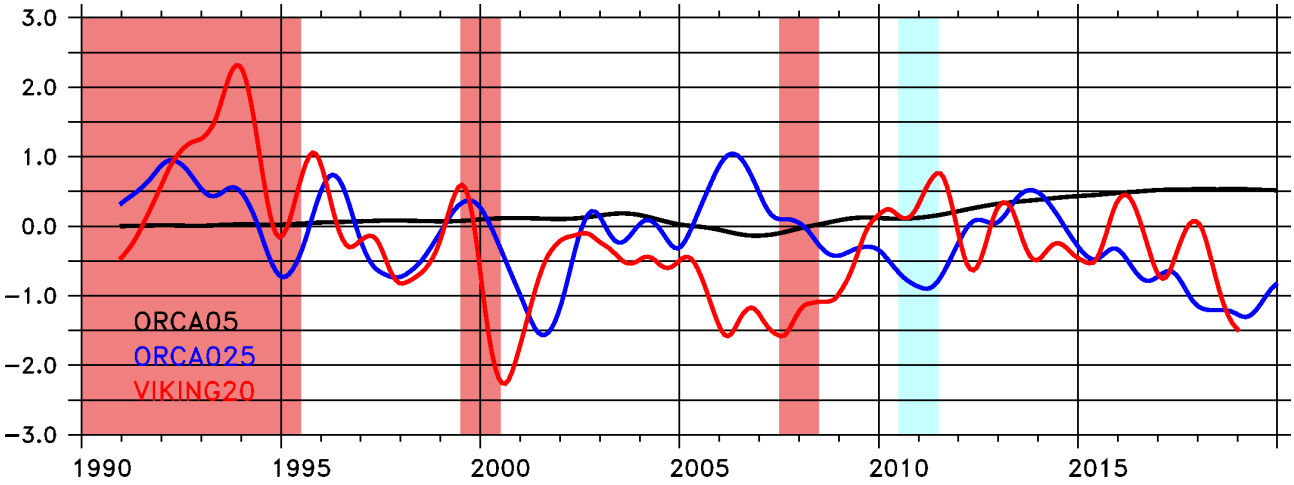

Figure 43.: Barotropic transport changes in the boundary current of the SPG: SPG strength anomaly from the barotropic streamfunction for the R-MELT scenario in Sv for the different configurations. Blue and red shading indicates $NAO^+$and NAO^+ phases. The timeseries are interannually filtered.

5.3. Basin-scale response of the subpolar and mid-latitude North Atlantic

The previous section described the meltwater related changes with focus on the Labrador Sea and the deep convection response. Obviously meltwater induced anomalies will not be confined to the Labrador Sea. The large scale spreading is described in the following section, starting with an analyses of "export pathways" of hydrographic anomalies to identify regions where the largest changes can be measured. The presented anomalies (temperature, salinity) have been averaged over the upper 2000 m, which represents the depth range of ARGO floats to increase their meaningfulness and robustness. Surface anomalies follow irrespectively of resolution mostly previous results of Swingedouw et al. (2012). Beside anomalies of temperature and salinity, the spreading of the meltwater (passive tracer vertical integral 0-2000m) and SSH is evaluated. It is furthermore tried to quantify expected changes in heat and freshwater content over the subpolar North Atlantic. These changes are compared to observed natural variability. In the first part of this section only results of the I-MELT scenario are presented and discussed. In section 5.3.5 the corresponding effects in the R-MELT scenario will jointly be presented.

5.3.1. The spreading of meltwater (passive tracer)

The spreading of the passive tracer (integrated over upper 2000 m) is governed mainly by the gyre circulation, especially within the SPG. After 10 years of hosing (Figure 44) the largest concentrations occur in the Baffin Bay and within the Labrador Current and in the course of the SPG heading towards the Nordic Seas. Meanwhile, a relative wide band of high concentrations from Newfoundland towards the Iceland-Scotland ridge is seen in ORCA05 and ORCA025 with concentrations exceeding 1 m^3/m^2.

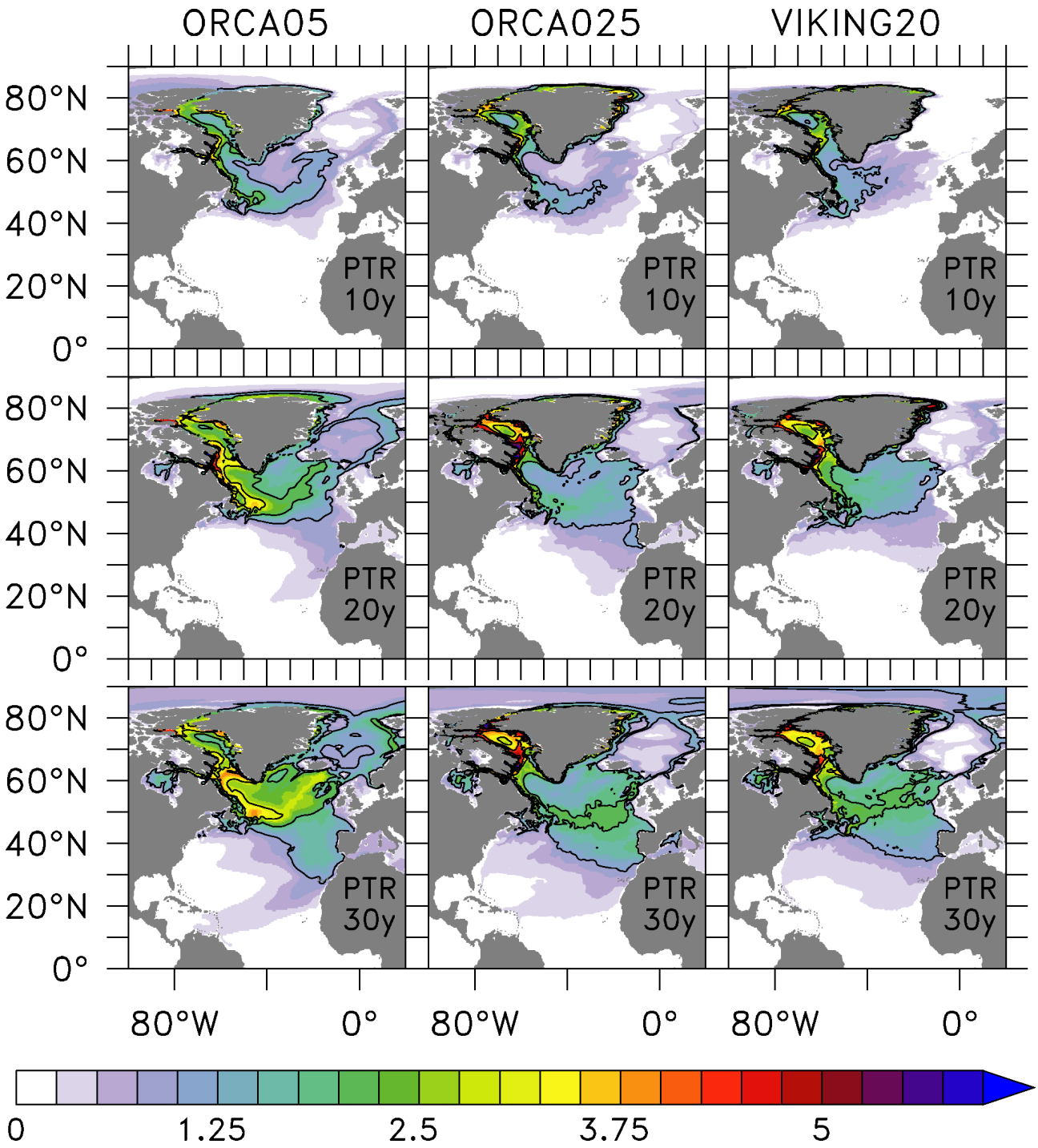

Figure 44.: Tracking the additional meltwater. Passive tracer distribution (vertical integrated 0-2000m) for certain periods (10, 20, 30 years, is based on monthly means) of the hosing in m^3/m^2 for the different model configurations in the I-MELT scenario. Contour lines indicate a 1 m^3/m^2 interval.

The spreading in VIKING20 is more concentrated to the Northwest SPG and does not support results of ORCA05 and ORCA025. The eastward spreading is linked with the representation of the NW Corner. This behaviour is more distinctly visible at a later point in time. For example after 20 and 30 years, when in both coarser simulations the passive tracer penetrates into the STG at the eastern subpolar North Atlantic and recirculates towards America. VIKING20 shows with respect to that aspect the lowest export from the SPG towards the STG, with most of the tracer staying within the SPG south of the Greenland-Scotland ridges. Despite the anticyclonic spreading within the SPG, there are also some indications of the southward spreading at the American coast, at least in ORCA025 and VIKING20 as part of the DWBC and SPG. This spreading is clearly visible after 30 years but not present in ORCA05. Beside the spreading to the subtropics, some portion has entered meanwhile the Nordic Seas with the Atlantic Inflow and follows the boundary currents along the Norwegian coast. A further pathway was identified by recirculations at the Greenland coast near Island (see section 5.1). The highest concentrations in the Nordic Seas are seen in both coarser configurations already after 10 years. VIKING20 suggested the lowest concentrations in that area over the entire hosing period. Based on that results some coherent patterns are expected in the salinity anomalies which are shown in the following subsection.

5.3.2. Effects on the salinity and temperature distribution

Changes in salinity After 10 years of Greenland melting the largest freshening signals (Figure 45) are seen within the boundary currents of Greenland, in the Baffin Bay and along the path of the SPG in agreement with the tracer spreading. The interior of the SPG and Nordic Seas at this stage show lower freshening signals than the boundary currents, which carry the majority of the anomaly signal. Some of this freshening signal is not directly related to the presence of meltwater but rather due to large scale circulation changes. That effect is confirmed by the passive tracer spreading results, described above. The freshening signal around the Canary Current is to a certain amount related to changes in the gyre circulation (subtropical) and partly to direct presence of meltwater. This export pathway from the SPG to the STG was already described as “comma shape” and freshwater leakage by Swingedouw et al. (2012). This signal becomes more prominent over time and is emphasised in ORCA05 and ORCA025 compared to VIKING20. In both coarser configurations the path of the NAC is shifted to the south and does not show a presence of the NW Corner, contrary to VIKING20. Therefore, the freshwater anomalies spread more easily to the east and leave the SPG, while this export parthway is more impeded in VIKING20 by a better represented NW Corner. That is also indicated by the tracer distribution in Figure 44. As a consequence, more direct freshwater related anomalies remain within the SPG in VIKING20 compared to the other configurations. The NW Corner in VIKING20 however is eroded over time (Figure 56) and moves to the south. That response is in agreement with sensitivity studies by Zhang et al. (2011). The accompanying circulation changes are the reason for the largest freshening signal in VIKING20 over that area. After about 20 years, a positive anomaly develops

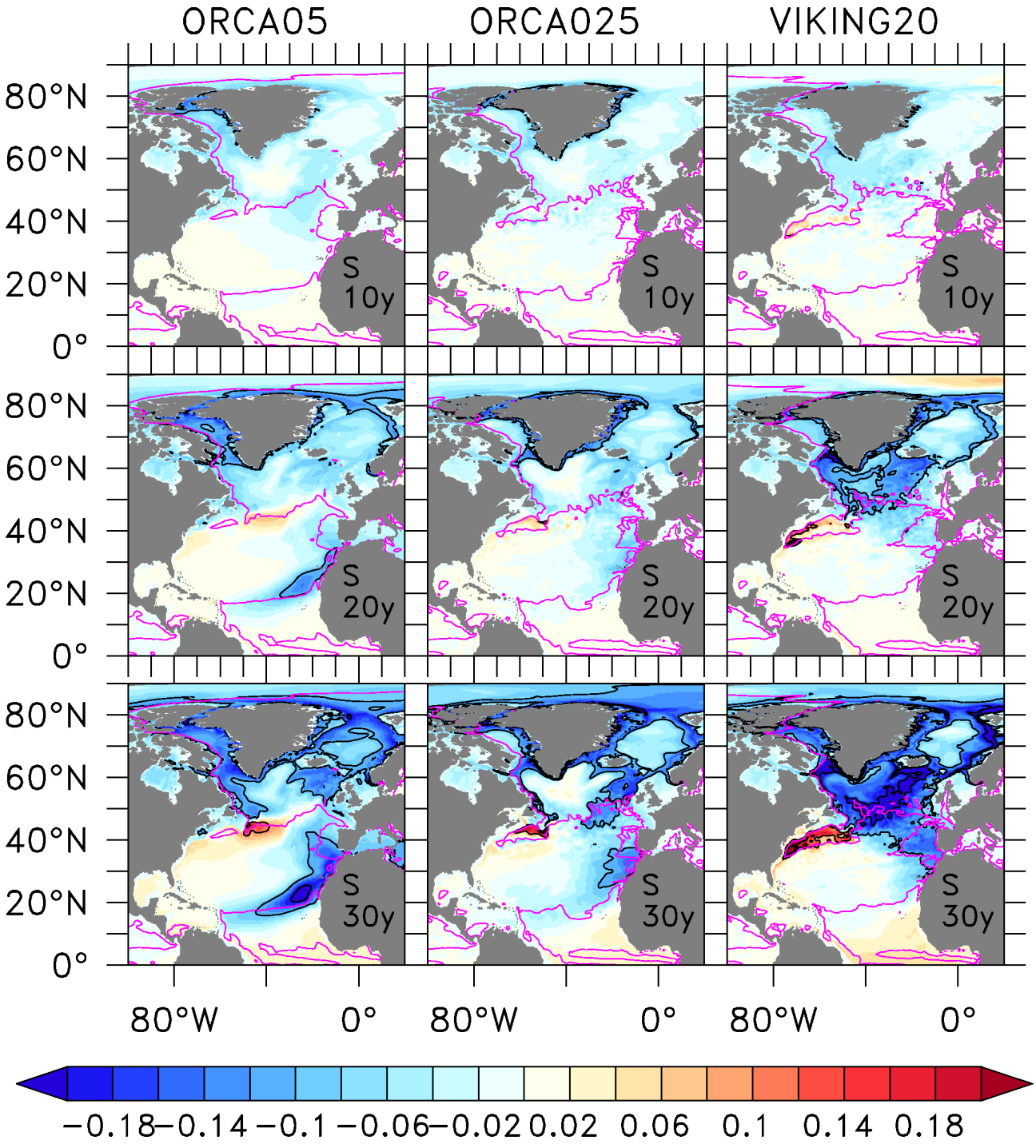

Figure 45.: Salinity anomalies (psu) averaged over the upper 2000 m for the different model configurations in the I-MELT scenario and after certain periods (10, 20, 30 years, are based on 5 yearly means) of hosing. Magenta contour line mark the 0 line of the mean (1998-2007) barotropic streamfunction to indicate the SPG and STG. Black contour lines indicate a 0.1 psu interval.

along the path of the Gulf Stream south of Nova Scotia in all configurations. This positive anomaly is caused by a northward shift of the path of the Gulf Stream. Therefore the transports of salty water into this normally fresh regions are intensified. That positive anomaly evolves further in time and becomes more distinct after 30 years of melting. The most prominent positive signal in that respect shows VIKING20. The passive tracer results in VIKING20 suggested lower meltwater transports into the Nordic Seas compared to the other configurations. On the other hand the salinity anomalies concentrated in the boundary currents are largest compared to all other configurations. That result points again to distinct circulation changes in the salt advection, associated with the NAC. These changes will be investigated further in section 5.4.4.

Changes in temperature After 10 years a warming signal is a common feature among all configurations (Figure 46) in the Labrador Sea, Baffin Bay as well as in the Gulf Stream path. That confirms the earlier mentioned northward shift of the Gulf Stream in the region around Nova Scotia . A general cooling tendency is visible in the North East Atlantic (around Island and Scotland), in the Nordic Seas and partly in the Arctic Ocean. The warming signal, which is originating from Labrador Sea and Baffin Bay is caused by the reduced convection and less mixing of cool surface waters to depth during winter conditions. This warming further increases over the first 30 years in that area and exceeds 1 °K. After that period the warming switches to a cooling (shown in Figure 48) due to lower northward meridional heat transports. The warming south of Nova Scotia is persisting over the entire hosing period instead. The above mentioned better representation of the NW Corner in VIKING20 and its hosing related shift (eroding), cause a large cooling signal there, which is not present in the coarser simulations. A further strong cooling is present at the Norwegian shelf break, probably due to a large reduction of warm water inflow from the subpolar North Atlantic into the Nordic Seas in VIKING20. That is confirmed by corresponding salt anomalies. ORCA05 and ORCA025 exhibit a cooling (similar to the salinity anomalies) at the south eastern boundary of the STG. The South Atlantic reveals a positive anomaly (~ 0.3 °K). The warming signal seen in the Gulf Stream (around Nova Scotia) could be related and describe the possible underlying mechanism to the long-term observed changes in that area(Wu et al. (2012)).

5.3.3. Equivalent freshwater and heat content changes

In the following section the simulated anomalies in the equivalent freshwater and heat content over the subpolar North Atlantic are compared to the decadal variability observed during the past 50 years, as discussed in the study by Boyer et al. (2007). (see also section 2.3.5)

Equivalent freshwater content

The observed anomaly from 1960 to 2002 is indicated by the black line (Figure 47) and shows a multidecadal variability. Since the early 1990s a decrease of the freshwater content over the subpolar

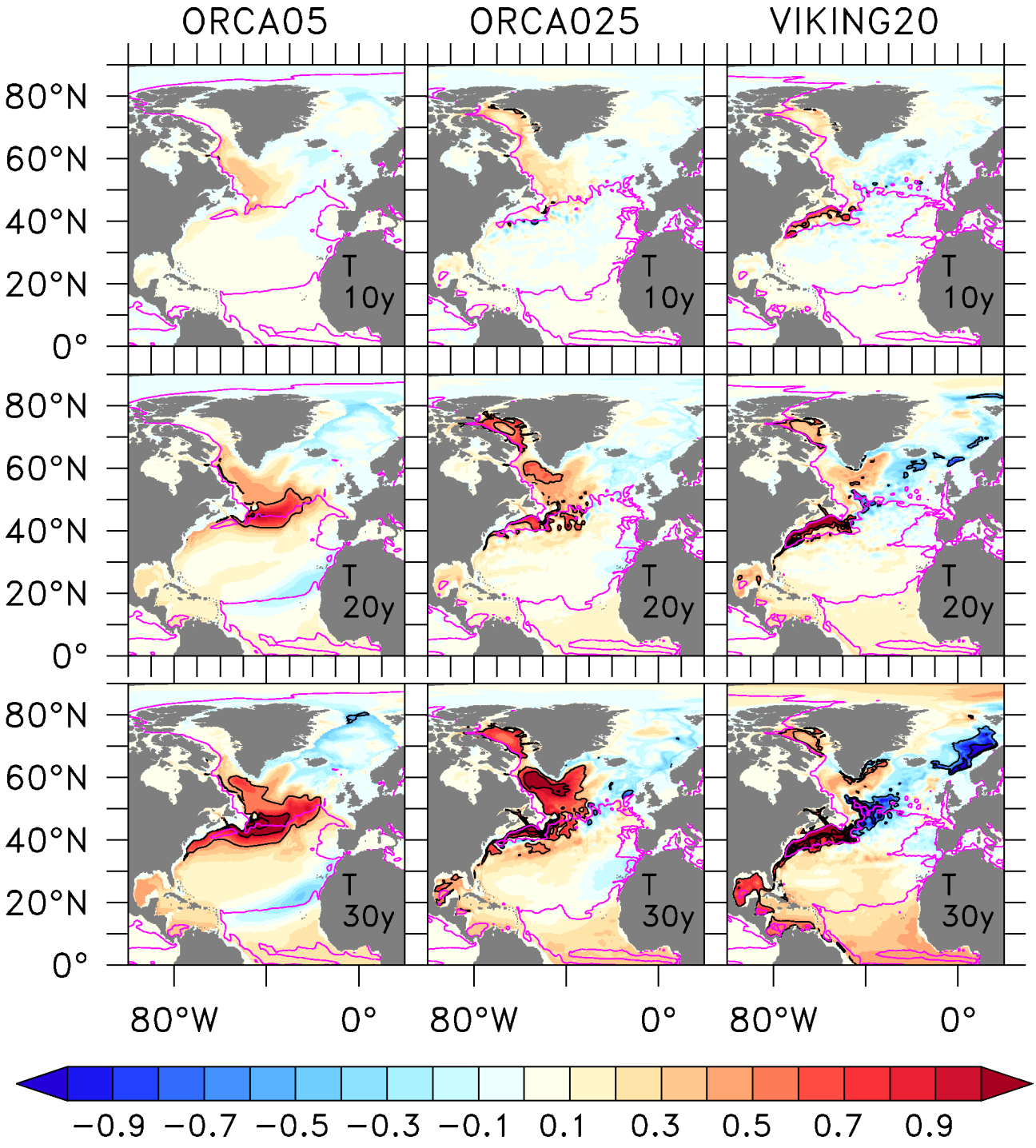

Figure 46.: Temperature anomalies (°K) averaged over the upper 2000 m for the different model configurations in the I-MELT scenario and after certain periods (10, 20, 30 years, are based on 5 yearly means) of hosing. Magenta contour line mark the 0 line of the mean (1998-2007) barotropic streamfunction to indicate the SPG and STG. Black contour lines indicate a 0.5 °K interval.

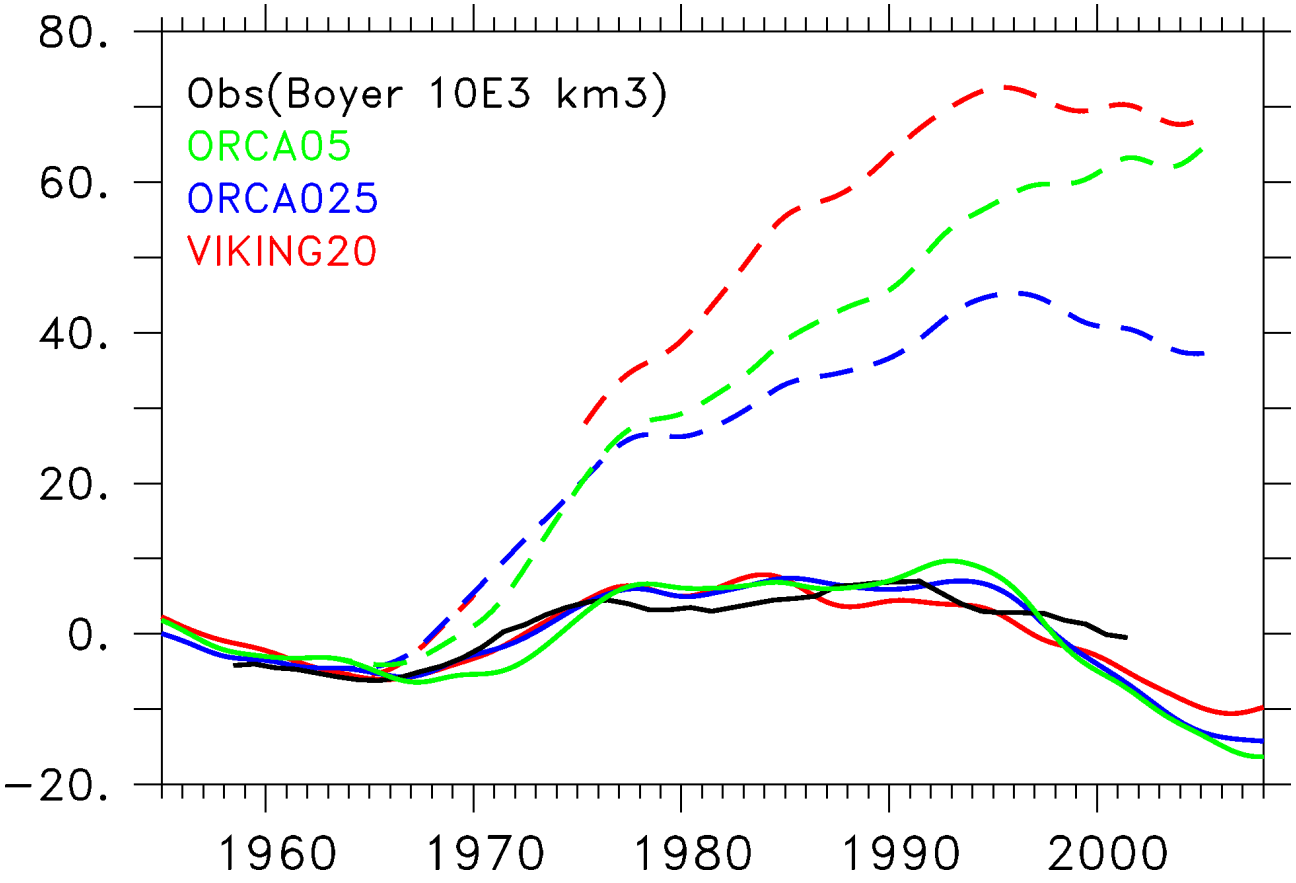

Figure 47.: Freshwater content anomaly (0-2000m) in 10^3 km^3 for the subpolar North Atlantic from observations (black solid line) and different simulations and configurations (reference simulation in solid and I-MELT scenario results in dashed). The region for the computation is indicated in Figure 8. The linear trend of each reference simulation over the period of observation is removed from the reference and I-MELT simulation. The gap in the VIKING20 R-MELT simulation is caused by lost data.

region (50°N-80°N) is visible. All reference simulations (solid lines) follow the observations closely and show the observed variability. The hosing simulations (dashed) exhibit a clear freshwater content increase instantly at the beginning of the melting simulation (1965). The increase over the first ten years (until 1975) is nearly linear due to the constant meltwater release rate and the fact that no freshwater has left that region. After ten years the freshwater increase becomes more gradual. ORCA05 exhibits the lowest further increase followed by ORCA025. That behaviour is consistent with the fact that both lower resolution models show the pronounced "comma shape" of an enhanced export pathway of freshwater anomalies from the SPG to the STG. VIKING20 on the other hand exhibits the largest increase with a leveling off about ∼70.000 km^3, which is about 12 times larger than the observed natural variability. The spread between the configurations is caused by the differences in the export of freshwater anomalies out of the subpolar North Atlantic. The results suggest that the exports in ORCA025 are largest compared to the other two configurations. The study of Curry and Mauritzen (2005) quantified the freshwater increase from the 1960s to the 1970s to about ∼9000 km^3. They further estimated that this amount applied to the upper 1000 m of the Nordic Seas, would

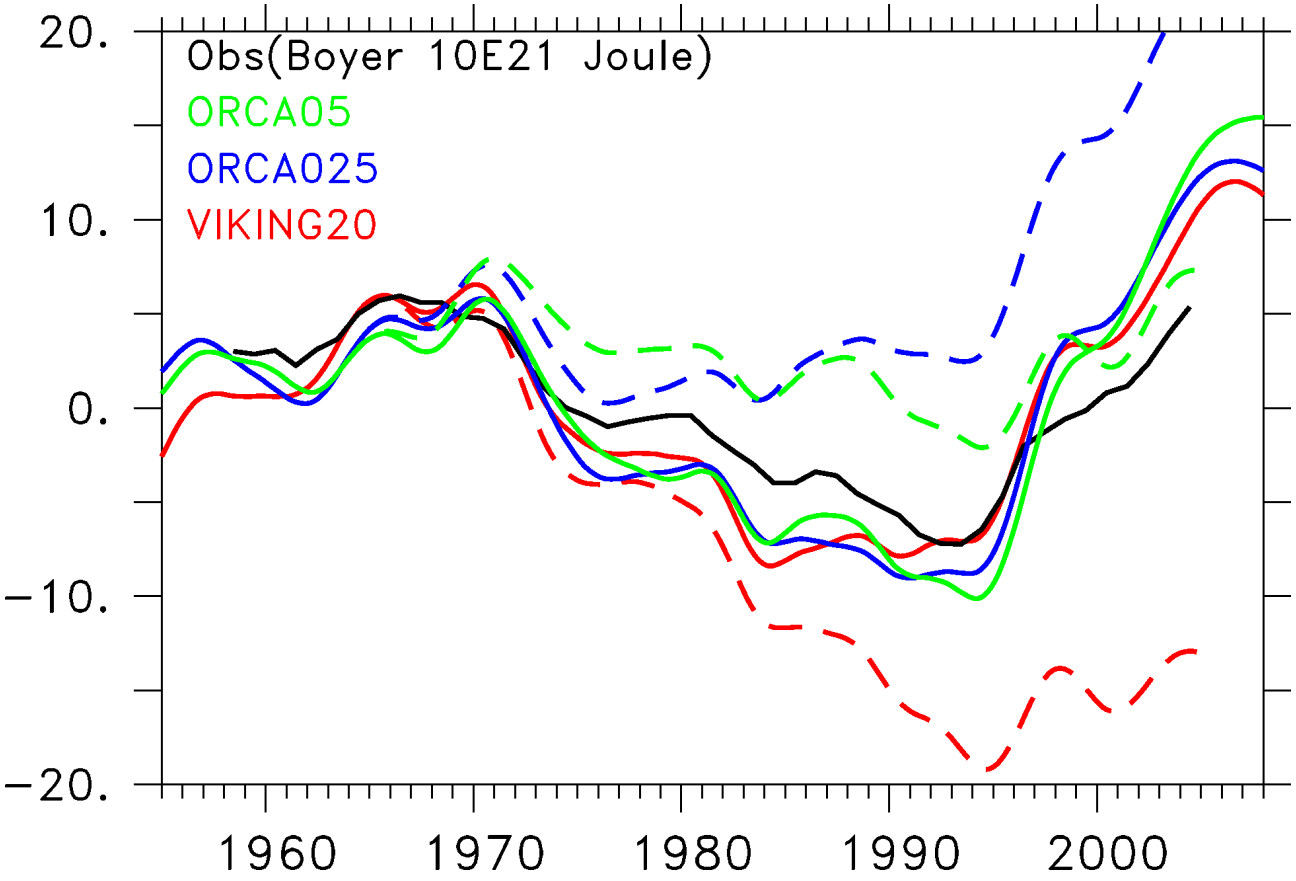

Figure 48.: Heat content anomaly (0-2000 m) in 10^{21} Joule for the subpolar North Atlantic from observations (black solid line) and different simulations and configurations (reference simulation in solid and I-MELT in dashed). The region for the computation is indicated in Figure 8. The linear trend of each reference simulation over the period of observation is removed from the reference and I-MELT simulation.

alter the density of the overflows substantial with significant consequences for the AMOC. Two times this amount of freshwater of a GSA (18000 km^3) could lead to a complete shut down of the deep convection in the Nordic Seas. At the end of the hosing simulation (2007) freshwater anomalies in the upper 1000 m of the Nordic Sea are about 20710 km^3 (ORCA05), 15940 km^3 (ORCA025) and 15640 km^3 (VIKING20). These anomalies suggest that the convection in the Nordic Seas should be close to a shut down with substantial implications of the overflows as well as on the AMOC. (Results are presented in section 5.3.8 and 5.4.2)

Heat content

The heat content change over the subpolar North Atlantic shows a multidecadal variability (black line), which is anti-correlated to the freshwater content (Figure 47, 48, Boyer et al. (2007)). That means during periods with decreasing freshwater content, for example after 1990, the heat content increases. That behaviour is explained by advective anomalies within the NAC propagating from the STG to SPG, through the transition zone of the so called inter-gyre gyre (Scheinert (2008)). The reference

simulations (solid lines) basically follow the observed variability (black line). With respect to heat content changes the picture is not as consistent as for the freshwater content, which is also indicated by the horizontal maps of the temperature anomalies in Figure 46. VIKING20 (red dashed) suggests a loss of energy of up to 20 $\times 10^{21}$ J compared to the reference simulation (red solid) at the end of the hosing period. ORCA05 (green dashed) shows a slight increase until 1995 but then a clear decrease compared to the reference. ORCA025 exhibits an overall warming tendency over the hosing period in the GrIS melting simulation (blue dashed). That behaviour is related to the positive temperature anomaly originating from the overestimated convection in the Labrador Sea and its abrupt shut down. Since the largest negative anomalies occur in VIKING20 in the region of the NW Corner and near the Norwegian coast (Figure 46), it is very likely that these anomalies are induced by reduced advection of heat from the south due to changes in the NAC and subsequently lead to differences in the Atlantic Inflow to the Nordic Seas (also confirmed by a strong decline of the AMOC 61). The representation of this advective pathway differs between these configuration and possibly explains the differences in the heat content response. In the coarser configurations the largest heat content anomalies (positive) are more related to changes in the mixed layer depths (Labrador Sea), which points to the importance of changes in the surface heat fluxes in contrast to an advective process. That contrast reveals a significant difference between VIKING20 and the two coarser configurations and highlights differences in the mechanisms between coarse and eddy resolving configurations. It should be noted that ocean-only simulations are strongly linked to the applied air temperatures, while in a coupled system there are several feedbacks involved and the atmosphere can freely react on oceanic anomalies. However as indicated by (Swingedouw et al. (2012)) the atmospheric feedbacks seem to be of minor importance in the I-MELT case and most changes are oceanic driven. As a reminder these results are based on coarse coupled climate models.

5.3.4. Changes in the surface circulation and the related impact on the SSH

Beside changes in the temperature which have an important impact on the atmosphere and climate conditions, changes in sea surface height are relevant for inhabitants of coastal areas. It is known that the volume of the GrIS is approximately 2.8×10^6 km³ (Bamber et al. (2001)). With an assumed runoff of 0.1 Sv (I-MELT) it would last about $\sim$ 887 years to melt this ice sheet completely and $\sim$ 552 years in the R-MELT simulation. A melting of the entire GrIS would lead to a global SSH rise of about 7.8 m ($\sim 2.8 \times 10^6$ km³ / 357×10^6 km² $\times$ 1000 m, pure volumemetric). The SSH rise is characterised by strong regional variations (Cronin (2012)). These variations are related to the redistribution of mass (changes in the gravitational potential), thermal expansion and circulation changes. Changes in the gravitational potential and thermal expansion, which can dominate on regional scales (Landerer et al. (2007)), are not taken into account for the following diagnostic. Due to a melting of the GrIS, the mass attraction of Greenland would decrease and counteract to a certain amount the SSH rise caused by the additional meltwater volume. This could lead to a drop of SSH around Greenland compared

to the global mean (Kopp et al. (2010)). To investigate the regional SSH pattern independently from the expected global mean that value was subtracted from the anomalies (10 years = 8.8 cm, 20 years = 17.5 cm and after 30 years = 26.5 cm). The results (Figure 49) after 10 years suggest a enhanced increase of about 10 cm around Greenland and the North American coast, compared to the global expected mean (8.8 cm). Differences between the configurations are seen in the eastward extent of anomalies towards Europe and Africa. Both coarser configurations suggest an increased SSH rise there, while VIKING20 tends to a slight decrease instead. The SSH anomaly pattern of ORCA05 follows very much the results of Landerer et al. (2007) in the subpolar North Atlantic. In the following decades the principal pattern evolves further and becomes more pronounced. Anomalies exceed 0.50 cm compared to the global expected mean, near Greenland, Labrador Sea and Newfoundland. In later decades VIKING20 also show an increased SSH rise along the European coast of about 10 cm. The regions of the NAC and Nordic Seas show a striking difference compared to the other configurations. In both regions a distinct negative anomaly ($\sim$ -10cm) compared to the global mean is suggested. Both coarser configurations do not confirm that and are tending more to the classical "comma" shape pattern, described by Swingedouw et al. (2012). The presence of the NW Corner inhibits the direct eastward propagation of these anomalies, which marking a clear deficit of the coarser models. Irrespectively of resolution the most affected regions are the coastal waters around Greenland and of North American. The horizontal resolution is important for the eastward propagation over the Atlantic Ocean.

5.3.5. The importance of details in the GrIS melting scenario (R-MELT)

In the following paragraph the anomalies of temperature, salinity and SSH in the R-MELT scenario and the tracer spreading after 30 years of hosing will be evaluated and compared to the I-MELT results to identify differences in the response. That allows to estimate the effect of the applied melting scenario on the oceanic response.

Meltwater spreading (passive tracer)

Similar to the results from the I-MELT scenario the spreading of the meltwater is governed by the large scale circulation (Figure 50). In agreement to the I-MELT results the largest concentrations are found in the Baffin Bay and along the Labrador coast. With increasing horizontal resolution less tracer is carried into the Nordic Seas and less spreading occurs to the east across the North Atlantic. That behaviour is important for differences in the long-term response between the different configurations. The eastward spreading is clearly related to the course of the NAC, also found in the I-MELT scenario, with clear deficits in the coarser simulations. The export path within the DWBC also present below 2000m and storage in the northern recirculation gyre of the Gulf Stream (Hogg et al. (1986)) south of Nova Scotia become more important with increasing resolution, clearly seen in VIKING20. That is indicated by the southernmost extension of the tracer along the American coast. That pathway is

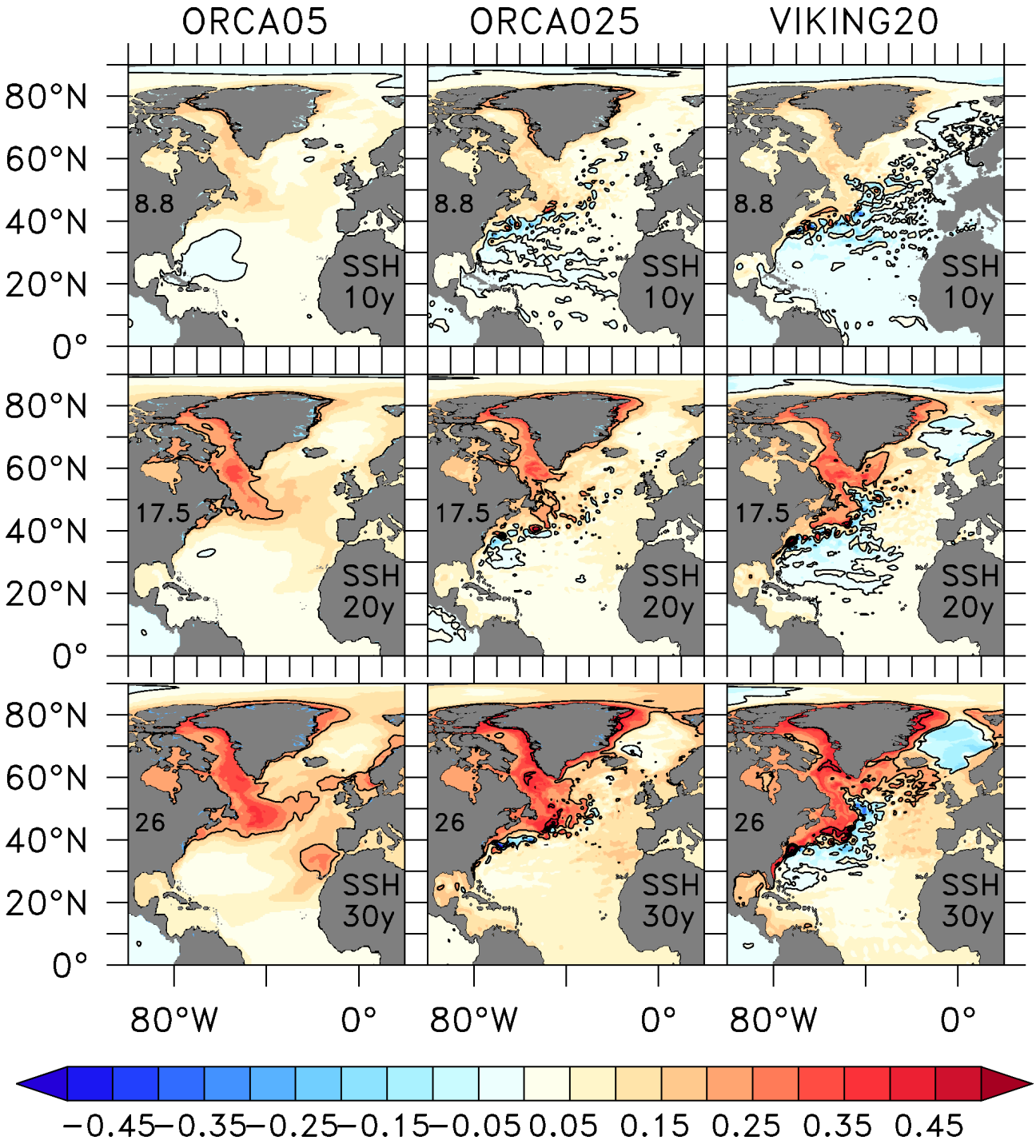

Figure 49.: SSH anomalies (m) after certain periods (10, 20, 30 years, are based on yearly means) referenced to the expected global mean SSH rise at that stage (8.8 cm, 17.5 cm and 26 cm respectively) for the different model configurations. Contour lines indicate each 25 cm interval. The numbers indicate the global mean SSH rise.

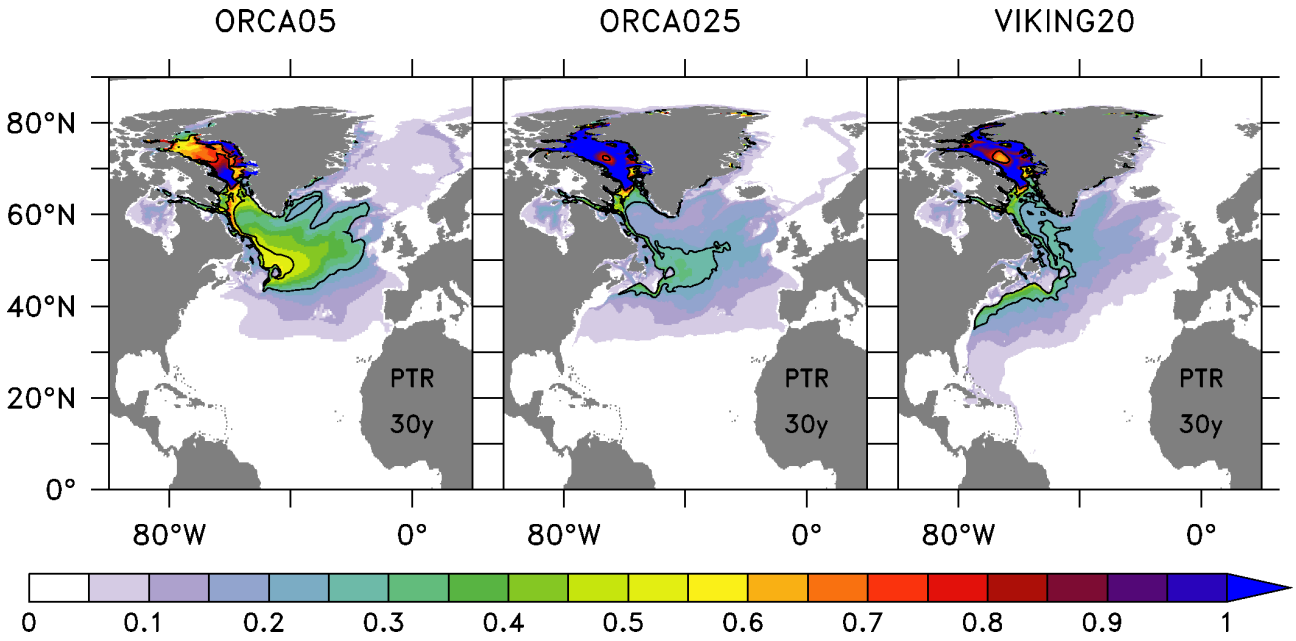

Figure 50.: Tracking the additional meltwater. Passive tracer distribution (is based on monthly means) after 30 years of hosing (vertical integrated 0-2000m in m^3/m^2) for the different model configurations in the R-MELT scenario. Contour lines indicate a 0.25 m^3/m^2 intervals.

enhanced in the R-MELT case compared to the residual spreading in the North Atlantic and to results in the I-MELT scenario. Irrespective of the large scale distribution, the largest amount of tracer is found in the Baffin Bay in agreement to the I-MELT results (Figure 44) and suggesting largest salinity anomalies there. ORCA025 and VIKING20 show the largest amount in that region, while ORCA05 tends to flush this meltwater to and into the SPG.

Changes in the salinity distribution

The salinity anomalies (0 - 2000 m) of the R-MELT scenario show similarities to the I-MELT simulations, i.e. a pronounced freshening in the Baffin Bay and over the subpolar North Atlantic (Figure 51). The signals over the NAC are dominated by mesoscale variability in ORCA025 and VIKING20 and cover a possible melting signal. The largest negative anomaly is found in ORCA025 ($<$ -2 mpsu) in Baffin Bay and in the east North Atlantic. Both coarser configurations suggest larger negative anomalies in the central subpolar North Atlantic and in the NAC and show hints of the export pathway from the SPG to the STG at the African coast. The reasons for the large positive anomaly in ORCA025 in the Arctic is unclear. Contrary to the I-MELT results, VIKING20 does not exhibit the largest freshening signal over the NW Corner region. That effect might point to the existence of a certain threshold in the freshwater forcing and to the importance of details in applied melting scenario, which lead to different results. The freshening in the NAC extension and in parts along the Norwegian coast is present. Despite the freshening signal in the subpolar North Atlantic there are also indications of a salinification in the western STG and south of the equator, which is also seen in the

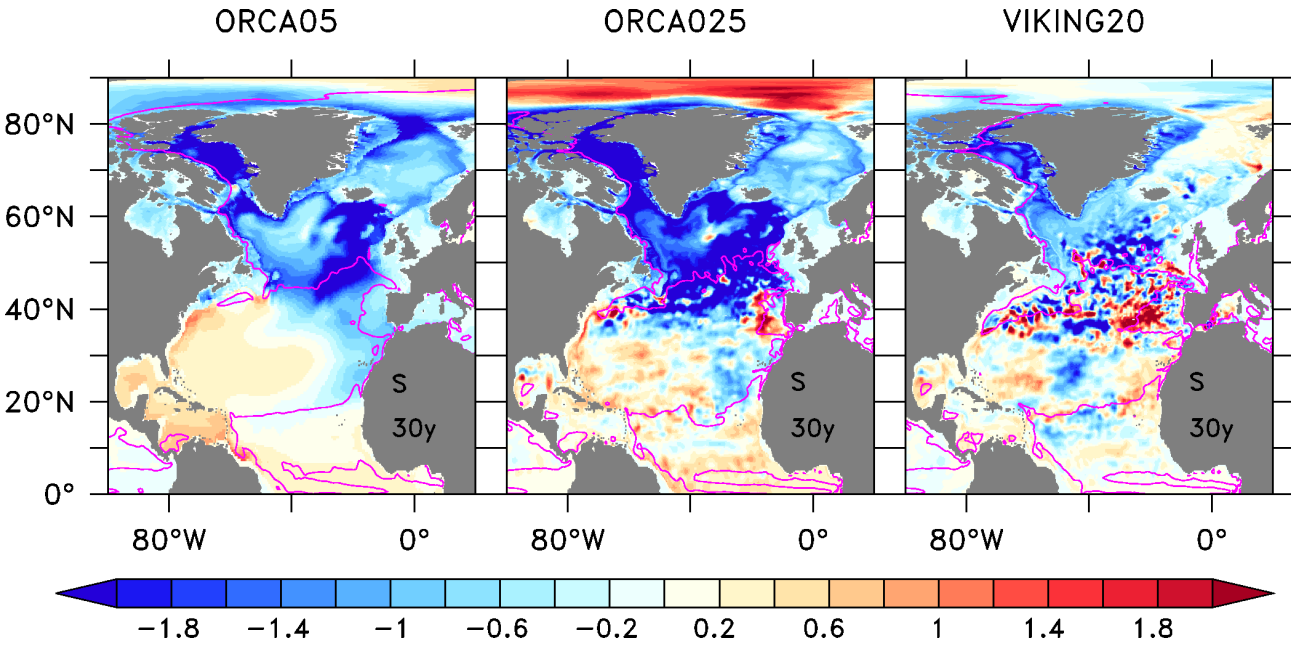

Figure 51.: Salinity anomalies (averaged 0 - 2000 m) between hosing and reference simulation in mpsu after 30 years (are based on 5 yearly means) of hosing for the different model configurations. The magenta contour line indicate the 0 line of the mean (1998-2007) barotropic streamfunction to illustrate the SPG and STG.

I-MELT simulations. The reasons are yet unclear but might be related to changes in the meridional transports of salt and heat. That is also confirmed by a similar pattern for temperature anomalies (Figure 52). The northern shift of the NAC is only seen in both coarser configurations, which cause the slight positive anomalies south of Nova Scotia.

Changes in the temperature distribution

The temperature anomalies (Figure 52) suggest a warming in the Baffin Bay and in the near coastal waters of North America, associated with a northward shift of the NAC path. That shift is hardly detectable in VIKING20. The cooling anomaly ($\sim$ -1.5 °K) south of Iceland and west of Ireland seems robust among all configurations. That indicates lower heat transport within the NAC into this region. The large warming signal in the interior Labrador Sea, due to the shutdown of convection in the I-MELT scenario, is partly seen in ORCA05. That response is in agreement with diagnostics in the interior Labrador Sea (Figure 33), which suggested the largest response on the convection in ORCA05. The Nordic Seas do not show a consistent picture between the configurations, while some warming pattern in the interior seems to be robust between the configurations, which can be crucial for the formation of the dense overflows and a remote control for the AMOC. This impact will be discussed in section 5.4.1. South of 15°N, all configurations suggest a warming which goes along with positive salinity anomalies.

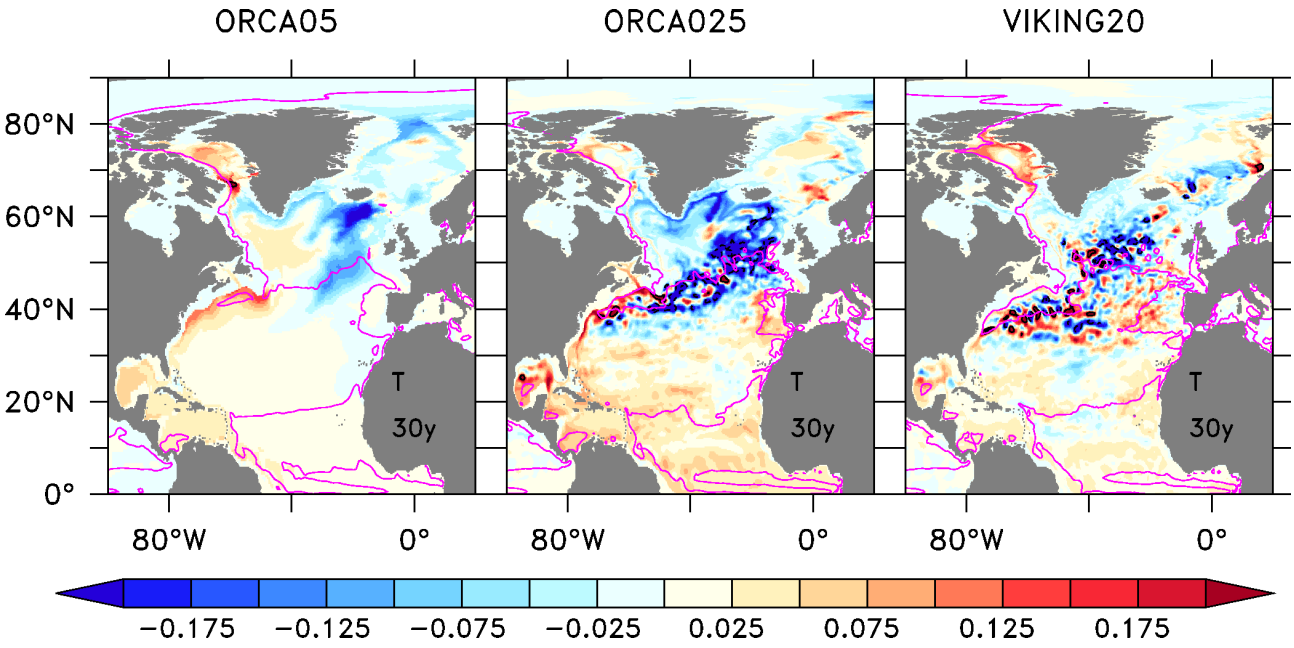

Figure 52.: Temperature anomalies (averaged 0 - 2000 m) between hosing and reference simulation in °K after 30 years (are based on 5 yearly means) for the individual model configurations. The magenta contour line indicate the 0 line of the mean (1998-2007) barotropic streamfunction to illustrate the SPG and STG. Black contour lines indicate anomaly intervals of 0.25 °K.

Changes in the surface circulation and related impacts on the SSH

The R-MELT results (Figure 53) confirm with respect to the SSH changes the general findings in the I-MELT scenario. The largest SSH rise is seen along the Greenland and North American coast with values up to 4 cm above the global expected mean of 2.75 cm after 30 years. In the coarse ORCA05 a positive anomaly expands into the Newfoundland basin, similar to the tracer pattern (see 50). In VIKING20 this penetration is not seen due to the large mesoscale variability and inhibition by the North West Corner. A slight positive anomaly (1-2 cm above the global expected mean) is also visible in both coarser configuration along the European coast, which is not present in VIKING20 during that time.

Equivalent freshwater content

Due to the lower amount of released meltwater compared to the I-MELT scenario the quantitative response on the freshwater content is also lower (Figure 54). The applied repeating year (2007) forcing beyond 2007 inhibits all interannual variability and induces an arbitrary tendency. VIKING20 (red solid curve) shows beyond 2007 a further decrease of the freshwater content, while ORCA05 (green solid curve) tends to an increase in the control simulation. ORCA025 shows first an increasing and after 2010 a decreasing tendency. Irrespectively of that behaviour in the reference simulations all hosing experiments (dashed) show a freshwater increase from the arbitrary reference state. The largest increase is displayed by ORCA025 with 7.5 $\times$ 10^3 km^3, followed by ORCA05 with 6 $\times$ 10^3

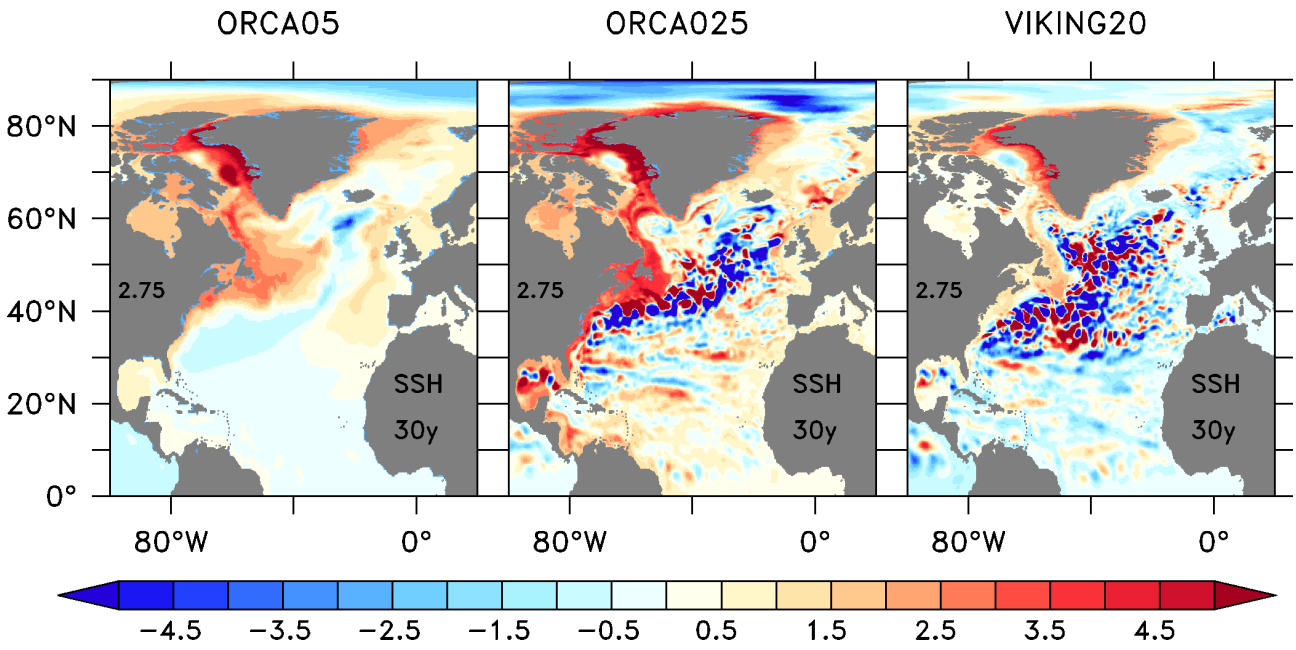

Figure 53.: SSH anomalies between hosing and reference simulation in cm after 30 years (are based on yearly means) relative to the expected global mean SSH rise (2.75 cm) for the individual model configurations.

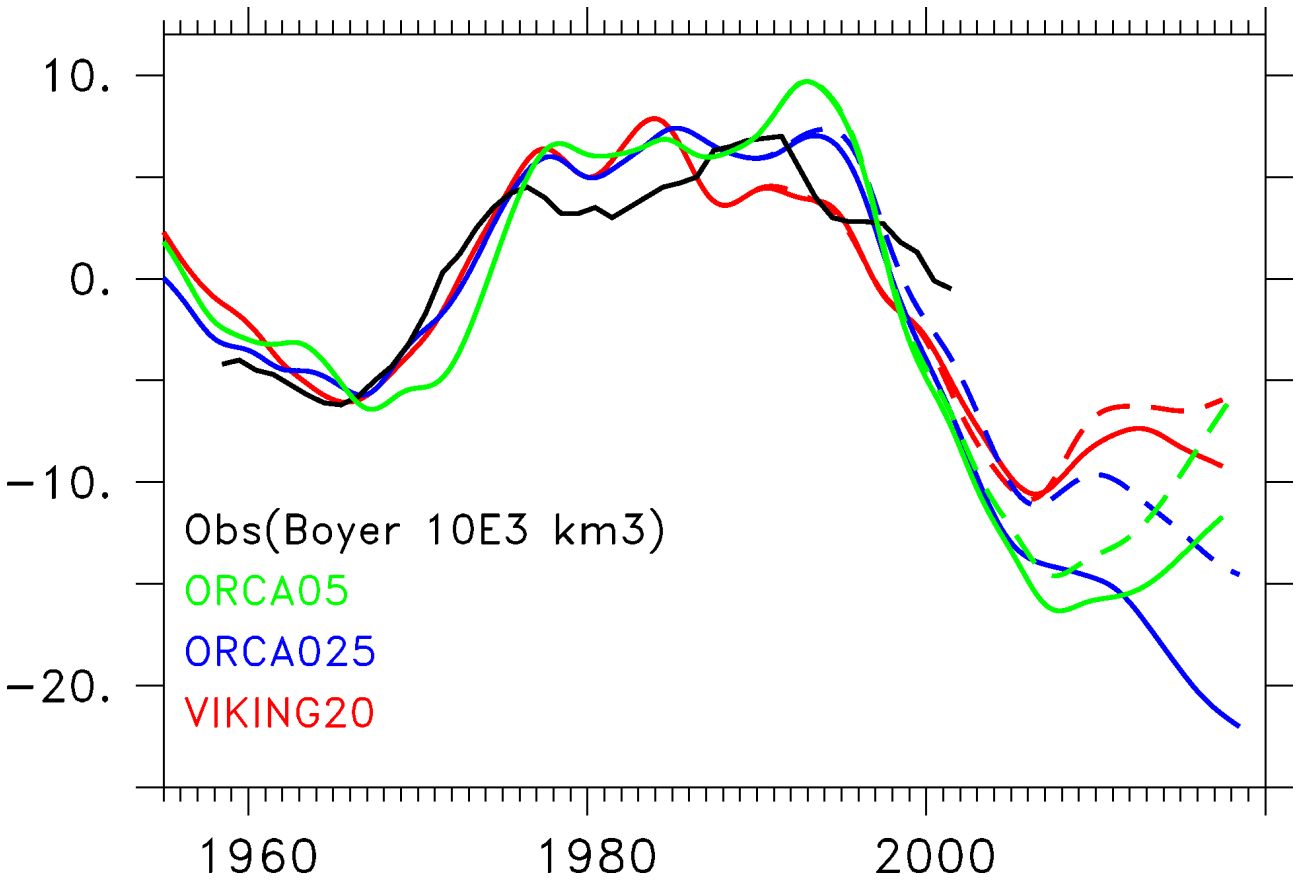

Figure 54.: Freshwater content anomaly (0-2000m) in 10^3 km^3 for the subpolar North Atlantic from observations (solid black line) and different simulations (reference simulations in solid and R-MELT simulations in dashed). The region for the computation is indicated in Figure 8.

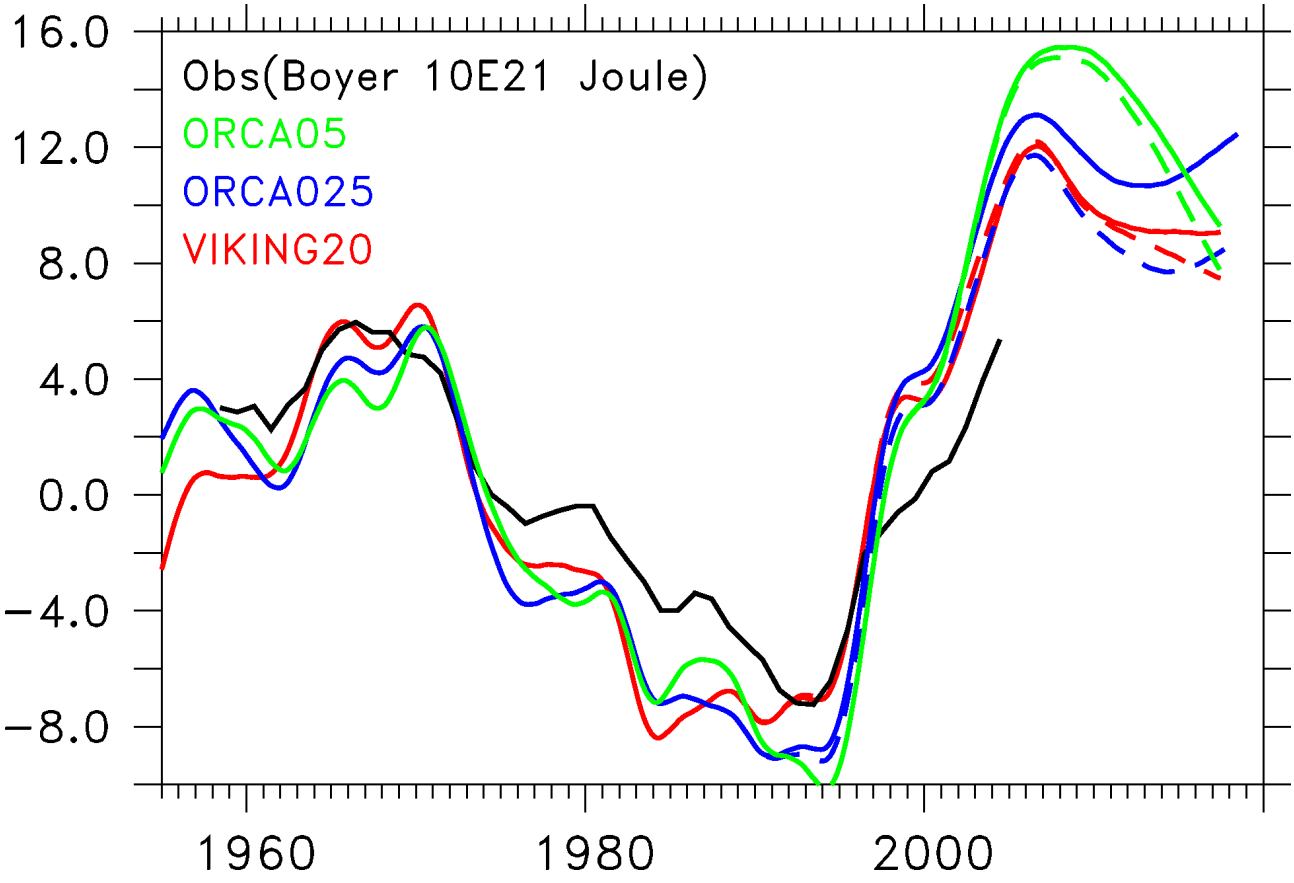

Figure 55.: Heat content anomaly (0-2000m) in 10^{21} Joule for the subpolar North Atlantic from observations (black solid line) and different simulations (reference simulations in solid and R-MELT simulations in dashed). The region for the computation is indicated in Figure 8.

km³ and VIKING20 with 5×10^3 km³ at the end of the hosing period. Anomalies in the upper 1000 m of the Nordic Seas are 1174 km³ (ORCA05), 1191 km³ (ORCA025) and 614 km³(VIKING20) and suggesting according to Curry and Mauritzen (2005) only small changes in the overflow density. Based on this values the smallest effect is expected in VIKING20, which shows the lowest freshwater anomaly, indicating the largest freshwater export compared to the other configurations. These results are in line with the salinity anomalies presented in Figure 51. Taking a natural multidecadal variability of approximately $\pm$ 10 $\times$ 10^3 km³ into account, the freshwater anomalies exhibited after 30 years in this scenario are within that range of natural variability and therefore hard to measure.

Heat content

The anti-correlation between freshwater and heat content anomalies (Figure 55) is valid as suggested by Boyer et al. (2007) even with arbitrary atmospheric condition. The control simulations (solid lines) show a drop in the heat content after 2007. That is probably related to the repeated 2007 atmospheric forcing, while the further development of the heat content varies between the configurations. Irrespectively to the tendency of the control run, all R-MELT simulations (dashed) suggesting a de-

crease at the end of the hosing simulation, strongest in ORCA025 of about -4 $\times$ 10^{21} Joule, somewhat lower in ORCA05 and VIKING20 ($\sim$ -1 to -2 $\times$ 10^{21} Joule). The suggested anomalies in the melting simulations are small compared to the natural variability ($\pm$ 6 $\times$ 10^{21} Joule).

Summary: Large scale anomalies in the I-MELT and R-MELT scenario

With respect to salinity anomalies (0 - 2000 m) the simulations show an overall freshening of the subpolar North Atlantic, irrespectively of resolution and melting scenario. The temperature response (0 - 2000 m) suggests a cooling at the ocean surface but also a convection response related warming in the interior Labrador Sea and Baffin Bay at least in the I-MELT scenarios. All simulations exhibit in the I-MELT scenario a northward shift of the Gulf Stream south of Nova Scotia which produce a warming and positive salinity anomaly there. The sea surface height shows the largest increase around Greenland and along the North American coast.

The response in the R-MELT scenario follows in principle the I-MELT behaviour, but is distinctly reduced and partly covered by mesoscale variability, at least in the higher resolution configurations in the region of the Gulf Stream. However a crucial difference between both coarser configurations and VIKING20 is the path of the NAC. This path seems to act as a buffer for the eastward propagation of anomalies across the Atlantic (temperature, salinity, SSH) at least in VIKING20. The coarser simulations show a comma shape export pathway reaching from SPG to the STG following results from (Swingedouw et al. (2012)). That effect is relevant for melting simulations in coupled climate models, mostly suffering from deficits in the representation of NAC. The propagation of anomalies indicates that some portion can leave the subpolar North Atlantic due to the exchange between both gyres. That export pathway is enhanced in the coarser configurations A significant export pathway of meltwater is accomplished by the DWBC, which is only present in the higher resolution configurations. The presented diagnostics reveal substantial changes in the Nordic Seas, which are critical for the formation of dense water masses and subsequently for the overflows. The according changes within the Nordic Seas will be investigated in section 5.3.7.

5.3.6. SPG and STG circulation and the Gulf Stream

As earlier stated some anomalies are related to circulation changes, rather than to the presence of meltwater from Greenland. A possible way to illustrate shifts in fronts and gyres is to investigate changes in the barotropic streamfunction, shown in Figure 56. Shown are means over the last decade of reference simulation (upper panel) and I-MELT simulation (lower panel). The 0 contour is used to define the separation between SPG (cyclonic) and STG (anticyclonic). It was found that a northward shift of the NAC south of Nova Scotia is suggested by related T, S and SSH anomalies. That behaviour can be seen in a slight northward shift of the 0 contour line, or at least a weakening of the cyclonic circulation in that region like indicated in VIKING20. Somehow suspicious is the effect around the NW

Corner. In this region it seems that in the hosing simulations the representation of the NW Corner is improved at least in both coarser resolution configurations. That is related to the slight weakening of the SPG. However an opposing behaviour is seen in VIKING20 which shows a well located NW corner in the reference simulation and an eroding (southward shift) in the hosing simulation, associated with according large anomalies of temperature and salinity in that region. The proposed difference between ORCA05/ORCA025 and VIKING20 with respect to the development of the comma shape (export pathway) is not visible from that diagnostic straight away. In the R-MELT scenario, the circulation changes are too small compared to stochastic mesoscale variability and therefore not visible in the barotropic streamfunction.

5.3.7. Hydrographic changes in the Nordic Seas and implications for the overflows

After investigating the large scale horizontal anomaly pattern the focus is set on the Nordic Seas, the area where the dense overflows are formed (Macrander et al. (2007); Strass et al. (1993); Hansen and Osterhus (2000)). It is known that changes in the deep convection in the Labrador Sea have an impact on the interannual variability of the AMOC (Biastoch et al. (2008a)). Changes in the overflows from Nordic Seas to the subpolar North Atlantic trigger long-term changes in the meridional overturning and induce anomalies in the related meridional transport of heat and salt (Zhang et al. (2011), Latif et al. (2006)). To investigate the local changes in the Nordic Seas a similar diagnostic as applied in the Labrador Sea is used. Therefore area-means of temperature, salinity, SSH, tracer concentration and mixed layer depth of the reference simulation have been compared to the hosing results. Beside the remote control of the Nordic Seas on the AMOC, changes in this region have also implications for the regional climate and environment of Scandinavia (Koenigk et al. (2005)).

Response in the I-MELT scenario

The temperature anomalies over the Nordic Seas differ from those derived in the Labrador Sea (Figure 57a). ORCA025 and VIKING20 tend to a cooling from the surface to depths of 600 - 800 m, which emerges after about 10 years ($\sim$ 1975). That timescale roughly agrees with the time, the previously described anomalies (temperature and salinity) need to propagate within the SPG into the Nordic Seas. A possible shortcut by recirculations from the ECG into the Nordic Seas (Strass et al. (1993)) as well as through the Denmark Strait was introduced in recent investigations Våge et al. (2011) proposing that some portion of DSOW is formed close to the northern coast of Iceland, thus could triggering a quicker response of the DSOW. The cooling of water in the overflow range exceeds 1 °K in ORCA025 and VIKING20 after about 10 to 20 years. No clear mid depth warming signal is visible like in the Labrador Sea in all configurations, due to the collapse of the convection. Somehow unusual, ORCA05 shows a distinct warming of the top 400 m which is also found in most results in (Swingedouw et al. (2012)). The explanation for that positive anomaly is the following: The surface

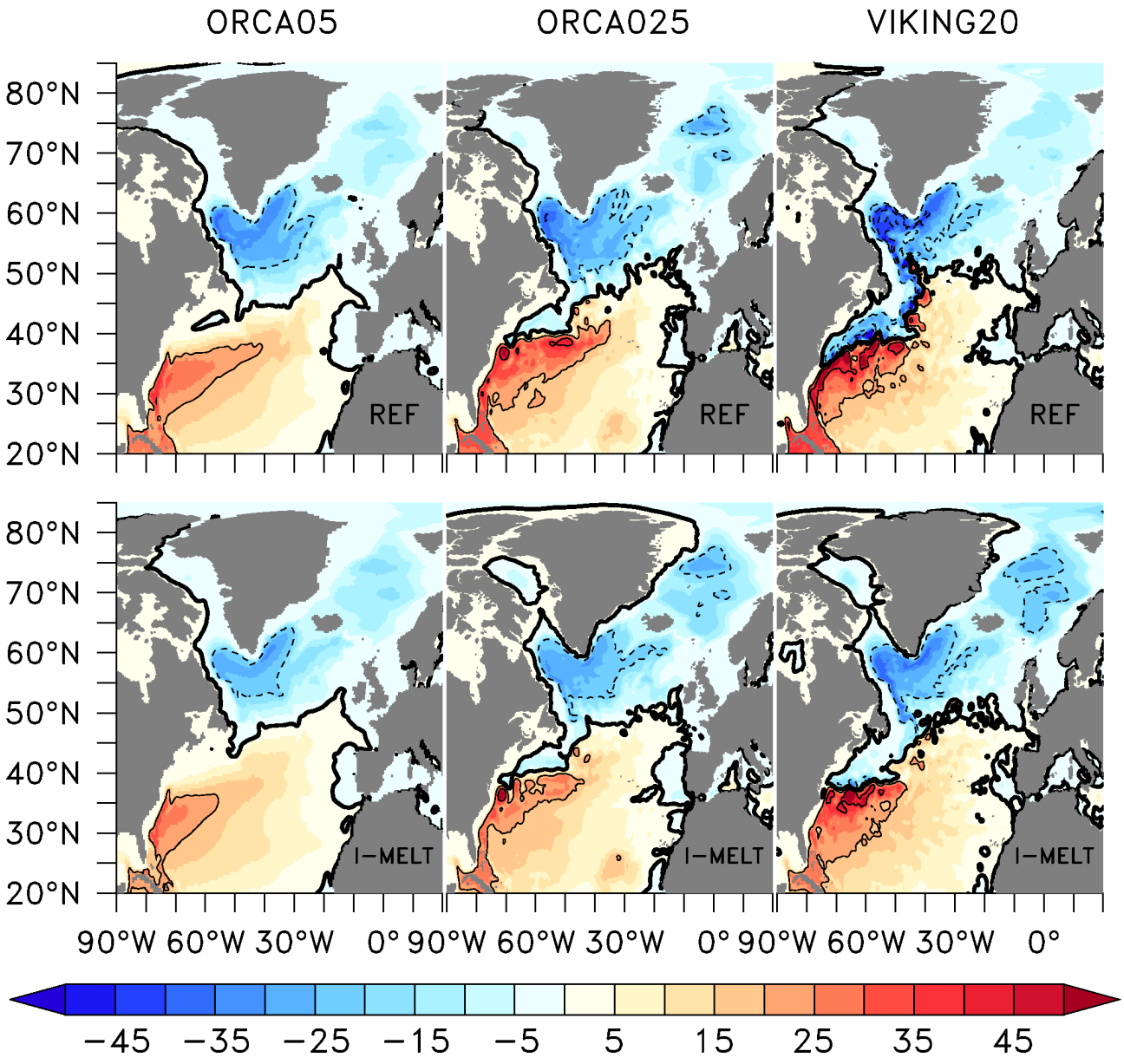

Figure 56.: Mean barotropic streamfunction (1998-2007) of the reference simulation (upper panels) and for I-MELT simulations (lower panels). Negative values indicate cyclonal and positive anti-cyclonal flow. Contour lines indicate 20 Sv intervals.

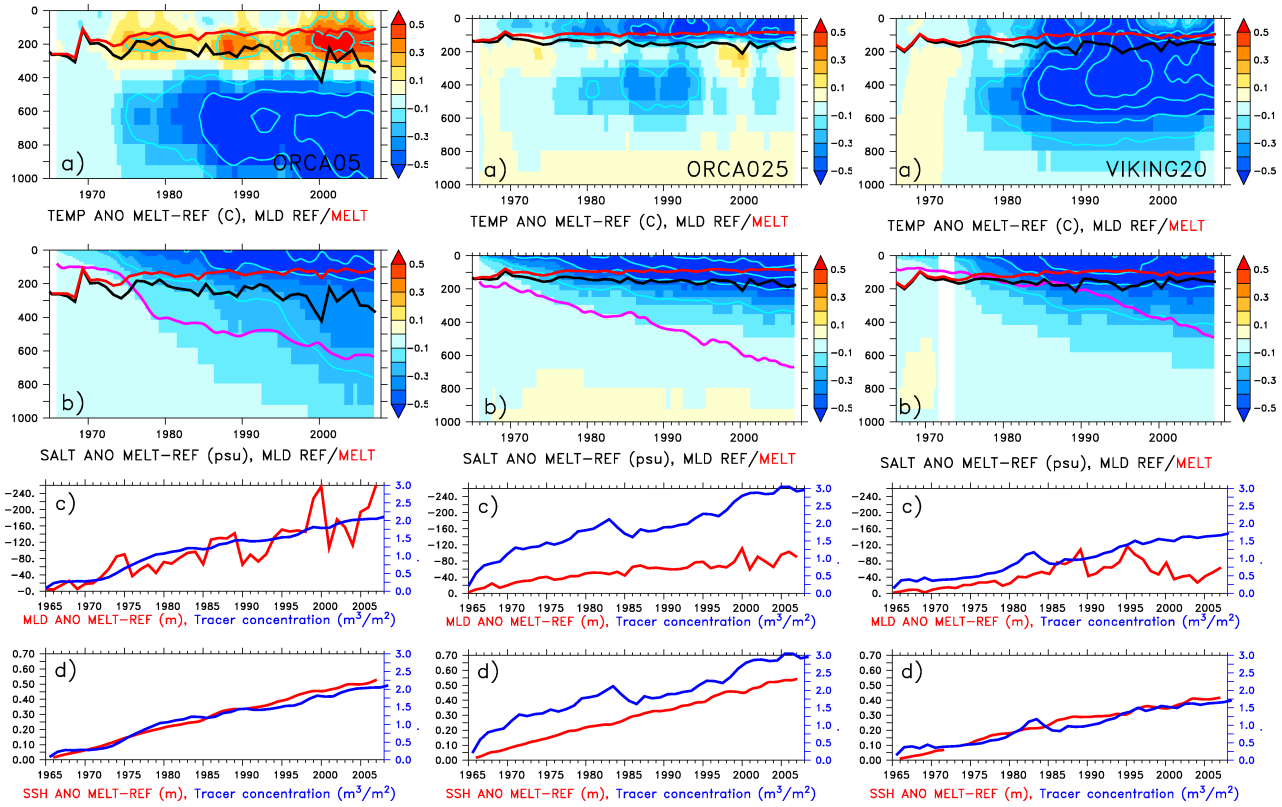

Figure 57.: Anomalies of hydrographic quantities between hosing (I-MELT) and reference (REF) simulation in the different model configurations. (a) temperature (°K), (b) salinity (psu), (c) March-MLD (m, in red) and vertical integrated passive tracer concentration (m^3/m^2, in blue) and (d) SSH (m, in red) and vertical integrated passive tracer concentration (m^3/m^2, in blue). The thick lines in (a) and (b) indicate the March-MLD in the reference (black) and hosing (red) simulation. The magenta line in (b) mark the 0.001 m^3/m^3 isosurface of the passive tracer to illustrate the freshwater spreading. The light blue contour lines in (a) mark a 0.25 °K interval and 0.25 psu in (b). All anomalies are interannually filtered.

heat losses of Atlantic inflowing water are reduced by the shielding effect of the freshwater cap on top, due to lower vertical mixing. This leads to an earlier outcropping of these water masses in the region of the Nordic Seas instead of the Arctic Ocean. Obviously, with increasing resolution and presence of eddies, that response seems to differ substantially from the coarser results. ORCA05 shows below that warming layer a clear cooling pattern propagating to a depth of 1200 m. Since the averaging area (entire Nordic Seas) is comparatively large, the signal of the mixed layer depth is not as pronounced as in the Labrador Sea. However, the mixed layer depth in ORCA05 is somewhat deeper (around 400 m) than in the other two configurations (around 200 m). The MLD clearly marks the transition zone between the near surface inflow of warm waters and cool outflows, which is indicated by the temperature anomalies. In the GrIS melting simulations the mixed layer depths show a shoaling by about 200 m in ORCA05 and only a few tens of meters in the higher resolution configurations.

The salinity anomalies suggest a clear freshening, propagating from surface to depth of 1200 m and somewhat shallower in ORCA025 (400 m). The salinity anomalies exceed 0.5 psu after about 20 years. The meltwater concentration (magenta line) is not as strongly linked to the salinity anomalies as in the Labrador Sea. That reflects that only some portion of the salinity anomalies are caused by the direct presence of meltwater. Circulation changes and associated changes in the meridional freshwater transport into the Nordic Seas gain in importance and contribute significantly to the freshening signal.

The close relation between MLD and tracer is only visible in ORCA05. In ORCA025 and VIKING20 both quantities are more unrelated than in the Labrador Sea. The reason for that behaviour seems again linked to the importance of the circulation changes, rather than to the actual amount of meltwater, which affects the MLD.

The conjunction between SSH and tracer concentration on the other hand is still seen with some exceptions in VIKING20 and ORCA05. VIKING20 shows the lowest meltwater concentrations and SSH rise of all simulations. ORCA05 and ORCA025 exhibit an increase of about 0.5 m over 43 years, while VIKING20 exhibits only 0.4 m over that period. From that diagnostic robust features seem to be the freshening signal and the SSH rise among all configurations. A clear resolution effect is not seen. This diagnostic would suggest that the overflowing water becomes fresher and colder, but from that it is unclear which contributes most to the important density change of the overflow (shown later).

The response in the R-MELT scenario

The R-MELT results (Figure 58) show a similar reaction as in the I-MELT simulation. The temperature signal in the higher resolved simulation however is dominated by the mesoscale variability. The warming of the near surface waters and cooling at depth develops again in ORCA05. Relative little or no effect is seen in the depth of the mixed layer. The most pronounced signal among all quantities

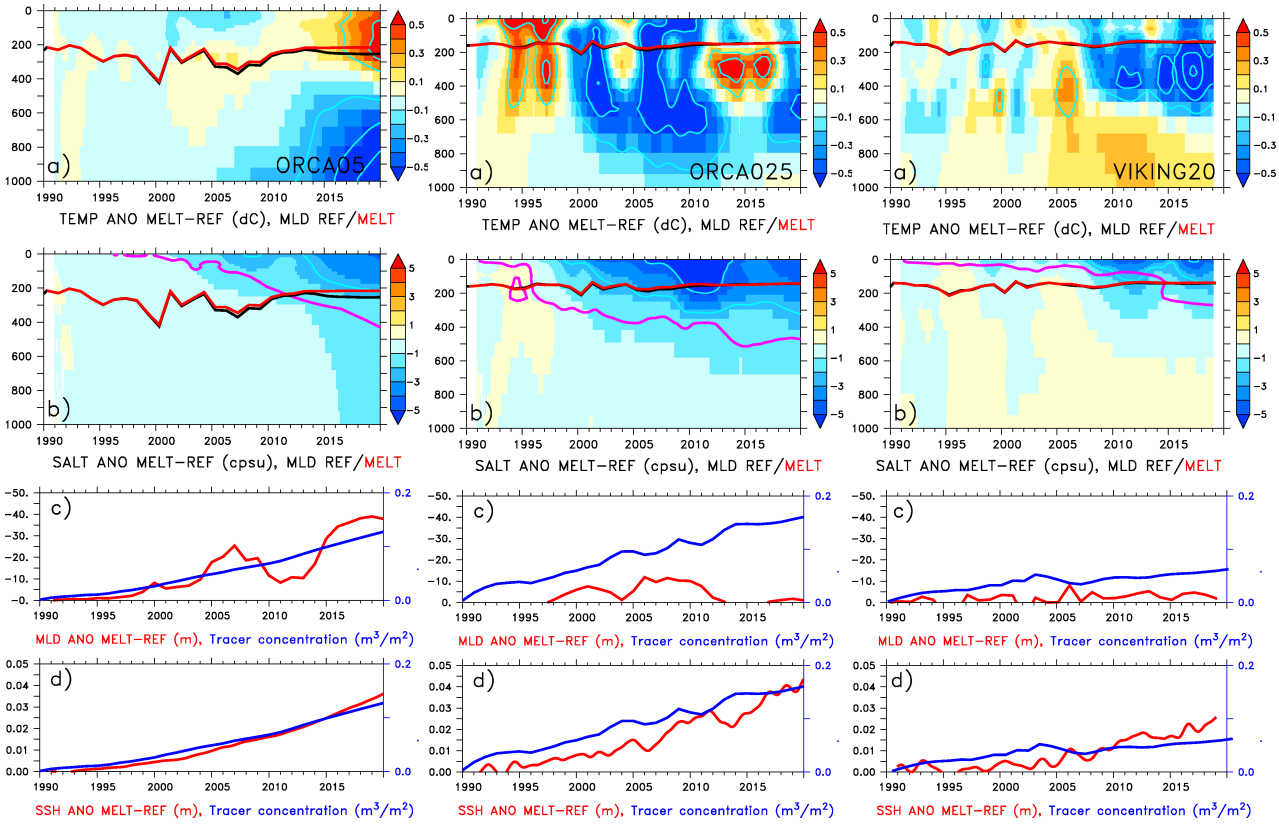

Figure 58.: Anomalies of hydrographic quantities between hosing (R-MELT) and reference (REF) simulation in the different model configurations. (a) temperature (°dK), (b) salinity (cpsu), (c) March-MLD (m, in red) and vertical integrated passive tracer concentration (m^3/m^2, in blue) and (d) SSH (m, in red) and vertical integrated passive tracer concentration (m^3/m^2, in blue). The lines in (a) and (b) indicate the March-MLD in the reference (black) and hosing (red) simulation. The magenta line in (b) mark the 0.0001 m^3/m^3 isosurface of the passive tracer to illustrate the freshwater spreading. The light blue contour lines in (a) mark a 0.025 °K interval and 0.025 psu in (b). All anomalies are interannually filtered.

is seen in the salinity anomaly, which shows a surface intensified freshening signal, slowly propagating to depth. A relative large difference occurs in the timing and vertical extent of those anomalies over all configurations. A slight immediate freshening is present in ORCA05 with an acceleration after about 15 years (2005). That acceleration occurs approximately 5 years earlier (2000) in ORCA025, while VIKING20 displays only after 20 years (2010) a persisting near surface freshening signal. With respect to the SSH rise, both coarser configurations suggest a SSH rise of about 3 - 4 cm after 30 years, while VIKING20 shows only 2 cm over the melting period, which coincides with the smallest salinity anomalies over that region.

5.3.8. Changes of the DSOW density in the Denmark Strait

As shown in Behrens et al. (2013), the model results suggest a close link between the overflow density (σ_0) of DSOW and AMOC. Similar results are presented by (Latif et al. (2006)). Measuring the AMOC requires a large effort, while changes in a key location like the Denmark Strait require much

less efforts and give the opportunity to infer on the AMOC which is of greatest interest. The changes in the overflow density (Figure 59a) in the I-MELT scenario indicate a relative small decrease within the first ten years ($\sim$ 1975) in line with earlier results. (Substantial anomalies need to reach the Nordic Seas and influence the dense water formation). That confirms that the anomalies originating from Labrador Sea or induced in the NAC have to propagate within the SPG into the Nordic Seas. Local effects within EGC and interactions within the Nordic Seas seem of minor importance for changes of the overflow density, which would trigger a faster response. After 10 years the formation of dense water masses in the Nordic Seas is considerably affected and leads to an accelerated decline of dense water masses feeding the lower limb of the AMOC and indicating a positive feedback (Griffies et al. (2009)). All simulations show a similar decline in the DSOW density until 1988 ($\sim$ 20 years of hosing). Further on VIKING20 projects a larger decline than ORCA05 and ORCA025. After 43 years the maximum density of the overflow has dropped by -0.28 kg/m^3 and -0.16 kg/m^3, for VIKING20 and ORCA05/ORCA025 respectively, compared to the reference simulation. These results suggest a larger declining response in the VIKING20 configuration. It should be noted that the initial density of the overflow differs between all configurations due to differences in the resolved physical processes as well as in unavoidable differences in the initial state at the beginning of the hosing simulation. (Means are 28.03 kg/m^3 (ORCA05), 27.95 kg/m^3 (ORCA025) and 28.11 kg/m^3 (VIKING20) for the period from 1998-2007, observations suggests $\sim$ 28.1 kg/m^3 Macrander et al. (2007))

The response in the R-MELT scenario (Figure 59b) is more affected by short term variability, but a clear decline starts after 15 years in ORCA05 and ORCA025 and continues over the entire hosing simulation. Opposing to these evolutions the density in VIKING20 is recovering during that last 10 years to values of the reference simulation, while ORCA05 and ORCA025 show an ongoing decline of the DSOW density of $\sim$ -0.008 kg/m^3 instead. That result corresponds to the smallest anomalies (temperature and salinity) seen in VIKING20 over the Nordic Seas at the end of the hosing simulation. From these findings and former results a conclusion could be drawn, that the I-MELT simulation is extensive and forces all models to the same response. In a more realistic melting simulation with resolved eddies the tendency is not clear, at least for the overflow density, while some other quantities behave similar to the realistic runoff forcing.

5.4. Repercussions for the Meridional Overturning Circulation

5.4.1. Connection between DSOW density and AMOC strength

As presented in Behrens et al. (2013) the relation between density of the overflow and AMOC strength holds and is also seen in VIKING20 and in GrIS (I-MELT) simulations (Figure 60). The decline is nearly linear in all simulations until the AMOC is reduced by about 50%. The largest decline of AMOC and DSOW density shows VIKING20. After that linear decline the further drop becomes

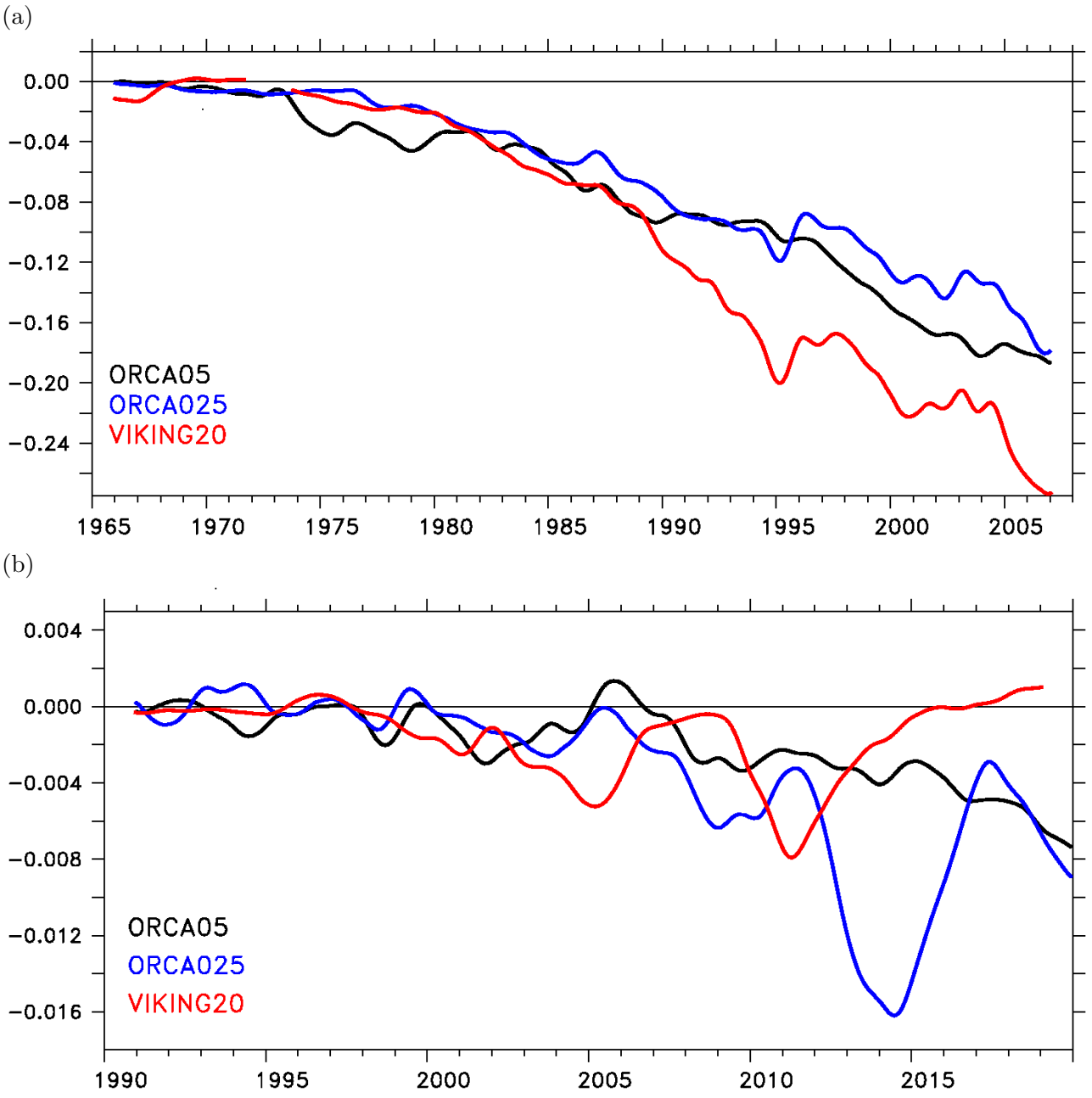

Figure 59.: Density anomaly (σ_0) between hosing and reference simulation of the overflowing water at the sill depth in the Denmark Strait for the individual model configurations in kg/m^3. (a) For the I-MELT scenario and (b) for the R-MELT scenario. The timeseries are interannually filtered.

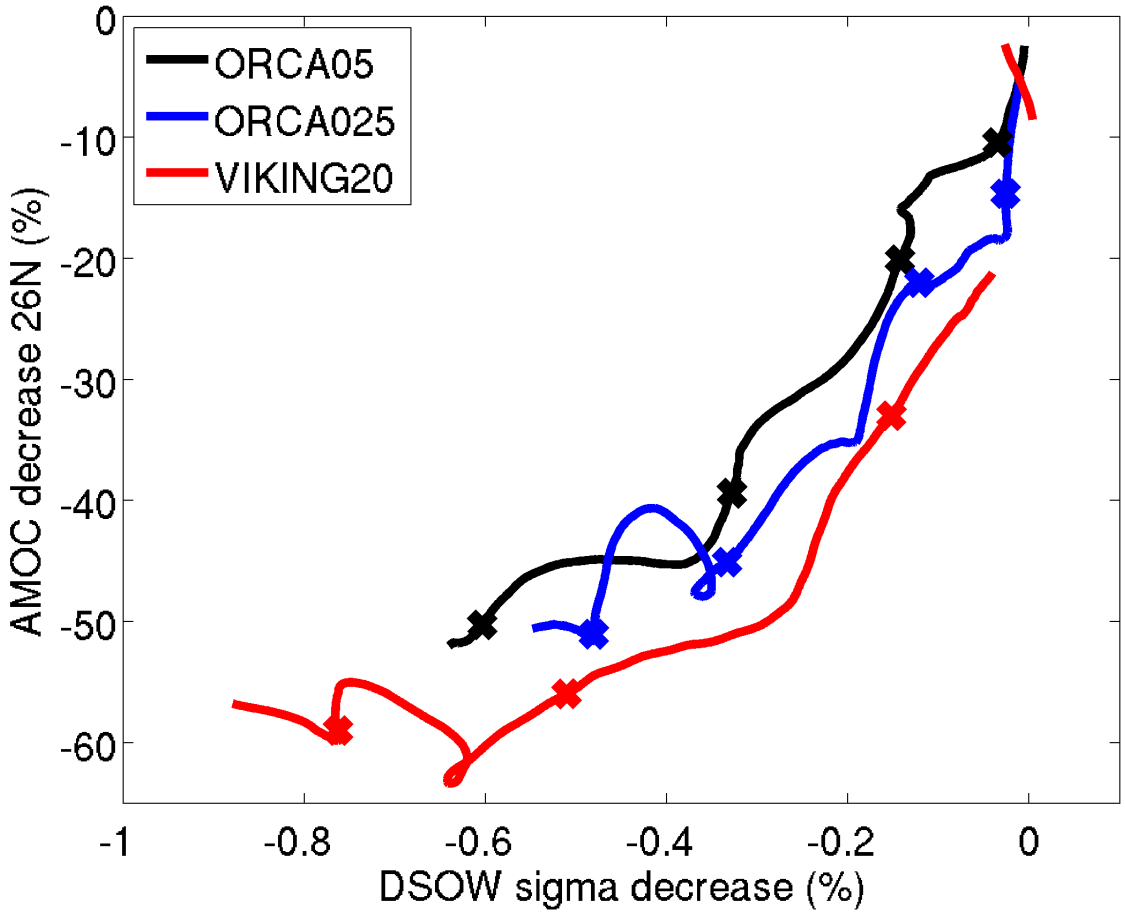

Figure 60.: Relation between relative changes (%) of the DSOW density (σ_0)and AMOC strength at 26°N between hosing (I-MELT) and references (REF) simulation for the different model configurations. Timeseries are smoothed with a decadal running mean. The crosses indicate each decade since the start of the hosing. The first cross in VIKING20 is missing due to lost data.

more gradual. It should be highlighted that very small changes in the overflow density have a large impact on the AMOC.

5.4.2. The response of the AMOC in the subtropics (26.5°N)

Response in the I-MELT scenario

Here the AMOC response at 26.5°N is evaluated to investigate the large scale response a allow the comparison to observations. The mean (1998-2007) vertical structure of the AMOC is shown on the left hand side for the reference simulations (solid) and hosing experiments (dashed) in Figure 61 (left panel). Observations suggest a mean AMOC of about 18.7 Sv ± 2.1 Sv at this latitude (Cunningham et al. (2010)). Both coarser models show a lack of about 3 Sv, while VIKING20 suggest 3 Sv larger overturning than the observations. As shown in Behrens et al. (2013) the mean value

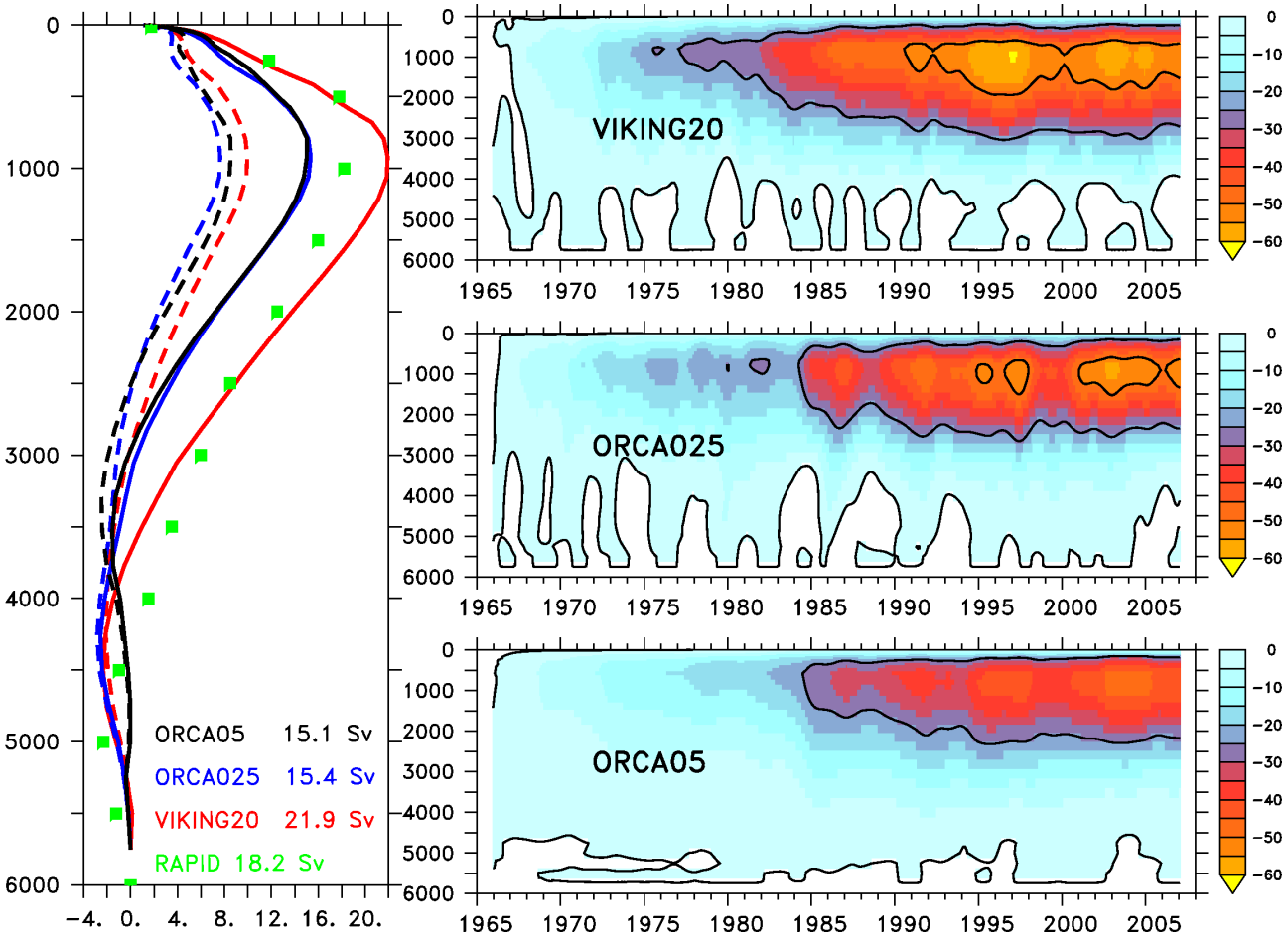

Figure 61.: AMOC 26.5°N response to Greenland melting (I-MELT). Vertical profile of the meridional streamfunction for control (solid) and hosing (dashed) simulations (left panel) averaged from 1998-2007 in Sv for each model configuration. Measurements of RAPID (2004-2009) are marked in green. Values indicate mean maximum values of the reference simulation over that period. Hosing related anomalies (in %) relative to the maximum value at that time in the reference simulation are shown in the right panels for the individual configurations. Each 25% interval is contoured. Hovmöller timeseries are interannual smoothed. Hovmöller timeseries are interannually smoothed.

of the AMOC is very sensitive to subpolar freshwater forcing. The applied atmospheric forcing is the same among all simulations, but differences in the northward transport of heat and freshwater are present and result in different ocean-atmosphere fluxes. The differences in the fluxes can also contribute to the different mean states. Irrespective of the differences in the maximum value, the vertical structures show consistent characteristics among all configurations. The maximum value of the streamfunction is located at a depth of 1000 m as suggested by observations (Cunningham et al. (2010)), with a southward flow from 1000 - 3500 m in ORCA05 and 1000 - 4500 m in the other two configurations. The near bottom flow is associated with the AABW, which is formed near Antarctica and penetrates in all ocean basins. Due to the differences in the mean AMOC values among the configurations, anomalies are referenced to the maximum value at 26.5°N of each configuration (shown in right panel). The largest reductions are visible in the upper 2500 - 3000 m, centered around 1000 m, the location of the maximum (Figure 61). The reduction is caused by reduced production rate and replenishment of dense water masses in the subpolar North Atlantic (shut down of Labrador Sea convection and decrease of DSOW density (Figure 59 and 36a). No significant changes are seen below 3000 m. The large decline in the DSOW density points to substantial changes in the density structure of the Atlantic and possible different depth ranges of returning water masses within the lower limb of the AMOC. The fastest significant (>20%) response is seen in VIKING20 and ORCA025 after about 10 years (right panel), which is also approximately the timescale when the overflow density is affected significantly. In ORCA05 similar changes are visible after approximately 20 years. The AMOC decline is steady (see also Figure 60) over the entire hosing period. Since the Labrador Sea convection is shut down within the first years, with implications for the AMOC, the progressing long-term decline has to be accomplished by the declining overflows. That is also supported by findings in Behrens et al. (2013) and indicates a mainly advective process for the signal propagation to south, with similarities to Biastoch et al. (2008b) for northward propagating signals from the Agulhas region. The delay in ORCA05 might be related to differences in the signal propagation in the DWBC, which is affected by the resolution in B-grid models (Getzlaff et al. (2005)) and not well resolved in ORCA05. However at the end of the hosing simulation (after 43 years), the AMOC shows a reduction of about 50%-60% from its maximum value, largest in the eddy resolving configuration.

Response in the R-MELT scenario

The corresponding R-MELT results are presented in Figure 62. The difference to the control simulation (2010-2019, left panel) suggests the largest decline in ORCA025 by about 1.2 Sv at a depth of about 1000 m. ORCA05 shows a decline of 0.5 Sv and VIKING20 by 0.4 Sv over that last decade. The relative changes (relative to the maximum AMOC value) are shown in the right panel. ORCA05 shows a steady decline exceeding 5 % in 2019. Both higher resolution simulations show larger variability, which is likely induced by a stochastic eddy variability superimposed to the melting signal. The mesoscale processes trigger wave processes, which induce the high AMOC variability in both higher resolution

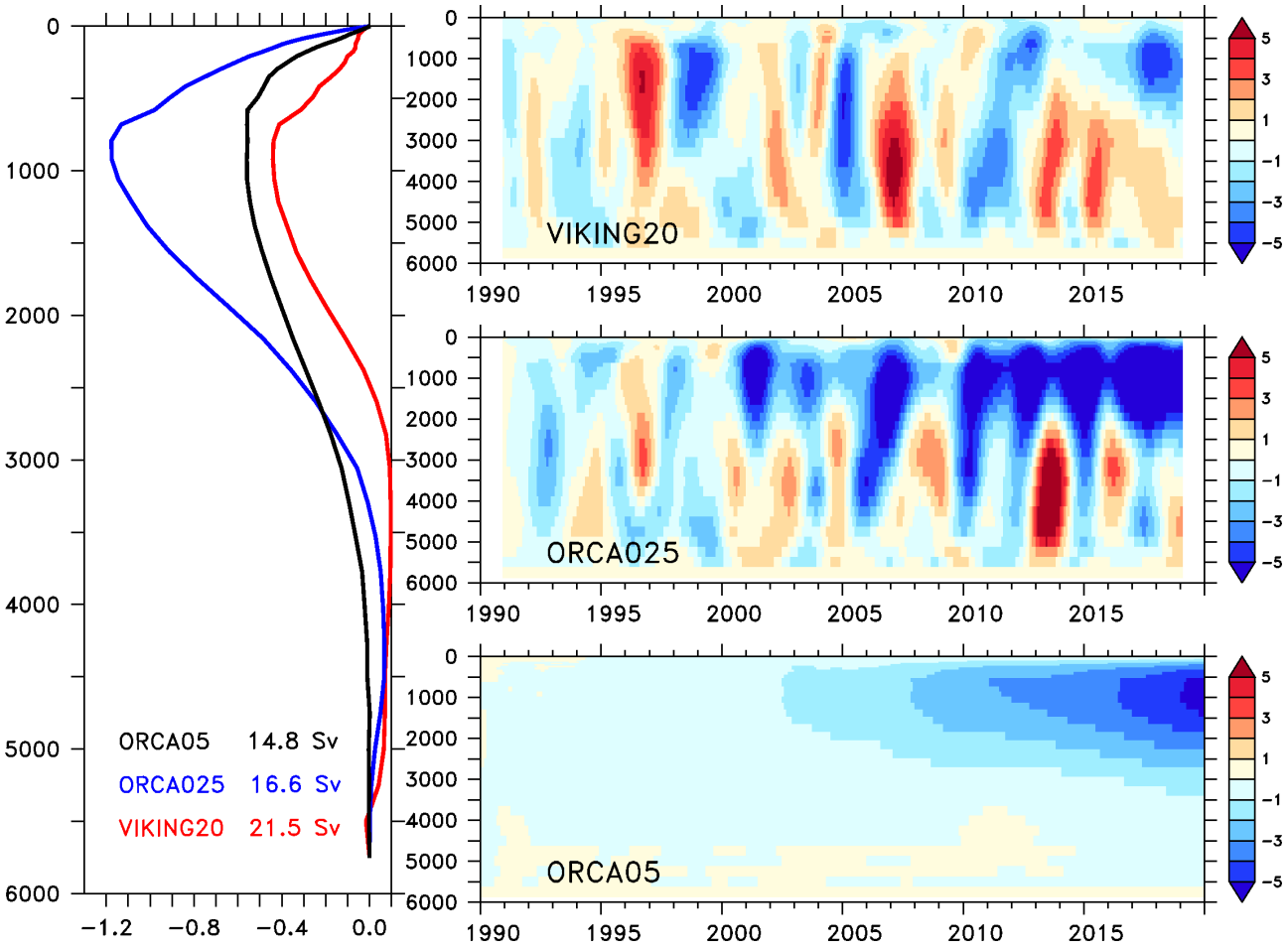

Figure 62.: AMOC 26.5°N response. Vertical profile of the meridional streamfunction difference between hosing (R-MELT) and reference (REF) simulations (left) and averaged from 2010-2019 in Sv. Values indicate mean maximum value of the reference simulation over that period. Hosing related anomalies (in %) relative to the maximum value at that time in the reference simulation are shown in the right panels for the individual model configurations. Hovmöller timeseries are interannually smoothed.

models (similar to Getzlaff et al. (2005)). Obviously, these wave processes in the I-MELT scenarios are small against the advective signals. All simulation share the same forcing, but only ORCA05 does not resolve these small scales and therefore does not show this type of variability. Eddy variability is in the order of about 5% compared to the maximum AMOC at that latitude (Treguier et al. (2012)). The largest negative anomaly exhibits ORCA025 with a reduction exceeding -5 % after 2010 continuously, followed by ORCA05 with negative anomalies of about $\sim$ -5 % at the end of the hosing simulation. VIKING20 does not show any clear declining tendency over the entire period. In the I-MELT scenario the melting signal is the dominating factor compared to the smaller mesoscale variability. These results suggest that in both simulations when eddies are resolved or an eddy parameterisation is applied, no or a weaker AMOC response occurs under the same melting scenario in comparison to the ORCA025 results. The explanation for that behaviour is linked to the local response of the deepwater formation in the SPG region in each individual configuration. However, based on these results it cannot be excluded that the initial conditions and long-term trend are affecting the AMOC response as well. On the other hand, simulations in the I-MELT scenario in ORCA05 with different initial conditions and different AMOC trends suggest that the initial conditions and long-term behaviour are of minor importance for the AMOC response (see Appendix A). A similar set of simulations in the R-MELT scenario was not performed. Finally it can by concluded from the VIKING20 results that the melting response is smaller compared to the stochastic mesoscale variability over the hosing period. Observations show no significant interannual variability at this latitude (McCarthy et al. (2012)). However, the models show interannual variations of about $\pm$ 2 Sv, which represents relative changes of about $\sim$ 10% compared to the maximum value. That means only ORCA025 shows AMOC changes in that order of magnitude at the end of the hosing simulation. The stable AMOC in VIKING20 is related to unchanged conditions in deep water formation and overflows.

5.4.3. Changes in the meridional heat transports

The reason for the enhanced interest in the AMOC is the fact that heat and freshwater transports are closely related to the AMOC strength in low and mid latitudes (Johns and Baringer (2011)). Changes in the northward heat transport are crucial for the European climate with far reaching consequences and therefore of largest interest.

Response in the I-MELT scenario

As mentioned above, the meridional heat transport is closely linked to the overturning strength in low and mid latitudes. Therefore the differences in the mean AMOC state between the individual configurations are also visible in an offset in the meridional heat transport (control simulation in solid lines, Figure 63, left panel). The largest heat transport shows VIKING20 with $\sim$ 1.2 PW close to the observed estimate of 1.3 PW by (Johns and Baringer (2011)). Lower maximum heat transports

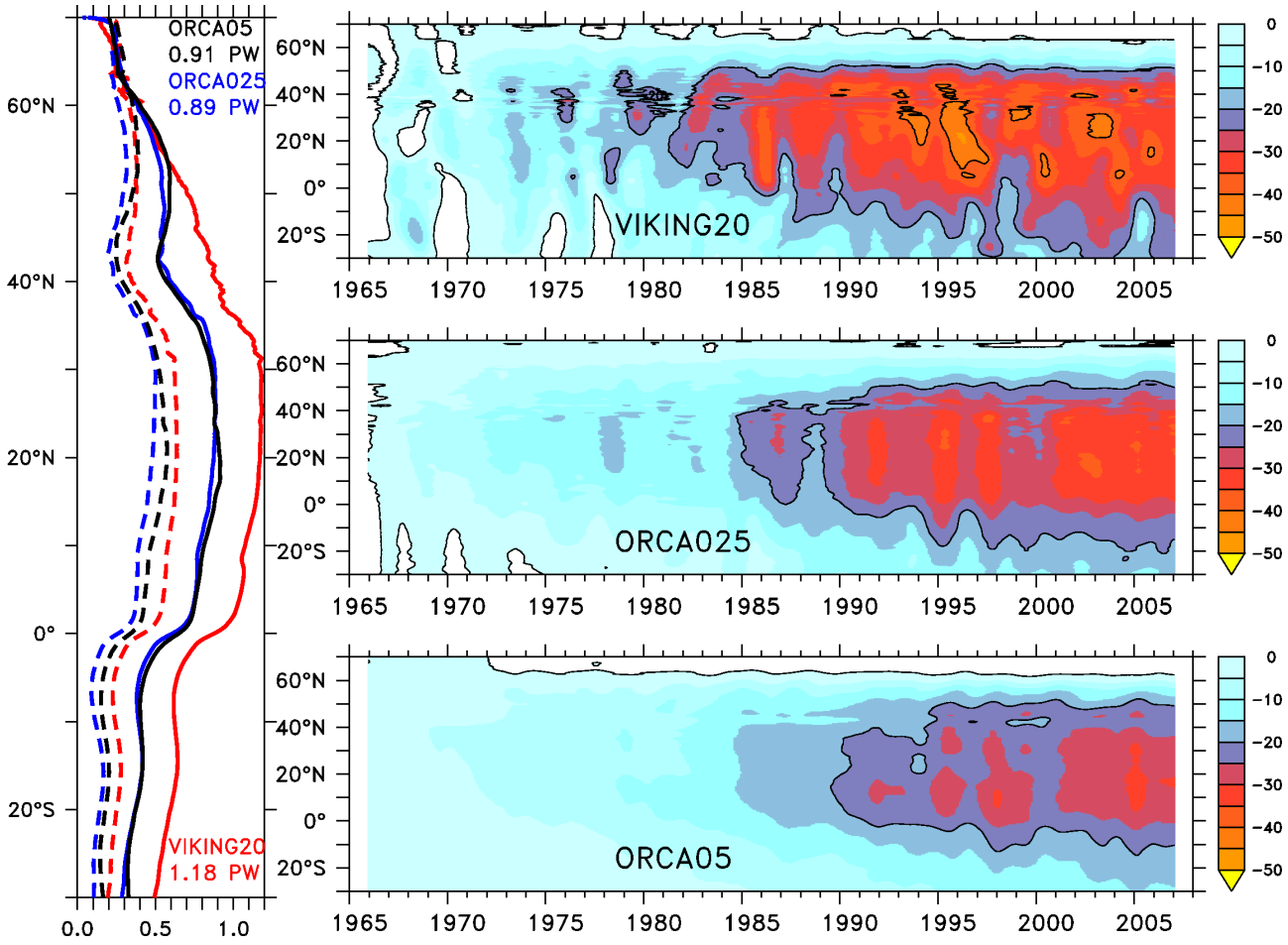

Figure 63.: Meridional heat transport in PW and its latitudinal dependence for control (solid) and hosing (I-MELT, dashed) simulations averaged over 1998-2007 (left panel). Values indicate the maximum value of the control simulation over that period for each individual model configurations. Meridional heat transport anomalies (in %) relative to the meridional maximum heat transport in the reference simulation of each model configuration are shown in the right panels. Each 25% interval is contoured. Hovmöller timeseries are interannually smoothed.

are obtained in ORCA05 and ORCA025 by $\sim$ 0.8 PW. In the melting simulations the weakening of the AMOC is a nearly meridional coherent signal (not shown), therefore the heat transports in the melting (I-MELT) simulation keeps the meridional structure but the overall value (26°N, Figure 63, both panels) is reduced. This is most pronounced in the location where the largest heat transport occurs. The first weakening signals (relative to the meridional maximum heat transport value, Figure 63 right panel) coincide with the weakening signals in the AMOC around 10 years after the beginning of the melting, somehow delayed in the coarser resolutions (1985, after 20 years). The reduction reaches up to 50 % in the VIKING20 (30 % - 35 % in ORCA05 and ORCA025), which is very similar to the AMOC decline and not restricted to the Northern Hemisphere where the largest response is visible (between 0° - 50°N).

Response in the R-MELT scenario

VIKING20 (2010-2019) shows the smallest reduction in the meridional heat transport at a value of about -0.02 PW, which slightly enhanced in ORCA05 (Figure 64 left panel). The largest reduction provides ORCA025, which is connected to the largest AMOC anomaly and produces a decline of -0.06 PW. Similar to the AMOC response in the R-MELT scenario, the mesoscale variability is dominating the heat transport anomaly and affects the expected weakening signal, at least in both higher resolution configurations (Figure 64, right panel). Those mesoscale variability can easily induce variability of $\pm$ 5 % compared to the maximum (Treguier et al. (2012)) and possibly trigger waves, which induce meridional propagating anomalies (like AMOC signals in Getzlaff et al. (2005)), as seen in right panel. Interannual variability accounts for anomalies of up to $\pm$ 15 %, which means that only ORCA025 exhibits anomalies with a similar magnitude. However, all simulations suggest a relative weakening of the northward heat transports, which is most pronounced in ORCA025 with anomalies exceeding -10 % between 10°N - 40°N compared to the meridional maximum heat transport. An ongoing decline in the heat transport shows again ORCA05, similar to the AMOC and emphasised after $\sim$ 10 years (2000) and not affected by any mesoscale variability. These results show similar to the AMOC response that both configurations with explicitly resolved or parametrised eddies exhibit the lowest decline in the maximum heat transport compared to the ORCA025 results. VIKING20 shows the weakest decline of all simulations as suggested by the lowest AMOC reduction.

5.4.4. Changes in the meridional equivalent freshwater transport

The last quantity which is of interest in combination with the meridional heat transport is the meridional freshwater transport. Both are contributing in conjunction to the large scale density and related gradients, which can have an impact on the circulation. The definition of the freshwater is provided in section 2.3.4. To quantify freshwater transports from observations is even more challenging than heat transport, due to the smaller variations in salinity compared to the temperature. However for

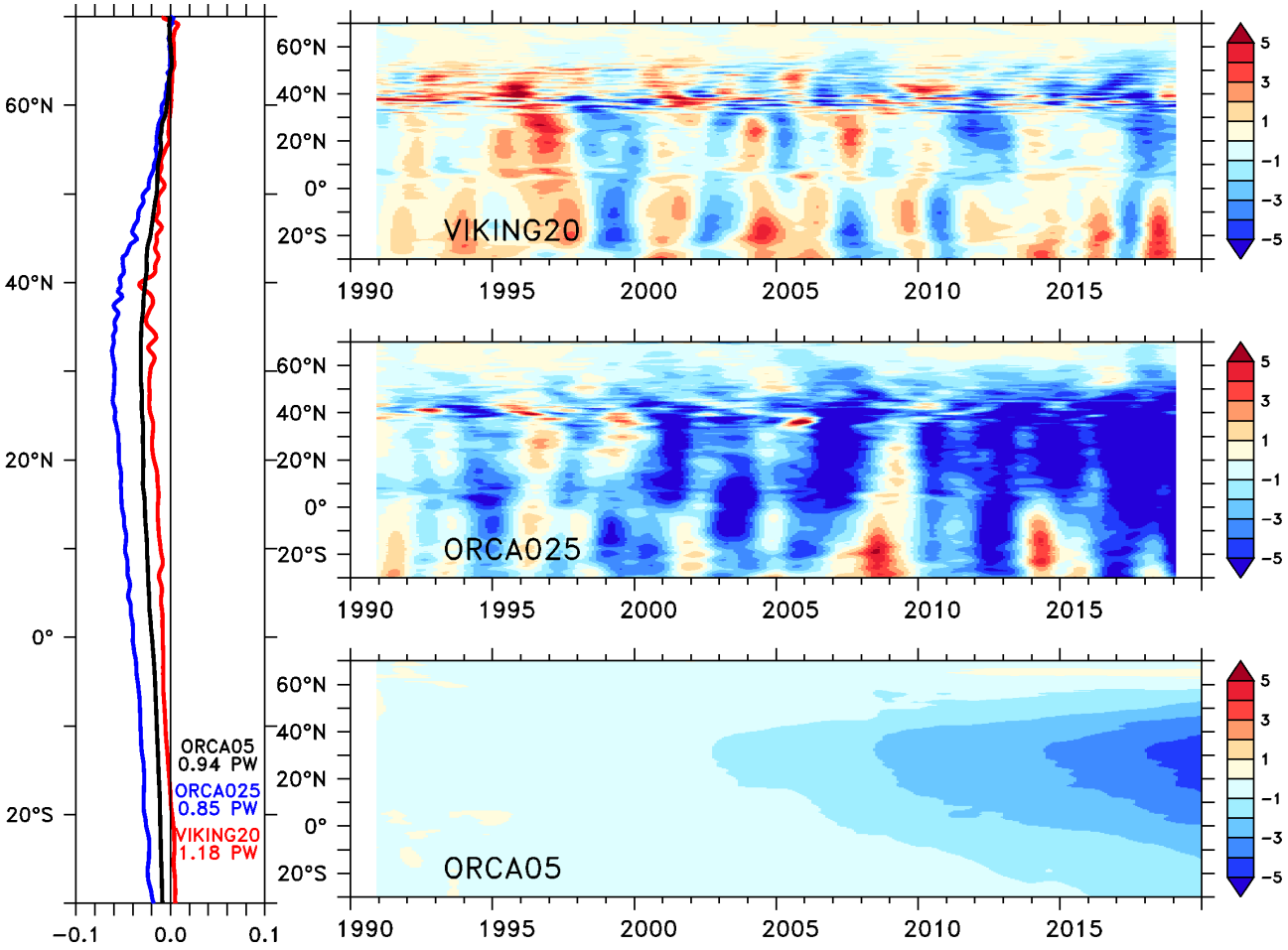

Figure 64.: Meridional heat transport anomaly between hosing (R-MELT) and reference (REF) simulation in PW averaged over 2010-2019 (left panel). Values indicate the maximum value over that period for reference simulation for each individual model configurations. Meridional heat transport anomalies (in %) relative to the meridional maximum heat transport in the reference simulation of each model configuration are shown in the right panels. Hovmöller timeseries are interannually smoothed.

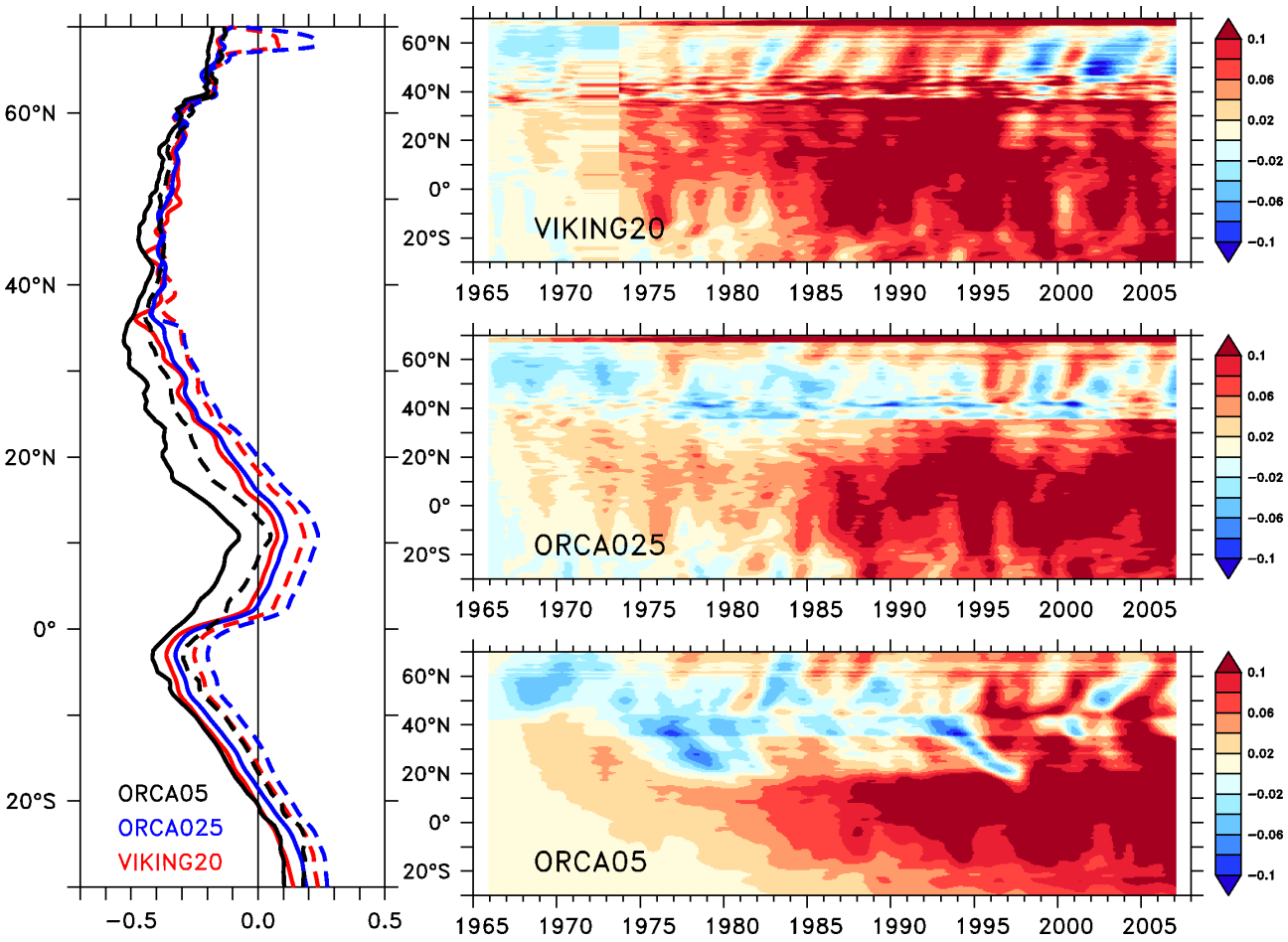

Figure 65.: Meridional equivalent freshwater transport in Sv for control (solid) and hosing (dashed) simulations averaged from 1998-2007 (left panel). Equivalent freshwater transport anomaly between hosing (I-MELT) and reference (REF) simulation in Sv for the individual model configurations (right panel). Hovmöller timeseries are interannually smoothed. The anomaly artifact in VIKING20 around 1972 is caused by a data loss.

ocean models it is a suitable diagnostic for discussion and investigation of large scale anomalies and their propagation.

Response in the I-MELT scenario

The meridional freshwater transport in the reference simulations (solid lines, Figure 65 left panel), shows the typical meridional structure (Lohmann (2003)). The northward freshwater transport decreases from the South Atlantic (30°S) towards the equator due to enhanced evaporation in the South Atlantic trade wind region. North of the equator the freshwater transport increases due to the northward shifted ITCZ and the surplus of precipitation. Further north (>10°N) the north trade wind region and the large evaporation leads to a decrease in freshwater transport with a minimum around 35°N. After that latitude the freshwater transport increases again pointing to positive net surface freshwater fluxes into the ocean. That behaviour indicates that the freshwater transport is strong related to the surface fluxes and moisture transports in coupled models (Marotzke and Stone (1995),

Lohmann (2003)). The transports of ORCA025 and VIKING20 are very similar, while the ORCA05 results tend to an overall reduced freshwater transport compared to the other configurations. (black line in 65, left panel)

The anomaly plots show an interesting pattern (65, right panel). Positive values indicate enhanced northward freshwater transport, while negative values can be thought of as enhanced freshwater transport to the south. The anomalies originate from the subpolar North Atlantic (50°N-60°N) and are moving southward over the first 10 years. These anomalies can be associated with enhanced meltwater transport within the SPG to the south of around 50°N. After 1975 (after 10 years) the sign of these anomalies begins to change from negative to positive and indicating an enhanced northward transport of freshwater partly south of the ridges but also partly into the Nordic Seas. VIKING20 exhibits the largest positive freshwater transport anomaly compared to the other configurations. These results are consistent with earlier described findings and presented anomalies in the Nordic Seas and North Atlantic. Transport north of 65°N has to be treated carefully due to the computation along distorted grid lines (tripolar grid). Irrespectively of that, ORCA05 and ORCA025 are showing between 20°N-60°N larger negative anomalies than VIKING20. That suggests a larger freshwater transport from Greenland to the south compared to the VIKING20. That corresponds to the fresh comma shape (export pathway) seen in both simulation in the east Atlantic, which is not visible to that order of size in VIKING20. The signal propagation speed in the nested region of VIKING20 (32°N- 85°N) differs in comparison the coarser models distinct. A transition region from the different propagation regimes can be seen at the southern boundary (32°N) in VIKING20. Overall, due to a weakening AMOC in the I-MELT simulations, the meridional freshwater (salt) transport is increased (decreased), leading to positive anomalies in comparison with the control simulation, which promotes an ongoing decline of the AMOC (positive feedback, Griffies et al. (2009)). These results cannot be directly compared to the freshwater content anomalies presented in section 5.3.3, due to differences in the depth range. For the freshwater content anomalies only the upper 2000 m have been considered, while for the meridional the entire water column was taken into account. However, the freshwater transports across 50°N at the beginning of the hosing are negative but larger than -0.1 Sv, which represents the source term of Greenland. In the consequence, the freshwater content north of 50°N has to increase, which is seen in Figure 47.

Response in the R-MELT scenario

The freshwater anomaly averaged over the last decade (2010-2019) of the simulations (Figure 66, left panel) indicates a positive northward freshwater transport anomaly for ORCA05 and ORCA025 south of 50°N - 60°N. VIKING20 displays only between 45°N and 15°S enhanced positive anomalies, differing strongly from the behaviour of both other configurations. The negative anomalies north of 45°N point to a freshwater transport to south and counteracting the enhanced freshwater anomaly from Greenland. That response stands in clear contrast to the both coarser results, which exhibit

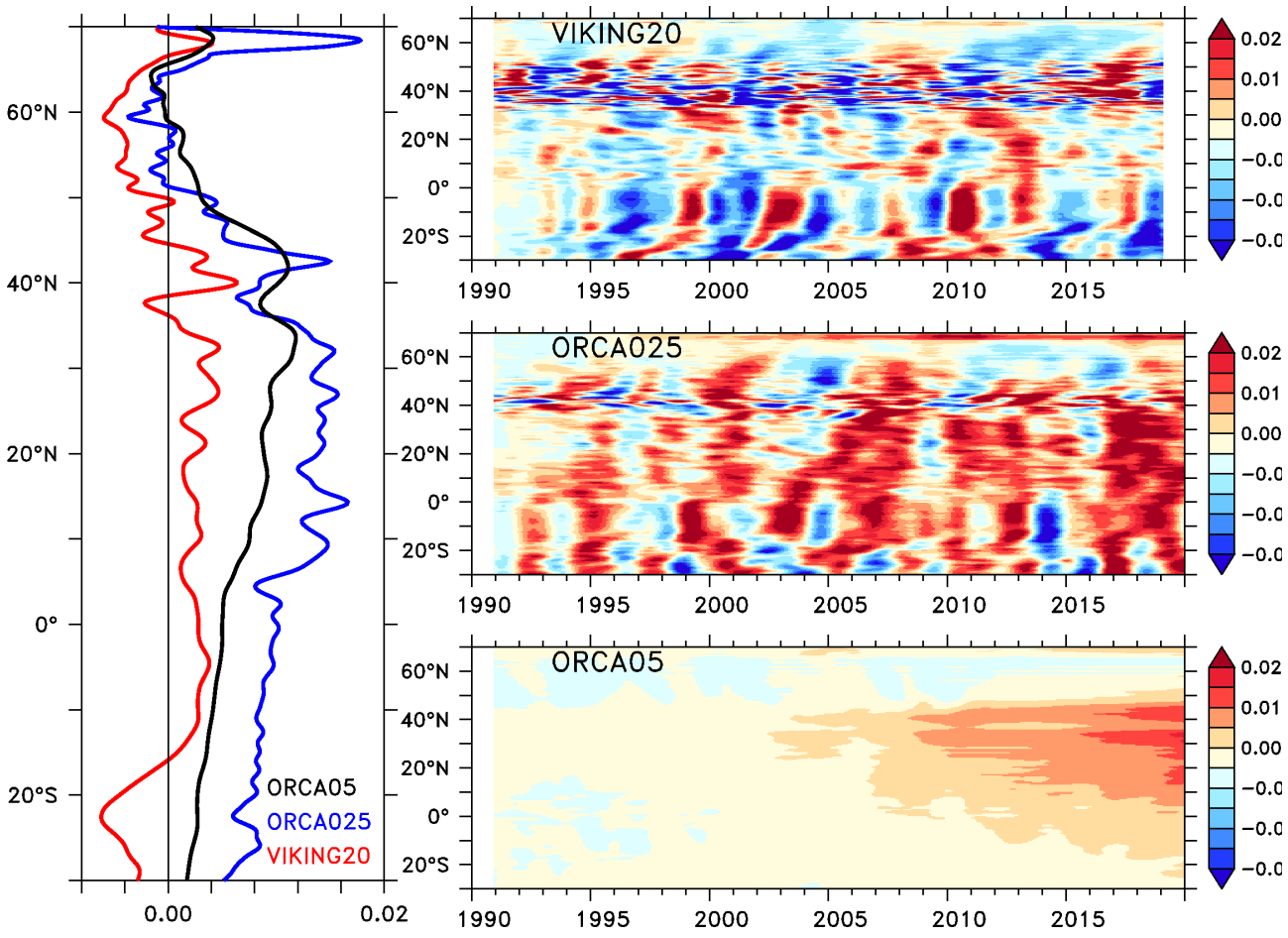

Figure 66.: Meridional freshwater transport anomaly in Sv between hosing (R-MELT) and reference (REF) simulation averaged from 2010-2019 are shown in the left panel. Freshwater transport anomaly between hosing (R-MELT) and reference (REF) simulation in Sv for the individual model configurations (right panel). Hovmöller timeseries are interannually smoothed.

mostly positive anomalies, having a negative impact on deep convection (positive feedback Griffies et al. (2009)). These findings confirm the previous results, where VIKING20 shows the smallest freshwater content increase north of 50°N, compared to the other configurations (Figure 54). In the Hovmöller plots (right side) the difference in the response between the configurations becomes more clear. The coarse ORCA05 shows right after the start of the hosing positive anomalies, almost not affected by any mesoscale variability and reaching values of 0.1 Sv at the end of the hosing simulation. ORCA025 also tends to positive northward propagating anomalies, exceeding partially 0.15 Sv. No clear preferred signal is visible in VIKING20, except the almost exclusively negative anomalies north of 50°N during the simulation. VIKING20 exhibits in this sense the potential to export the additional freshwater to the south with only little effect on the AMOC. That behaviour stands in contrast to both coarser simulations. This finding goes along with results of the SPG-strength and overflow (DSOW), which differ between VIKING20 and the other configurations. However the AMOC diagnostics in Figure 62 shows for all simulations at 26.5°N a decline but weakest in VIKING20. The results point to a different behaviour of VIKING20 compared to the other simulations. There are hints that the additional meltwater and freshwater can leave the SPG easier in VIKING20 by the DWBC (Figure 50) than in the other configurations. That is the reason for the smaller anomalies in VIKING20 in the SPG and AMOC.

6. Summary and Conclusion

In this study, a series of uncoupled ocean models with successively increasing horizontal resolution was used to investigate the effect of small scale ocean processes on the oceanic response to an increased melting of the Greenland Ice Sheet (GrIS). Previous studies showed that mesoscale eddies, especially around Greenland, have a strong impact on the local oceanic conditions. They affect for instance the deep convection processes and restratification and accomplish the cross-shelf transport of water from the fresh boundary currents into the interior Labrador Sea (Brandt et al. (2007); Gelderloos et al. (2011); Czeschel (2004); Chanut et al. (2008)). Most modelling studies, which already investigated an increased melting of the GrIS were based on relatively coarse models and thus did not resolve mesoscale processes in the high latitudes (e.g. Stouffer et al. (2006); Swingedouw et al. (2012); Gerdes et al. (2006)). Especially in Greenland melting scenarios it is assumed that these mesoscale eddies are important for the meltwater spreading (Weijer et al. (2012)), which potentially could alter the oceanic response significantly. Furthermore, most investigations assumed idealised meltwater rates from Greenland on the order of 0.1 Sv, a rate which could trigger a shut-down of the Atlantic Meridional Overturning Circulation (Latif et al. (2000); Rahmstorf (1996); Hofmann and Rahmstorf (2009); Gregory et al. (2003)). Actual estimates of the meltwater flux from Greenland are in the order of about 17 mSv - 20 mSv (Greve (2000); Bamber et al. (2012)) and the latter study diagnosed an increasing trend of about 0.53 mSv/a for the period of 1990 to 2010. Based on that fact, the assumed Greenland melting response was overestimated in most previous studies. Realistic Greenland melting projections with eddy resolving models were non-existent until now.

The main focus of this study is on the dependency of the oceanic response on the horizontal resolution of ocean models. Additionally, the importance of differences in the Greenland melting scenario on the oceanic response was assessed. The numerical ocean model is based on the NEMO code (Madec (2008)) and includes a sea-ice model (LIM2, Fichefet and Maqueda (1997); Goosse and Fichefet (1999)). Three different configurations have been used: a coarse (0.5°, ORCA05) setup, an eddy-permitting (0.25°, ORCA025) setup and an eddy-resolving (0.05°, VIKING20) setup.

The VIKING20 configuration constitutes a new development to address the given scientific questions (outlined in chapter 1). VIKING20 represents the oceanic conditions in the North Atlantic as realistic as possible. This configuration is based on a local grid refinement approach (Debreu et al. (2008)), allowing the embedment of a high resolution "nest" into a coarser (global) model domain, and permitting interactions between both models. The North Atlantic between $\sim$ 30°N and $\sim$ 85°N (north of Fram Strait) is covered by the high resolution nest with a resolution of 0.05°, resulting in grid sizes around 3 km near Greenland. The fine mesh ensures that mesoscale processes are resolved explicitly. VIKING20 is the first configuration with such a fine horizontal mesh in the North Atlantic, which is also successfully applied on the sea-ice model. Furthermore in this configuration several decades long simulations have been successfully performed. With this configuration significant improvements were achieved with respect to the separation of the Gulf Stream from the North American coast, the flow path of the NAC, the representation of the DWBC and in the eddy field in the North Atlantic, in comparison to the coarser configurations. Overall, the VIKING20 configuration captures many of the

observed characteristics in various regions, which is required for useful interpretation of the melting response and future implications.

In all configurations, a control hindcast simulation (1948-2007) has been performed using atmospheric conditions based on the CORE version 2 interannual varying products (Large and Yeager (2009)), following a 30 year spin-up phase and initial conditions given by climatological ocean fields (Levitus (1998)). The global coastal runoff in all configurations is based on Dai and Trenberth (2002) with slight modifications described in Bourdallé Badie and Treguier (2006). The polar precipitation north of 62°N was artificially decreased by 10% (14 mSv), which is still in the range of other reanalyse products. The modeled SSS has been restored to climatology (Levitus (1998)) with a very weak piston velocity of 16.4 mm/day, which correspond to restoring timescale of one year for a 6 m surface layer or equal to 8 years for a 50 m layer. Many previous forced GrIS melting simulations rather use a stronger restoring, which is assumed to counteract the melting response. Additionally, the restoring flux was further restricted to SSS differences between model and climatology to values lower than 0.5 psu, in line with suggestion of the CORE 2 protocol (http://data1.gfdl.noaa.gov/~nnz/mom4/COREv2/doc/CORE_notes_15feb2012.pdf). No restoring was applied in sea-ice covered regions, across a wide swath ($\sim$ 500 km) around Greenland, and in regions, where coastal runoff exists. That refined SSS restoring setting led to restoring fluxes of maximal 10 % of the precipitation fluxes. This refined surface freshwater setting permitted to investigate the oceanic response on a melting GrIS, where additional freshwater is release to the ocean and cause growing salinity anomalies.

With the same model setup, two GrIS melting simulations were performed. In the first, a rather extreme and idealised melting scenario (I-MELT), the coastal runoff was increased by 0.1 Sv, and equally distributed around the the Greenland coast. This simulation mimics a strong melting of the GrIS, which could occur in a future climate with a CO_2 concentration several times higher compared to present days values (Jungclaus et al. (2006a)). The simulation strategy was based on a related study by Swingedouw et al. (2012), which also showed that atmospheric feedbacks are negligible for the oceanic response over the first 4 decades. On longer time scale ocean-atmosphere feedbacks become important.

The second melting scenario (R-MELT) was based on the diagnosed increasing melting rates from Greenland over the period from 1990 to 2010 (Bamber et al. (2012)). Over that period, a linear trend of 0.53 mSv/a was implemented. That spatially varying trend was taken to modify the reference coastal runoff from Greenland accordingly, which leads to an increased runoff into the Irminger basin compared to the Labrador Sea as analysed by Bamber et al. (2012). Overall this scenario represents the actual best guess for the real future oceanic response to a realistic melting of the GrIS.

In both melting simulations a passive tracer was released according to the coastal runoff from Greenland, to investigate the spreading of meltwater.

In the following, the results from the R-MELT scenario in VIKING20 are considered as a reference case

to identify differences related to resolution and melting scenario. The following summary describes the main response in certain regions and quantities. The final conclusion is found in the last three paragraphs.

Short term surface response in the SPG

The additional meltwater enters the ocean around Greenland and is advected by the swift coastal currents off Greenland already toward the Labrador Sea and Baffin Bay within one year. The connected temperature and salinity anomalies are small compared to the mesoscale variability in VIKING20 over the first 5 years in the R-MELT scenario. Both coarser configurations do not show significant hydrographic anomalies at that stage. The amount of released freshwater in the two melting scenarios differs substantially during that period and explains why anomalies in the R-MELT scenario are not significant. Over the first 5 years only 500 km^3 of additional freshwater are released in R-MELT , while in I-MELT the amount exceeds 16000 km^3.

In the I-MELT scenario in the VIKING20 configuration a strong surface freshening ($<$ -1 psu) of the coastal waters around Greenland is present after 5 years of hosing. The freshening causes in the EGC and WGC a surface cooling ($<$ -1°K) due to increased stratification and less vertical mixing. Greenland melting results of Marsh et al. (2010) based on a previous version of ORCA025 show a similar anomaly pattern, but positive anomalies along the coast of Labrador, which could be related to differences in the SSS-restoring between both studies. A surface warming is present north of Greenland with anomalies around 0.2 °K over the entire hosing period. The reasons are still unclear.

The two coarser configurations follow most results of VIKING20 in the I-MELT scenario. However, ORCA05 shows the lowest peak anomalies in the comparison to the other configurations, which points to an overestimation of the lateral mixing in that configuration and produce increased cross-shelf transports into the Labrador Sea and Baffin Bay. Nevertheless a distinct contribution of the WGC eddies for an enhanced cross-shelf transport of meltwater into the interior Labrador Sea is resolved in VIKING20, which is absent in ORCA025. A remarkable difference between the VIKING20 results noted is in the eastward penetration of salinity anomalies across the North Atlantic. In ORCA025 and ORCA05, salinity anomalies reach the longitude of Iceland within 5 years, while anomalies in VIKING20 are found further west (30°W). These differences in the spreading of anomalies are also visible in the passive tracer distribution. The eastward spreading is linked to the representation of NW Corner, where ORCA05 and ORCA025 show distinct deficits compared to observations. Cooling and freshening anomalies around Greenland go along with southward shift of the sea-ice edge in the Labrador Sea and along the EGC south of the Denmark Strait. Most previous studies investigated the long term and large scale response, and preventing a comparison.

The initial spreading of the freshwater is in the R-MELT scenario similar to the I-MELT, while the hydrographic anomalies are small compared to the natural variability over the first years.

Anomalies in the interior Labrador Sea

In VIKING20, under the R-MELT scenario, a freshening anomaly of about -0.5 mpsu is visible at the surface in the interior of the Labrador Sea. Thereafter, the anomaly reaches depths of about 1600 m, which represents the maximum depth of the deep convection. No coherent anomalous temperature signal is seen over the entire hosing period in the interior Labrador Sea. The freshening concurs with a slight decrease (-100 m) of the maximum winter mixed layer depth at the end of the hosing simulation, while the LSW production rates are slightly enhanced ($\sim$ 1 Sv) compared to the control simulation. Inherently to the SPG strengthening, a SSH rise of about 3 cm compared to the reference simulation is found in the interior Labrador Sea, which is about half of the interannual variability of 4 to 6 cm, and slightly higher compared to the global expected mean of 2.75 cm (Wang et al. (2012)).

The two coarser configurations overestimate hydrographic anomalies in the interior of the Labrador Sea under the same scenario. ORCA05 and ORCA025 exhibit a clear surface intensified salinity anomaly ($\sim$ -2 mpsu) after 10 years. This points to enhanced net cross-shelf transports compared to VIKING20. The freshening in ORCA05 (ORCA025) goes along with a significant decline in the winter mixed layer depth of about 600 m (400 m), linked to a decrease in the LSW production rates of about -2 Sv in both configurations. The reduction of the maximum mixed layer depth introduces a slight positive temperature anomaly ($\sim$ 0.02 °K) at depth of 600 m to 2000 m in ORCA05, not found in the other configurations. ORCA025 shows a progressing negative temperature anomaly ($\sim$ -0.02 °K) over the entire period, since the MLD is less reduced compared to ORCA05.

In the stronger I-MELT scenario, a (instantaneous) surface cooling ($\sim$ -1 °K) and freshening ($\sim$ -1 psu) is visible, irrespectively of resolution, which leads to a fast shut down of the deep convection in the Labrador Sea within 5 years after the melting starts. In the depth ranges of previously ventilated water masses by winterly convection a positive temperature anomaly ($\sim$ 0.5 °K) develops. In a similar simulation, Weijer et al. (2012) found in a similar simulation a more gradual decline of the deep convection in a high resolution (1/10°) configuration compared to coarser (1°) results with an increased runoff from Greenland of about 0.1 Sv. This finding is not confirmed in the similar I-MELT scenario, since the behavior with respect to the MLD is very similar in all configurations and show a shutdown of the deep convection in the Labrador Sea within the first 5 years..

Response to the SPG circulation

Changes in the Labrador Sea, especially in the convection induce circulation changes, which can be traced in the strength of the SPG (Böning et al. (2006)). VIKING20, under the R-MELT scenario, interestingly tends to a slight increase of the SPG gyre circulation in the order of 1 Sv after 30 years. A similar increase is found in ORCA025. The reasons are still unclear, but be probably related to an enhanced cross-shelve gradient due to a fresher EGC. Only ORCA05 shows the expected decline, as a consequence of the largest reduction of the deep convection in the R-MELT scenario.

The I-MELT results suggest a weakening of the SPG gyre circulation ($\sim$ -4 Sv) at the end of the

hosing simulation, but enhanced (∼ -12 Sv) during periods where extensive deep convection occurs. During these periods the gyre circulation is reduced by 50%, while during "normal" conditions the gyre circulation weakens by about 20%, which has the same order of magnitude as the interannual variability. The results suggest that the SPG strength is not a good measure for changes, since even if the convection is collapsed the gyre is only weakened by -4 Sv. No clear dependence of the I-MELT results on resolution is found in that region.

Meltwater spreading

A clear dependence of the long-term spreading of the meltwater on the resolution in the subpolar North Atlantic is visible, especially in the R-MELT scenario. In VIKING20, the largest amount of meltwater is present in the Baffin Bay, along the path of the DWBC and within the northern Gulf Stream recirculation gyre, attached to the North American coast.

Both coarser configurations simulates high meltwater concentrations in the Baffin Bay, but not along the North American coast. Instead, they show an extensive eastward spreading across the subpolar North Atlantic. The differences in the freshwater spreading are caused by the under-representation of the NW Corner in both coarser configurations. In VIKING20 the NW Corner represents a barrier for the eastward penetration of meltwater across the North Atlantic. The DWBC produces on the other hand an additional export pathway to the south, which is missing in both coarser configurations, since the DWBC is not well resolved in these configurations.

In VIKING20, under the I-MELT scenario, the meltwater forcing seems strong enough to shift the NW Corner sufficiently, to allow an eastward spreading across the North Atlantic Ocean. However the spreading in VIKING20 is more limited to the subpolar North Atlantic, compared to the coarser results in the I-MELT scenario. They show a clear export pathway from the SPG to STG, which is know as "comma shape" (Swingedouw et al. (2012)). This behaviour seems to be an artifact of coarser configuration, which suffer from misplaced flow path of the NAC. Results of Weijer et al. (2012) suggest that the DWBC is important for the freshwater export in the high resolution configuration in the strong 0.1 Sv melting scenario. This result is only partly confirmed by the I-MELT results in VIKING20, which suggest the largest spreading within the SPG and only small portions of meltwater leave the SPG via the DWBC.

Long term salinity and temperature

According to the differences in the meltwater spreading, substantial discrepancies are also present in the large scale temperature and salinity anomalies (averaged from 0 - 2000 m) in the subpolar North Atlantic. In the R-MELT scenario in VIKING20 the strongest negative anomalies of salinity (∼ -1.5 mpsu) and temperature (∼ -0.1 °K) are present north of the flow path of the NAC near Iceland, probably due to slight southward shift of the flowpath of the NAC.

Both coarser configurations show also negative anomalies south of that flow path and at the eastern boundary of the STG as a consequence of an enhanced freshwater leakage. A pronounced freshening

occurs between Iceland and Ireland and in the Baffin Bay of about -2 mpsu, irrespectively of resolution in the R-MELT scenario.

The connected temperature anomalies (0 - 2000 m) in VIKING20 suggest a slight cooling (-0.1 °K) north of the NAC and parts of the Norwegian coastal current, indicating slight changes in the circulation and extend of the SPG. A slight warming of about 0.1 °K is present in the coastal regions of Baffin Bay. Both coarser configurations show the same anomaly pattern as VIKING20, but with larger anomalies, especially larger negative temperature anomalies.

The anomalies in the I-MELT scenario are several times larger than in the R-MELT scenario over the same hosing period. A freshening of about -0.2 psu over the upper 2000 m is present in the subpolar North Atlantic in VIKING20 after 30 years. Both coarser configurations suggest a weaker freshening in that area, but show an enhanced freshwater leakage from the SPG to the STG. All configurations exhibit a slight northward shift of the Gulf Stream extension south Newfoundland, which produce a pronounced positive salinity and temperature anomalies in that region. Additionally, the temperature anomalies for the upper 2000 m in VIKING20 suggest a strong cooling (-1 °K) in the NAC extension region and in the coastal current of Norway after 30 years. This cooling points to substantial changes in the transports of heat within the NAC towards the Nordic Seas. Most other regions experience a warming, which is linked to the reduction of convection and thus lower heat fluxes to the atmosphere or by adaptations of the meridional heat transport. The largest warming ($\sim$ 0.7 °K) occurs along east coast of America, south of Newfoundland, in the Baffin Bay and Labrador Sea in VIKING20 after 30 years.

Both coarser configurations do not support the strong cooling of VIKING20 in the Nordic Seas and NAC extension, but tend in contrast to larger positive anomalies, especially in the region of the Labrador Sea and around Newfoundland, which is connected to differences in the convection and the flow path of the NAC compared to VIKING20. None of the previous studies investigated salinity and temperature anomalies over the water column. In many studies only surface anomalies (e.g. Swingedouw et al. (2012)) were analysed to infer for changes on the ocean-atmosphere fluxes.

Freshwater and heat content anomalies in the subpolar North Atlantic

The freshwater content in the subpolar North Atlantic increase by $\sim$ 4000 km^3 in VIKING20 after 30 years in the R-MELT scenario. That amount is approximately less than half the amount of a of the decadal variability (Curry and Mauritzen (2005)). After 30 years of hosing a freshwater amount of 18500 km^3 in total has been released to the Atlantic Ocean. Both coarser models show larger values (ORCA025 7000 km^3, ORCA05 5000 km^3) implying that the southward export is enhanced with resolution. Approximately after further 5-10 years of hosing, these anomalies are in the magnitude of the natural variability ($\pm$ 10.000 km^3, Boyer et al. (2007)).

The heat content anomaly in VIKING20 and ORCA05 exhibit a similar decrease of -1 to -2 $\times$ 10^{21} J after 30 years of hosing. Only ORCA025 shows a stronger decline of about -4 $\times$ 10^{21} J. Overall the

projected anomalies in the R-MELT scenario are small compared to the natural variability of $\pm$ 8 $\times$ 10^{21} J.

In the I-MELT scenario, the freshwater content anomaly shows in agreement to a salinity anomalies a fast increase and exceeds already after 5 years the threshold of natural variability. Around 100000 km^3 of freshwater have been released in this scenario over the first 30 years of hosing, which is approximately five times larger than the amount in the R-MELT scenario. The largest freshwater content increase shows VIKING20, with values around 80000 km^3 at the end of the hosing simulation.

Both coarser models exhibit a lower freshwater gain, which is in agreement with the enhanced freshwater leakage from the SPG to the STG ("comma shape"). With respect to the heat content anomalies, the VIKING20 simulation reveals an opposite behaviour to the coarser results. VIKING20 prognoses a decline of the heat content by -15 $\times$ 10^{21} J after 30 years, which is approximately two times larger than the magnitude of interannual variability. ORCA025 and ORCA05 tend more to a heat content gain instead, which is related to the larger positive temperature anomalies, caused by the shut down of the deep convection.

Regional SSH rise pattern

SSH variations induced by the additional meltwater and circulation changes are important for the coastal regions. According to the amount of released meltwater a global mean SSH rise of 2.75 cm is projected for the R-MELT scenario and 26 cm in the I-MELT scenario after 30 years. Spatial variations are induced by changes in the circulation, mass attraction and thermal expansion (Cronin (2012)). The mass attraction and thermal expansion have been ignored in these simulations, which can dominate the SSH rise on regional scales (Landerer et al. (2007); Cronin (2012); Kopp et al. (2010)).

In VIKING20 in the R-MELT scenario the largest SSH rise is visible around Greenland and the coastal region of North American north of Cape Hatteras. The rise is on the order of 4 cm after 30 years compared to reference simulation, which is roughly twice the global mean at the end of the hosing simulation. All other regions show a SSH rise similar to the global mean or been heavily influenced by mesoscale variability, like the NAC. The coarser configurations suggest a larger SSH rise (up to 7 cm) in the same region as VIKING20 and at the European coast of about 3.75 cm, which is not seen in VIKING20. The latter response seems to be linked to the eastward propagating of anomalies (temperature and salinity) across the Atlantic Ocean, which is restricted by NW Corner in VIKING20.

In VIKING20 in the I-MELT scenario the SSH anomaly pattern is similar to the R-MELT scenario, except an also enhanced increase at European coast. The magnitude is large and varies between 60 cm around Greenland and North America and 10 cm at the European coast after 30 years. A fall of about -15 cm compared to the global mean of about 26 cm is seen along the flow path of the NAC and in Nordic Seas, after 30 years.

Response to the DSOW and meridional transports

Probably due to the exclusive export pathways along the North American coast in VIKING20 in the R-MELT scenario, less freshwater reaches the Nordic Seas compared to the other configurations. In consequence the maximum overflow density (σ_0) in the Denmark Strait in VIKING20 is not affected, which could alter the AMOC (Behrens et al. (2013)) over the hosing period. In contrast, both other configurations show a slight (-0.006 kg/m^3) decrease compared to the reference simulation instead. In the I-MELT scenario the decline is strongest in VIKING20, in the order of about -0.2 kg/m^3 after 30 years. In both coarser configurations the decline is weaker ($\sim$ -0.1 kg/m^3), but they suffer from deficits in maintaining a realistic overflow density of $\sim$ 28.1 kg/m^3 (Macrander et al. (2007)).

As a consequence of the unchanged density in the Denmark Strait, no substantial decline in the AMOC at 26.5°N is present in VIKING20 over the entire 30 years in the R-MELT scenario. Both other configurations suggest in contrast a weakening of about -5% to -10%, which concurs with the changes in the DSOW density. The presented model simulations suggest interannual variations in the order of $\pm$ 10% at that latitude. In the I-MELT scenario the behaviour is different. VIKING20 exhibits the strongest decline of the AMOC (50% - 60%), while both coarser configurations show only a decline of -40% to -50% after 30 years. This behaviour is in broad agreement to previous model studies, which showed a similar decline (e.g. Swingedouw et al. (2012); Stouffer et al. (2006); Weijer et al. (2012)).

The meridional heat transport which is strongly related to the AMOC in low latitudes, follows the AMOC results. No substantial decline is visible in VIKING20 over the 30 years in the R-MELT scenario, while both coarser configurations suggest a decline between -5% to -10% referenced to the maximum. In the I-MELT scenario, VIKING20 projects the largest decline, which exceeds -50% compared to the maximum. Lower reductions occur in both coarser configurations (-30% to -40%).

The results of the meridional freshwater transport support the previous findings of the freshwater content anomalies in the subpolar North Atlantic. VIKING20 in the R-MELT scenario show a slight negative anomaly between 45°N and 65°N, which represents the export pathway of freshwater along the North American coast. In contrast both coarser configurations show stronger positive freshwater transport anomalies, which induce a positive feedback on the AMOC (Griffies et al. (2009)) and lead to an ongoing declining AMOC. The I-MELT results of VIKING20 do not support the ability to export sufficient freshwater to the south, which seems to be the case in the R-MELT scenario as long the dense water formation is not collapsed. Both coarser configuration show that capability by an enhanced freshwater leakage from the SPG to the STG at the east North Atlantic ("comma shape", Swingedouw et al. (2012)), which is not supported in VIKING20.

Conclusion

Overall, the results suggest a remarkable weak meltwater response of VIKING20 in the realistic R-MELT melting scenario, compared to both coarser results. The reason is linked to detailed differences

in the meltwater spreading between VIKING20 and the coarser configurations, which is partly accomplished by mesoscale eddies directly. The DWBC, and the flow path of the NAC, and the representation of the NW Corner have been found to affect the meltwater spreading additionally. However certain key regions have been identified where pronounced anomalies occur, which are mostly small compared to natural variability in the 30 year long R-MELT scenario but provide the possibility to measure GrIS melting signals precociously. Two major differences between eddy resolving and not eddy resolving configurations have been identified. The location of the NW Corner affects the eastward spreading of meltwater and related anomalies across the Atlantic Ocean, which is restricted in VIKING20. Furthermore, VIKING20 exhibits the ability to transport a part of the additional freshwater within the DWBC southward and store meltwater within the northern recirculation gyre of the Gulf Stream, which is not well resolved in the coarser simulations. In consequence, the lowest freshwater content anomaly in the Nordic Seas is found in VIKING20 and therefore the smallest impact on the overflows, which could push the AMOC to a declining trajectory, as seen in both coarser configurations. There are also indications that the freshwater transport accomplished by WGC eddies from the boundary current into the interior Labrador Sea is reduced under Greenland melting conditions, by a weakening of the SPG, which promote a strengthening of convection and reveals a counteracting mechanism against the meltwater response. These eddies are not resolved in the coarser configurations and thus the counteracting mechanism is missing in those configurations.

The present results suggest that in the I-MELT scenario a certain threshold of the freshwater forcing from Greenland is exceeded and push all simulations to a similar melting response, irrespectively of resolution. All counteracting mechanisms seen in the R-MELT scenario are overwhelmed. In consequence, VIKING20 exhibits differences in the freshwater spreading, but tends to the same AMOC response as the coarser configurations in the I-MELT scenario. However, the previously described freshwater leakage ("comma" shape, Swingedouw et al. (2012)), transporting freshwater from the SPG to STG via the Canary Current is not supported in VIKING20, due to the blocking effect of the NW Corner.

The results of VIKING20 provide some new insights about the relevance of mesoscale processes for the oceanic response to an enhanced melting of Greenland, which are not well captured in present day climate models. However, further detailed investigations and simulations are required to confirm and validate the presented results of VIKING20, especially in the R-MELT scenario. Open questions are: How important are icebergs for a realistic response? How important is the seasonal cycle of the meltwater flux? How important are the initial condition and the atmospheric forcing for the oceanic response?

In summary, the results show that the combination of a resolved mesoscale and "realistic" Greenland melting matters for the oceanic response and to assess the consequences for future Greenland melting projections. That points to large demands to present day climate models and large challenges for reliable and realistic future projections. The present results also suggest that coarse models may be

used to investigate the response on meridional transports to large freshwater anomalies ($\sim$ 0.1 Sv), while hydrographic anomaly pattern have to been treated carefully.

Bibliography

Arakawa, A. and Y.-J. G. Hsu, 1990: Energy Conserving and Potential-Enstrophy Dissipating Schemes for the Shallow Water Equations. *Monthly Weather Review*, **118 (10)**, 1960–1969, doi:10.1175/1520-0493(1990)118<1960:ECAPED>2.0.CO;2. 9

Arakawa, A. and V. R. Lamb, 1977: Computational design of the basic dynamical processes of the ucla general circulation model. *Methods in computational physics*, **17**, 173–265. 8

Bamber, J., M. van den Broeke, J. Ettema, J. Lenaerts, and E. Rignot, 2012: Recent large increases in freshwater fluxes from Greenland into the North Atlantic. *Geophysical Research Letters*, **39 (19)**, doi:10.1029/2012GL052552. 2, 3, 5, 10, 15, 16, 18, 52, 53, 59, 126, 127

Bamber, J. L., R. L. Layberry, and S. P. Gogineni, 2001: A new ice thickness and bed data set for the Greenland ice sheet: 1. Measurement, data reduction, and errors. *Journal of Geophysical Research*, **106 (D24)**, 33 773, doi:10.1029/2001JD900054. 2, 15, 97

Barnier, B., L. Siefridt, and P. Marchesiello, 1995: Thermal forcing for a global ocean circulation model using a three-year climatology of ECMWF analyses. *Journal of Marine Systems*, **6 (4)**, 363–380, doi:10.1016/0924-7963(94)00034-9. 46

Barnier, B., et al., 2006: Impact of partial steps and momentum advection schemes in a global ocean circulation model at eddy-permitting resolution. *Ocean Dynamics*, **56 (5)**, 543–567, doi:10.1007/s10236-006-0082-1. 8, 28

Bates, M. L., S. M. Griffies, and M. H. England, 2012: A dynamic, embedded Lagrangian model for ocean climate models, Part II: Idealised overflow tests. *Ocean Modelling*, **59-60 (0)**, 60–76, doi:10.1016/j.ocemod.2012.08.003. 28

Behrens, E., A. Biastoch, and C. W. Böning, 2013: Spurious AMOC trends in global ocean sea-ice models related to subarctic freshwater forcing. *Ocean Modelling*, **69 (0)**, 39–49, doi:10.1016/j.ocemod.2013.05.004. 8, 10, 24, 28, 45, 46, 47, 49, 51, 52, 54, 110, 111, 113, 115, 133, 150, 157

Behrens, E., F. U. Schwarzkopf, J. F. Lübbecke, and C. W. Böning, 2012: Model simulations on the long-term dispersal of 137 Cs released into the Pacific Ocean off Fukushima. *Environmental Research Letters*, **7 (3)**, 034 004, doi:10.1088/1748-9326/7/3/034004. 8

Belkin, I. M., 2004: Propagation of the Great Salinity Anomaly of the 1990s around the northern North Atlantic. *Geophysical Research Letters*, **31 (8)**, L08 306, doi:10.1029/2003GL019334. 2, 35

Biastoch, A., C. W. Böning, J. Getzlaff, J.-M. Molines, and G. Madec, 2008a: Causes of Interannual-Decadal Variability in the Meridional Overturning Circulation of the Midlatitude North Atlantic Ocean. *Journal of Climate*, **21 (24)**, 6599–6615, doi:10.1175/2008JCLI2404.1. 8, 49, 106

Biastoch, A., C. W. Böning, and J. R. E. Lutjeharms, 2008b: Agulhas leakage dynamics affects decadal variability in Atlantic overturning circulation. *Nature*, **456 (7221)**, 489–492, doi:10.1038/nature07426. 12, 115

Blanke, B. and P. Delecluse, 1993: Variability of the Tropical Atlantic Ocean Simulated by a General Circulation Model with Two Different Mixed-Layer Physics. *Journal of Physical Oceanography*, **23 (7)**, 1363–1388, doi:10.1175/1520-0485(1993)023<1363:VOTTAO>2.0.CO;2. 9

Böning, C. W., M. Scheinert, and J. Dengg, 2006: Decadal variability of subpolar gyre transport and its reverberation in the North Atlantic overturning. *Geophysical Research Letters*, **33 (21)**, doi:10.1029/2006GL026906. 8, 20, 24, 87, 129

Bourdallé Badie, R. and A.-M. Treguier, 2006: A climatology of runoff for the global ocean-ice model ORCA025. Tech. rep., MOO–RP–425–365–MER pp. 10, 127

Bower, A. S., R. M. Hendry, D. E. Amrhein, and J. M. Lilly, 2013: Direct observations of formation and propagation of subpolar eddies into the Subtropical North Atlantic. *Deep Sea Research Part II: Topical Studies in Oceanography*, **85**, 15–41, doi:10.1016/j.dsr2.2012.07.029. 64

Boyer, T., S. Levitus, J. Antonov, R. Locarnini, A. Mishonov, H. Garcia, and S. A. Josey, 2007: Changes in freshwater content in the North Atlantic Ocean 1955-2006. *Geophysical Research Letters*, **34 (16)**, L16 603, doi:10.1029/2007GL030126. 20, 21, 22, 23, 93, 96, 104, 131

Brandt, P., A. Funk, L. Czeschel, C. Eden, and C. W. Böning, 2007: Ventilation and Transformation of Labrador Sea Water and Its Rapid Export in the Deep Labrador Current. *Journal of Physical Oceanography*, **37 (4)**, 946–961, doi:10.1175/JPO3044.1. 30, 126

Brandt, P., F. A. Schott, A. Funk, and C. S. Martins, 2004: Seasonal to interannual variability of the eddy field in the Labrador Sea from satellite altimetry. *Journal of Geophysical Research : Oceans*, **109 (C2)**, doi:200410.1029/2002JC001551. 3, 31, 43

Brearley, J. A., R. S. Pickart, H. Valdimarsson, S. Jonsson, R. W. Schmitt, and T. W. Haine, 2012: The East Greenland boundary current system south of Denmark Strait. *Deep Sea Research Part I: Oceanographic Research Papers*, **63**, 1–19, doi:10.1016/j.dsr.2012.01.001. 30

Carlson, A. E., D. W. Oppo, R. E. Came, A. N. LeGrande, L. D. Keigwin, and W. B. Curry, 2008: Subtropical Atlantic salinity variability and Atlantic meridional circulation during the last deglaciation. *Geology*, **36 (12)**, 991, doi:10.1130/G25080A.1. 3

Chanut, J., B. Barnier, W. Large, L. Debreu, T. Penduff, J. M. Molines, and P. Mathiot, 2008: Mesoscale Eddies in the Labrador Sea and Their Contribution to Convection and Restratification. *Journal of Physical Oceanography*, **38 (8)**, 1617–1643, doi:10.1175/2008JPO3485.1. 3, 30, 31, 43, 126

Chelton, D., 2013: Ocean-atmosphere coupling: Mesoscale eddy effects. *Nature Geoscience*, **6 (8)**, 594–595, doi:10.1038/ngeo1906. 3

Church, J. A. and N. J. White, 2006: A 20th century acceleration in global sea-level rise. *Geophysical Research Letters*, **33 (1)**, L01 602, doi:10.1029/2005GL024826. 2

Condron, A. and P. Winsor, 2011: A subtropical fate awaited freshwater discharged from glacial Lake Agassiz. *Geophysical Research Letters*, **38 (3)**, doi:10.1029/2010GL046011. 58

Cronin, T. M., 2012: Rapid sea-level rise. *Quaternary Science Reviews*, **56**, 11–30, doi:10.1016/j.quascirev.2012.08.021. 2, 73, 97, 132

Cunningham, S., et al., 2010: The present and future system for measuring the Atlantic meridional overturning circulation and heat transport. OceanObs'09. 22, 24, 50, 55, 113, 115

Curry, R. and C. Mauritzen, 2005: Dilution of the Northern North Atlantic Ocean in Recent Decades. *Science*, **308 (5729)**, 1772–1774, doi:10.1126/science.1109477. 2, 95, 104, 131

Czeschel, L., 2004: The role of eddies for the deep water formation in the Labrador Sea. Deutsche Nationalbibliothek. 126

Dai, A. and K. E. Trenberth, 2002: Estimates of Freshwater Discharge from Continents: Latitudinal and Seasonal Variations. *Journal of Hydrometeorology*, **3 (6)**, 660–687. 9, 10, 127

Danabasoglu, G., W. G. Large, and B. P. Briegleb, 2010: Climate impacts of parameterized Nordic Sea overflows. *Journal of Geophysical Research*, **115 (C11)**, doi:201010.1029/2010JC006243. 28

Danabasoglu, G., J. C. McWilliams, and W. G. Large, 1996: Approach to Equilibrium in Accelerated Global Oceanic Models. *Journal of Climate*, **9 (5)**, 1092–1110, doi:10.1175/1520-0442(1996)009<1092:ATEIAG>2.0.CO;2. 53

Debreu, L., C. Vouland, and E. Blayo, 2008: AGRIF: Adaptive grid refinement in Fortran. *Computers & Geosciences*, **34 (1)**, 8–13, doi:10.1016/j.cageo.2007.01.009. 8, 12, 126

Dickson, R. R., J. Meincke, S.-A. Malmberg, and A. J. Lee, 1988: The "great salinity anomaly" in the Northern North Atlantic 1968-1982. *Progress In Oceanography*, **20 (2)**, 103–151, doi:16/0079-6611(88)90049-3. 2

Dijkstra, H. A., 2007: Characterization of the multiple equilibria regime in a global ocean model. *Tellus A*, **59 (5)**, 695–705, doi:10.1111/j.1600-0870.2007.00267.x. 13

DRAKKAR Group, 2007: Eddy-permitting ocean circulation hindcasts of past decades. *Clivar Exchange*, 12, 3. 8

Dufresne, J.-L., et al., 2013: Climate change projections using the IPSL-CM5 Earth System Model: from CMIP3 to CMIP5. *Climate Dynamics*, **40 (9-10)**, 2123–2165, doi:10.1007/s00382-012-1636-1. 54

Eden, C. and C. W. Böning, 2002: Sources of Eddy Kinetic Energy in the Labrador Sea. *Journal of Physical Oceanography*, **32 (12)**, 3346–3363, doi:10.1175/1520-0485(2002)032<3346:SOEKEI>2.0.CO;2. 31

Eden, C., R. J. Greatbatch, and C. W. Böning, 2004: Adiabatically Correcting an Eddy-Permitting Model Using Large-Scale Hydrographic Data: Application to the Gulf Stream and the North Atlantic Current. *Journal of Physical Oceanography*, **34 (4)**, 701–719, doi:10.1175/1520-0485(2004)034<0701:ACAEMU>2.0.CO;2. 3

Falina, A., A. Sarafanov, H. Mercier, P. Lherminier, A. Sokov, and N. Daniault, 2012: On the Cascading of Dense Shelf Waters in the Irminger Sea. *Journal of Physical Oceanography*, **42 (12)**, 2254–2267, doi:10.1175/JPO-D-12-012.1. 30

Fichefet, T. and M. A. M. Maqueda, 1997: Sensitivity of a global sea ice model to the treatment of ice thermodynamics and dynamics. *Journal of Geophysical Research*, **102 (C6)**, 12 609–12 646, doi:10.1029/97JC00480. 9, 126

Fischer, J. and F. A. Schott, 2002: Labrador Sea Water Tracked by Profiling Floats-From the Boundary Current into the Open North Atlantic. *Journal of Physical Oceanography*, **32 (2)**, 573–584, doi:10.1175/1520-0485(2002)032<0573:LSWTBP>2.0.CO;2. 38, 62

Fischer, J., M. Visbeck, R. Zantopp, and N. Nunes, 2010: Interannual to decadal variability of outflow from the Labrador Sea. *Geophysical Research Letters*, **37 (24)**, doi:201010.1029/2010GL045321. 30, 33

Gelderloos, R., C. A. Katsman, and S. S. Drijfhout, 2011: Assessing the Roles of Three Eddy Types in Restratifying the Labrador Sea after Deep Convection. *Journal of Physical Oceanography*, **41**, 2102–2119, doi:10.1175/JPO-D-11-054.1. 3, 43, 126

Gelderloos, R., F. Straneo, and C. A. Katsman, 2012: Mechanisms behind the temporary shutdown of deep convection in the Labrador Sea: Lessons from the Great Salinity Anomaly years 1968-1971. *Journal of Climate*, **25**, 6743–6755, doi:10.1175/JCLI-D-11-00549.1. 30

Gerdes, R., W. Hurlin, and S. M. Griffies, 2006: Sensitivity of a global ocean model to increased run-off from Greenland. *Ocean Modelling*, **12 (3-4)**, 416–435, doi:10.1016/j.ocemod.2005.08.003. 3, 4, 13, 55, 126

Getzlaff, J., C. W. Böning, C. Eden, and A. Biastoch, 2005: Signal propagation related to the North Atlantic overturning. *Geophysical Research Letters*, **32 (9)**, 3–6, doi:10.1029/2004GL021002. 115, 117, 119

Girton, J. B. and T. B. Sanford, 2003: Descent and Modification of the Overflow Plume in the Denmark Strait*. *Journal of Physical Oceanography*, **33 (7)**, 1351–1364, doi:10.1175/1520-0485(2003)033<1351:DAMOTO>2.0.CO;2. 28

Goosse, H. and T. Fichefet, 1999: Importance of ice-ocean interactions for the global ocean circulation: A model study. *Journal of Geophysical Research*, **104 (C10)**, 23 337–23 355. 126

Gordon, C., C. Cooper, C. A. Senior, H. Banks, J. M. Gregory, T. C. Johns, J. F. B. Mitchell, and R. A. Wood, 2000: The simulation of SST, sea ice extents and ocean heat transports in a version of the Hadley Centre coupled model without flux adjustments. *Climate Dynamics*, **16 (2-3)**, 147–168, doi:10.1007/s003820050010. 54

Gregory, J. M., O. A. Saenko, and A. J. Weaver, 2003: The role of the Atlantic freshwater balance in the hysteresis of the meridional overturning circulation. *Climate Dynamics*, **21 (7-8)**, 707–717, doi:10.1007/s00382-003-0359-8. 2, 126

Gregory, J. M., et al., 2005: A model intercomparison of changes in the Atlantic thermohaline circulation in response to increasing atmospheric CO 2 concentration. *Geophysical Research Letters*, **32 (12)**, L12 703, doi:10.1029/2005GL023209. 2

Greve, R., 2000: On the Response of the Greenland Ice Sheet to Greenhouse Climate Change. *Climatic Change*, **46 (3)**, 289–303. 10, 52, 53, 126

Griffies, S. M., et al., 2009: Coordinated Ocean-ice Reference Experiments (COREs). *Ocean Modelling*, **26 (1-2)**, 1–46, doi:10.1016/j.ocemod.2008.08.007. 4, 8, 10, 31, 47, 49, 111, 122, 124, 133

Haak, H., 2003: Formation and propagation of great salinity anomalies. *Geophysical Research Letters*, **30 (9)**, 1473, doi:10.1029/2003GL017065. 2

Häkkinen, S., 1999: A Simulation of Thermohaline Effects of a Great Salinity Anomaly. *Journal of Climate*, **12 (6)**, 1781–1795, doi:10.1175/1520-0442(1999)012<1781:ASOTEO>2.0.CO;2. 2

Hall, M. M., D. J. Torres, and I. Yashayaev, 2013: Absolute velocity along the AR7W section in the Labrador Sea. *Deep Sea Research Part I: Oceanographic Research Papers*, **72**, 72–87, doi:10.1016/j.dsr.2012.11.005. 30, 35, 36

Hansen, B. and S. Osterhus, 2000: North Atlantic-Nordic Seas exchanges. *Progress in Oceanography*, **45 (2)**, 109–208, doi:10.1016/S0079-6611(99)00052-X. 106

Hansen, B. and S. Osterhus, 2007: Faroe Bank Channel overflow 1995-2005. *Progress in Oceanography*, **75 (4)**, 817–856, doi:10.1016/j.pocean.2007.09.004. 35

Hofmann, M. and S. Rahmstorf, 2009: On the stability of the Atlantic meridional overturning circulation. *Proceedings of the National Academy of Sciences of the United States of America*, **106 (49)**, 20 584–9, doi:10.1073/pnas.0909146106. 2, 13, 126

Hogg, N. G., R. S. Pickart, R. M. Hendry, and W. J. Smethie, 1986: The northern recirculation gyre of the gulf Stream. *Deep Sea Research Part A. Oceanographic Research Papers*, **33 (9)**, 1139–1165, doi:10.1016/0198-0149(86)90017-8. 98

Houghton, R. W. and M. H. Visbeck, 2002: Quasi-decadal Salinity Fluctuations in the Labrador Sea. *Journal of Physical Oceanography*, **32 (2)**, 687–701, doi:10.1175/1520-0485(2002)032<0687:QDSFIT>2.0.CO;2. 2

Hu, A., G. A. Meehl, W. Han, and J. Yin, 2009: Transient response of the MOC and climate to potential melting of the Greenland Ice Sheet in the 21st century. *Geophysical Research Letters*, **36 (10)**, doi:200910.1029/2009GL037998. 3, 55

Hurrell, J. W., Y. Kushnir, G. Ottersen, and M. Visbeck, 2003: *The North Atlantic Oscillation: Climatic Significance and Environmental Impact*, Geophysical Monograph Series, Vol. 134. American Geophysical Union, Washington, D. C., 1-279 pp., doi:10.1029/GM134. 30, 87

Jochumsen, K., D. Quadfasel, H. Valdimarsson, and S. Jónsson, 2012: Variability of the Denmark Strait overflow: Moored time series from 1996-2011. *Journal of Geophysical Research*, **117 (C12)**, C12 003, doi:10.1029/2012JC008244. 28, 30, 53

Johns, W. and M. Baringer, 2011: Continuous, array-based estimates of Atlantic Ocean heat transport at 26.5 N. *Journal of Climate*, **24**, 2492–2449. 23, 117

Jones, E. P., 2003: Tracing Pacific water in the North Atlantic Ocean. *Journal of Geophysical Research*, **108 (C4)**, 3116, doi:10.1029/2001JC001141. 64

Jungclaus, J. H., H. Haak, M. Esch, E. Roeckner, and J. Marotzke, 2006a: Will Greenland melting halt the thermohaline circulation? *Geophysical Research Letters*, **33**. 2, 13, 127

Jungclaus, J. H., et al., 2006b: Ocean Circulation and Tropical Variability in the Coupled Model ECHAM5/MPI-OM. *Journal of Climate*, **19 (16)**, 3952–3972, doi:10.1175/JCLI3827.1. 52

Jungclaus, J. H., et al., 2013: Characteristics of the ocean simulations in the Max Planck Institute Ocean Model (MPIOM) the ocean component of the MPI-Earth system model. *Journal of Advances in Modeling Earth Systems*, **5 (2)**, 422–446, doi:10.1002/jame.20023. 54

Kanzow, T., et al., 2010: Seasonal Variability of the Atlantic Meridional Overturning Circulation at 26.5ï¿œN. *Journal of Climate*, **23 (21)**, 5678–5698, doi:10.1175/2010JCLI3389.1. 22, 24

Kieke, D., M. Rhein, L. Stramma, W. M. Smethie, J. L. Bullister, and D. A. LeBel, 2007: Changes in the pool of Labrador Sea Water in the subpolar North Atlantic. *Geophysical Research Letters*, **34 (6)**, L06 605, doi:10.1029/2006GL028959. 23, 76

Koenigk, T., U. Mikolajewicz, H. Haak, and J. Jungclaus, 2005: Variability of Fram Strait sea ice export: causes, impacts and feedbacks in a coupled climate model. *Climate Dynamics*, **26 (1)**, 17–34, doi:10.1007/s00382-005-0060-1. 106

Kopp, R. E., J. X. Mitrovica, S. M. Griffies, J. Yin, C. C. Hay, and R. J. Stouffer, 2010: The impact of Greenland melt on local sea levels: a partially coupled analysis of dynamic and static equilibrium effects in idealized water-hosing experiments. *Climatic Change*, **103 (3-4)**, 619–625, doi:10.1007/s10584-010-9935-1. 98, 132

Landerer, F. W., J. H. Jungclaus, and J. Marotzke, 2007: Regional Dynamic and Steric Sea Level Change in Response to the IPCC-A1B Scenario. *Journal of Physical Oceanography*, **37 (2)**, 296–312, doi:10.1175/JPO3013.1. 39, 73, 97, 98, 132

Large, W. and S. Yeager, 2009: The global climatology of an interannually varying air-sea flux data set. *Climate Dynamics*, **33**, 341–364, doi:10.1007/s00382-008-0441-3. 5, 9, 12, 48, 127

Latif, M., C. Böning, J. Willebrand, A. Biastoch, J. Dengg, N. Keenlyside, U. Schweckendiek, and G. Madec, 2006: Is the Thermohaline Circulation Changing? *Journal of Climate*, **19 (18)**, 4631–4637, doi:10.1175/JCLI3876.1. 53, 106, 110

Latif, M., E. Roeckner, U. Mikolajewicz, and R. Voss, 2000: Tropical Stabilization of the Thermohaline Circulation in a Greenhouse Warming Simulation. *Journal of Climate*, **13 (11)**, 1809–1813, doi:10.1175/1520-0442(2000)013<1809:L>2.0.CO;2. 13, 126

Lavender, K. L., R. E. Davis, and W. B. Owens, 2000: Mid-depth recirculation observed in the interior Labrador and Irminger seas by direct velocity measurements. *Nature*, **407**, 66–69, doi:10.1038/35024048. 32, 33, 38, 39, 62

Lee, T. and P. Cornillon, 1996: Propagation and Growth of Gulf Stream Meanders between 75ï¿œ and 45ï¿œW. *Journal of Physical Oceanography*, **26 (2)**, 225–241, doi:10.1175/1520-0485(1996)026<0225:PAGOGS>2.0.CO;2. 41

Levermann, A. and A. Born, 2007: Bistability of the Atlantic subpolar gyre in a coarse-resolution climate model. *Geophysical Research Letters*, **34 (24)**, L24 605, doi:10.1029/2007GL031732. 71

Levitus, 1998: Introduction. Vol. 1, World Ocean Database NOAA Atlas NESDIS 18,. *NOAA/NESDIS, U.S. Dept. of Commerce, Washington, D.C*, **1**. 9, 10, 23, 46, 48, 49, 50, 127

Lévy, M., P. Klein, A.-M. Tréguier, D. Iovino, G. Madec, S. Masson, and K. Takahashi, 2010: Modifications of gyre circulation by sub-mesoscale physics. *Ocean Modelling*, **34 (1-2)**, 1–15, doi:10.1016/j.ocemod.2010.04.001. 3

Lilly, J. M., P. B. Rhines, F. Schott, K. Lavender, J. Lazier, U. Send, and E. D'Asaro, 2003: Observations of the Labrador Sea eddy field. *Progress In Oceanography*, **59 (1)**, 75–176, doi:10.1016/j.pocean.2003.08.013. 30

Lohmann, G., 2003: Atmospheric and oceanic freshwater transport during weak Atlantic overturning circulation. *Tellus A*, **55 (5)**, 438–449, doi:10.1034/j.1600-0870.2003.00028.x. 121, 122

Lorbacher, K., S. J. Marsland, J. A. Church, S. M. Griffies, and D. Stammer, 2012: Rapid barotropic sea level rise from ice sheet melting. *Journal of Geophysical Research*, **117 (C6)**, C06 003, doi:10.1029/2011JC007733. 4

Macrander, A., R. Käse, U. Send, H. Valdimarsson, and S. Jónsson, 2007: Spatial and temporal structure of the Denmark Strait Overflow revealed by acoustic observations. *Ocean Dynamics*, **57 (2)**, 75–89, doi:10.1007/s10236-007-0101-x. 30, 106, 111, 133

Madec, G. Madec, P. Delecluse, M. Imbard, and C. Lèvy, 1998: OPA 8.1 Ocean General Circulation Model Reference Manual. 9

Madec, G., 2008: NEMO the Ocean Engine. *Tech. Rep., Notes de l IPSL*, **27 (1288-1619)**, 193. 8, 126

Marotzke, J. and P. H. Stone, 1995: Atmospheric Transports, the Thermohaline Circulation, and Flux Adjustments in a Simple Coupled Model. *Journal of Physical Oceanography*, **25 (6)**, 1350–1364, doi:10.1175/1520-0485(1995)025<1350:ATTTCA>2.0.CO;2. 121

Marsh, R., D. Desbruyères, J. L. Bamber, B. A. de Cuevas, A. C. Coward, and Y. Aksenov, 2010: Short-term impacts of enhanced Greenland freshwater fluxes in an eddy-permitting ocean model. *Ocean Science*, **6 (3)**, 749–760, doi:10.5194/os-6-749-2010. 3, 4, 55, 128

Marshall, J., H. Johnson, and J. Goodman, 2001: A Study of the Interaction of the North Atlantic Oscillation with Ocean Circulation. *Journal of Climate*, **14 (7)**, 1399–1421, doi:10.1175/1520-0442(2001)014<1399:ASOTIO>2.0.CO;2. 22

McCarthy, G., et al., 2012: Observed interannual variability of the Atlantic meridional overturning circulation at 26.5ï¿œN. *Geophysical Research Letters*, **39 (19)**, doi:10.1029/2012GL052933. 117

Meese, D. A., et al., 1997: The Greenland Ice Sheet Project 2 depth-age scale: Methods and results. *Journal of Geophysical Research*, **102 (C12)**, 26 411, doi:10.1029/97JC00269. 2

Msadek, R., W. E. Johns, S. G. Yeager, G. Danabasoglu, T. L. Delworth, and A. Rosati, 2013: The Atlantic Meridional Heat Transport at 26.5ï¿œN and Its Relationship with the MOC in the RAPID Array and the GFDL and NCAR Coupled Models. *Journal of Climate*, **26 (12)**, 4335–4356, doi:10.1175/JCLI-D-12-00081.1. 23

Neem community Members, ., 2013: Eemian interglacial reconstructed from a Greenland folded ice core. *Nature*, **493 (7433)**, 489–94, doi:10.1038/nature11789. 3, 18

Otterå, O. H., M. Bentsen, H. Drange, and L. Suo, 2010: External forcing as a metronome for Atlantic multidecadal variability. *Nature Geoscience*, **3 (10)**, 688–694, doi:10.1038/ngeo955. 54

Paiva, A. M. and E. P. Chassignet, 2001: The impact of surface flux parameterizations on the modeling of the North Atlantic Ocean. *Journal of Physical oceanography*, **31 (7)**, 1860–1879, doi:10.1175/1520-0485(2001)031<1860:TIOSFP>2.0.CO;2. 46

Pickart, R. S., D. J. Torres, and R. A. Clarke, 2002: Hydrography of the Labrador Sea during Active Convection. *Journal of Physical Oceanography*, **32 (2)**, 428–457, doi:10.1175/1520-0485(2002)032<0428:HOTLSD>2.0.CO;2. 31

Pokhrel, Y. N., N. Hanasaki, P. J.-F. Yeh, T. J. Yamada, S. Kanae, and T. Oki, 2012: Model estimates of sea-level change due to anthropogenic impacts on terrestrial water storage. *Nature Geoscience*, **5 (6)**, 389–392, doi:10.1038/ngeo1476. 10, 73

Rahmstorf, S., 1996: On the freshwater forcing and transport of the Atlantic thermohaline circulation. *Climate Dynamics*, **12 (12)**, 799–811, doi:10.1007/s003820050144. 2, 3, 126

Rattan, S., P. G. Myers, A.-M. Treguier, S. Theetten, A. Biastoch, and C. W. Böning, 2010: Towards an understanding of Labrador Sea salinity drift in eddy-permitting simulations. *Ocean Modelling*, **35 (1-2)**, 77–88, doi:10.1016/j.ocemod.2010.06.007. 50

Rhein, M., et al., 2002: Labrador Sea Water: Pathways, CFC Inventory, and Formation Rates. *Journal of Physical Oceanography*, **32 (2)**, 648–665, doi:10.1175/1520-0485(2002)032<0648:LSWPCI>2.0.CO;2. 23, 76

Rhein, M., et al., 2011: Deep water formation, the subpolar gyre, and the meridional overturning circulation in the subpolar North Atlantic. *Deep Sea Research Part II: Topical Studies in Oceanography*, **58 (17-18)**, 1819–1832, doi:10.1016/j.dsr2.2010.10.061. 76

Ridley, J. K., P. Huybrechts, J. M. Gregory, and J. A. Lowe, 2005: Elimination of the Greenland Ice Sheet in a High CO 2 Climate. *Journal of Climate*, **18 (17)**, 3409–3427, doi:10.1175/JCLI3482.1. 2

Rignot, E., M. Koppes, and I. Velicogna, 2010: Rapid submarine melting of the calving faces of West Greenland glaciers. *Nature Geosci*, **3 (3)**, 187–191, doi:10.1038/ngeo765. 2

Rignot, E., I. Velicogna, M. R. van den Broeke, A. Monaghan, and J. Lenaerts, 2011: Acceleration of the contribution of the Greenland and Antarctic ice sheets to sea level rise. *Geophysical Research Letters*, **38**, 5 PP., doi:201110.1029/2011GL046583. 2

Rossby, T., V. Ozhigin, V. Ivshin, and S. Bacon, 2009: An isopycnal view of the Nordic Seas hydrography with focus on properties of the Lofoten Basin. *Deep Sea Research Part I: Oceanographic Research Papers*, **56 (11)**, 1955–1971, doi:10.1016/j.dsr.2009.07.005. 41

Scheinert, M., 2008: Causes and Impacts of teh Northern Atlantic Freshening. Ph.D. thesis. 96

Spall, M. A. and R. S. Pickart, 2001: Where Does Dense Water Sink? A Subpolar Gyre Example*. *Journal of Physical Oceanography*, **31 (3)**, 810–826, doi:10.1175/1520-0485(2001)031<0810:WDDWSA>2.0.CO;2. 88

Spence, J. P., M. Eby, and A. J. Weaver, 2008: The Sensitivity of the Atlantic Meridional Overturning Circulation to Freshwater Forcing at Eddy-Permitting Resolutions. *Journal of Climate*, **21 (11)**, 2697–2710, doi:10.1175/2007JCLI2103.1. 59

Stammer, D., 2008: Response of the global ocean to Greenland and Antarctic ice melting. *Journal of Geophysical Research*, **113 (C6)**, doi:10.1029/2006JC004079. 3

Sterl, A., et al., 2011: A look at the ocean in the EC-Earth climate model. *Climate Dynamics*, **39 (11)**, 2631–2657, doi:10.1007/s00382-011-1239-2. 54

Stouffer, R. J., J. Yin, J. M. Gregory, and K. Dixon, 2006: Investigating the causes of the response of the thermohaline circulation to past and future climate changes. *Journal of Climate*, **19**, 1265–1387. 3, 4, 13, 55, 126, 133, 150

Strass, V. H., E. Fahrbach, U. Schauer, and L. Sellmann, 1993: Formation of Denmark Strait overflow water by mixing in the East Greenland Current. *Journal of Geophysical Research*, **98 (C4)**, 6907, doi:10.1029/92JC02732. 106

Swingedouw, D., et al., 2012: Decadal fingerprints of freshwater discharge around Greenland in a multi-model ensemble. *Climate Dynamics*, **41**, 695–720, doi:10.1007/s00382-012-1479-9. 2, 3, 4, 13, 31, 45, 54, 55, 56, 57, 58, 59, 61, 89, 91, 97, 98, 105, 106, 126, 127, 130, 131, 133, 134, 150, 157

Talley, L. D. and M. S. McCartney, 1982: Distribution and Circulation of Labrador Sea Water. *Journal of Physical Oceanography*, **12 (11)**, 1189–1205, doi:10.1175/1520-0485(1982)012<1189:DACOLS>2.0.CO;2. 30

Treguier, A. M., J. Deshayes, C. Lique, R. Dussin, and J. M. Molines, 2012: Eddy contributions to the meridional transport of salt in the North Atlantic. *Journal of Geophysical Research: Oceans*, **117 (C5)**, C05 010, doi:10.1029/2012JC007927. 117, 119

Trenberth, K. E., 2010: Global change: The ocean is warming, isn't it? *Nature*, **465**, 304, doi:10.1038/465304a. 50

Vancoppenolle, M., T. Fichefet, H. Goosse, S. Bouillon, C. Konig Beatty, and M. A. Maqueda, 2008: LIM3, an advanced sea ice model for climate simulation and operational oceanography. 12

Våge, K., R. S. Pickart, M. A. Spall, H. Valdimarsson, S. Jónsson, D. J. Torres, S. Ø sterhus, and T. Eldevik, 2011: Significant role of the North Icelandic Jet in the formation of Denmark Strait overflow water. *Nature Geoscience*, **4 (10)**, 723–727, doi:10.1038/ngeo1234. 62, 106

Wang, X., Q. Wang, D. Sidorenko, S. Danilov, J. Schröter, and T. Jung, 2012: Long-term ocean simulations in FESOM: evaluation and application in studying the impact of Greenland Ice Sheet melting. *Ocean Dynamics*, **62 (10-12)**, 1471–1486, doi:10.1007/s10236-012-0572-2. 3, 4, 13, 55, 73, 129

Weese, S. R. and F. O. Bryan, 2006: Climate impacts of systematic errors in the simulation of the

path of the North Atlantic Current. *Geophysical Research Letters*, **33 (19)**, L19 708, doi:10.1029/2006GL027669. 39

Weijer, W., M. E. Maltrud, M. W. Hecht, H. A. Dijkstra, and M. A. Kliphuis, 2012: Response of the Atlantic Ocean circulation to Greenland Ice Sheet melting in a strongly-eddying ocean model. *Geophysical Research Letters*, **39 (9)**, doi:10.1029/2012GL051611. 3, 4, 13, 55, 58, 126, 129, 130, 133

Wu, L., et al., 2012: Enhanced warming over the global subtropical western boundary currents. *Nature Climate Change*, **2 (3)**, 161–166, doi:10.1038/nclimate1353. 93

Yashayaev, I., 2007: Hydrographic changes in the Labrador Sea, 1960-2005. *Progress in Oceanography*, **73 (3-4)**, 242–276, doi:10.1016/j.pocean.2007.04.015. 32, 35

Yashayaev, I. and J. W. Loder, 2009: Enhanced production of Labrador Sea Water in 2008. *Geophysical Research Letters*, **36 (1)**, doi:200910.1029/2008GL036162. 23, 31, 35, 38, 71

Zhang, R., 2010: Latitudinal dependence of Atlantic meridional overturning circulation (AMOC) variations. *Geophysical Research Letters*, **37 (16)**, doi:10.1029/2010GL044474. 24

Zhang, R., T. L. Delworth, A. Rosati, W. G. Anderson, K. W. Dixon, H.-C. Lee, and F. Zeng, 2011: Sensitivity of the North Atlantic Ocean Circulation to an abrupt change in the Nordic Sea overflow in a high resolution global coupled climate model. *Journal of Geophysical Research*, **116 (C12)**, doi:201110.1029/2011JC007240. 91, 106

A. Sensitivity simulations of the oceanic response (AMOC at 36°N) on an enhanced melting of the GrIS to differences in the AMOC history and AMOC trend.

The following paragraph addresses the question of the robustness of the presented results and to provide some kind of error estimate. At that point only the AMOC strength at 36°N is taken as measure to keep the paragraph clear. The related Figure A-1a provide an overview about all performed simulation pairs in ORCA05 and the previously presented simulations in ORCA025 and VIKING20, which consists of a reference (solid, referred to as "REF") simulation (1948 - 2007) and a perturbation simulation with the I-MELT (dashed, referred to as "FW") scenario (1965-2007). Further performed simulations pairs in ORCA025 did not provided additional insights to the ORCA05 results and have been excluded. In total they accumulate to a pair of 15 simulations, which mainly differ in the horizontal resolution from ORCA05 over ORCA025 to VIKING20 (referred to as "05","025" and "0.05" respectively) and in details in the applied freshwater forcing, which leads to large difference in the AMOC and its long-term tendency (Figure A-1).

The freshwater forcing includes variations in the polar rain reduction from 55°N to 62°N and between 7.5% and 10% (referred accordingly) and furthermore in details of the SSS restoring. Two different SSS restoring settings have been used, a regional uniform SSS restoring with a piston velocity of 16.4 mm/day and simulations where no SSS restoring is applied in the wide swath ($\sim$ 500 km) around Greenland (referred to as "noGR") to avoid an immediately restoring effect on the additional meltwater from Greenland. In both settings the restoring fluxes are limited to a difference between modelled SSS and climatology of about 0.5 psu to inhibit dominating restoring fluxes.

In the ORCA05 configuration the entire CORE 2 forcing period is not only applied once (referred to as "1.it") but also up to two times (referred to as "2.it") with the oceanic state of 2007 from

the previous iteration. Last but not least, simulations with a so called "mixed boundary condition" (referred to as "MIXED") and without restoring (referred to as "NO") have been performed. In the mixed boundary condition simulations the restoring fluxes of an existing reference simulation have been analyzed and applied instead of any further SSS-restoring in the according subsequent reference and melting simulation.

All these differences in details in the model configuration lead to a large spread in the AMOC strength and its long term tendency (Figure A-1a) in the reference simulations (solid) and in line with results of Behrens et al. (2013). The main previous presented simulations are marked heavy bold. The AMOC strength of the reference simulation varies between 10 Sv (REF05 noGR 7.5% 55N 1.it) and 22 Sv (REF05 10% 55N 2.it) and most of the reference simulations show a slight ongoing trend over the simulation period, related to the freshwater forcing (Behrens et al. (2013)). Irrespectively of the initial AMOC strength or ongoing trend of the reference simulation, all Greenland melting simulations (dashed) suggest a decline in comparison to the reference simulations, with values between 12 ((FW05 10% 55N 2.it) and 7 Sv (FW025 noGR 10% 62N 1.it) in 2007. Taking the AMOC strength of each individual reference simulation as reference value and diagnose relative changes, the spread is substantially reduced (Figure A-1a). All relative AMOC changes converge to values between -42% to -62%, while the host of simulations projects a decline of about -45% at the end of the hosing simulation, which is in broad agreement to previous studies with similar meltwater rates (e.g. Swingedouw et al. (2012); Stouffer et al. (2006)). The results suggest further that the remaining SSS restoring is of minor importance for the oceanic response, which is indicated by similar results of configurations with no SSS restoring or mixed boundary condition in comparison to simulation with SSS restoring. Furthermore the results show that the initial AMOC strength and long-term trend are also of minor importance for the AMOC response at least in the I-MELT melting scenario. A similar large set of simulations in the R-MELT scenario has been not conducted to test the robustness of the R-MELT results.

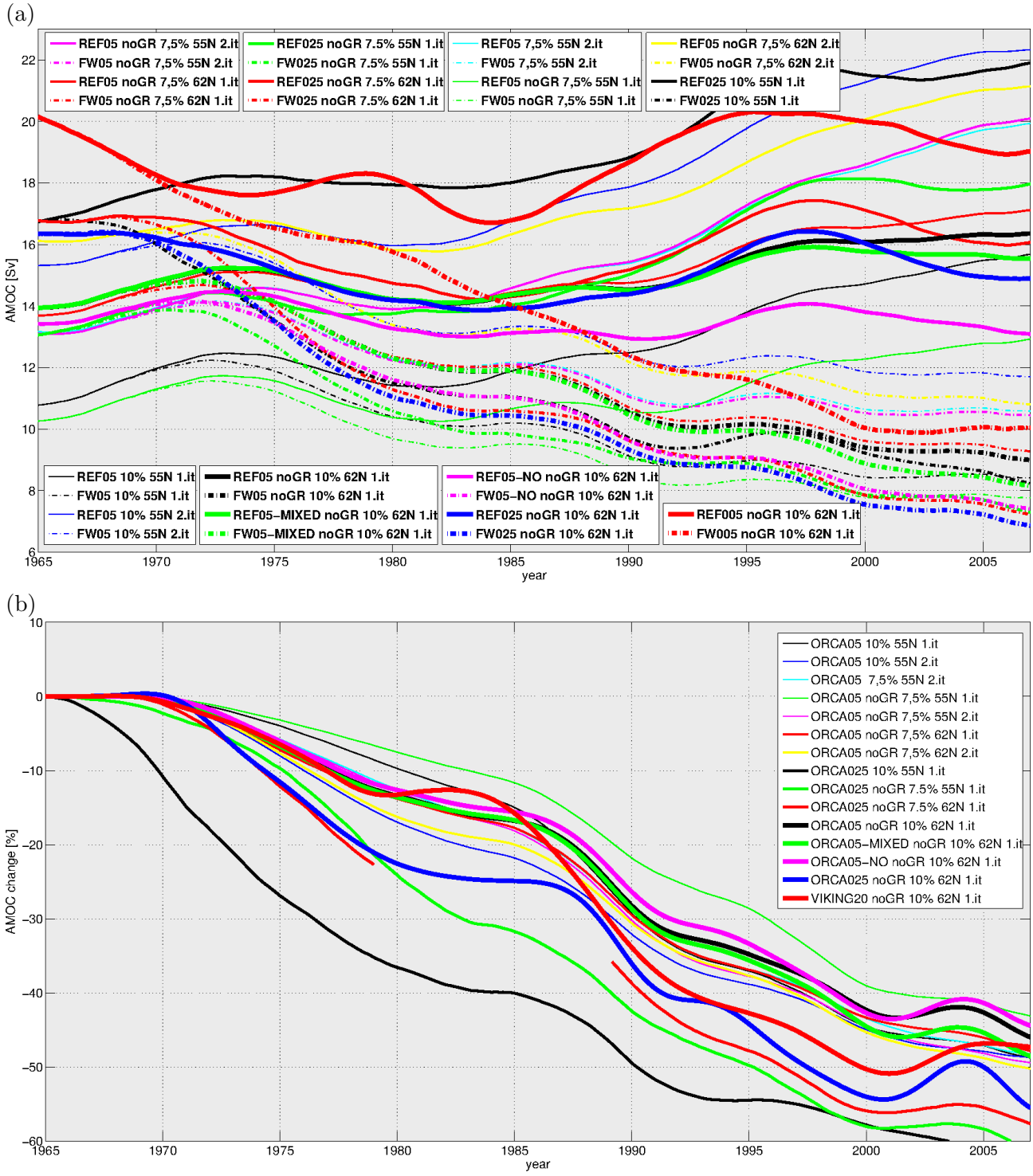

Figure A-1.: AMOC strength at 36°N: (a) Maximum AMOC in Sv for the reference and hosing (I-MELT) simulation and in (b) the relative changes (in %) to the maximum value are shown. Simulations differ in their horizontal resolution (0.5° and 0.25°), the polar freshwater forcing, in details of the SSS restoring and number of iterations. The simulation "REF05 noGR 10 % 55N 1.it" indicates a reference simulation in ORCA05 with a polar reduction of precipitation by 10 % north of 55N and around Greenland no SSS restoring is applied. This simulation corresponds to the first iteration of the CORE2 forcing (1948-2007). For all other simulations the nomenclature is accordingly. FW indicates I-MELT simulation. The major important simulations are heavy bold.

Nomenclature

AABW Antarctic Bottom Water

AMOC Atlantic Meridional Overturning Circulation

DSOW Denmark Strait Overflow Water

EGC East Greenland Current

GrIS Greenland Ice Sheet

LSW Labrador Sea Water

MLD Mixed Layer Depth

NAC North Atlantic Current

NADW North Atlantic Deep Water

NAO North Atlantic Circulation

NW Corner North-West Corner

S salinity

SPG Subpolar Gyre

SSH sea surface height

STG Subtropical Gyre

T temperature

WGC West Greenland Current

Danksagung

Mein besondere Dank gilt meinem Dokotorvater Prof. Claus W. Böning, der mir stets hilfreiche Anregungen und Unterstützungen während der Promotion gegeben hat.

Desweiteren danke ich Prof. Arne Biastoch für seine ständige Hilfsbereitschaft und nützliche Diskussionen, die diese Arbeit deutlich voran gebracht haben.

Ich möchte besonders Franziska Schwarzkopf und ihrer Vorarbeit mit AGRIF danken, ohne die diese Arbeit nicht in dem Zeitrahmen zu bewerkstelligen gewesen wäre. Außerdem möchte ich mich für stetige Unterstützung während der Promotion bedanken.

Ein weiterer wichtiger Punkt, ist die breite technische Hilfe von Dr. Markus Scheinert, dem eine große Bedeutung für die wissenschaftliche Leistung der Forschungsgruppe zu kommt.

Ich bedanke mich weiterenhin bei den lieben Vorablesern meiner Arbeit, die mein Englisch verbessert haben (Jonathan Durgadoo, Hendrik Behrens, Stefan Gary, Markus Scheinert und Lavinia Patara).

Zu guter letzt möchte ich mich noch bei allen anderen Personen bedanken, die mich bei der Arbeit in jeglicher Form unterstützt haben. Danke!

Erklärung

Hiermit erkläre ich, dass ich die vorliegende Dissertation, abgesehen durch die Beratung meiner akademischen Lehrer, selbstständig verfasst habe und keine weiteren Quellen und Hilfsmittel, als die hier angegebenen verwendet habe.

Diese Arbeit hat weder ganz, noch in Teilen, bereits an anderer Stelle einer Prüfungskommission zur Erlangung des Doktorgrades vorgelegen.

Ich erkläre, dass die vorliegende Arbeit gemäß der Grundsätze zur Sicherung guter wissenschaftlicher Praxis der Deutschen Forschungsgemeinschaft erstellt wurde.

Folgende Abbildungen sind bereits veröffentlicht und Teil wissenschaftlicher Arbeiten mit meiner Beteilung während der Promotion:

Abbildungen 25, 26 and 27 sind Swingedouw et al. (2012) entnommen und die Abbildungen 22, 23 und 24 aus Behrens et al. (2013). Texte oder Texteile sind nicht verwendet wurden.

Kiel, den 10.12.2013

Erik Behrens